In-process Monitoring and Control for Nd:YAG Laser Material Processing

By

Christopher N. D. Peters

October 2000

A thesis submitted for the degree of Doctor of Philosophy of the University of Liverpool

Department of Mechanical Engineering
Liverpool University
Liverpool
L69 3BX

Declaration

I declare that no part of this thesis has been submitted in support of any other qualification.

Christopher Peters

Oct 1998

Acknowledgements

A special thank you to The Royal Commission for the Exhibition of 1851 for their vision and hands-off support throughout, and to GSILumonics Ltd, for their faith and commitment to people development.

I would like thank Professor W.M.Steen for his guidance as my academic supervisor and a seemingly endless flow of ideas and, to my industrial supervisor, Dr Ian Norris, for his support.

I would also like to thank Dr Duncan Hand and Dr Frank Haran of the Department of Physics, Heriot-Watt University for their help, wisdom, enthusiasm, guidance and friendship during (and I hope beyond) this project.

Finally I would like to thank my wife, Jenny for her support and encouragement throughout this experience

Abstract

The objectives of this thesis were to develop techniques that can be employed to monitor process quality on-line in industrial Nd:YAG laser material processing applications

Work was carried out to develop sensors that will be practical for use in industrial conditions. These sensors were then used to observe process behaviour during processing and in particular laser welding.

Optical sensing was favoured because of light's inherent immunity to noise and the ease in which it can be transmitted though simple optics.

The techniques employed were found to be both flexible and sensitive to the events occurring within the process.

From this work a range of techniques have been developed which can be used for monitoring changes from the normal condition, and indicate a change in quality. These include a method for accurately monitoring of laser beam focus position with potential for closed loop control, a method for determining changes in laser beam coupling efficiency, penetration monitoring and a method for discriminating between different causes of penetration defects.

List of Symbols

Symbol	Meaning	Units
I(r)	beam intensities at a radius distance r from the centre of the beam	Wcm^{-2}
I(o)	beam intensity at the centre of the beam	Wcm^{-2}
w	radius of the beam corresponding to the intensity $1/e^2$ of the peak intensity.	m
P	total power within a Gaussian beam.	W
Z	distance in the direction of beam propagation	m
Z_R	Rayleigh range	m
d	beam waist diameter	m
g	beam radius factor	-
λ	laser beam wavelength.	m
w_0	laser beam waist radius	m
b	depth of focus	m
f	focal length of a lens	m
D	beam diameter at the lens	m
θ	full angle beam divergence	rads
$\theta_{act.}$	actual full angle divergence of a given laser beam	rads
n_1 and n_2	refractive indices of dielectric material	-
n_i	refractive index of incident material	-
n_t	refractive index of transmitting material	-
θ_1 and θ_2	angle of light ray incidence relative to the normal	rads
NA	fibre optic numerical aperture	-
n_o	refractive index of air	-
A_i	absorption in an ideal material	-
A_D	absorption due to free electron collision (Drude)	-
A_A	absorption due to anomalous skin effect	-
A_{IB}	absorption due to inter-band transitions	-
A_o	initial absorption.	-
A_r	absorption in a real material	-
A_{ext}	absorption due to extrinsic material properties	-
A_{int}	absorption due to intrinsic material properties	-
N_{ion}	density of ionised atoms	cm^{-3}
N_{neu}	density of neutral atoms	cm^{-3}
T	temperature	K
K	Boltzmann constant	$J K^{-1}$
U_i	ionisation energy	J
h	Planck constant	$J Hz^{-1}$
ν	photon frequency	Hz
n_e	electron density number	cm^{-3}
z	charge number	-
e	electron charge	V
c	velocity of light	ms^{-1}
ε_o	dielectric constant of the medium	-
ε	dielectric constant of the particle	-
K_{sca}	coefficient of Rayleigh scattering	-
m_e	mass of an electron	kg
ω	angular frequency of the incident wave	$rads^{-1}$
ω_p	angular frequency of plasma oscillation	$rads^{-1}$
Λ	Coulomb	C
V_p	particle volume	cm^3
R	distance from particle	m

Φ	angle of scattering	rads
ω_{oo}	angular frequency for ground mode	$rads^{-1}$
E	dielectric constant of the particle	-
N	number density of particles	cm^{-3}
B	restoring pressure	Nm^{-2}
Q	average mass density of the liquid phase	$kg\ m^{-3}$
a	equilibrium keyhole radius	m
C	ratio of weld-pool radius and keyhole radius	-
m	azimuthal mode number	-
k	wave number of axial mode	-
K'	derivative of the Bessel function	-
γ	coefficient of surface tension	-
K_n	modified Bessel function	-
P	density of the melt	kgm^{-3}
l	axial mode number	-
h	weld-pool depth	m
E_{bb}	total energy radiated by black body per unit area time	$J\ m^{-2}s^{-1}$
E_{nb}	total energy radiated by non-black body per unit area time	$J\ m^{-2}s^{-1}$
σ	Stefan's constant	$Wm^{-2}K^{-4}$.
H	total emissivity of a body	-
x_{nm}	excitation potential from level m to n	-
E_n	energy level	-
g_n	statistical weight of ground or excited state	kg
A_{nm}	probability of energy transition	-
I_{nm}	spectral intensity	Wcm^{-2}
V	ionisation energy	J
R_1 and R_2	lens surface radii	m
n_{lens}	refractive index of lens material	-
T_{ip}	thickness of molten material ahead of beam impingement point	m
b'	keyhole length	m

Contents

1 Introduction

1.1 Development of the Nd:YAG Laser

It was in 1917 that Einstein [1] first introduced the idea of stimulated emission when he showed that to describe fully the interaction of radiation with matter, a process must be included, where an atom in an excited state is induced to decay to a lower state by the interaction of radiation.

Gordon, Zeiger and Townes [2] demonstrated the first practical device showing stimulated emission with an ammonia MASER (Microwave Amplification by Stimulated Emission of Radiation) in 1954. The first LASER (Light Amplification by Stimulated Emission of Radiation) followed shortly afterwards when Maiman [3] demonstrated oscillating action at 693.4nm in ruby, in 1960.

The solid state Neodymium: Yttrium Aluminium Garnet (Nd:YAG) laser and gas based Carbon Dioxide (CO_2) laser were later developed in the Bell Laboratories in 1964 [4].

The total world market for laser systems (machines incorporating laser sources) in 2000 is estimated [5,6] at nearly 4 billion US dollars. This includes the use of lasers for such diverse applications as telecommunication, optical storage, medical applications and material processing such as welding, cutting and drilling. The material-processing sector, widely regarded as the industrial sector, is estimated to be worth just over $1.0bn per annum in revenue.

Industrial lasers, used for material processing applications, comprise approximately 8% of the machine tool market and are now expected to experience similar 10% p.a. growth as this sector. The industrial laser market is now dominated by the CO_2 and Nd:YAG laser sources. The

Nd:YAG laser employs a solid crystal usually in the form of a cylindrical rod or rectangular slab. The Carbon Dioxide laser employs a mixture of gases (helium, nitrogen and carbon dioxide) as the medium to generate the laser beam. The principal output wavelengths of the Nd:YAG and the CO_2 laser beam is 1.064μm and 10.6μm respectively.

The CO_2 laser currently has the lion's share of the industrial market, accounting for over 50% of the market revenue and units sold. Solid state lasers (within which Nd:YAG is the principal source) account for approximately 38% of both revenue and units.

The biggest area of application for industrial lasers is for marking and cutting, however there is strong growth (17-20%) predicted for welding applications, mainly in the automotive sector over the next ten years. The main automotive applications are welding of body components on-line, such as roof to body side and, tailored blank welding. Other non-automotive applications include welding of domestic products such as radiators.

A particular attribute of the Nd:YAG laser, by virtue of its shorter wavelength, is that common optical materials such as fused silica, can be used for its beam delivery. An attractive and flexible option available to these lasers is the use of a fibre optic for beam delivery.

1.2 Nd:YAG Laser Material Processing Performance.

Driven partly by market demand and partly by technological interest the Nd:YAG laser has undergone extensive development in recent years and is now becoming more widely available at higher power levels (1-4kW). Some Nd:YAG lasers at this power level have the capability of providing both continuous wave and pulsed output from the same source.

The use of Nd:YAG lasers for materials processing is now commonplace for a variety of applications the most common being welding, cutting and drilling of metals. Claimed performance data such as maximum speed, depth of penetration is commonly available mainly as product data from manufacturers of sources and applications publications. Figure 1.1 shows a graph compiled from data from a variety of manufacturers of welding performance for mild steel. The data have been presented in the form of maximum processing speed against thickness of material for full penetration, for several levels of laser mean power. For comparison similar data for CO_2 laser sources have also been plotted. All Nd:YAG laser data are for fibre optic beam delivery.

This is a common way of presenting such data and is generally intended to give an indication of potential performance for more specific applications. It is interesting to note that the absolute welding performance of Nd:YAG lasers, compared with reported performance 8 years ago [7], has, in the thinner materials (0.5-1.0mm) more than doubled and, in the medium thickness materials (3-5 mm) increased by a factor of 5-10. It can also be seen that the relative welding performance of an Nd:YAG laser with 3.5kW at the work-piece is capable of higher welding speeds than a 4 kW CO_2 source and can be shown to be approximately the same as a 5 kW source. High performance has mainly been achieved through improved beam quality, allowing greater intensity and mean power at the work-piece.

Very high welding speeds can be achieved by welding without the use of the shielding gas [8], normally used to prevent oxidation of the molten metal in the weld. At these high speeds, the beam interaction time seems sufficiently short to prevent adverse oxidation. This approach does not seem practical with the CO_2 laser because of excessive beam absorption in the plasma above

the work-piece and as a consequence is making the Nd:YAG laser attractive to tailored blank manufacturers [9] who require high speed, low cost welding in thin steel sheet.

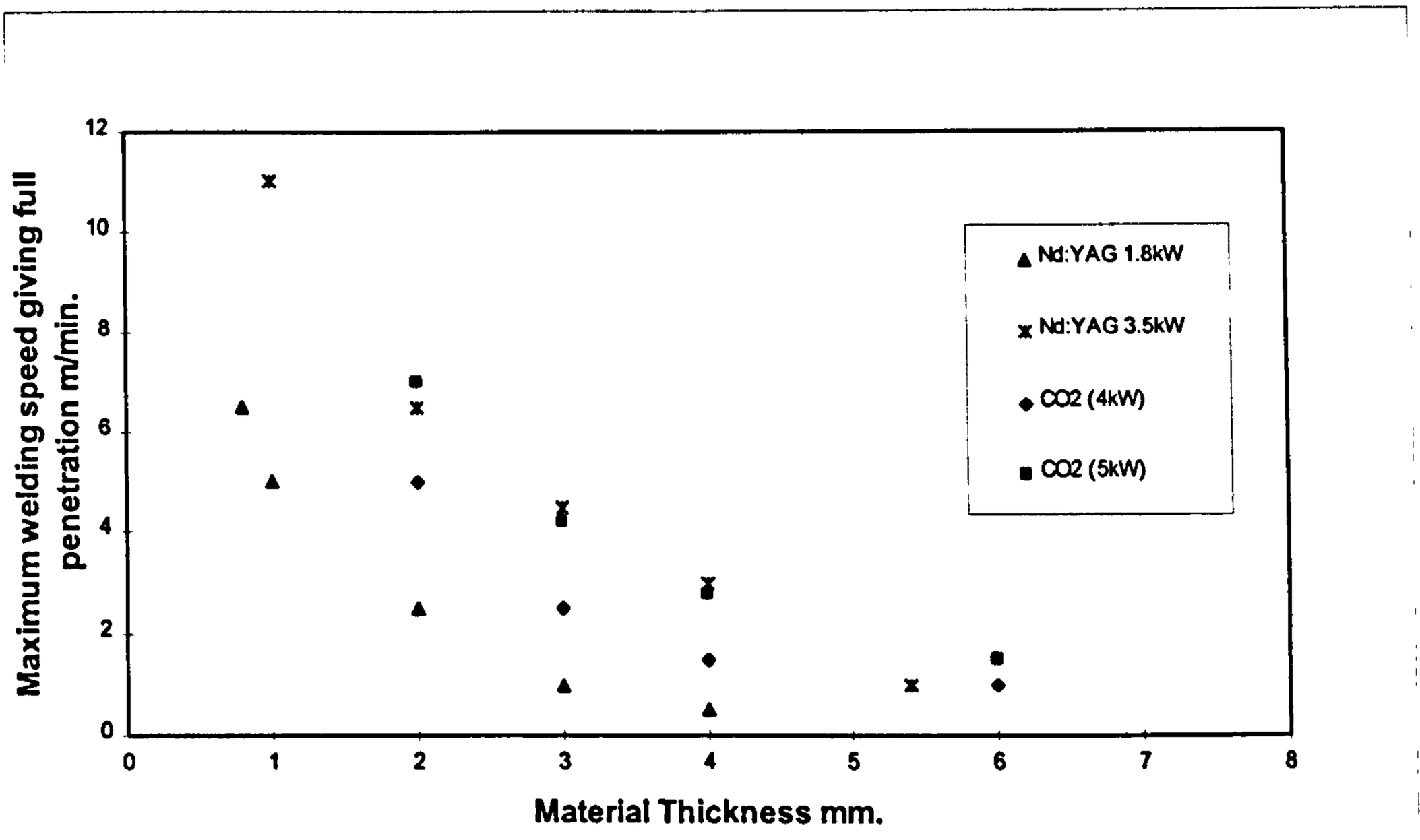

Figure 1.1. Comparison of laser welding performance for industrial lasers [10, 11]

Fibre optic beam delivery has been proven to be both flexible and easy to maintain and greatly simplifies the task of delivering the beam for processing complex three-dimensional components.

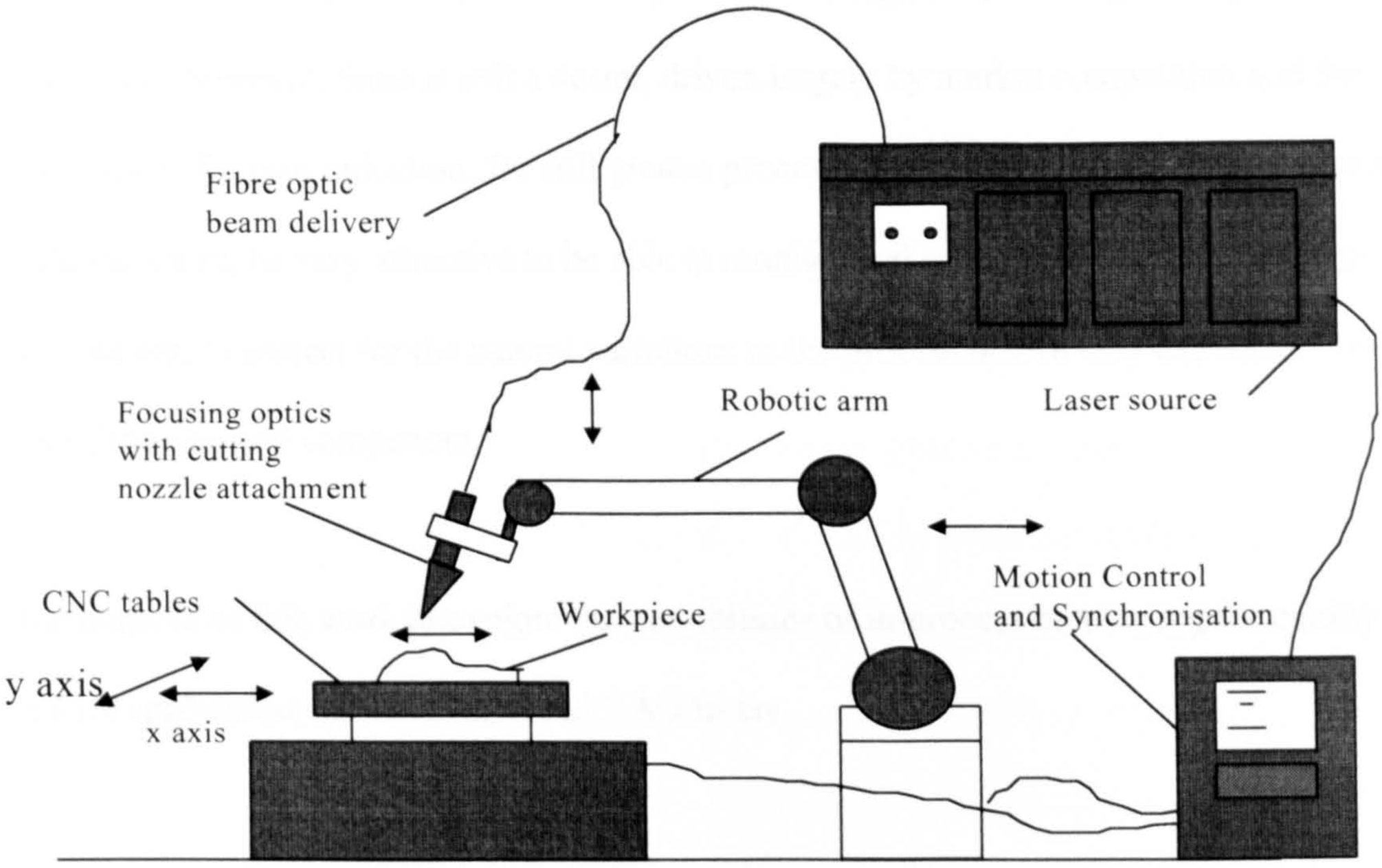

Figure 1. Typical Automated Nd:YAG laser system showing laser source,beam delivery focusing optics, workhandling and control and process ancillaries.

Figure 1.2 shows a schematic of a typical automated Nd:YAG laser system featuring fibre optic beam delivery [12].

As a result of the increased power, fibre optic beam delivery and the laser's inherent suitability to automation there is now considerable interest in applying Nd:YAG lasers to on-line production, particularly in the automotive manufacturing industry.

Processing performance is not the whole story however; probably the biggest overriding consideration for an industrial user, when considering any machine tool, is the cost of ownership [13]. One way of calculating this is by cost per part or per metre of weld. Such a costing takes into account running costs (electricity and other consumables), depreciation of capital cost, laser availability and of course reject rate.

The reliability of these systems has also been proven to be high [14] and in general productivity is being realised; however, there is still a desire, driven largely by market competition and the relentless quest for cost reduction, for still greater process repeatability and assurances of quality. It would therefore, be very attractive to be able to monitor and control the integrity of the process in real time and to correct for the natural variations in the process before they can affect the quality of the finished component.

It is the purpose of this work to explore the possibilities of in-process monitoring for quality control for application with industrial Nd:YAG lasers.

1.3 Project Objectives and Strategy

The principal objective of this work was to explore the possibility of using monitoring methods to observe optical process phenomena occurring during laser welding with a Nd:YAG. The work was carried out with specific attention to both understanding the nature of phenomena and understanding their significance to monitoring of process quality. In particular, determining optical activity capable of discriminating between the different faults, so as to offer the potential for fast diagnosis and adaptive control of the process.

The strategy employed for this work can be summarised into four main areas:

- To develop practical techniques for observing signals from the process.
- To observe the various signals emanating from the laser-material interaction process.
- To correlate signals with events occurring within the process and to the quality aspects of that process.
- To use these signals in an in-process monitoring system which can be used to provide an alarm or to correct for process errors.

2 Lasers Used for Material Processing

2.1 Laser Sources

There are three main types of laser source that have found greatest up take for industrial applications, the carbon dioxide laser, the excimer laser and the Neodymium: Yttrium Aluminium Garnet (Nd:YAG) laser. These are characterised by the media used to produce the laser beam.

The carbon dioxide laser produces laser light from a mixture of gases including nitrogen, helium and carbon dioxide. This type of laser can produce a range of wavelengths from 9000 to 11000nm but the wavelength normally used for industrial applications is 10,600nm. The CO_2 laser is currently available at mean powers up to 25kW for industrial applications.

The excimer laser can radiate at a number of wavelengths, depending on the gaseous mixture employed. Its emission is dependent on the excitation of rare-gas halides; these are shown in table 1 below:

Excimer Laser Type	Wavelength (nm)
ArF	193
KrCl	222
KrF	249
XeCl	308
XeF	350

Table 1. Showing the common excimer laser types by gas mixture and wavelength [15]

Neodymium:Yttrium Aluminium Garnet (Nd:YAG) lasers differ to the CO_2 and excimer types in that, instead of a mixture of gases, a solid crystal is used as the source material. The YAG crystal ($Y_3\ Al_5\ O_{12}$), is relatively strong and, exhibits relatively good thermal and optical properties. The cubic structure contributes to a narrow line width that gives high gain and low laser threshold. This combined with the four level energy transitions makes it suited to high peak power and high mean power operation.

Typically 0.5-1.2% yttrium ions (Y^{3+}), depending on the desired mode of operation, is substituted with neodimium ions (Nd^{3+}) in the lattice. Larger amounts can produce additional gain but produce significant distortion in the crystal lattice. YAG is readily available in rod and slab form, cut from a boule that is grown using the Czochralski [16] method at typical growth rates of 0.5mm/hr. Thus, to grow typical rod lengths of 150-200mm several weeks are required. Typical output power range for commercially available industrial lasers with a single Nd:YAG rod is 500-700 watts [17]. It is now commonplace, particularly with higher mean power continuous wave sources to optically couple several rods in series (typically between 2 and 8) in a single oscillator or arranged in an oscillator/amplifier configuration to give outputs in the range 1 to 5kW.

Common in solid-state lasers is a phenomenon known as thermal lensing and thermal birefringence that arises because of uneven heating of the rod. A large proportion (90-95%) of the flash lamp output is of no use for excitation of the laser action and goes instead to heat the laser rod. Management of the total amount of heat in the rod is therefore critically important and cooling of the rod (and flash-lamps) is usually achieved by flowing cooled water over its outer surface. The process of cooling, however, creates temperature gradients in the rod that lead to temperature and stress dependent variations in refractive index across the rod cross-section and length. The effect of this is to create additional beam divergence that has an adverse affect on the degree to which the laser beam can be focused.

2.2 Beam Characteristics

2.2.1 Transverse Electromagnetic Modes (TEM_{mn})

The spatial distribution of a laser beam may have significant effects on its material processing performance. Due to the nature of laser resonators the distribution of amplitudes and phases reproduce themselves on repeated reflections within the resonator. Certain modes are favoured and low order modes can produce distinctive spatial patterns that can be described using a notation indicating the mutually perpendicular null points within the distribution. This is known as the Transverse Electromagnetic Mode (TEM_{mn}) notation and can be described in either Cartesian (TEM_{mn}) or cylindrical (TEM_{pl}) co-ordinates. The lowest order mode is known as TEM_{00} and describes a Gaussian distribution. The Gaussian spatial intensity distribution is described by the following:

$$I(r) = I(o)\exp\left(-2r^2/w^2\right) \qquad (2.1)$$

Where I(r) and I(o) are the intensities (W/cm^2) at a radius distance r, from the centre and at the centre of the beam respectively. 'w' is the radius of the beam corresponding to the intensity $1/e^2$ or 13.5% of the peak intensity.

The total power in the Gaussian or TEM_{00} beam is related to the peak intensity by the equation:

$$P = \frac{\pi w^2}{2} I(o) \qquad (2.2)$$

where P = total power (watts) within a Gaussian beam.

High power (>100W) lamp pumped Nd:YAG lasers typically exhibit high order modes and cannot be conveniently described using the TEM notation, instead the term used to describe their beam distribution is "multi-mode".

2.3 Beam Quality

An important consideration in laser material processing is the degree to which the laser beam can be focused onto the work-piece. Power density or intensity (laser beam power divided by the focused spot area) is important since it is the magnitude of the intensity that governs the type of events occurring at the work-piece such as heating, melting and vaporisation. For a given wavelength the focusability of a laser beam is governed by a parameter termed as the 'beam quality'. A laser with good beam quality can be focused more readily to a fine spot compared to one with poorer beam quality.

When a laser beam propagates from the laser cavity it usually converges to form a waist of finite length (Rayleigh length or range) and then begins to diverge at a constant rate. This is shown in figure 2.1. The divergence of a laser beam is generally small, usually measured in milli-radians, and can be specified as either full or half angle.

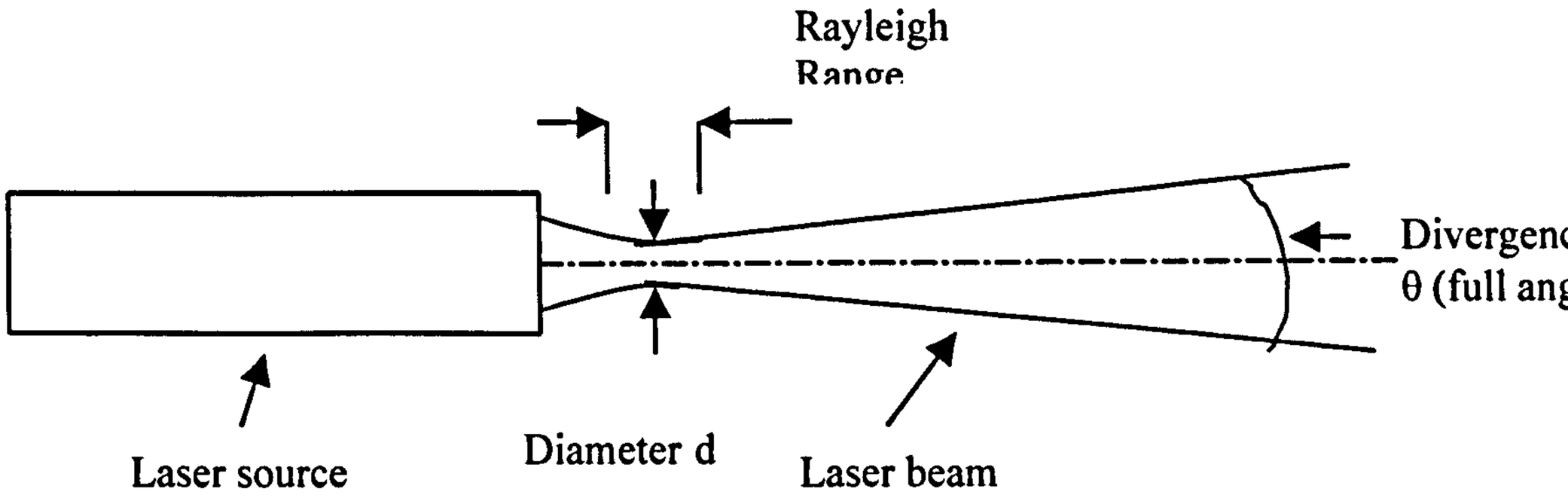

Figure 2.1 Schematic of beam propagation from a laser source

For a Gaussian beam profile, the radius of the beam at any point of a focusing beam whether it is after the resonator or after transmission through a perfect lens is given [18], with reference to figure 2.2 by the following:

$$W(z) = W_0\left[1+\left(\frac{Z}{Z_R}\right)^2\right]^{1/2} \qquad (2.3)$$

where z is the distance in the direction of propagation and Z_R is known as the Rayleigh range, which is the term, used to describe the distance over which the beam radius increases from w_0 to $\sqrt{2}w_0$ and is given by the equation:

$$Z_R = \frac{\pi w_0^2}{\lambda} \qquad (2.4)$$

Where λ is the laser beam wavelength.

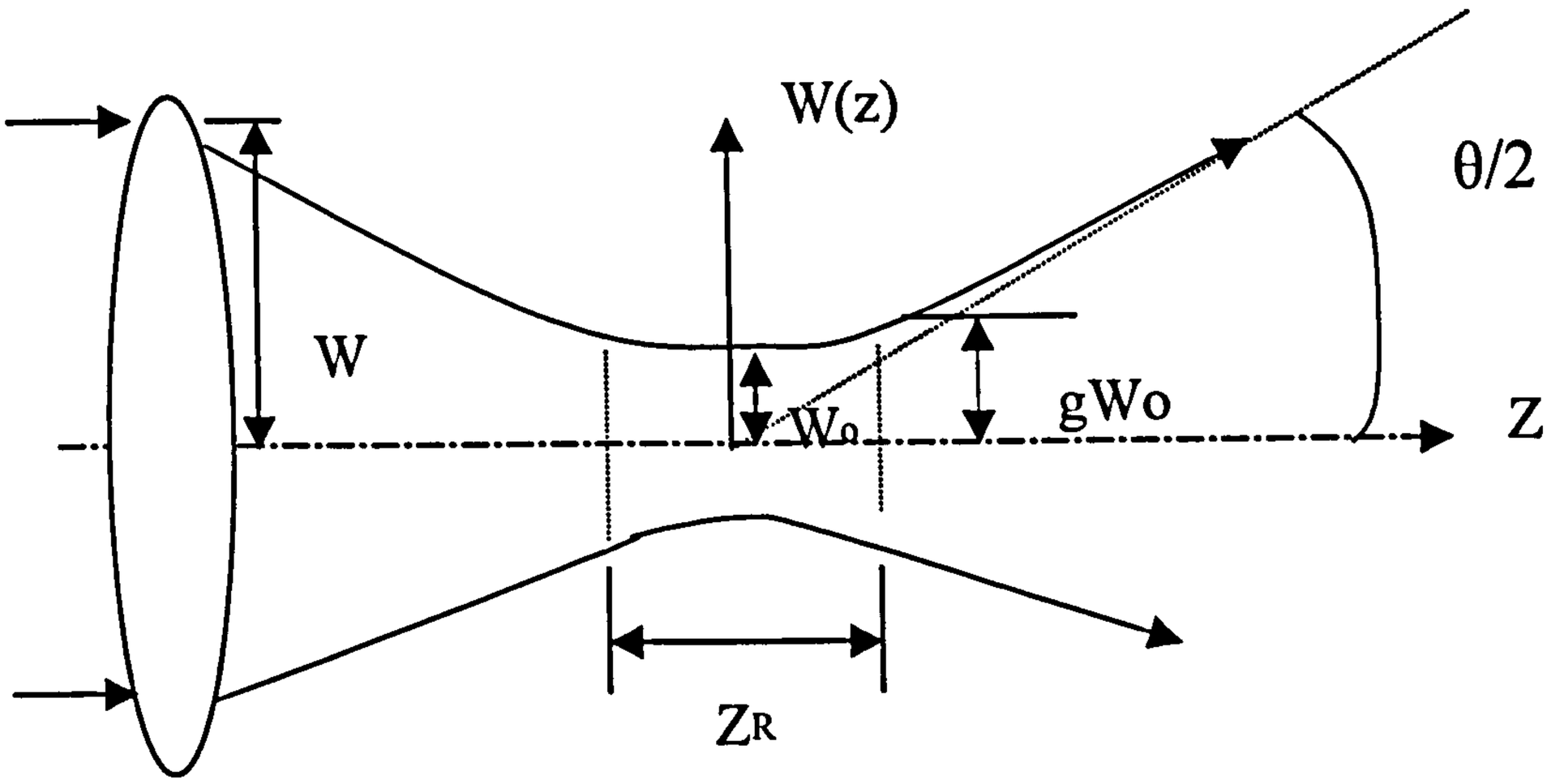

Figure 2.2 Laser beam focusing through a lens.

An asymptote taken from the centre of the beam waist w_0 at an angle of $\theta/2$ defines the half angle far field divergence of the propagating beam. The full divergence angle for the fundamental mode as z tends to infinity is given by:

$$\theta_{diff.} = \lim_{z\to\infty} \frac{2w(z)}{z} = \frac{2\lambda}{\pi w_0} = 1.27\frac{\lambda}{(2w_0)} \qquad (2.5)$$

Where $2w_0$ is the waist diameter 'd', hence,

$$\theta_{diff.} = \frac{1.27.\lambda}{d} \qquad (2.6)$$

Equation 2.6 shows that for given waist diameter the beam size increases linearly with distance and hence the divergence is constant. From this we can also see that the smaller the beam waist

the higher the divergence and vice versa. In fact, an important parameter of the laser beam is that at any point in its propagation the product of waist diameter and divergence is constant and this is often used to describe the beam quality of the laser beam. From equation 2.6 we can see for a diffraction-limited beam from an Nd:YAG laser the divergence-diameter product will be 1.35mm.mrads. and for a carbon dioxide laser beam 13.4mm.mrads.

We can apply this property when considering focusing the beam through a lens for the purpose of materials processing. If the Gaussian beam is propagated through a lens such that the beam is focused to a waist at the focal plane of the lens, the radius of the waist will be:

$$w_0 = \frac{\lambda . f}{\pi . w} \qquad (2.7)$$

and

$$d = \frac{4 . \lambda . f}{\pi D} \qquad (2.8)$$

where 'f' is the focal length of the lens and 'D' is the beam diameter at the lens.

The term f/D is a term known as the f-number.

For both Gaussian and non-Gaussian beams the radii of the focused spot can be approximated using the equation:

$$d \approx f . \theta_{act.} \qquad (2.9)$$

Where $\theta_{act.}$ is the actual full angle divergence (mrads) of a given laser beam. This equation is a very useful tool for calculating relative spot size when selecting different lenses. Beam divergence can be modified by selective beam expansion techniques. Care should be taken when using equation 2.9, to ensure that the actual divergence is calculated taking into account magnification of beam expansion i.e. beam quality divided by beam expansion.

It can be determined that the fundamental mode (TEM_{00}) gives the smallest focused spot size and that as the order of the mode increases so does the divergence and the smallest achievable spot size increases. It can be seen therefore that the beam quality has a significant bearing on the focusability of a given laser beam.

2.3.1 Other Measures of Beam Quality

For some applications is has become commonplace to express the actual divergence of a laser beam in terms of the diffraction limited beam at that wavelength.

Two conventions have emerged; 'M squared' (M^2) and k factor. They are related by the following:

$$d_{act.}.\theta_{act.} = M^2.d_{diff}.\theta_{diff.} = (1/k).d_{diff}..\theta_{diff.} \qquad (2.10)$$

Thus for a TEM_{00} or diffraction limited beam $M^2 = 1$ and $k = 1$. Hence, substituting into the above equations the calculated spot size for a real laser beam, becomes:

$$d_{act.} = \frac{1.27.M^2.\lambda.f}{D} \qquad (2.11.)$$

and

$$d_{act.} = \frac{1.27.\lambda.f}{k.D} \qquad (2.12)$$

2.3.2 Depth of Field

Another important parameter for processing is one commonly called the depth of focus or tolerance to focus that relates to the length over which the size of the beam waist remains within certain limits.

For material processing it is often important to maintain the beam intensity at the work-piece within certain limits to ensure quality is maintained. Let us consider a distance either side of w_0 where the waist radius becomes some proportion larger, say g times w_0 either side of the focused waist. By substitution of $g.w_0$ and equation 2.4 into equation 2.3 it can be shown that the length over which this change occurs 'b' can be calculated thus;

$$b = \frac{2\pi.w_0^2}{\lambda}\left(g^2 - 1\right)^{1/2} \qquad (2.13)$$

Of interest to note is the quadratic nature of the relationship between the spot size and the depth of focus 'b'; that is, if the spot size is halved, the depth of focus will reduce by four.

Combining equations 2.7 and 2.13 gives:

$$b = \frac{8\lambda}{\pi}.\left(\frac{f}{D}\right)^2\left(g^2 - 1\right)^{1/2} \qquad (2.14)$$

This equation shows that to achieve tolerance to variation in lens to work-piece distance it is more favourable to use a longer focal length lens. For practical laser systems the beam quality is always finite, and for some never good enough. Since, in broad terms higher process performance (speed and depth) is achieved with smaller spot size and tolerance to misalignment comes from trading-off spot size for depth of field, the challenge for the laser processing engineer is to achieve a balance between the two.

2.4 Beam Delivery Methods for Nd:YAG Lasers

For any laser processing system it is essential to be able to deliver the laser beam from the laser source to the work-piece that might be some tens of metres away. Two principal methods exist for beam delivery [19, 20]; direct or conventional beam delivery, and fibre optic beam delivery. The principle of direct beam delivery is quite well known, employing a combination of mirrors and lenses to steer the beam, often through gaitering to the work-piece in what is essentially a series of straight lines. This is illustrated below in figure 2.3. Gaitering in the form of tubing is often used to keep out dust and dirt and to ensure safety of personnel.

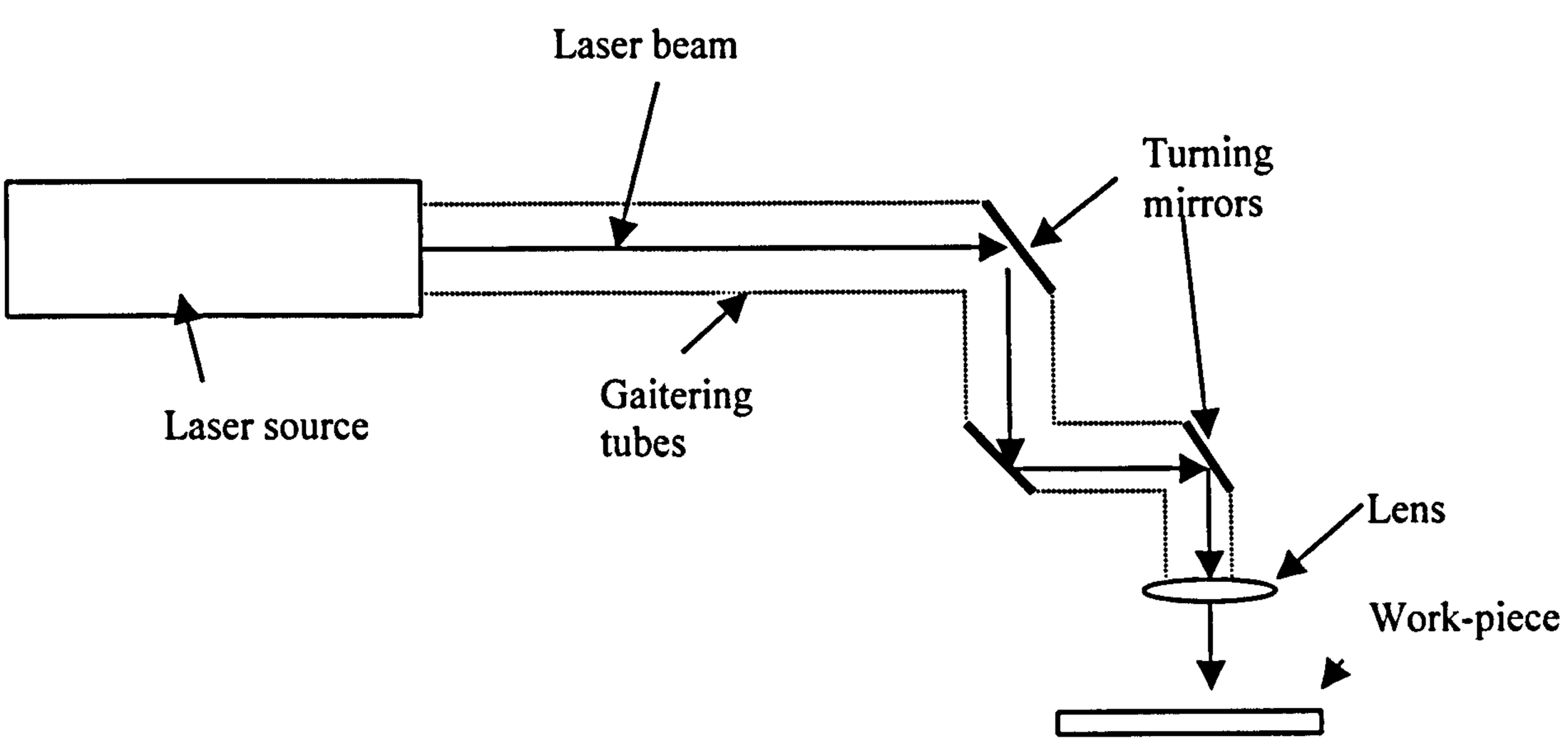

Figure 2.3 Schematic of direct or conventional beam delivery

2.4.1 Fibre Optic Beam Delivery

Where as conventional beam delivery steers light from the laser in straight lines by use of a series of discrete reflecting surfaces, fibre optic beam delivery provides the benefits of a continuous reflecting surface.

The phenomenon of light being guided by multiple reflections within a channel was first demonstrated in 1870 by John Tyndall [21] to the Royal Society when he showed light travelling within a jet of water. Possibly the first practical applications of this were in the late 1920's when acrylic rods were used to light aircraft instrument panels and clad fibres where first introduced in the early 1950's for optical communications [22].

The benefits of using a flexible optical fibre have lead to widespread adoption of this technique for Nd:YAG laser beam delivery [23, 24, 25] and, has stimulated work on the development of light guides in the form of tubes, for the CO_2 laser [26, 27]

Total internal reflection is the limiting case of refraction. Snell's law [28] relates angles of incidence and refraction to each other:

$$n_1 Sin\theta_1 = n_2 Sin\theta_2 \qquad (2.15)$$

Where n_1 and n_2 = Refractive index of the dielectric material

θ_1 and θ_2 = Angle of incidence relative to the normal

This can be re-written as

$$Sin\theta_2 = \left(n_1 / n_2\right) Sin\theta_1 \qquad (2.16)$$

Assuming $n_1 > n_2$ the refracted angle will always be greater than the angle of incidence. Thus, it can be seen that there is a point where θ_2 becomes 90° at an angle of incidence that is less than 90°. Hence total internal reflection occurs at the interface between two dielectrics of differing refractive index when:

- The light is incident on the dielectric of higher index.
- The angle of incidence exceeds a critical value.

Taking the limiting case for internal reflection to occur

$$Sin\theta \geq n_2 / n_1 \qquad (2.17)$$

The value of input angle for a given reflection can be written as follows:

$$Sin\theta_1 \leq {}^{1}\!/_{n_o}\left(n_1^2 - n_2^2\right)^{1/2} \qquad (2.18)$$

Thus the largest angle at which light can be accepted by the fibre and transmitted by a meridional ray can be found when two sides of the above equation are equal.

If, RHS = 1

θ_1 can be up to 90° where the limiting value of refraction is encountered

If, RHS > 1

θ_1 is greater than 90° and the limiting value of refraction is encountered

Hence, the term $${}^{1}\!/_{n_o}\left(n_1^2 - n_2^2\right)^{1/2} \qquad (2.19)$$

is an important quantity in fibre optics and is termed the numerical aperture (NA) of the fibre.

The NA is usually defined in air, hence,

$$\text{NA}=\left(n_1^2 - n_2^2\right)^{1/2} \qquad (2.20)$$

This expression is independent of the fibre diameter and holds to fibres of diameter 5μm, whereupon the geometrical approach becomes no longer valid.

2.4.1.1 Meridional and Skew Rays

Two types of light rays propagate through an optical fibre, meridonal and skew rays. Meridional rays pass through the central axis of the fibre. Skew rays pass through the fibre but never through the central axis of the fibre. Their path forms a helix through the fibre.

2.4.1.2 Losses in Optical Fibres

The fraction of the input energy emerging from the output face is called the transmission of the optical fibre. The value of transmission for an optical fibre is determined by the following losses:

2.4.1.2.1 Fresnel Losses.

Accounting for approximately 8-10% due to differences between the refractive index at the interfaces between input and output. Reflectance can be calculated from the equation,

$$R = \left(\frac{n_t - n_i}{n_t + n_i} \right)^2 \qquad (2.21)$$

where n_t and n_i are the refractive indices of the transmitting and incident materials. For example n for air and fused silica (common material for fibre optics) is 1.000 and 1.458 giving a reflective loss calculated from equation 2.21 of 4%.

2.4.1.2.2 Absorption Losses

Caused by absorption of light by the fibre material. This type of loss is wavelength dependent and thus can be reduced by appropriate use of material for the application. Absorption losses

generally limit the use of the commonly used fibres to wavelengths between 0.4μm and 2.0μm.

Typical loss in fibres used for beam delivery of Nd:YAG laser radiation <4db/km.

2.4.1.2.3 Reflection Losses

Are caused by inhomogeneities between fibre and fibre cladding interface. Generally negligible compared with other losses.

2.4.1.2.4 Scattering Losses

Due to inhomogeneities within the core material light rays are scattered and reach an angle of incidence that allows them to escape from the core.

In the author's experience, Fresnel losses dominate the losses within optical fibres used for laser beam delivery. The figure of 4 % per optical face is for practical consideration an accurate value to use since the minimum value is determined by the physical properties of the materials present. If the loss is found to be significantly more than this value it is probably associated with misalignment of the laser beam to the fibre or damage to the fibre ends. Either way the result can lead to rapid fibre failure.

3 Laser Interaction with Material

3.1 Reflectivity and Absorption

The rate at which a material is initially heated by an incident laser beam is dependent on the absorptivity of the material to the laser beam. The absorptivity A, is defined as the ratio of energy absorbed by a material to the incident energy. Alternatively it may be more convenient to think in terms of reflectivity which is defined as R = 1 –A. At room temperature most metals

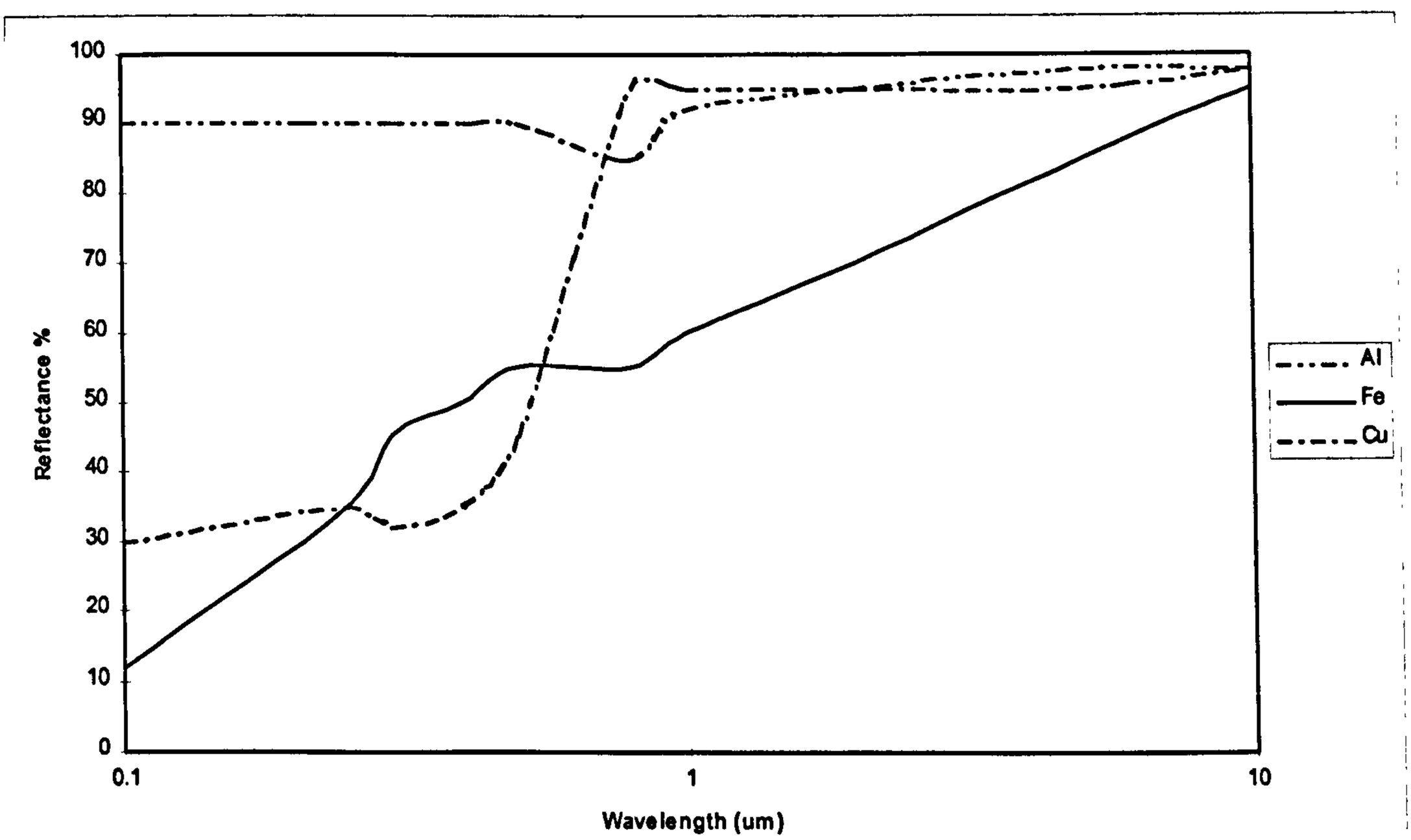

Figure 3.1 Reflectivity of some materials to electromagnetic radiation of varying wavelength at normal incidence and room temperature (20° C) [29].

exhibit very high reflectivity which is dependent on wavelength. It is worth noting that at room temperature an apparently small difference in reflectivity 0.98 to 0.99, produces a change in absorptivity by a factor of two i.e. from 0.02 to 0.01. For the majority of metals there is a trend

towards reduced reflectivity (and therefore greater absorption) with decreasing wavelength. Figure 3.1 shows a plot of reflectance for various materials against laser wavelength showing this trend.

One could be forgiven for thinking after a first glance at the reflectivity characteristics of metals that there would be no point in employing lasers for welding and cutting metal. Practise however has demonstrated that they are practical tools for metal processing and the high reflectivity is not as problematical as it first seems. This is mainly because of other mechanisms that work to increase the coupling of the beam energy into the metal surface. An attempt has been made to try and describe these processes.

3.1.1 Initial Absorption

Figure 3.2 shows the effect of a Nd:YAG laser pulse on the reflectivity of a polished copper target [29]. It can be seen that as the pulse increases to full intensity the reflectivity decreases dramatically after several tens of nanoseconds. Several attempts have been made to try and describe the mechanisms producing this effect. The Drude model [30, 31] describes

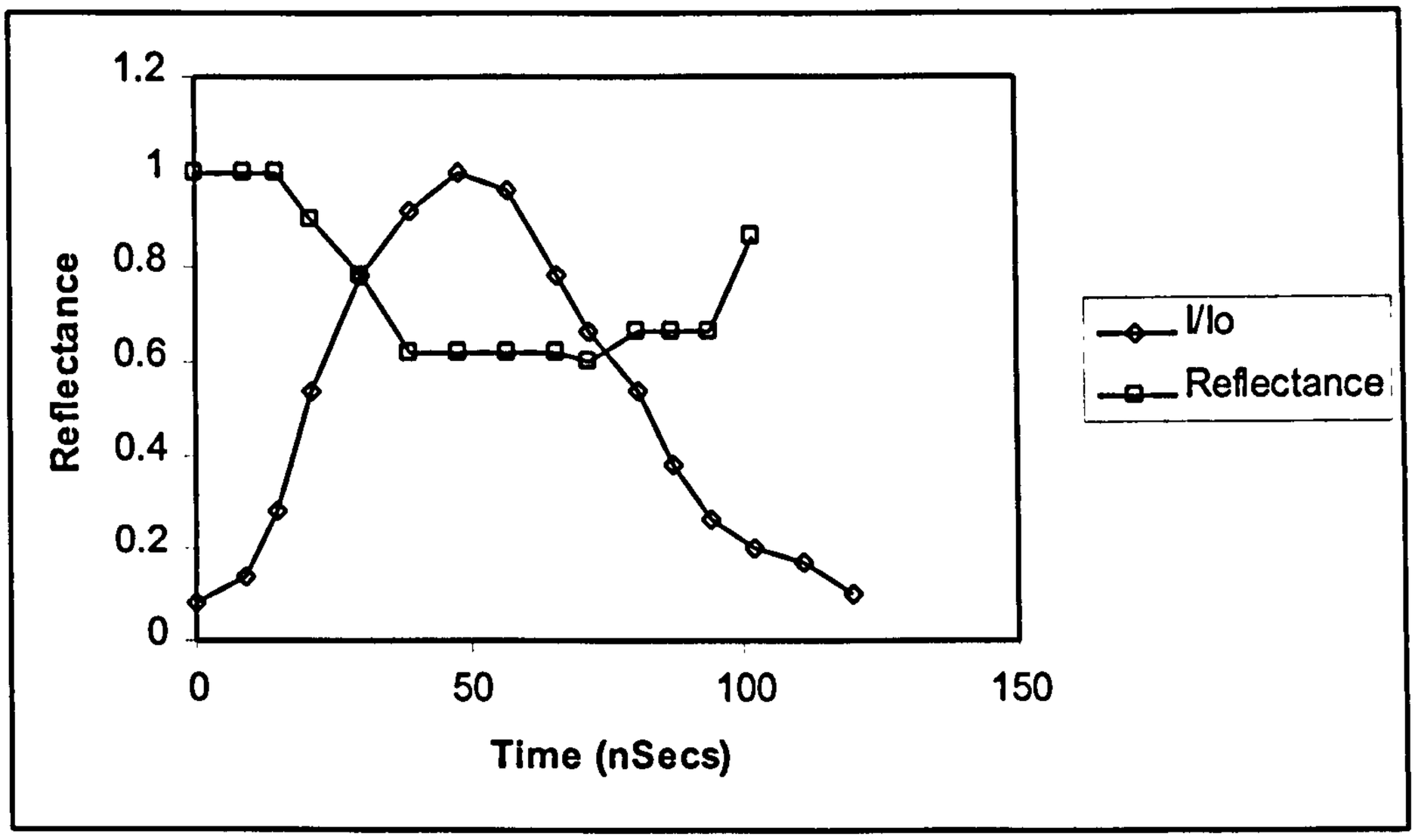

Figure 3.2 Decrease in reflectance of a copper target with laser beam interaction time for a Nd:YAG laser [29].

the heating of a metal surface by free-free electron transitions. The Drude free electron model assumes that energy from the laser beam is not absorbed directly, that is by Fresnel absorption, but through the intermediary of the electrons that transmit through collisions, their energy to the metal's crystalline lattice.

Absorptivity of an ideal metal (A_i) can be thought of as being made up of several absorptivities, such that:

$$A_i = A_D + A_A + A_{IB} \qquad (3.1)$$

Where A_D is the absorption due to free electron collision (Drude)

A_A is the absorptivity due to anomalous skin effect

A_{IB} is the absorptivity due to interband transitions (important in non-metals)

3.1.1.1 Real Materials

A number of factors such as surface roughness, surface contamination and defects, and oxidation can increase the absorption of the laser beam so that reflectivity and coupling are made easier. There is usually a large dispersion in data on absorption that is attributed to the departure of the test sample from the ideal.

Surface roughness generally influences absorption in localised areas where the beam incidence is not normal to the work-piece or in the case of grooves or cracks where wave-guide propagation is favoured. Dust and other surface impurities can increase local absorption and also promote oxidation which in itself will increase absorption in some cases by an order of magnitude [29]. Thus it is better to consider absorption for real engineering materials as being made up of its intrinsic absorption A_{int} plus an additional absorption due to its extrinsic properties A_{ext} .

Therefore from equation. 3.1 the real absorption A_r, becomes:

$$A_r = A_{int} + A_{ext} \qquad (3.2)$$

In general the absorptivity of real engineering metals is expected to be higher than the ideal metal.

3.1.2 Temperature Dependence of Absorption

In the solid phase it can be shown both through theoretical calculation that absorptivity linearly increases with temperature. The precise nature of this effect has not been determined

experimentally, mainly because of the difficulty in obtaining pure metals with perfect structure. However, the behaviour can be generally described by the simple function below:

$$A(T) = A_o + A_1 T \qquad (3.3)$$

Where A_o is the initial absorption.

Most pure metals exhibit higher absorption in their liquid phase. As the metal changes from a solid to liquid state it can be shown [32] that the absorptivity generally increases by a step change as it reaches the melting temperature.

3.1.3 Anomalous Absorption

For some time it has been observed [33] that at the point of melting the absorptivity of a metal is much higher than can be explained by temperature dependence alone. At relatively low beam intensity, below a critical value, I_c (I_c for steel approx.10^4 W/cm^2) and below the material melting point, absorption of laser beam energy into the surface of a work-piece is dependent on surface condition and independent of intensity. However above this intensity more complex heat transfer mechanisms begin to occur. At higher intensities>10^6 W/cm^2 significant vaporisation of the work-piece surface begins and has been shown to be coincident with the formation of a plasma [30, 31] at the surface of the material. Figure 3.3 shows the effect of intensity on the reflectivity of steel. This effect has been shown to be independent of wavelength [33].

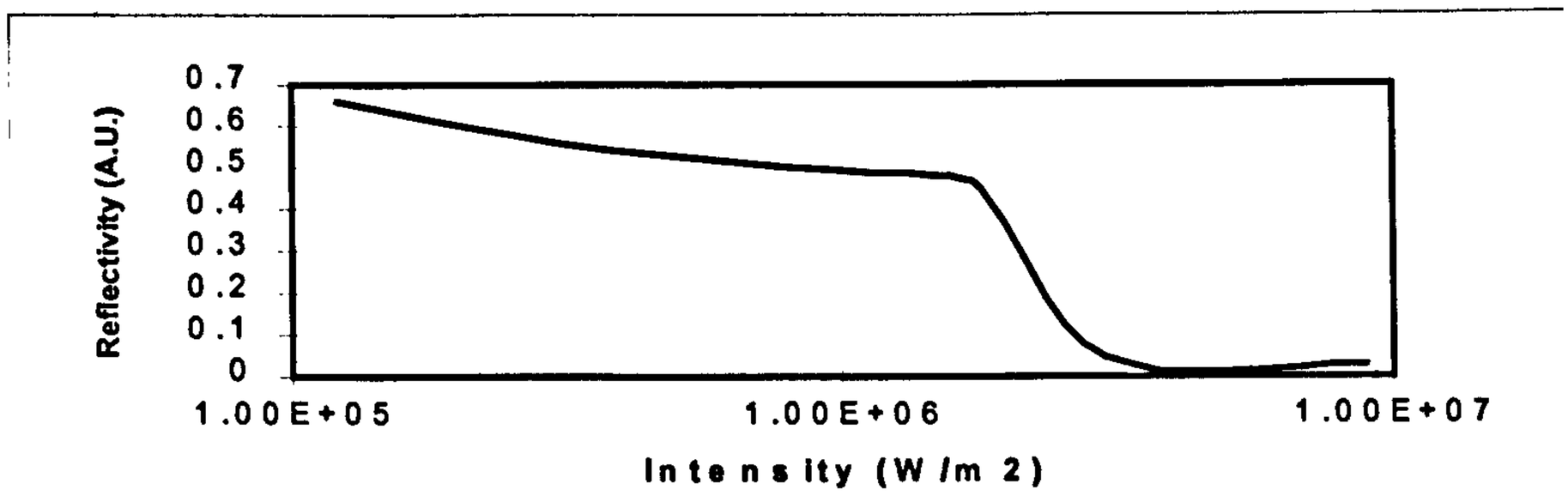

Figure 3.3 Dependence of reflectivity on laser beam intensity for steel.

Plasma formation occurs when free electrons present in the surface of the work-piece are accelerated by the laser radiation until the kinetic energy is sufficient to ionise the atmosphere of gas and metal vapour around the interaction zone. A further increase in the number of electrons available occurs by avalanche ionisation.

A useful definition [34] of plasma :

A plasma is a quasineutral gas of charged and neutral particles which exhibits collective behaviour.

The Saha equation predicts the amount of ionisation present in a gas in thermal equilibrium;

$$\frac{N_{ion}}{N_{neu}} \approx 2.4x10^{15} \frac{T^{3/2}}{N_{ion}} e^{-U_i/KT} \qquad (3.4)$$

Where, N_{ion} and N_{neu} are the density of ionised and neutral atoms respectively (number per cm^3)

T is the gas temperature of the gas

K is Boltzmann constant

U_i is the ionisation energy

It can be seen that the equation includes the term:

$$e^{-u/KT} \tag{3.5}$$

from the Boltzmann distribution law.

The significance of the Saha equation is that atoms within gases have a range of thermal energy. An atom will become ionised if it collides with another particle of sufficient energy so as to remove an electron. If the gas is thermally cold then the availability of particles of high enough ionising energy is low and the frequency also correspondingly low. The exponential factor expresses the fact that the number of energetic atoms falls exponentially with U_i/kT. An ionised atom remains charged until it recombines with an electron. The rate of recombination depends on the density of electrons which can be taken as n_i ; the equilibrium ion density should decrease with n_i, hence its appearance on the right hand side of equation 3.4.

Once a plasma has begun to form at the work-piece surface the primary absorption mechanism of the laser energy is by electronic excitation by absorption of a photon [35,36,37]. For metals this process involves free electron transitions. A conduction electron increases its kinetic energy, by energy $h\nu$ (where h is Planck's constant and ν is the frequency of the photon). This process is the opposite to the Bremsstrahlung process where radiation is emitted when a free electron loses energy when it is slowed in the Coulomb field of an ion, and is therefore known as 'Inverse Bremsstrahlung' or Bremsstrahlung absorption [38,39,40]. Absorption by the Inverse

Bremsstrahlung process causes the temperature of the conduction electron gas to rise by electron-phonon interaction; the energy is transferred in part to the motion of the atoms or ions making up the metallic lattice. Transfer of this energy takes place in times of the order of 10^{-10} - 10^{-13} secs for most materials [41,42].

The hot electron plasma will expand taking atoms with it to maintain overall neutrality; the plasma will continue to expand unrestrained by the bonding forces within the lattice structure as a rarefaction wave.

3.2 Interaction of Plasma/Plume with the Laser Beam

The phenomenon of reduced penetration depth that has been attributed to the interaction of the laser beam with the plasma/plume has been well documented [43,44,45]. There are believed to be two mechanisms occurring: absorption through inverse Bremsstrahlung and by losses caused by scattering. Absorption through inverse Bremsstrahlung (A_{ib}) can be calculated using the equation derived from plasma physics as:

$$A_{ib} = \frac{z^2 e^6 n_e^2 \ln\Lambda}{3\omega^2 c\varepsilon_o^3 (2\pi m_e k_B T)^{\frac{3}{2}} \sqrt{1-\left(\frac{\omega_p}{\omega}\right)^2}} \qquad (3.6)$$

Where, n_e is the electron density number

N_{ion} is the ion number density

z is the charge number

e is electron charge

c is the velocity of light

ε_o is dielectric constant

m_e is the mass of an electron

K is boltzmann constant

T is temperature

ω angular frequency of the incident wave

ω_p is the angular frequency of plasma oscillation

ln Λ is the Coulomb logarithm

This equation tells us that the absorptivity of the plasma is proportional to the product of $n_e.n_i$ and inversely proportional to ω and $T^{3/2}$. Hence absorption is expected to become less as the wavelength becomes shorter and the plasma temperature increases.

Scattering is another mechanism by which energy is prevented from reaching the work-piece. Scattering is caused by the ultra-fine particles within the plume produced by the evaporation of the work-piece. Matsunawa [46] determined that particle size was dependent on ambient pressure conditions, getting larger with increasing pressure. Even at high pressure (200kPa) particle size is several orders of magnitude smaller than the laser wavelength. Rayleigh scattering by a small particle is given by the equation:

$$\frac{I_{sca}}{I_{inc}} = \frac{2\pi^2 V_p^{\,2}}{r^2 \lambda^4}\left(\frac{\varepsilon - \varepsilon_o}{\varepsilon_o}\right)\left(1+\cos^2\phi\right) \qquad (3.7)$$

Where, V_p is particle volume

R distance from particle

Φ is the angle of scattering

ε_o is the dielectric constant of the medium

ε is the dielectric constant of the particle

λ is the wavelength of the incident beam

The equivalent absorption coefficient of the Rayleigh scattering by many particles is given by:

$$K_{sca} = \frac{8\pi^3 N V_p^{\,2}}{3\lambda^4}\left(\frac{\varepsilon - \varepsilon_o}{\varepsilon}\right)^2 \qquad (3.8)$$

Where N is the number density of particles

It can be seen from equation 3.8 that the scattering loss is inversely proportional to the fourth power of the wavelength. Hence the shorter the wavelength, the more scattering occurs. Thus it is thought that the principal mechanism for absorption in the plume for the Nd:YAG laser is by scattering and for the CO_2 laser inverse Bremsstrahlung.

Essien [47] reported seeing as a result of observation of the plume using a Schlieren photography technique, high and low density regions that exhibited differing refractive index. It was postulated from this work and Beck et al [48] that such refractive index gradients caused by high temperature gradients in the plasma could cause defocusing of the beam relative to the work-piece and resulting changes of penetration depth and profile. The results also suggested a periodic element to this interaction where the beam initially, when sharply focused, melts the surface of the target and in doing so creates a plume, this in-turn defocuses the beam which reduces the efficiency of the interaction, reduces penetration and in-turn reduces the plume effects and the beam is refocused and so on.

Various techniques have been developed, principally for higher power CO_2 laser welding, to combat the effects of the plasma including high velocity plasma suppression jets [49,50] that are used to blow across the opening of the keyhole.

3.3 Keyhole Formation

At relatively low intensity ($<10^6$ W/cm^2) transfer of heat into the bulk of the work-piece material is limited by the rate at which heat is conducted by the material. The radius of the melt is determined by interaction time [48]. The melt isotherm being determined when a steady state condition is reached whereby the energy being provided by the laser beam is balanced by the conduction into the metal, losses to atmosphere and reflective loss. At higher intensity significant vaporisation of the work-piece begins to occur and the surface of the melt becomes depressed under the recoil pressure of vaporisation and a keyhole begins to form. The keyhole is stabilised by the combination of recoil and vapour pressure attempting to keep the keyhole open and surface tension and hydrostatic pressure attempting close it. When fully penetrating, the keyhole is expected to be more stable as the surface tension acts to keep the keyhole open.

Semak et al [51] proposed a more complete explanation of keyhole formation. Figure 3.4 shows schematic diagrams of the sequence of keyhole formation to assist in this explanation.

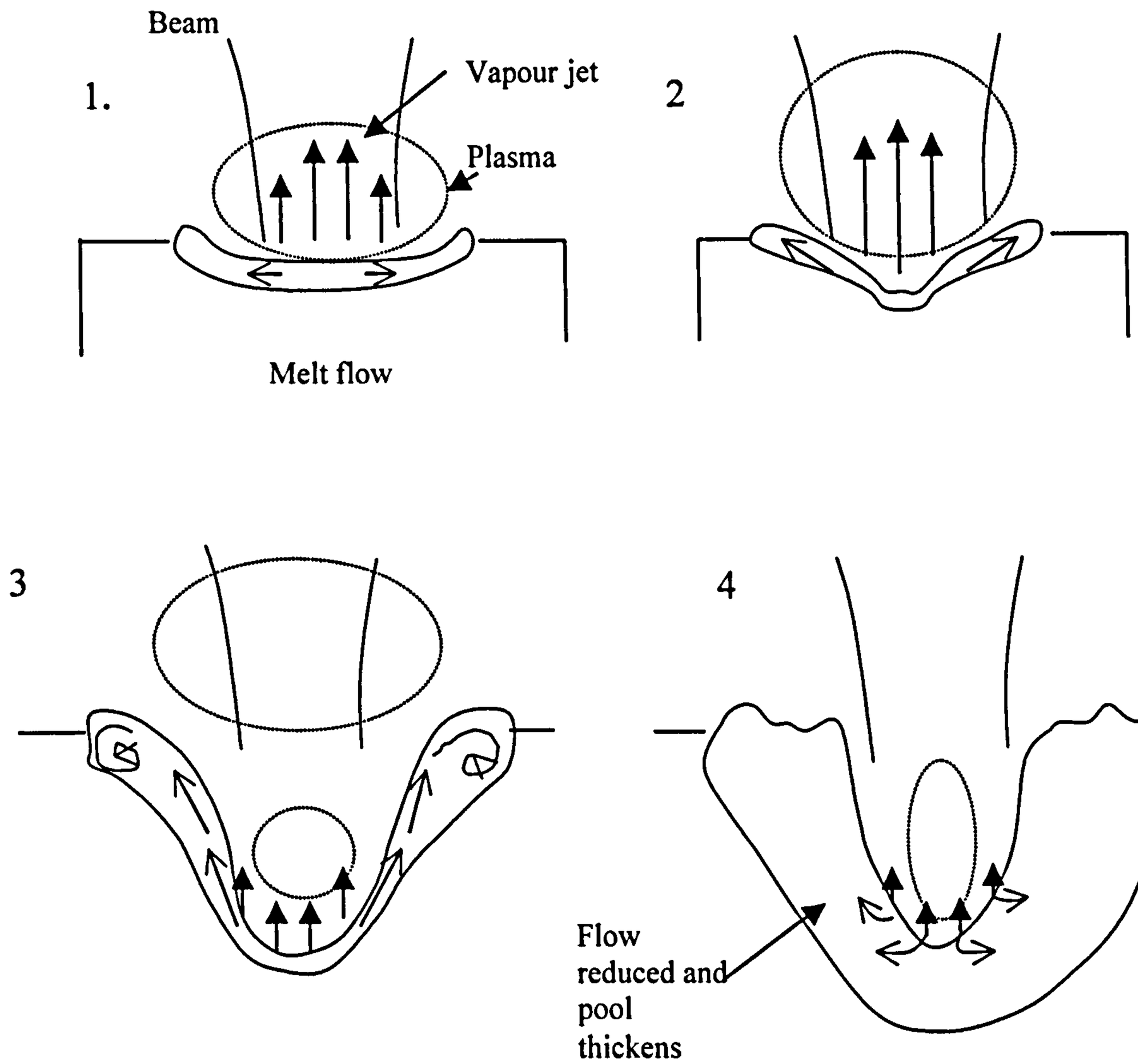

Figure 3.4 showing stages of keyhole formation (after Semak [51])

1. After initial melting, a vapour jet is produced which generates recoil pressure on the surface of the melt. The temperature within the envelope of the laser beam exceeds that outside of it and therefore there is a recoil pressure gradient between the centre and sides of the melt that promotes motion of the melt out from the centre to the sides. In addition it is known that for pure metals the surface tension of the melt tends to reduce with temperature [52] so additional flow is created by the surface tension gradient.

2. Motion of molten liquid away from the centre of the beam reduces the melt thickness and the vapour/liquid interface moves downwards with velocity V, allowing the keyhole to begin to form.
3. Molten material moving up the sides of the keyhole is not expelled but is contained by surface tension and instead circulates near the entrance of the keyhole. With relatively high electron densities plasma is formed within the keyhole which, serves to partially absorb the beam reducing the amount of laser radiation directly reaching the keyhole sides. Higher absorption in the plasma can also raise its temperature and increase the amount of radiative and conductive heat transfer to the walls.
4. The keyhole will continue to extend until the plasma reaches a length where it prevents the beam reaching the keyhole walls. At this point the surface tension and hydrostatic pressures balance the recoil pressure within the keyhole. The keyhole stops growing and the melt depth increases heat conduction, thickening the melt and in doing so reduce the amount of flow within the melt. In the case of shorter wavelengths (such as 1064nm) the plasma is more transparent and absorption is known to be low. In this case, a limiting mechanism to keyhole depth could be when the vapour pressure at the entrance to the keyhole becomes substantially smaller than the surface tension pressure causing the melt to slump into the cavity closing the keyhole. Closure of the keyhole has been observed under simulated conditions of laser beams interacting with transparent fluids [53] where no plasma was detected; such a mechanism is therefore thought to be possible. An alternative explanation is that at the high temperatures within the keyhole, refractive index gradients are formed and cause the beam to be defocused, thereby reducing its intensity.

Fujinaga et al [54] in some interesting work using combined power from three Nd:YAG laser sources observed the formation of the keyhole using micro-focus X-ray and high speed video.

The results of these trials showed that the plasma/plume above the surface of the work-piece began to form within 0.2ms, the keyhole began to form after approximately 0.7ms and reached full depth (4mm) within 1.5ms of initial irradiation. Semak et al [55] carried out a similar study, looking at penetration depth dynamics using a metal/glass sandwich with a CO_2 source. This determined that ignition of plasma at the surface of the work-piece also occurred after 0.2ms, and average penetration velocity was estimated as 4m/s. A strong dependence was found between penetration velocity and the formation of plasma which reduced the penetration velocity rate.

3.3.1 Moving Source

In the case of a moving laser beam source, the centre of keyhole becomes displaced relative to the centreline of the beam [55,56]. The beam axis moves forwards relative to the movement of the beam and work-piece. Figure 3.5 shows this effect.

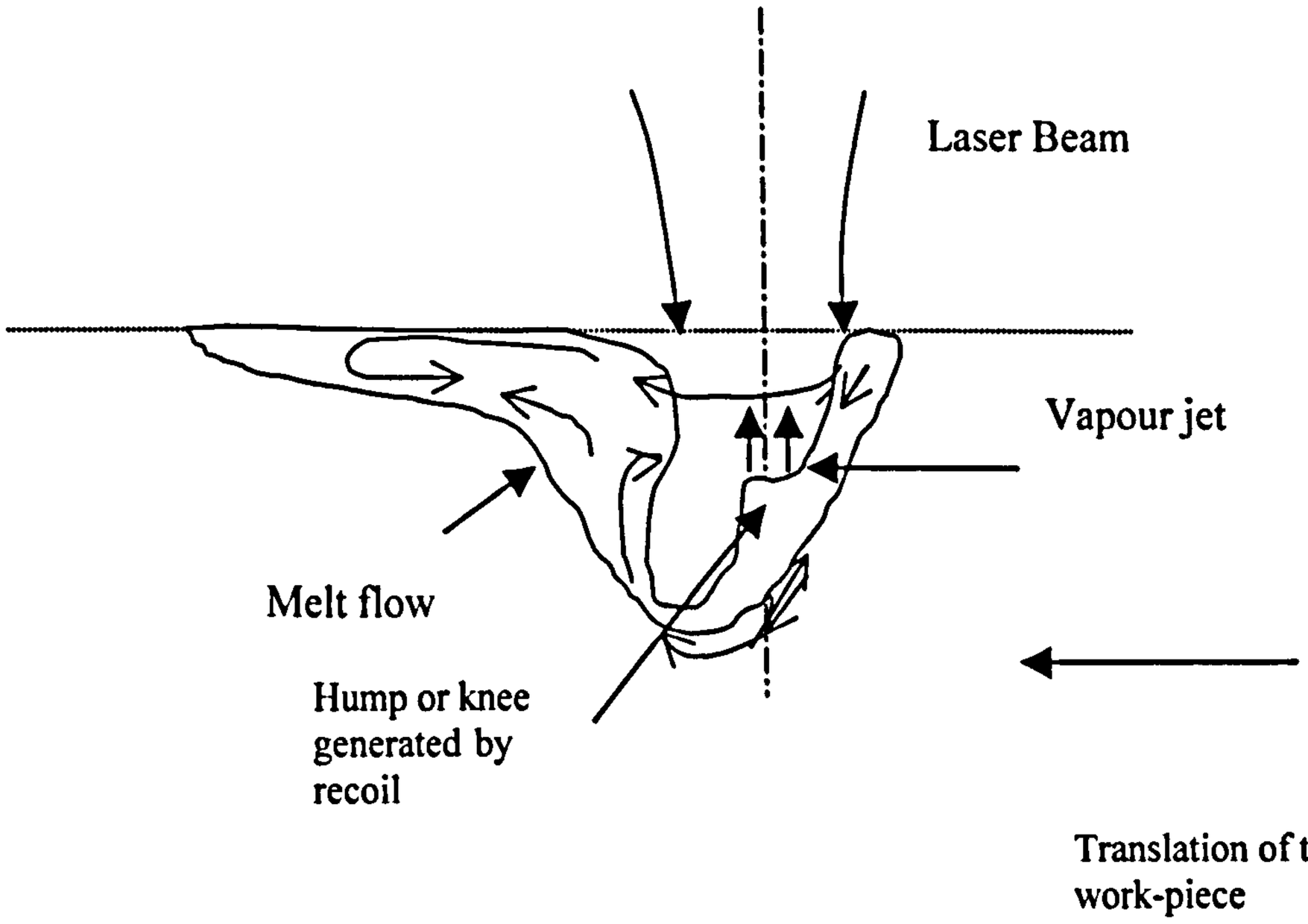

Figure 3.5 showing effect of beam translation on interaction point within keyhole

3.4 Weld-pool and Keyhole Dynamics

There is no doubt that the interaction of a laser beam with molten material will create vigorous activity within the keyhole.

Recoil force is thought to play the biggest part in promoting motion of the molten liquid within the keyhole. Its influence so vigorous that it is also thought to promote instability within the keyhole itself, which has been widely observed. Williams et al [57] reported seeing chaotic wave patterns in the weld-pool surrounding in the welding keyhole seemingly made up of circumferential and radial waves, with a wavelength of approximately 0.3mm, emanating from the keyhole itself. Semak et al [58], also using high-speed video techniques, observed oscillation of the weld-pool opening at a frequency in excess of 1kHz associated with the keyhole opening, collapsing periodically. Shannon [59] reported seeing humping of the weld bead during seam welding caused by the vigorous flow of molten material from behind the keyhole.

Duley [60] in trials using a low power CO_2 laser demonstrated keyhole-type behaviour in water. The benefit of this approach is that subsurface effects could be observed through the transparent fluid. Periodic closure of the keyhole, described as 'Spiking', due to flow and surface tension effects resulted in formation of bubbles. Closure was monitored acoustically and revealed frequencies in the range 2-3kHz.

Hugel et al [61, 62, 63] presented studies into the modelling and prediction of pressure and velocity gradients around the keyhole, finding that the pressure and flow was greatest along the centreline of the weld pool, with the prospect of reverse flow taking place at the edges of the weld-pool close to the keyhole. Hugel shows that welding speed has largest influence on the kinetic energy of the melt flowing around the keyhole. Further evidence of the vigorous

processes occurring within the keyhole is the loss of material through spatter which can sometimes occur particularly in spot welding. Matsunawa et al [56], again using high speed imagery, observed violent oscillation of the keyhole. Acoustic (AE) and light (LE) emissions were also measured and found to have distinctly separate frequency ranges at lower speeds (<100mm/s). At higher speed (300mm/s) both AE and LE had common peaks in the 3 – 4kHz range. The general trend was towards higher frequency oscillation with increasing speed. It was postulated that LE fluctuation spectra carries information about keyhole opening dynamics and AE spectra reflect keyhole front wall interaction. Matsunawa also observed high velocity flow estimated at 1m/s within the weld pool (approx three times the work-piece translation velocity), coexisting with the existence of reverse flow, in the sense of flow backwards relative to the translation direction, within the weld-pool.

Several workers have attempted to model the oscillatory nature of the keyhole within the weld-pool. Lord Rayleigh [65], with great foresight for the laser community, identified the nature of instabilities in cylindrical fluid surfaces as far back as 1892. Klein et al [66] identified three basic modes of oscillation for a fully penetrating cylindrical keyhole; radial, azimuthal and axial modes, these modes are shown in figure 3.6:

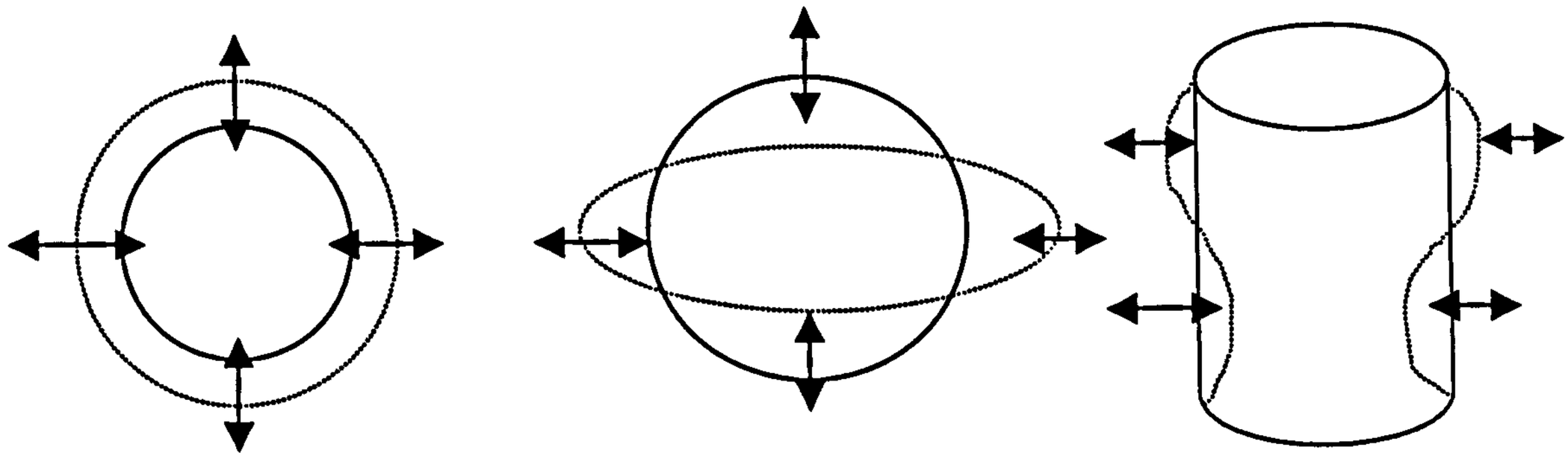

Radial Mode
(0,0)

Azimuthal
(n,0)

Axial
(0,1)

Figure 3.6 oscillation modes of keyhole (after Klein [66])

In the simplest case 'ground' mode the keyhole is thought to oscillate radially with the keyhole expanding and contracting in and out equally around its circumference. Klein assumed that the weld-pool was circular with a concentric keyhole and showed the calculation for the angular frequency for the ground mode to be the following:

$$\omega_{\infty}^{2} = \frac{B}{Q.a.\ln C} \qquad (3.9)$$

Where ω_{∞} is the angular frequency,

B is the restoring pressure,

Q is the average mass density of the liquid phase

a is the equilibrium keyhole radius

C is the ratio of weld-pool radius and keyhole radius a.

For axial and azimuthal oscillations the following expression was developed:

$$\omega_{nl}^2 = \frac{ka\left|K_n'(ka)\right|}{K_n(ka)}\left[\frac{\gamma}{a^3 Q}\left(m^2 + k^2 a^2\right) + \frac{B}{aQ}\right] \qquad (3.10)$$

where k is the wave number of axial mode

K' is the derivative of the Bessel function with respect to its argument

γ is the Coefficient of surface tension

K_n is the Modified Bessel function

m is the azimuthal mode number

Haran et al [67] plotted the fundamental values for natural frequency for an application involving a 2kW Nd:YAG laser and showed that eigenvalues were expected in the range of 2 to 5kHz in sheet materials.

Postacioglu et al [68, 69] showed a derivation for calculating the natural frequencies of weld pool oscillation with a concentric, fully penetrating circular keyhole. The keyhole radius was assumed to be independent of depth. In this work several conditions are analysed, with constant surface tension, with varying surface tension due to temperature gradients, and oscillation of the weld-pool due to forced oscillation of the keyhole. Such a situation is representative of the welding condition where motion in the keyhole is expected to be stimulated from changes in recoil pressure that are caused by interaction with the beam. The use of dimensionless quantities was employed for ease of numerical calculation and comparison with other work. Translation, as in the case of the welding, was considered but ignored since the oscillatory motion of the translation

was thought to be at least an order of magnitude less than the natural frequency. What is helpful is that Postacioglu presents a numerical solution that can be applied relatively easily to real data.

$$\omega^2 \approx \gamma \frac{k^3}{\rho} \tanh kh \qquad (3.11)$$

Where ρ is the density of the melt

γ is the surface tension

k is the wave number of axial mode and is calculated

$$k = \frac{l\pi}{h} \qquad (3.12)$$

l is the axial mode number and h is the weld-pool depth

3.5 Sources of Optical Signal

All bodies or objects give out electromagnetic radiation at temperatures above absolute zero. This is a function of the oscillation and transitions of the atoms making up the body.

A blackbody is a theoretical concept describing the behaviour of a body that is both a perfect emitter and absorber of electromagnetic radiation. It can be seen that only a fraction of the radiation being emitted is of visible light even at high relatively high temperature. At a given temperature T the energy radiated is a maximum for a certain wavelength λ_{max} that becomes

progressively shorter as the temperature increases. It can be shown that the following relationship exists:

$$\lambda_{max} T = \text{constant} \qquad (3.13)$$

This is known as Wien's Displacement Law. The value for Wien's constant is 2.9×10^{-3} mK.

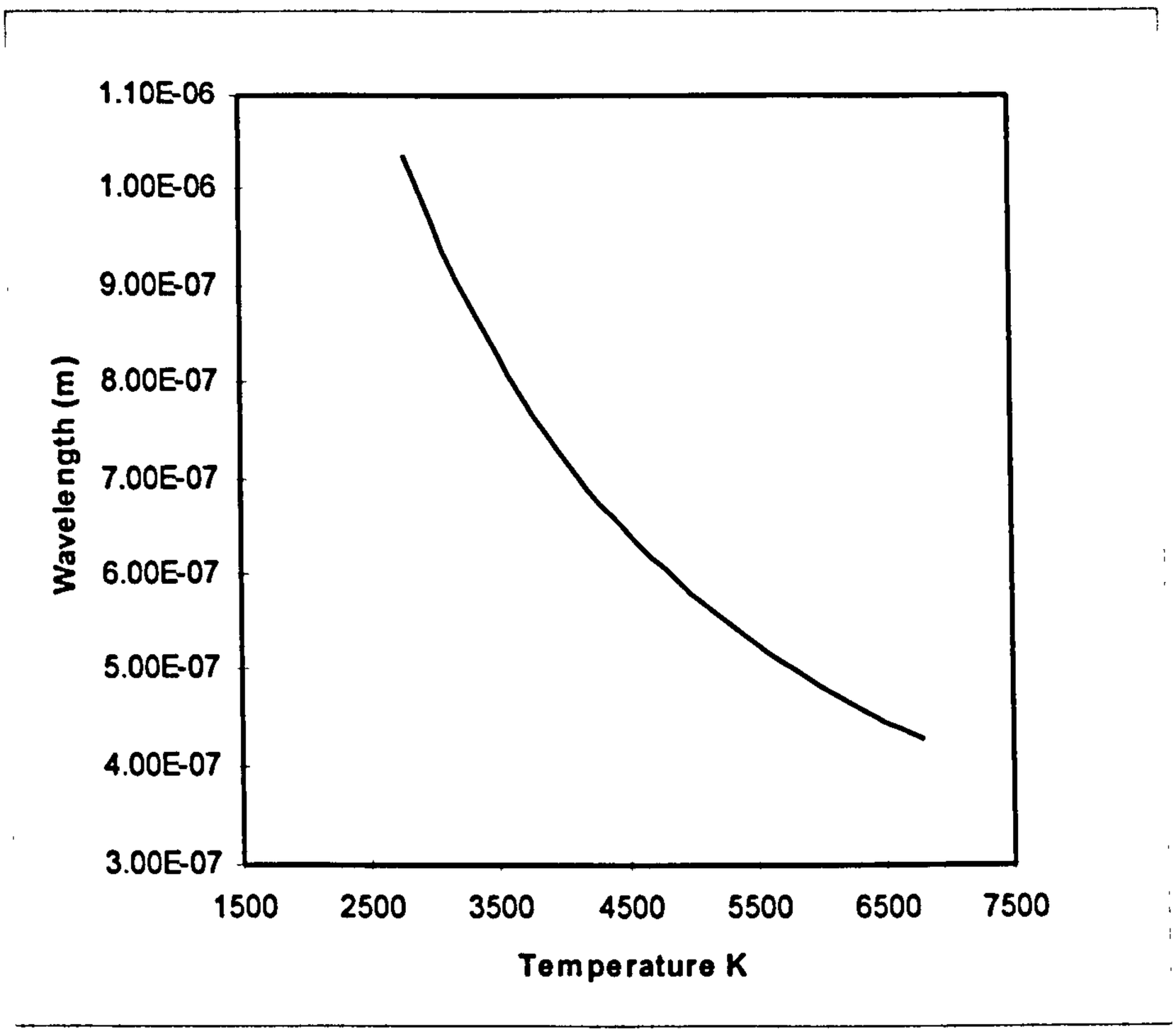

Figure 3.7 Wavelength with maximum intensity at different temperatures

Stefan's Law states that the total energy E_{bb} radiated of all wavelengths per unit area per unit time at thermodynamic temperature T is equal to:

$$E_{bb} = \sigma T^4 \qquad (3.14)$$

where σ is known as Stefan's constant which is equal to 5.7 x 10^{-8} $Wm^{-2}K^{-4}$.

For a non-blackbody Stefan's Law can be modified as follows:

$$E_{nb} = \mathrm{H}\sigma T^4 \qquad (3.15)$$

where H is known as the emissivity and is the ratio of the emitted energy for the non-blackbody with that of a blackbody at the same temperature.

The emissivity of real engineering materials is dependant on a number of additional factors including the material type, surface roughness, temperature, surface condition (i.e. oxidation), and wavelength.

4 Welding Process Quality

4.1 Definition

Weld quality can be defined [70] as:

'The totality of features and characteristics of a weld or welded component that bear on its ability to satisfy stated or implied needs'.

This can be extended to embrace laser processing in general, i.e. cutting, drilling as well as welding but for the sake of this thesis we will concentrate on welding.

Clearly, the quality specification to satisfy stated and implied needs will be dependent on the environment a welded component is subjected to and, the consequence of failure of that component.

In contemplating the direction for development of in-process monitoring and control systems for Nd:YAG laser welding, it is important to consider which defects such a system may have to monitor and control.

It is therefore, important to consider which defects can occur during laser welding, their significance to weld quality, and the relative likelihood of those defects occurring under automated production conditions.

4.2 Factors Affecting Laser Weld Quality.

Weldability is a term used to describe the ease by which a material or component can be welded.

The International Institute of Welding (I.I.W.) has defined weldability [71] in the following terms:

' A metallic material is considered weldable, to a certain degree, by a given process, and for a given purpose, when a continuous metallic connection can be obtained by welding using a suitable procedure, so that the joints comply with the requirements specified both in regard to their local properties and their influence on the construction of which they form part.'

The weldability of a component can be affected by one or more of the following [72]:

- The chemical properties of the material; oxidation resistance (if a material oxidises readily it may be more difficult to protect during welding) the nature of surface films which may provide a barrier to good cohesion; impurity content which may lead to cracking and porosity.
- The physical properties such as thermal conductivity and reflectivity will influence the ability of the material to be melted. High or low viscosity will influence the way the molten material flows and the eventual shape of the solidified weld. The surface tension of the melt can also influence flow and the ability of the melt to retain itself within the joint.
- Metallurgical properties of the joint must be given in the respect of the effect of the welding process on the properties of the parent material and the structure and properties of the weld metal.

The design of the joint or component to be welded may also have a significant influence on the weldability of the component. Accessibility and restraint are the principal factors having influence in this respect. Poor accessibility will almost certainly result in an increase in defect levels whilst excessive restraint will produce high residual stresses and could result in distortion or cracking.

The I.I.W proposed a list of six main categories of weld defect;

1. Cracks.
2. Cavities (porosity, shrinkage cavities).
3. Inclusions (e.g. oxides or slag).
4. Lack of fusion and lack of penetration.
5. Shape defects.
6. Miscellaneous (e.g. Spatter, marks caused by post weld treatments).

4.2.1 Cracking.

There are three categories of cracks that may be encountered in laser welding. These are:

- Hot Cracking, so called because cracks are formed when the temperature of the weld-metal is such that some constitutes are still molten, occurring during the solidification of the weld.
- Cold cracking, this type of cracking takes place below the solidification temperature and can occur in all materials where ductility is low and high stresses are present.
- Delayed or Hydrogen cracking. So called because it occurs sometime after the weld has cooled. Occurring mainly in thicker section (>5.0mm) ferritic steels, it is caused by the presence of hydrogen in the weld metal.

4.2.2 Porosity

Porosity can be caused when the molten weld metal becomes supersaturated with gases such as hydrogen, nitrogen or carbon monoxide. Upon cooling these gases, no longer able to remain in solution, will nucleate out and form pores or cavities in the solidified weld metal.

Gases can enter the weld-pool through breakdown of the gas shield, either by entrainment or contamination of the shielding gas, or through contamination of the work-piece surface, grease or moisture, or through chemical reactions in the weld-pool.

In laser welding the high intensity beam generates a keyhole in the work-piece that is sustained by a combination of surface tension, vapour pressure, recoil forces and hydrostatic forces [73]. The periodic collapse of the keyhole is not uncommon, and can result in the entrapment of gases and vapour leaving pore-like voids. This can be reduced by appropriate positioning of the laser focus relative to the plane of the work-piece surface [74].

4.2.3 Solid Inclusions.

This is usually a problem with arc welding processes using fluxes and slags to protect the weld but can arise with laser welding, particularly when welding materials, which have oxide films on their surface such as aluminium alloys. Parts of this oxide can become embedded within the solidified weld metal.

4.2.4 Lack of Fusion and Lack of Penetration.

This can be a problem with laser welding, particularly when butt welding, where the combination of small beam diameter and lack of proper fit-up will prevent effective melting and join of the plate edges. It can also be a problem when laser welding overlapping metal sheet when there is

inadequate contact between the top and bottom sheets. This can result either in inadequate penetration of the underlying sheet or failure to join both sheets together.

The narrow nature of the weld fusion zone created by high energy density processes also presents difficulties of alignment with the joint line in butt-welding. This may also be exacerbated by the characteristic 'wine glass' shaped cross-section [75], often exhibited by laser welds. Narrowness of the 'stem' together with inherent variability in aligning the laser with the joint line may also cause lack of fusion defects, which are not visible from the surface.

4.2.5 Shape Defects

These include a range of defects related to the cross-section shape, profile of the top and under-bead and general smoothness of the weld-bead.

Laser welds can exhibit a number of shape defects which include undercut, concavity and humping [76] of the weld top and under bead which can give rise to reduced static and fatigue strength in laser welds and affect their aesthetic appearance.

These defects can arise through incorrect selection of parameters such as speed and laser power but can also be caused by variability in material edge preparation and alignment of the beam with the joint line [77].

4.2.6 Miscellaneous Weld Defects

The ejection of material from the weld pool as spatter can be a common problem during laser welding because of the rapid and sometimes violent evaporation of material caused by the high energy density at the work piece. It can also arise as a consequence of lower melting point constituents, such as protective coatings on the material surface, escaping through the weld pool.

Excessive spatter can result in a reduction of material in the weld bead, which will reduce its strength and affect the cosmetic appearance of the finished part if it adheres to the component surface. Hot spatter adhering to the surface of some sensitive materials can act as a crack initiation point and may promote premature failure in service.

4.3 The Likelihood of Various Defects Arising in Automated Laser Welding.

Rogerson [72], in considering the manual arc welding processes, proposed that welding defects should be classified into two main categories;

i. Technological defects; defects resulting from a major inconsistency in the welding operation such as incorrect materials, joint design and weld procedure. Factors that should have been established at the development stage of the process and are beyond the control of the operator.

ii. Commonplace or workmanship defects: defects arising from the inherent variability of the process or chance error by the operator for example, variations in the positioning of the welding arc relative to the weld joint, inadequate cleaning of parent materials.

Rogerson proposed that the majority of cracks occurring in welding can be considered as technological defects, whereas the majority of cavities, solid inclusions, shape and miscellaneous defects can be considered as workmanship defects.

It is reasonable to relate these ideas to the application of in-process monitoring for in Nd:YAG laser welding.

As a starting point we must assume that the basic process procedure is sound; that is, technological defects will not arise, and the defects that need to be detected by in-process

monitoring (IPMC) are most likely to arise as a consequence of the natural variance in the process.

4.4 Common Causes of Defect in Laser Welding.

A number of workers have looked at defects and root causes of defects, which can arise during laser welding; Tönshoff [78] and Decker [79] in consultation with end users determined common defects and their root causes occurring in laser based welding systems. These data has been summarised in table 4.1.

It can be seen from these data that the most likely defects encountered are those that can be described as workmanship defects. Significantly there is generally no common root cause for these defects that has important implications when considering the possibility of automatically correcting defects. Clearly if there are many possible root causes, the difficulty of being able to select and correct the right error is greatly increased.

Cause\Defect	Incorrect penetration	Seam Interrupts	Incorrect seam position	Cracks	Porosity	Spatter	Poor weld bead shape
Defective Optical Components	√						√
Defective Laser source	√	√		√		√	√
Work-piece Distortion	√	√	√				√
Out of Focus	√	√			√		
Incorrect speed	√				√		√
Defective process gas flow	√	√		√	√	√	√
Incorrect power	√				√		√
Poor work-piece cleanliness		√		√	√	√	
Incorrect nozzle diameter					√		
Beam alignment	√		√				

Table 4.1 Common causes of defects in laser welding

5 Review of Literature Relevant to In-process Monitoring

Prior to consideration of the techniques available for IPMC of laser welding process it is worth reflecting on work carried out in development of similar systems for the automated arc welding process as by virtue of the maturity of the welding process might be more highly developed.

5.1 In-process Monitoring for Arc Welding

Several authors [80, 81] have carried out reviews of currently available in-process monitoring technology for use in arc welding and it is obvious that many techniques have been investigated. The majority of development has been in the field of techniques for penetration monitoring, these can be placed into two generic groups: those monitoring from the underside of the weld and those monitoring from the topside.

Back light sensing was one of the earliest techniques developed to monitor penetration from the underside of the weld. The technique uses an individual or array of photosensitive devices to detect the radiation emitted by the weld under-bead. The intensity of the emitted radiation was used to indicate the degree of penetration. By using selective filtering the sensor device could be made to be more sensitive to radiation emitted by hotter material [82]. An alternative, more complex and more expensive approach was to observe the image of the weld under-bead using a video camera. Both techniques involved the use of feedback to control welding current. The principal drawback with back-face monitoring systems is the need for access to the under-bead and the alignment and synchronisation of the heat source with the sensor and as a consequence this type of sensor, to the author's knowledge, has experienced only limited uptake.

This use of ultrasonic has been one of several methods employed for controlling penetration from the topside of the weld. Here, an ultrasonic wave is directed towards the weld by sensors, positioned either side of the weld bead, on the surface of the component.

A calculation to determine the time of flight for the sound wave is performed by a computer, which can give an indication of both full and partial penetration. The main drawback of this type of system appears to be the need for intimate contact with the work piece and the synchronisation of the sensor movement with the heat source.

Several systems have been developed to determine the onset of full penetration by monitoring the sagging of the weld bead. One such system detects the onset of sagging through the arc. As the weld begins to sag so the arc lengthens and the arc voltage increases. Similar in principle, another system uses a displacement transducer that monitors the movement of an arc voltage control system, which moves in order to maintain a constant arc length.

A further system that detects the displacement of the weld surface uses a laser beam, which is used to illuminate the surface of the weld pool. A proportion of the laser light is reflected onto a detector that is sensitive to position. This system has the benefit of being independent of arc parameters and could therefore be used for other welding processes such as laser. However, a significant drawback must be that it does not provide information about partially penetrating welds.

More recently techniques have been developed which involve the use of video cameras to observe the weld pool. One such system uses a camera mounted coaxially within a specially adapted welding torch. The camera is sensitive to the arc light reflected from the surface of the weld pool. A computerised image processor is used to detect the edges of the pool. Weld penetration is

controlled indirectly by varying power source parameters and speed, to control weld pool size and shape. This type of system offers the flexibility of not being confined to only arc processes but would be both complex and costly to implement.

Research has shown that the oscillation frequency of the weld pool is lower for a fully penetrating weld than for one that is only partially penetrating. Several penetration control systems have been developed around this phenomenon. One way of detecting weld pool oscillation is through the arc parameters such as arc voltage. A spike of welding current is introduced periodically to excite the weld-pool into oscillation and as the pool surface oscillates up and down the arc length and therefore voltage changes. A computer is used to calculate the frequency of voltage oscillation and a control system acts on that information to make adjustments to the power source to maintain the appropriate weld-pool depth. Similar in principle an optical system has also been developed which observes the fluctuations in arc light during oscillation of the weld-pool. This type of system may hold considerable promise for use with laser processes where either the reflected laser beam light or light from an external source could be monitored.

Measurement of the temperature distribution around the weld-pool has been used as an indirect indication of depth of penetration. Measurement can be achieved either by direct contact with the weld using a temperature measuring device such as a thermocouple or indirectly with an infrared video camera. The main disadvantage of the former is the need for the device to be in physical contact with the work-piece. Similarly the optical technique is susceptible to errors caused by variations in material thermal emissivity and surface condition.

Acoustic-Emission sensing is still largely undeveloped for arc welding. The principle works on the phenomenon that thermal stresses formed in the material during welding generate acoustic

emissions that travel throughout the work piece. The amount of emission is therefore a function of the amount of fused material.

In summary, the experience from arc welding techniques demonstrated that practical in-process monitoring and control systems must possess five important features [80] if they are to be successful. These are:

1. They must sense from the front side of the weld as access to the under-bead is not always possible.
2. The sensor used should be non-contact and not intrude upon the processing area.
3. Penetration monitors need to be capable of both full and partial penetration measurement.
4. Should be independent of the process, ideally independent of the welding process used (i.e.Arc , laser)
5. The technique should be simple, reliable and cost effective.

It is expected that attributes outlined above can be applied equally well to laser processing.

5.2 In-process Monitoring Techniques for Laser Welding.

The use of optical energy for welding, in the form of a laser beam, offers a number of opportunities for sensing signals from the process containing information indicative of the processes occurring and quality of those processes.

Figure 5.1 shows a diagram indicating the signals that are available from the laser process for in-process monitoring. These are discussed in more detail in the following.

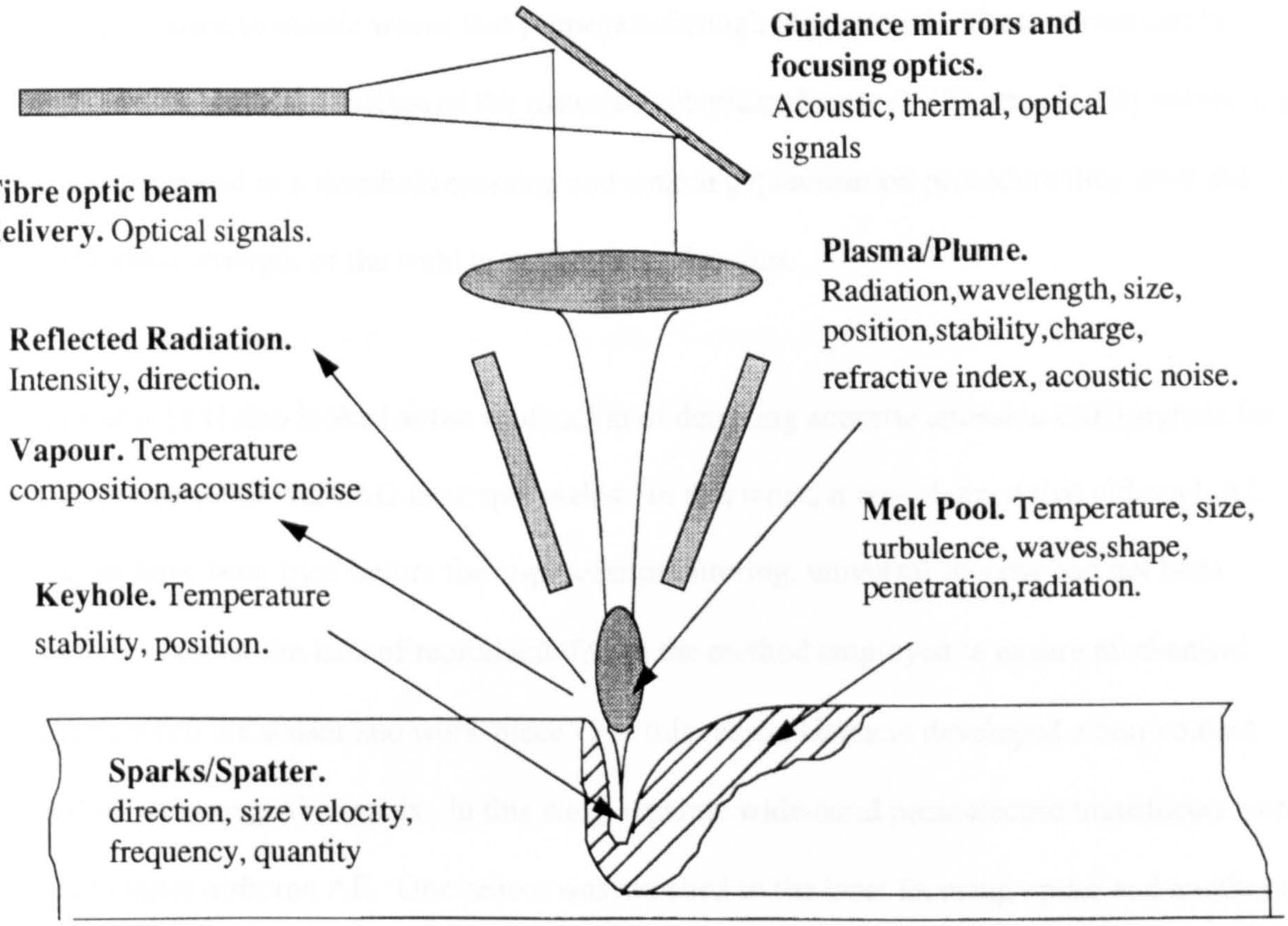

Figure 5.1 Opportunities for in-process monitoring of laser processes (after Steen [4])

5.2.1 Acoustic Emission Sensing.

A number of investigators have looked at the acoustic emissions (AE) from the laser process as a possible indicator of process quality.

Saifi and Vahaviolos [83] developed a contact technique for monitoring the AE emitted during welding of copper wire to terminal posts with a pulsed Nd:YAG laser. In this case they referred to AE as Stress Wave Emissions (SWE).

In this context AE (SWE) occurred as a consequence of being released as a solid undergoes (elastic) plastic deformation and fracture. The absorption of the laser beam releases AE energy, which is converted to elastic waves that propagate through the material. These waves can be detected as they reach the surface of the material with piezoelectric (PZT) sensors. By subjecting the signal generated to a threshold crossing and counting quantisation procedure they were able to relate the shear strength of the weld to the number of counts.

Hamann et al [84] also looked at the application of detecting acoustic emission (AE) signals for the quality control of Nd:YAG laser spot welds. In this work, it was claimed that although AE techniques have been tried before for in-process monitoring, universal success had not been achieved because of the lack of reproducibility in the method employed to ensure mechanical contact between the sensor and work-piece. For this reason Hamann developed a non-contact method for detecting AE signals. In this work separate wide-band piezoelectric transducers were used to monitor airborne AE. One sensor was attached to the laser focusing optics and another to the surface of the work-piece. A photo-detector was used to monitor the temporal profile of the laser pulse developed by the laser and was used as a trigger for sampling. A second photo-detector was used to monitor the development of the plume or plasma developed at the surface of the work-piece.

Hamann's results, when welding steel and aluminium alloys, indicated that an AE sensor with no direct contact with the work-piece can be used to monitor AE successfully from the spot welding process.

Further more, it was found that by calculating the AE energy (by taking the time integral of the measured signal, squared) the non-contact AE method could be used to monitor penetration depth in both the steel and aluminium samples. A drawback with this technique is that the non-contact

AE sensor is susceptible to heating, by back-scattered laser radiation, which generates additional background AE.

Li and Steen [85] developed a similar technique for detecting airborne AE signals that was used for seam welding, cutting and drilling with a carbon dioxide laser. The technique involved attaching piezoelectric transducers to part of the processing nozzle, insulated from heat conducted through the nozzle and shielded from back-scattered laser radiation. A similar transducer was also attached to one of the turning mirrors in the laser beam delivery; this arrangement has been shown to provide information on the laser beam characteristics.

Three sources of AE were postulated by Li and Steen [85];

1. Vapour/Plasma initiated acoustic waves,
2. Phase transformations within the material; either solid phase, liquid/solid or liquid/gas transformations.
3. As a consequence of the impacting gas jets such as from the assist gas from a cutting nozzle.

Due to practical considerations, only sources 1 and 3 could be sensed as airborne AE.

Their findings were consistent with those of Hamann in the respect that AE becomes significant only when vaporisation begins, a keyhole is generated and plasma is formed in the interaction zone.

The results of their work show that there is a relationship between the AE and the traverse speed, incident power and plasma density with the AE first increasing to a maximum and then decreasing as these variables are increased.

Li and Steen also examined the frequency domain of the AE signals. This they found to be broadband and similar for a number of different welding conditions. The lack of change was attributed to the masking or 'blanketing' effects of the plasma produced at the laser interaction zone.

Farsen et al [86] carried out detailed time-frequency analysis of airborne AE data collected from welds made using a high power CO_2 (14kW) laser. The materials were stainless steel sheet arranged in lap a joint, with a combined thickness 0.107inches (approx. 2.6mm.). Welds were made under a number of conditions that included full and partial penetration welds, and welds with and without gap between the overlapping sheets. Full and partial penetration welds, were made both by holding the laser mean power constant and welding at different speeds and by holding the speed constant and welding at different laser power settings. Analysis of these data showed, that for fully penetrating welds significant energy was found in the spectral region 1-2kHz which was not present for partially penetrating welds.

Trials where a progressively increasing gap was introduced between the overlapping plates showed that the total energy in the AE spectrum reduced as the gap became severe. The actual gap size and its effect on weld quality were not specified.

5.2.2 Electrical Charge Sensors.

Li et al [87, 88] investigated the use of the so called, Plasma Charge Sensor (PCS) for monitoring the space charge between the end of an insulated nozzle and the work-piece.

The origin of the charge was believed to be the partially ionised plasma that was formed by the interaction of the laser beam with the target material. As a consequence the sensor was found to

be relatively insensitive to welds made at sufficiently low laser intensities such that plasma or keyhole was not formed.

The intensity of the laser beam at the target surface and the density of the metal vapour govern the density of the plasma.

It is postulated that although the plasma has a net charge of zero by virtue of it possessing an equilibrium number of positively charged ions and negatively charged electrons, the higher mobility of the lighter electrons allows them to migrate to the edges of the plasma where they can be detected.

Experiments with a 2kW CO_2 laser showed that the PCS could be used to discriminate between a number of different welding conditions;

Variations in penetration (induced by varying welding speed) produced a characteristic increase in amplitude of the PCS signal. The suggested reason for this was the increase in plasma density associated with greater metal vaporisation and keyhole depth.

The PCS sensor was found to be able to detect start and stop craters (with the signal increasing and decreasing respectively), vapour craters or pitting in the top weld bead, changes in shield gas flow, loss of the keyhole, weld bead humping and undercut, and variations in laser power.

5.2.3 Optical Sensing

Optical sensing of the process light represents the biggest area of research into in-process monitoring techniques for laser processing.

The origins of optical radiation emanating from the laser welding process can be summarised in three areas:

1) Scattered and reflected radiation from the laser source.

2) Emitted, reflected and scattered radiation from the hot metal in the weld pool.

3) Emitted and scattered radiation from the plasma in the keyhole and above the weld pool.

Many workers have explored the use of optical radiation as an indicator of quality in the laser welding process.

Chen et al [89] used a technique of monitoring the UV and IR components emanating from the weld zone during laser welding of mild steel plates of different thickness. Two types of photo-detector were used, a GaP photodiode sensitive to wavelengths in the range 300 to 500nm and a Ge photodiode with a Si filter with a sensitivity to the wavelength range 1000 to 1800nm. Three arrangements were used to detect light from the welding process: by directing the photodiodes directly at the welding zone from the side, by gathering light via an optical fibre from the side and by gathering light via an optical fibre directed at the process zone, positioned within the final turning mirror of the beam delivery optics. A number of normal welding conditions were explored as well as introducing a number of deliberate defects. Chen claimed that the system was capable of detecting variations in the specific energy (J/mm^2) introduced into a weld by changes in speed and power. Excessive specific energy resulting in weld sagging and drop-through

caused both the IR and UV signals to rise; too little energy resulted in inadequate penetration and caused both signals to drop significantly.

Keyhole failure, instigated by varying focus position relative to the work-piece produced a step increase in both UV and IR signal levels. Of significant interest was the observation that the UV signal changed prior to keyhole collapse (approx. 100ms) and prior to changes in the IR signal, giving the signal a predictive element. The suggested reason for this was that the plasma (main source of UV) within the keyhole become unstable due to defocusing before the keyhole itself became unstable and before absorption of the laser beam was affected. Other instabilities in the process, probably due to variations in the reflectivity of the work-piece surface were also detectable. Variations in the velocity of the shielding gas could also be detected by virtue of its influence on the production of welding plasma. At low velocity the plasma almost completely blocked the laser beam from the work-piece, the effect was a significant increase in the UV signal detected.

Semak et al [90] described a technique of monitoring keyhole stability during spot welding of stainless steel, with a 2.4kW CO_2 laser, by using a low power argon probe laser. This technique involved the illumination of the welding keyhole from one side using the probe laser. A photo-multiplier fitted with a band pass filter corresponding to the wavelength of the probe laser was positioned so as to collect the reflected radiation from the probe laser. This technique allowed an assessment of the time taken to break down the reflectivity of the material surface and an assessment of whether effective coupling was taking place.

Miyamoto et al [91] describes a method of monitoring the plasma plume within the welding keyhole produced by a CO_2 laser of 1.5kW in mild steel sheet. An off-beam axis detector was used to gather light from the process and deliver it to a monochromator. The intensity of light

was time integrated (to overcome the effect of rapid fluctuations in the plasma) in the wavelength range 364.874 to 382.782nm. Miyamoto made the assumption that the plasma was in local thermodynamic equilibrium (LTE). The plasma can be considered to be in LTE when the collision transition is much larger than the radiation transfer that is, when the following equation is satisfied

$$n_e \geq 9.2 \times 10^{11} x_{nm} \sqrt{T} \qquad (5.1)$$

where n_e is electron density

x_{nm} is excitation potential from level m to n.

Assuming LTE allowed the following equation to be used to calculate average plasma temperature from the relative intensities of spectral lines.

$$\ln \frac{I_{nm}\lambda}{g_n A_{nm}} = -\frac{E_n}{KT} + const. \qquad (5.2)$$

Where λ is the line wavelength

K is Boltzmann constant

E_n is the energy level

g_n is the statistical weight of ground or excited state

A_{nm} is the probability of energy transition

I_{nm} is the spectral intensity.

By using a Boltzmann plot it was determined that a linear relationship exists between $\ln(I_{nm}\lambda/g_nA_{nm})$ and E_n this allowed the average plasma temperature to be determined as the slope of the graph and was found to be in the range 7500 - 8800K.

The temperature of the plasma was found to vary when the laser focus position was moved relative to the material surface. At focus, the temperature was found to be at a minimum, rising either side of focus.

Again assuming LTE, the electron density was determined by using the Saha [35] equation;

$$n_e = 4.83\times10^{15} T^{3/2} \frac{g_n^{+} A^{+} v^{+} I}{g_n A v I^{+}} \exp\left(\frac{E_n - E_n^{+} - V}{KT}\right) \qquad (5.3)$$

Where V is ionisation energy,

E energy level

T temperature and

I spectral intensity

The subscript + indicates the value of ionised species and no subscript atomic species. Using this equation electron density was calculated for FeI (285.18nm) and FeII (292.659nm) and was found to be in the range 1 to 4 x 10^{16} cm^{-3}. Also the electron density was found to be a minimum at the focus position.

A more precise estimate of temperature and the distribution of electron density in the plasma was achieved by mapping the plasma with the monochromator in steps of 0.25mm. This yielded a higher temperature of approx. 9500K close to the centre of the plasma out to a radius of 0.25mm,

beyond this the temperature was constant at 8500K. Electron density at the centre was calculated as 10^{17} /cm^3. Clearly with consideration of equation (5.3) it is was safe to assume LTE. Miyamoto also calculated the absorption coefficient of the CO_2 laser beam; A, via inverse Bremsstrahlung using the equation 5.4.

$$A = 3.69 \times 10^8 \frac{n_e^2}{v^3 \sqrt{T}} [1 - \exp(-\frac{hv}{KT})] \qquad (5.4)$$

where n_e is the electron density

T is temperature

v is the frequency of laser beam

K is Boltzmann constant

h is Planck's constant.

At a value 10^{17} cm^{-3} the absorption coefficient was calculated as A=0.2cm^{-1} or an absorption depth of approximately 5cm, much higher than the plasma depth which was observed as approx. 0.5mm which equates to 1% absorption.

Miyamoto proceeded to utilise the effect of changes in the plasma with laser parameters for process monitoring. Four photodiodes with peak sensitivity at 800nm were arranged every 15° in a vertical arc adjacent to and viewing the welding plasma. A fifth photodiode was positioned beneath the work-piece to view breakthrough of the weld under-bead. Using this arrangement optimum focus producing full penetration was found when the signal from the diode positioned at the highest angle i.e. looking into the keyhole, reached a minimum. This arrangement was also found to be capable of sensing changes in speed. At low speeds the output from the sensors spread over a range of values, with the high angle sensor having the greatest value and the low

angle the lowest. At higher speeds the output of the lower angle sensors rose and converged on that of the highest angle sensor. This was attributed to a greater fraction of the plasma being ejected at high speeds and interacting with the beam.

Shield gas flow rate was also found to affect the signal level with lower values being recorded at higher flow rates. This was attributed to higher flow rates reducing the plasma height.

Griebsch et al [92] carried out work to investigate the possibility of monitoring penetration depth of seam welds produced with a 520W pulsed Nd:YAG laser by monitoring the reflected laser radiation from the keyhole. Griebsch determined that a clear relationship existed between the aspect ratio; penetration depth divided by focused spot diameter and the degree, expressed as a percentage, of absorbed laser energy in the weld, for both the Nd:YAG and CO_2 laser wavelengths.

This being the case, since focused spot size can be kept constant the relationship could be used to calculate weld penetration depth.

A photodiode with an interference filter (1064nm) positioned behind a turning mirror in the focusing head was used to monitor the temporal characteristics of the reflected laser radiation during the welding pulse. The measured signal revealed three phases of beam interaction with the metal target. In the first phase, within 0.2ms, the reflected radiation reached peak intensity. This was attributed to initial high reflectivity of the work-piece. Over a further 0.2ms the peak decayed to a value approximately half that of the initial peak as heating of the work-piece increased absorption. It was thought that the keyhole was formed during this period. After the initial rapid decay the signal settled and decayed more slowly until the end of the laser pulse where the signal was lost.

Griebsch identified that poor welds exhibiting melt expulsion had the characteristic initial peak in the reflected signal missing. A linear relationship was found between the value of the difference between the initial and final amplitude of the reflected signal and the depth of penetration. This relationship held true for a number different pulse widths and peak powers in the range 3.5 to 7.5ms and 1300 to 2700W.

6 Equipment used in Experimental trials

A large variety of equipment was used during the experimental trials. Rather than attempt to include each item within the experimental procedures that follow this chapter describes the equipment in detail.

6.1 Laser Sources.

Four different laser sources were used during material process trials, these are detailed below:

1. A free running lamp pumped pulsed Nd:YAG laser (Lumonics JK702H) rated to give a specified mean power output of 350W. The power supply design was switch-mode, capable of giving pulse widths in the range 0.5 to 20ms typically but also capable of giving continuous wave output. Pulse frequency range is 0.3 to 500Hz. The power supply software was capable of providing pulse shaping but this was not used in the trials. The resonator layout consisted of a single rod pumping chamber using two flash lamps, with ceramic reflectors within the cavity. A schematic of the optical layout of this laser is shown in figure 6.1. The laser system construction consisted of a separate laser head and power supply, which allows the laser head to be mounted onto a work-handling machine if required. The laser can be used with either conventional or fibre optic beam delivery. For the trials the laser was used exclusively with fibre optic beam delivery.

2. A continuous wave carbon dioxide laser (PRC Oerlikon LE2000, Type LE2000T000A, serial number 3C2006) with conventional beam delivery giving a rated maximum power of 1800W and a beam quality of <26mm.mrads, TEM_{01} . This was used with conventional beam delivery.

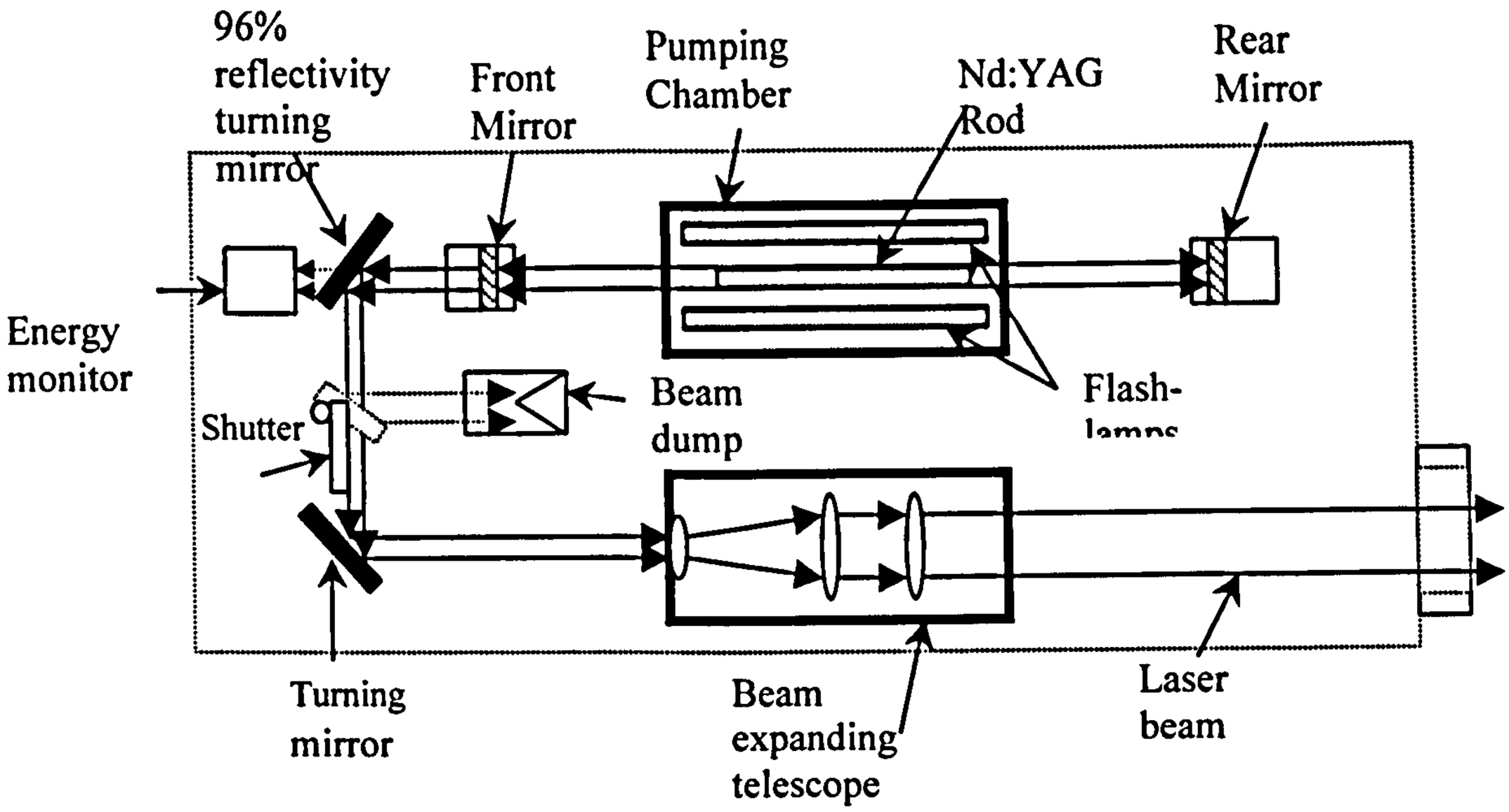

Figure 6.1 Layout of pulsed Nd:YAG laser

3. A continuous wave Nd:YAG laser (Lumonics MultiWave™ 2000) capable of giving 500 to 2000watts output (measured at the source). The laser equipment consisted of a single unit containing both power supplies, optics and cooling system. The resonator consisted of four pumping chambers each containing a cylindrical rod and two flash lamps arranged in a periodic resonator, see figure 6.2. After leaving the resonator a portion of the beam (approximately 4%) is directed into a silicon diode based monitor for power measurement. The remaining portion of the beam, when not being used for processing was absorbed using a water-cooled beam dump. The shutter is operated by raising turning mirror 1 into the beam which redirects the beam from the beam dump to turning mirror 2 which in turn directs the beam to the fibre input lenses.

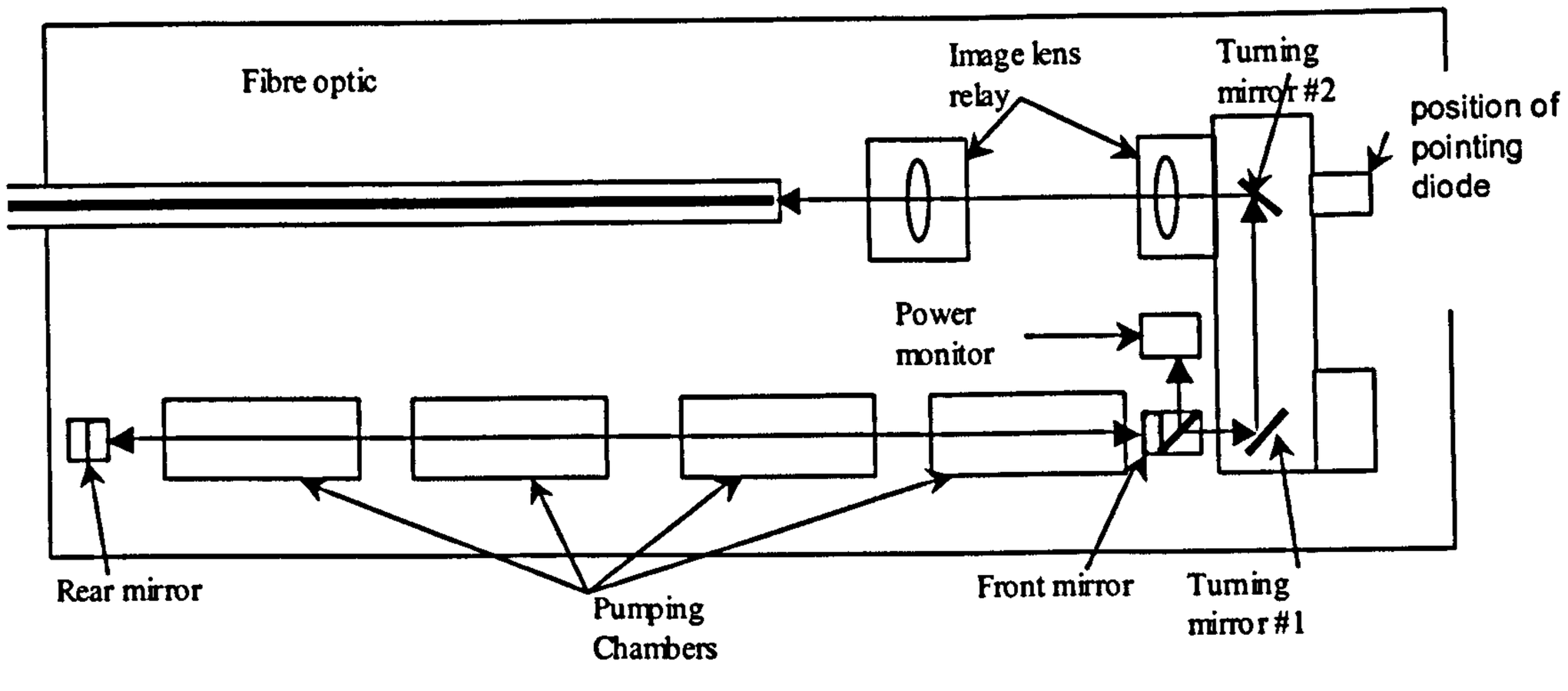

Figure 6.2 Layout of 2kW continuous wave Nd:YAG laser

The beam is then focused using a pair of lenses, arranged as an imaging relay, into the core of a fibre optic cable. The fibre optic cable consisted of a single core fused silica step index fibre of 1000μm core diameter, housed in a flexible armoured jacket. This laser was used for the majority of experimental trials. Figure 6.3 shows the output power and beam quality characteristics of this laser.

4. A prototype continuous wave Nd:YAG laser (built by Lumonics as part of a high power development programme) consisting of an 3 chamber oscillator and 5 chamber amplifier optical arrangement, see figure 6.4. An imaging relay was used to focus the beam into a single core step index fused silica fibre with 600μm diameter core. The laser was capable of producing in excess of 5kW mean power at the work-piece i.e. after the final focusing lenses and protective cover-slide. This equates to a mean power at the source of approximately 5.9kW.

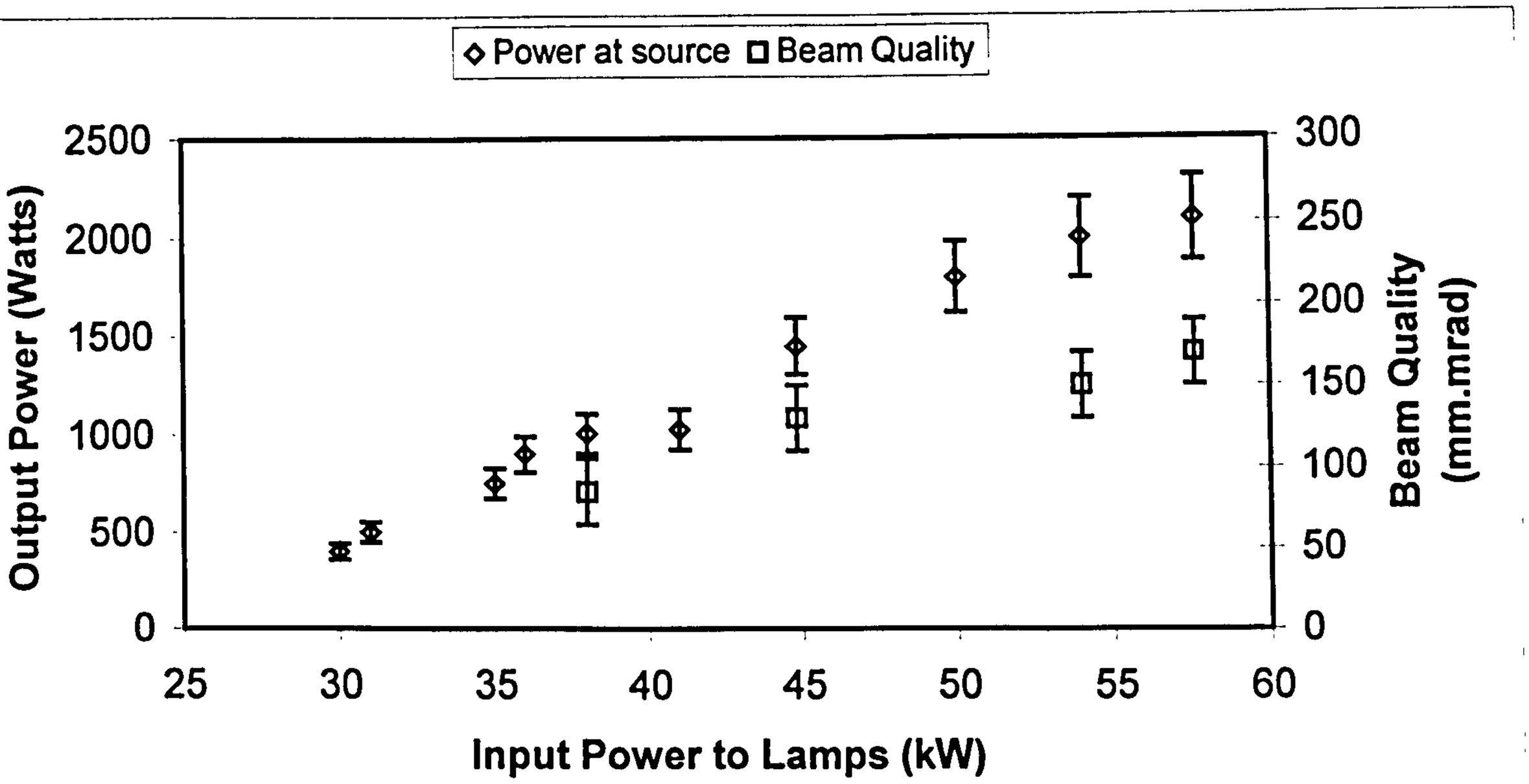

Figure 6.3 Output power and beam quality characteristics with respect to input power for the 2kW continuous wave laser.

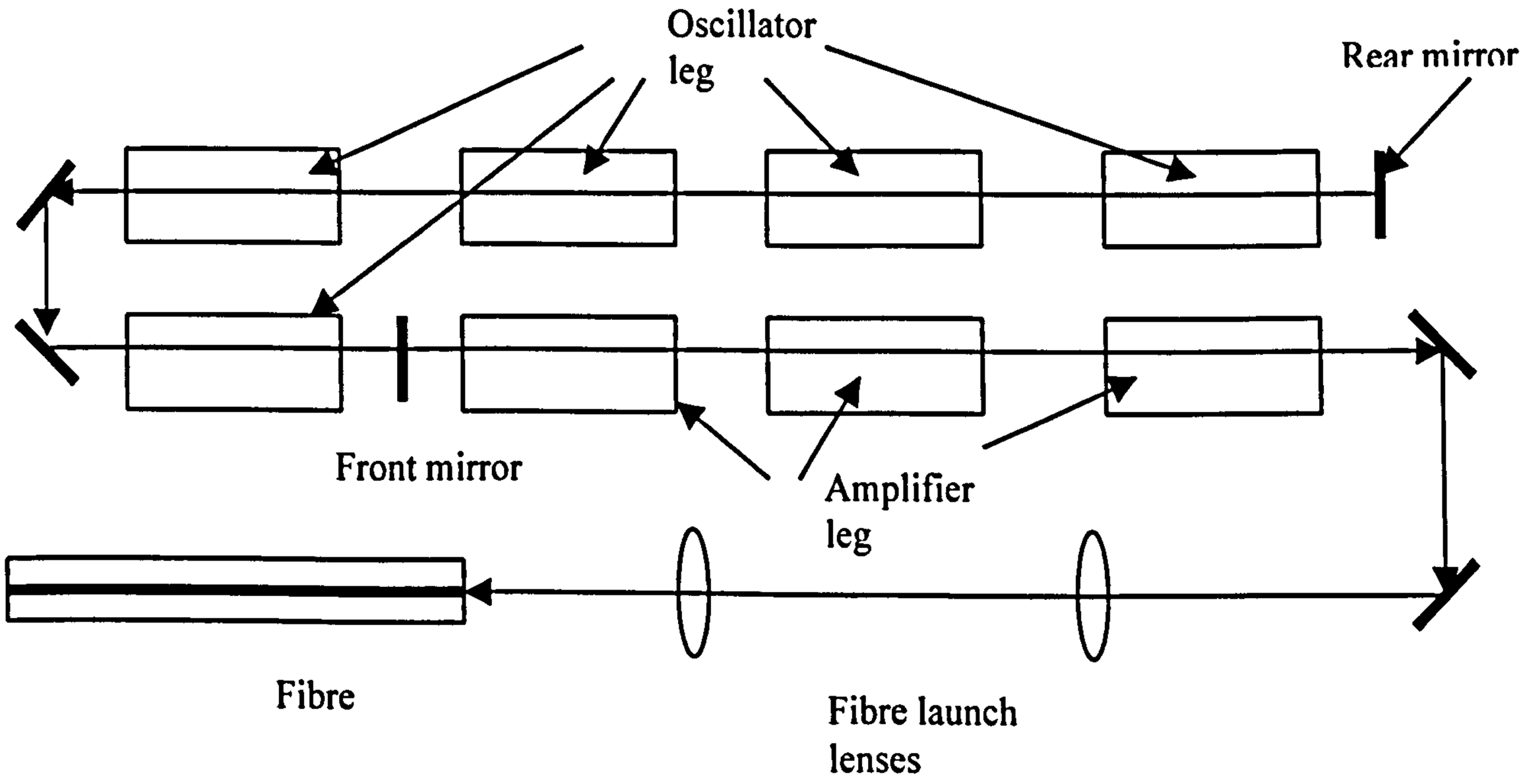

Figure 6.4 schematic of prototype 6kW Nd:YAG laser system

6.2 Monitoring Equipment

6.2.1 Off-axis monitor

This sensor is shown in figure 6.5, and consisted of a single cemented positive achromat lens of diameter 25mm, with a focal length of 60mm with the end of a 1.0mm fused silica fibre positioned in its conjugate focus plane.

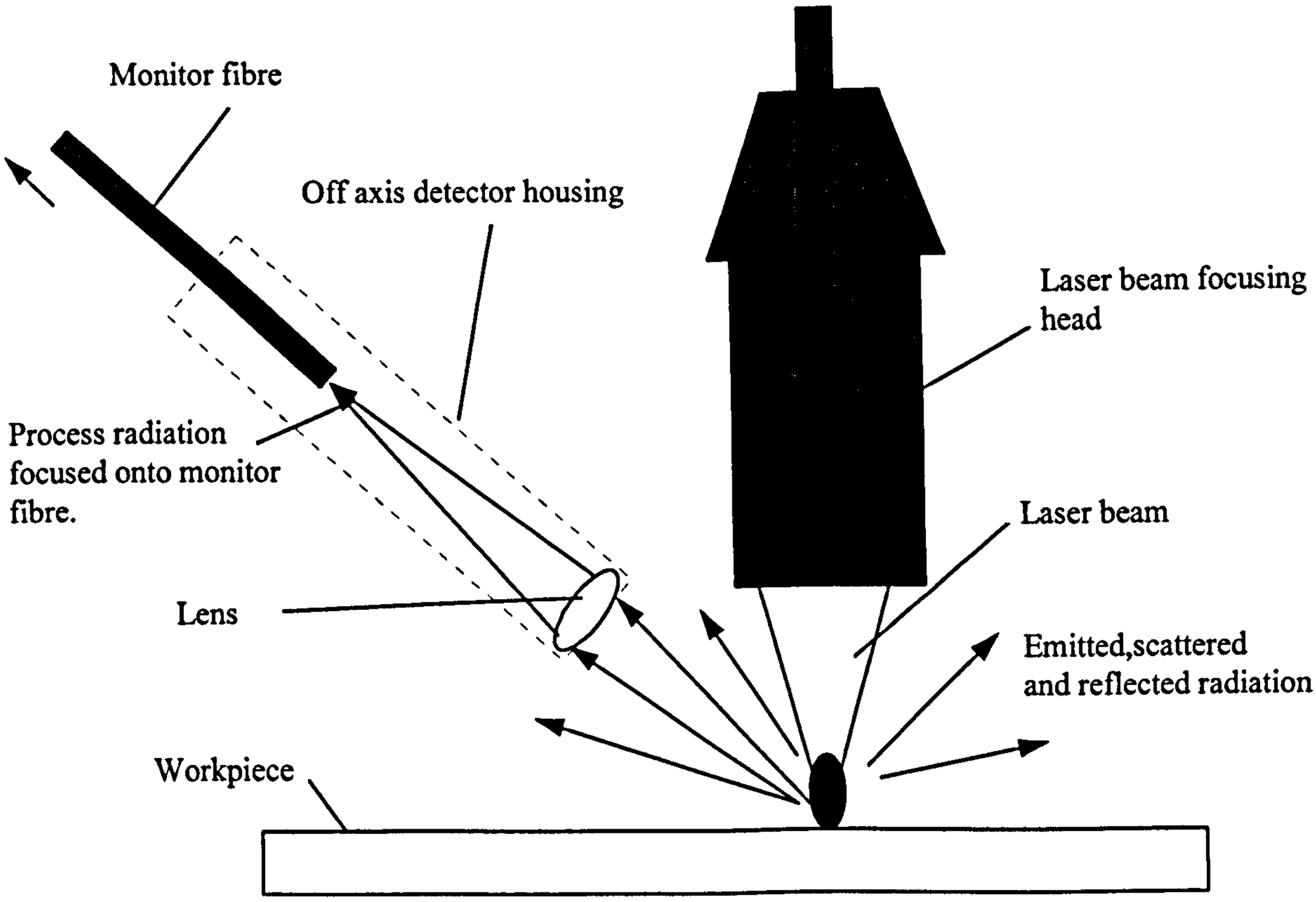

Figure 6.5 Schematic of off-axis detector

The sensor was positioned adjacent to the output optics of the laser beam delivery at an angle typically 45 °– 60° from the vertical and directed at the interaction point. The method employed to position the sensor was to shine white light from the opposite end of the fibre through the lens to create an image at the work-piece. The distance between fibre end and lens was fixed so as to give a 1.0 –1.5mm image at the work-piece. The sensor was placed so that its collection zone was positioned symmetrically about the interaction point. A hood was placed around the lens so

as to minimise the ambient light entering the detector. This design of optical sensor proved to be a convenient and simple way of gathering light from the process and was suitable for use with either Nd:YAG or CO_2 lasers.

6.2.2 Bi-directional Cladding Power Monitor (CPM).

Figure 6.6 shows a schematic diagram of a cladding power monitor (CPM). This sensor was designed to be an integral part of a fibre optic beam delivery and consisted of a small fused silica fibre optic (200μm core diameter) which was optically coupled to the cladding of main beam delivery fibre using a refractive index matching gel or adhesive. After attachment the junction between the two fibres was given protection with a sheath made of a metal tube sealed at both ends with epoxy adhesive. Each end of the monitor fibre was terminated within a glass capillary tube using epoxy adhesive and polished using a diamond wheel to 1μm finish. The main fibre ends were also polished to 1μm and terminated in a metal ferrule compatible with the laser beam delivery. This arrangement allowed light entering the cladding at either end of the fibre and in particular that emanating from the process, to travel along the cladding by a process of total internal reflection to be coupled out at the junction between the main fibre and the smaller CPM fibre. A proportion of this light leaves the cladding and enters the smaller monitor fibre where it is guided to its end. No light is coupled out of the core of the main delivery fibre and there is therefore no insertion loss associated with it. The main expected factors affecting the performance of this device [93] are the coupling efficiency between monitor fibre and cladding of the main fibre and the amount of cross-talk between the laser radiation travelling in both directions being detected by the photodiodes. For the purposes of in-process monitoring the wavelengths of interest are beyond that of just the laser wavelength and therefore cross talk was not considered a problem.

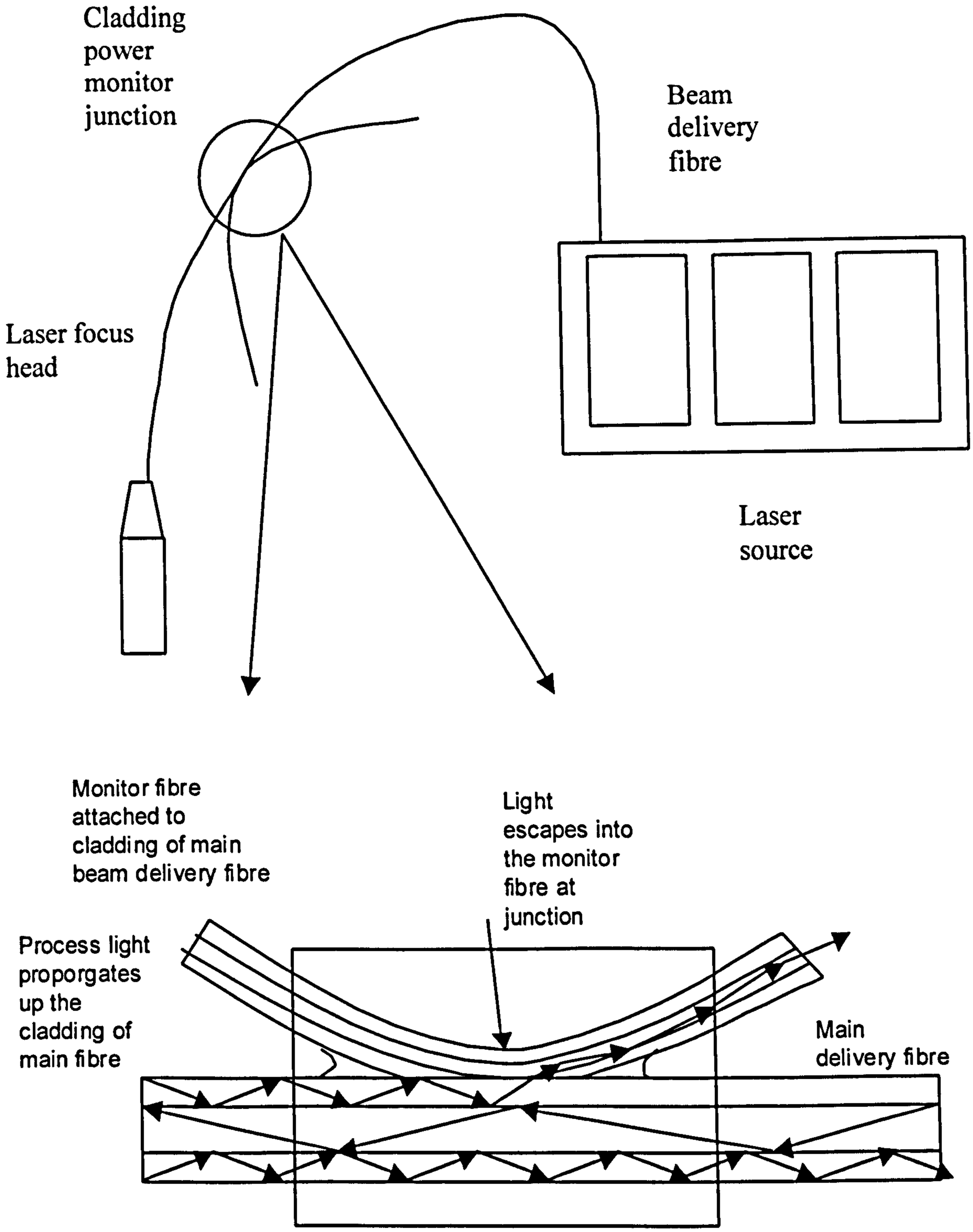

Figure 6.6 Schematic of the cladding power monitor arrangement

Light escaping from the junction was scattered and absorbed by the surrounding protective enclosure around the CPM junction.

6.2.3 Fibre Core Monitor

This device is so called because it was used to monitor process light, which travelled back up the core of the main beam delivery fibre in the opposite sense to that of the incident laser beam.

Light from the process enters the optics in the focusing head where it is focused back onto the output end of the main beam delivery fibre.

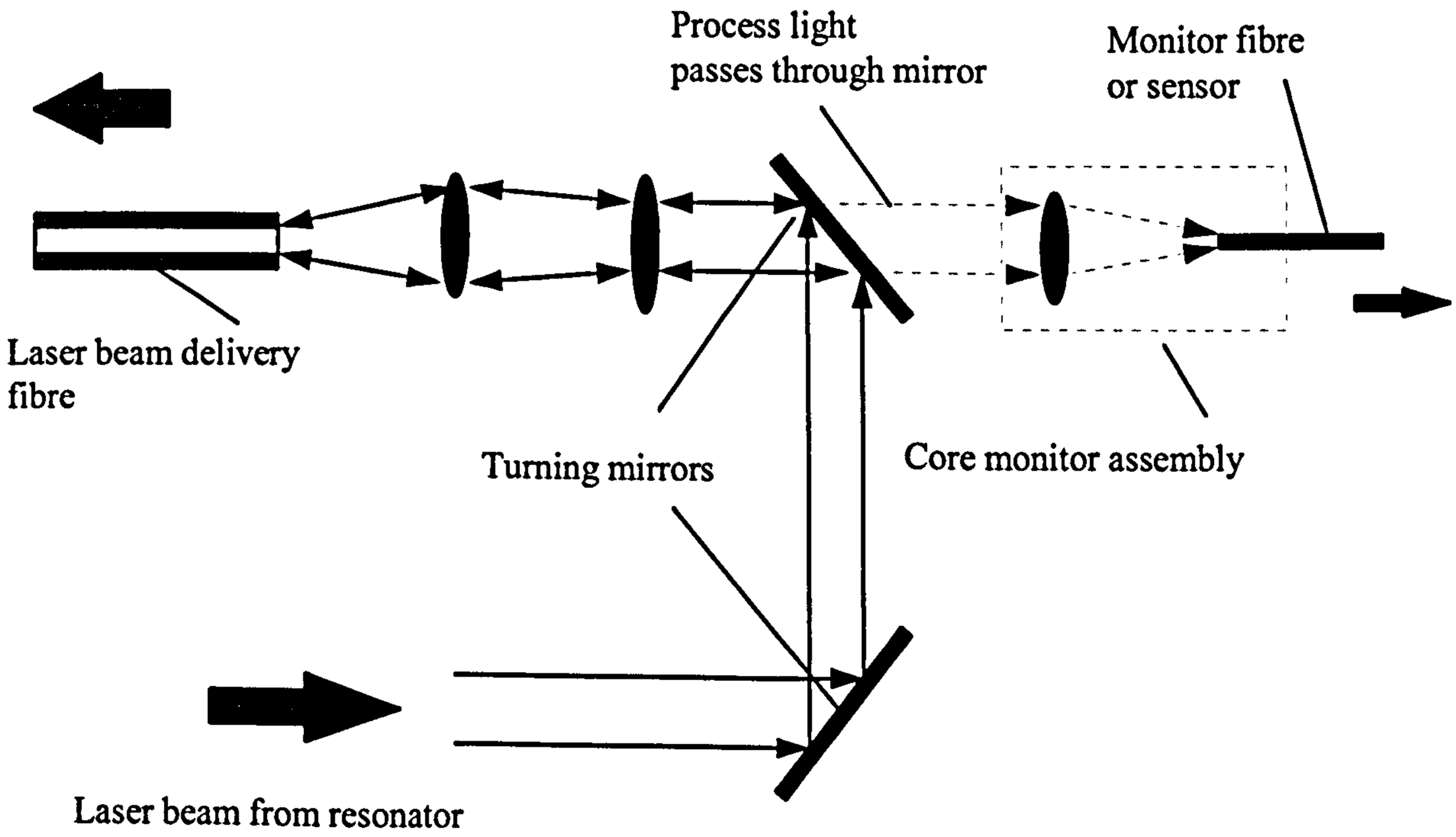

Figure 6.7 Schematic of the optical layout for the core monitor within the laser head

Figure 6.7 shows a schematic of the layout of a sensor in relation to the other optical elements within the laser head. The arrangement uses a series of silica lenses to image the input end of the main beam delivery fibre onto the end of a smaller fibre. This allows a significant amount of

process light to be imaged back from the work-piece into the fibre core by the focusing optics in the focusing head to be detected. The core monitor was designed in such a way that the fibre could be moved independently in the Z direction, of the lens so that it could be accurately positioned at the waist position of the lens. Both lens and monitor fibre could be moved in the X-Y position relative to the fibre axis for alignment with the optical axis of the fibre see figure 6.8.

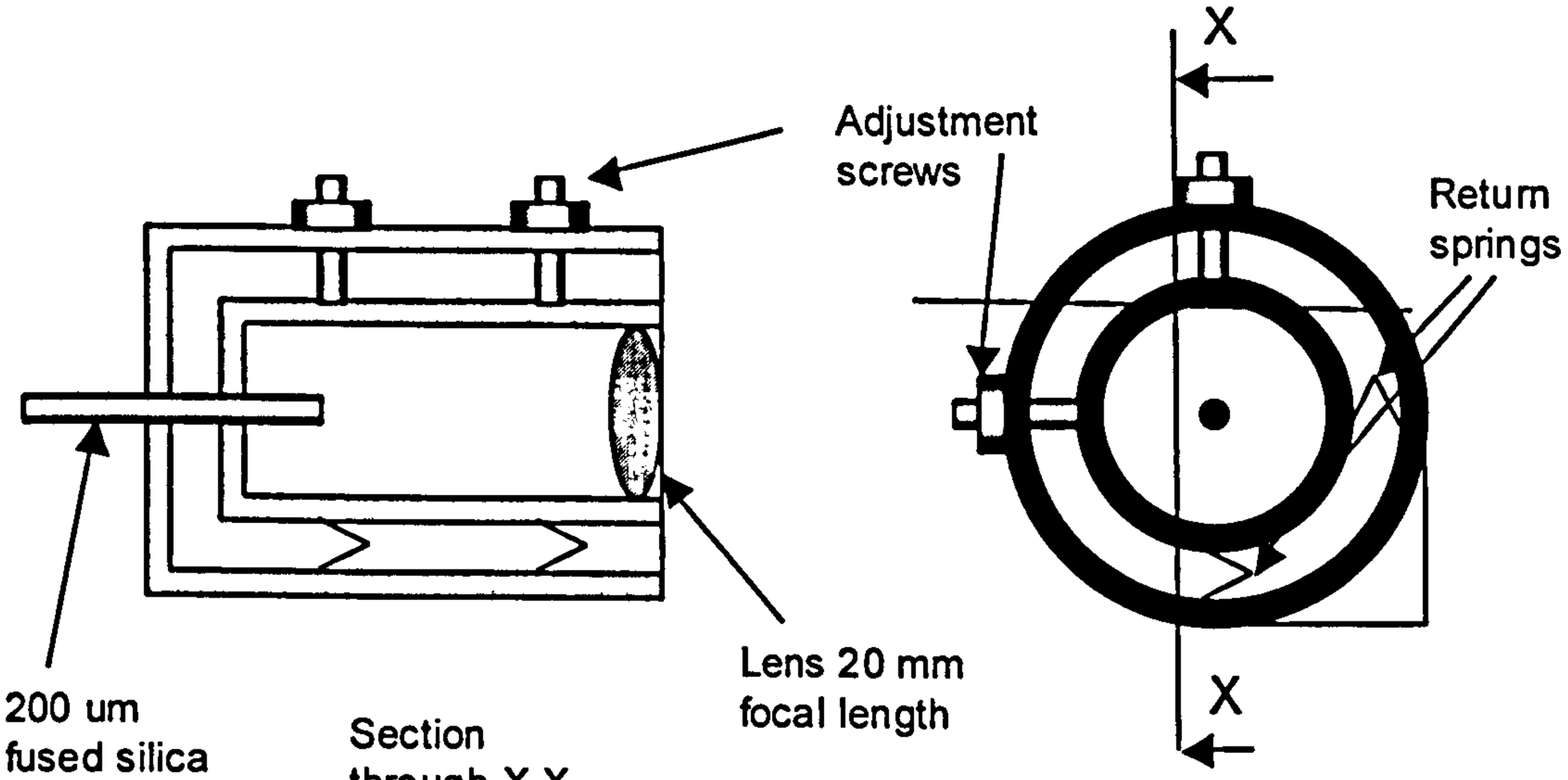

Figure 6.8 Schematic of 'core monitor' assembly

Figure 6.9 shows a photograph of this device mounted inside the head of the 2kW Lumonics MultiWave™ Nd:YAG laser.

Both the CPM and core monitors, by virtue of them being positioned on the same axis as the laser beam gather process light directly from the centre of the laser-material interaction zone.

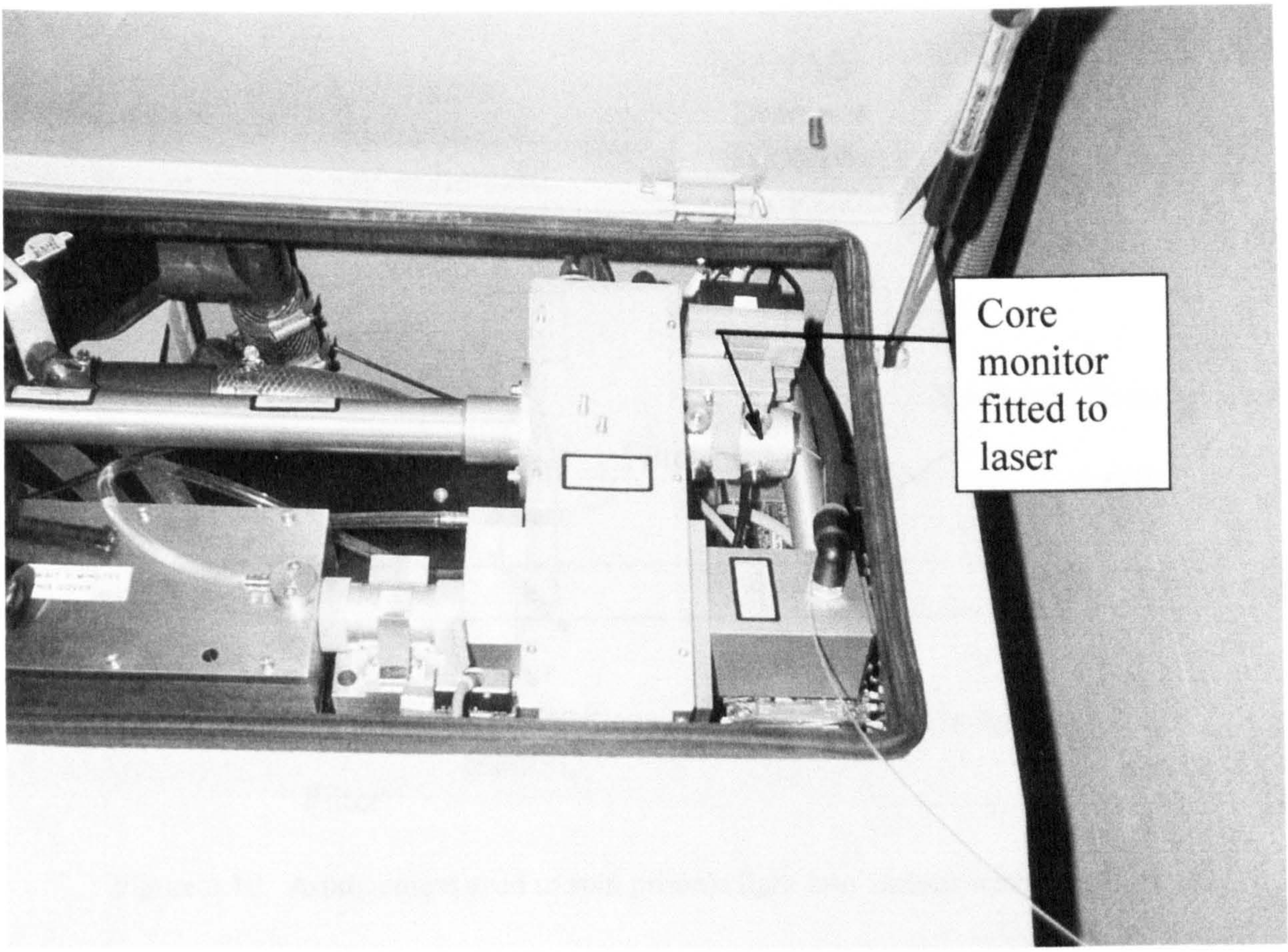

Figure 6.9 Location of Core monitor within laser

6.3 Sensing Equipment

Process light, collected by the optical sensors was delivered to a wavelength splitter arrangement via their respective optical fibres, see figure 6.10. The optical splitter allowed the process light to be split into three wavelength ranges, given the following names for convenience; Nd:YAG = 1064nm, IR = >1100nm and UV/Visible = < 900nm.

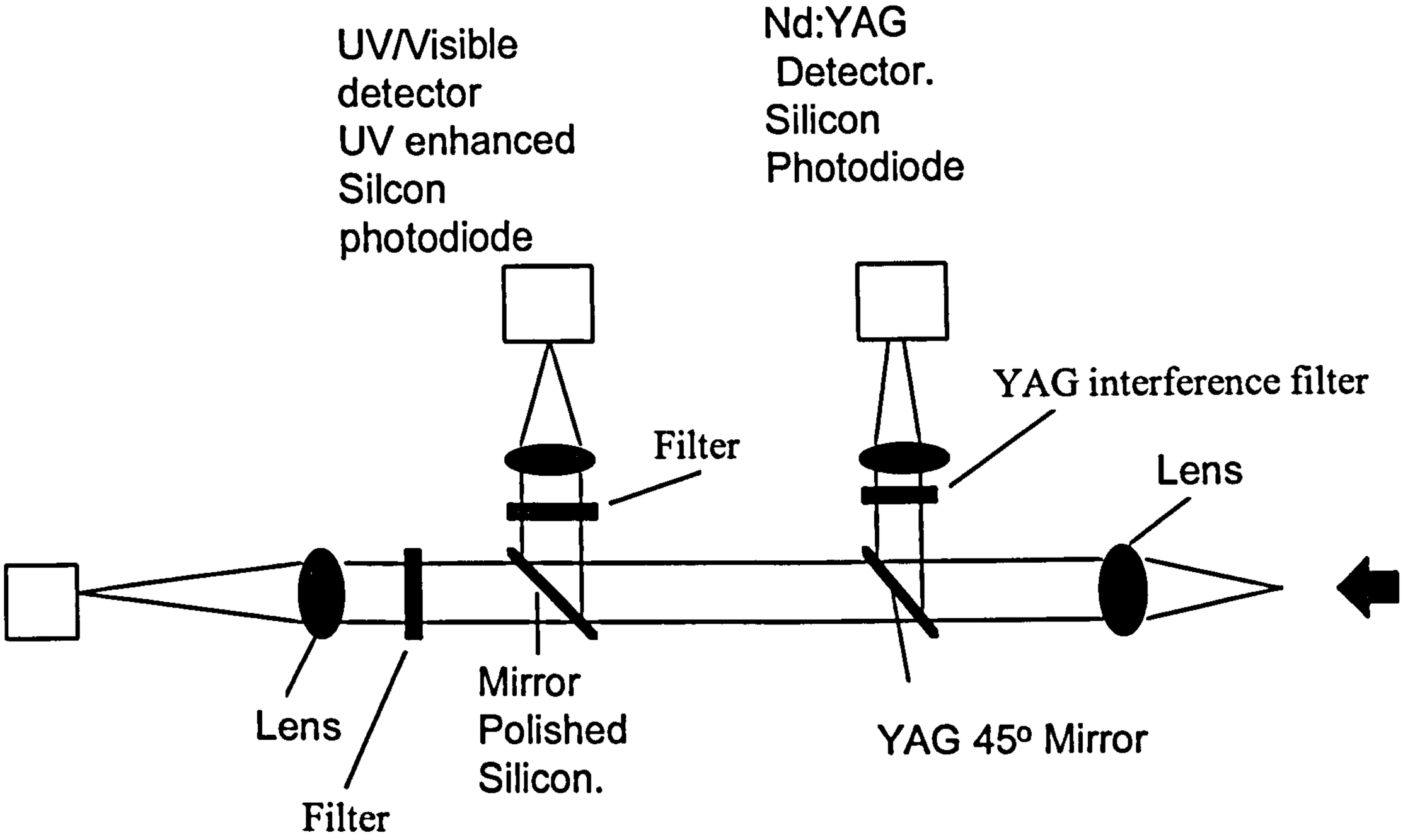

Figure 6.10. Arrangement used to split process light into various wavelength ranges.

After leaving the monitor fibre optic, a lens was used to collimate the light (note: complete collimation was not possible as the light from the process was not monochromatic). The collimated beam was firstly intercepted by a 45° mirror coated to reflect radiation at a wavelength of 1064nm which was used to reflect laser radiation through an interference filter centred on a wavelength 1064nm with a band width of 10nm through a microscope objective onto a silicon photodiode. The light in the UV/ visible range, having passed through the YAG mirror, was then reflected at 45° by a silicon mirror (0.5mm thick, polished on both sides 1μm using diamond paste). A coloured glass filter was used to remove radiation with wavelength greater than 700nm then the beam was focused onto a UV enhanced silicon diode using a microscope objective. Radiation with wavelengths of >1.1μm passed through the silicon mirror and was focused onto an Indium Gallium Arsenide (InGaAs) photodiode using a microscope objective. The actual layout of the wavelength splitter is shown in figure 6.11. Voltage signals from all the

photodiodes were subject to amplification prior to recording on either a digital oscilloscope or a PC based data acquisition system (Compuscope).

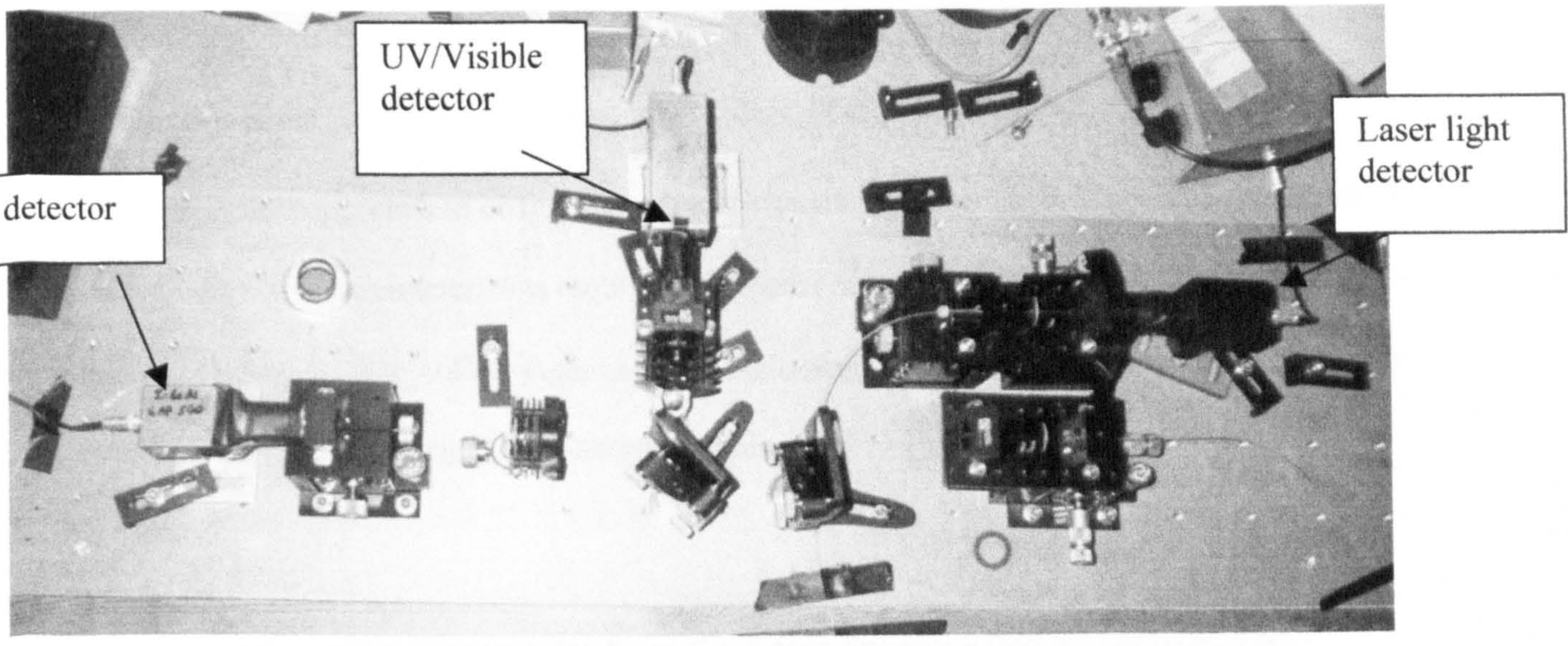

Figure 6.11 Photograph of wavelength splitter apparatus

7 Experimental Trials to Observe the Temporal Behaviour of Optical Signals from the Laser Beam Interaction Zone

7.1 Introduction

By far the simplest approach to observing radiated signals from the work-piece, and one which is most conducive to the characteristics required of process monitoring for industrial applications, as outlined in chapter 5, is to collect them using a single simple sensor viewing the interaction zone as a whole. This effectively gives an integrated view of the interaction zone radiation.

7.2 Observation of Optical Spectra from the Laser Process using a Spectrometer

7.2.1 Objectives

These experiment were carried out primarily to determine the characteristics of the light signature from the Nd:YAG laser process, as this would have an influence on the choice of sensors for in-process monitoring.

7.2.2 Experimental Trials

An Jarrell-Ash optical monochromator with a 450 blaze grating at 150 gratings per mm was used to collect light signals from the beam interaction zone under a number of conditions to determine the spectra of the process at various intensities. The spectrometer was configured with a 400μm diameter fused silica fibre of 2 metres in length, which allowed light from a distance to be collected from a localised zone. The spectrometer system was fitted with a multi-channel optical analyser (Alton Instruments Corp, LAMDA^{TM} LS-2000 series). This was a PC software based system based on a 2048 element silicon based, linear Photodiode Charge Coupled Device

(PCCD) detector which is positioned in the diffracted beam within the monochromator. This system allowed high speed capture of spectral distributions in the wavelength range 200 to 1100nm the sensitivity of the detector although outside of the range 400 to 950nm the detector is diminished response and could not therefore pick up the laser wavelength. Calibration of the monochromator was achieved by using a number of sources with known wavelength i.e. mercury lamp, helium neon laser.

The optimum laser focus position relative to the work piece surface was found prior to carrying out experimental trials. This was done by producing a series of bead-on-plate welds on 1.0mm thick mild steel, at constant power and speed settings and varying the focus position, using a linear Z-axis, relative to the plate surface. The optimum focal position was the one that gave the fullest weld penetration through the plate.

Two methods of detection were used; off-axis detection and core monitor detection. To collect the signal the spectrometer fibre was mounted in a specially constructed fixture together with a 100mm focal length cemented achromat imaging lens positioned 140mm from the fibre and 400mm from the interaction zone so as to image a small area of approximately 2.8mm around the laser interaction zone.

With the side detector arrangement a white light source was shone back through the spectrometer to emerge at the distal end of the fibre to be focused by the achromat lens. The point of focus for white light was relatively easily seen in low light conditions and could be accurately positioned relative to the diode targeting laser from the Nd:YAG laser source, to image the area coincident with the laser interaction point. The off axis detector was positioned in such a way as to view at an angle of 60^0 from the vertical.

In addition, for comparison, signals were captured from the plume above the work piece close to the work piece surface by placing the off axis detector in a position behind the laser beam interaction zone parallel with the work piece surface. The image height above the surface was determined by again imaging a white light source this time onto the surface of the graduations on a height gauge.

The core monitor was specially adapted to accept the spectrometer fibre to allow light from the interaction zone travelling back up the core of the main beam delivery to be collected by the Core Monitor and spectrometer. In this way the spectrometer signal was sampled directly on axis with the laser beam and the interaction point.

Melting of the target material was carried out using a number of different laser sources including 2kW and 4kW continuous wave Nd:YAG and 2kW carbon dioxide lasers.

7.2.3 Results of Spectrometer Trials

All results presented have been corrected for the spectral response of the silicon based PCCD detector and are presented as intensity levels on the detector array.

Figures 7.1 and 7.2 show typical spectra from welds made in mild steel using the 2kW Nd:YAG laser source at two travel speed conditions; 2 and 4m/min . Each speed produced a good weld with smooth top and under bead and full penetration through 1.0mm sheet material using argon to protect the melt-pool from oxidation.

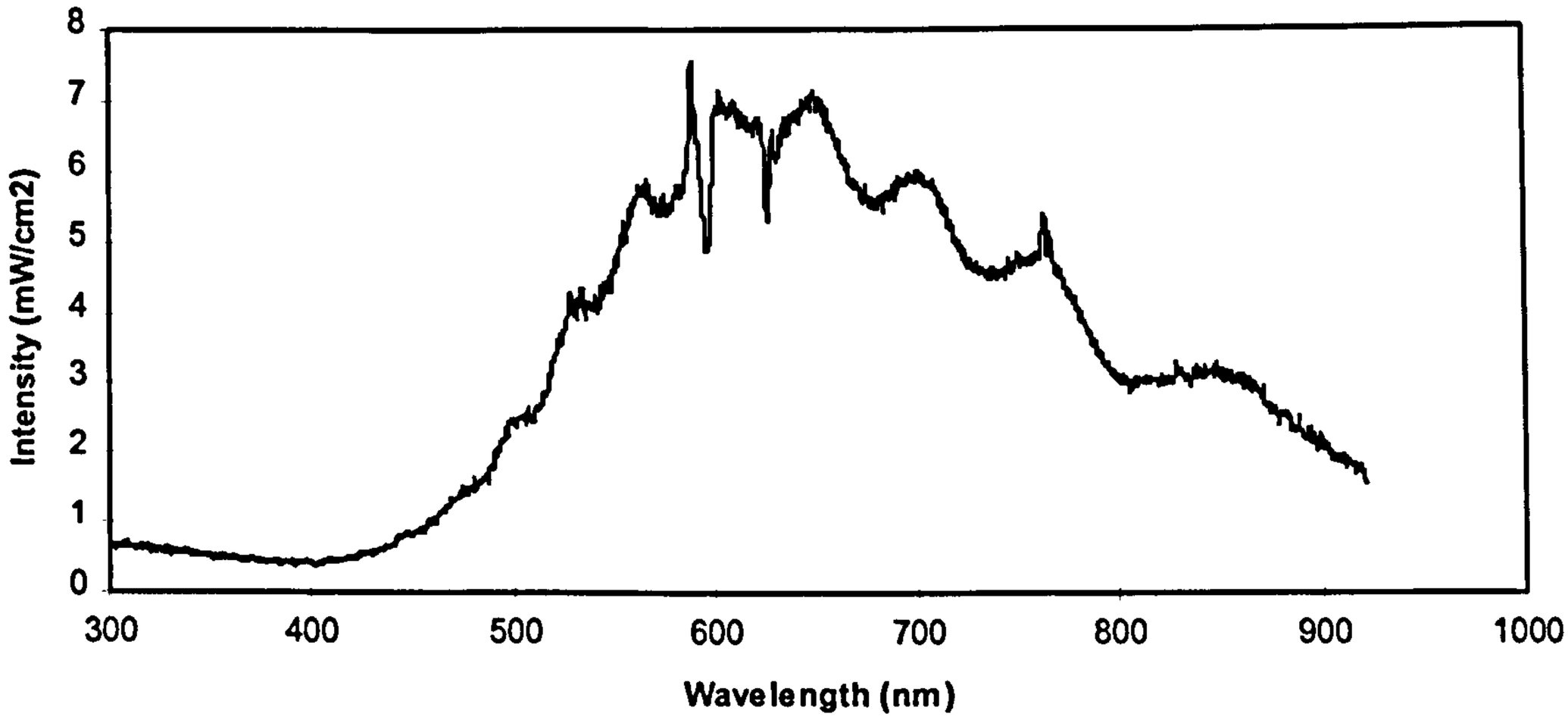

Figure 7.1 Spectral distribution of light from a 1.0mm thick mild steel sheet welded with a CW Nd:YAG laser at 2kW and 2m/min and argon gas shielding. Off-axis detector.

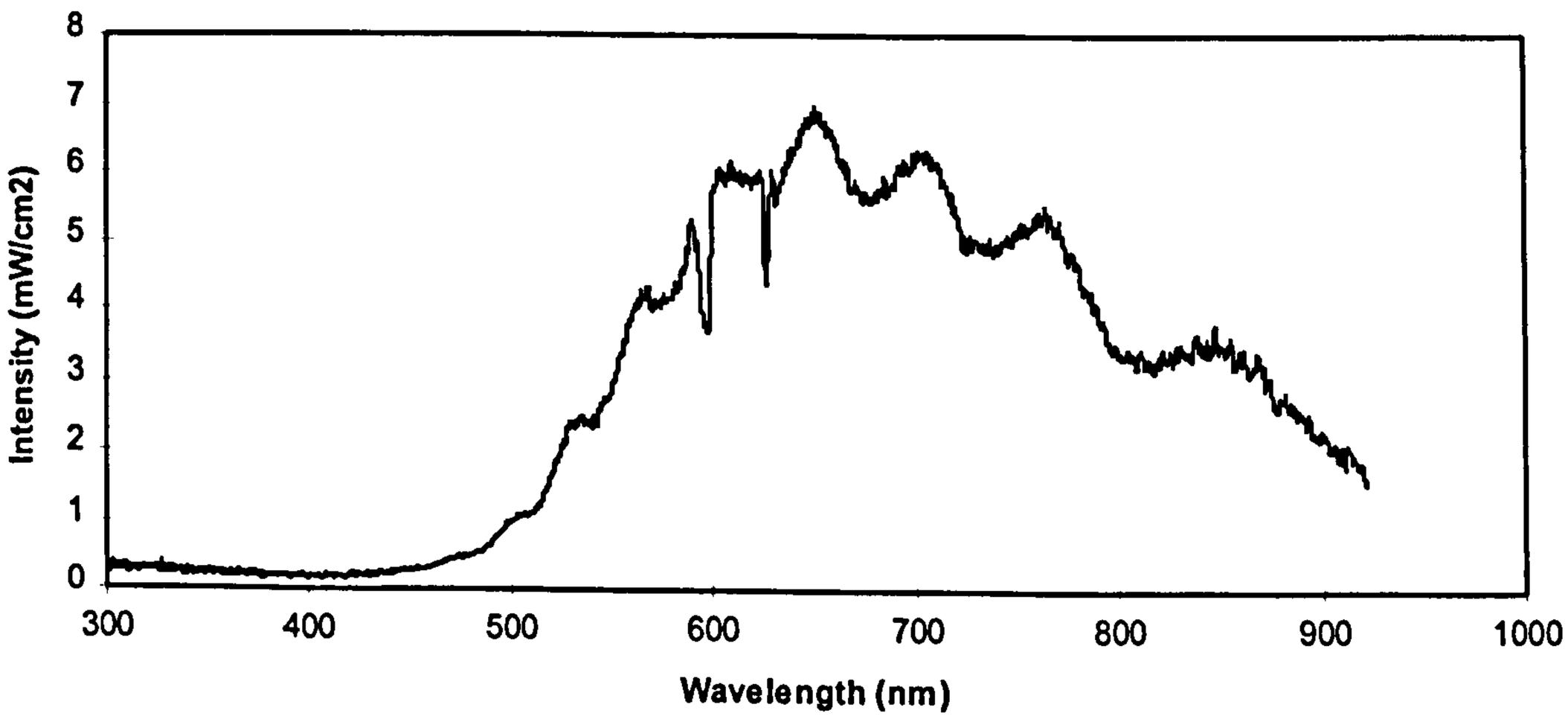

Figure 7.2. Spectral distribution of light from a 1.0mm thick mild steel sheet welded with a CW Nd:YAG laser at 2kW and 4m/min and argon gas shielding. Off-axis detector.

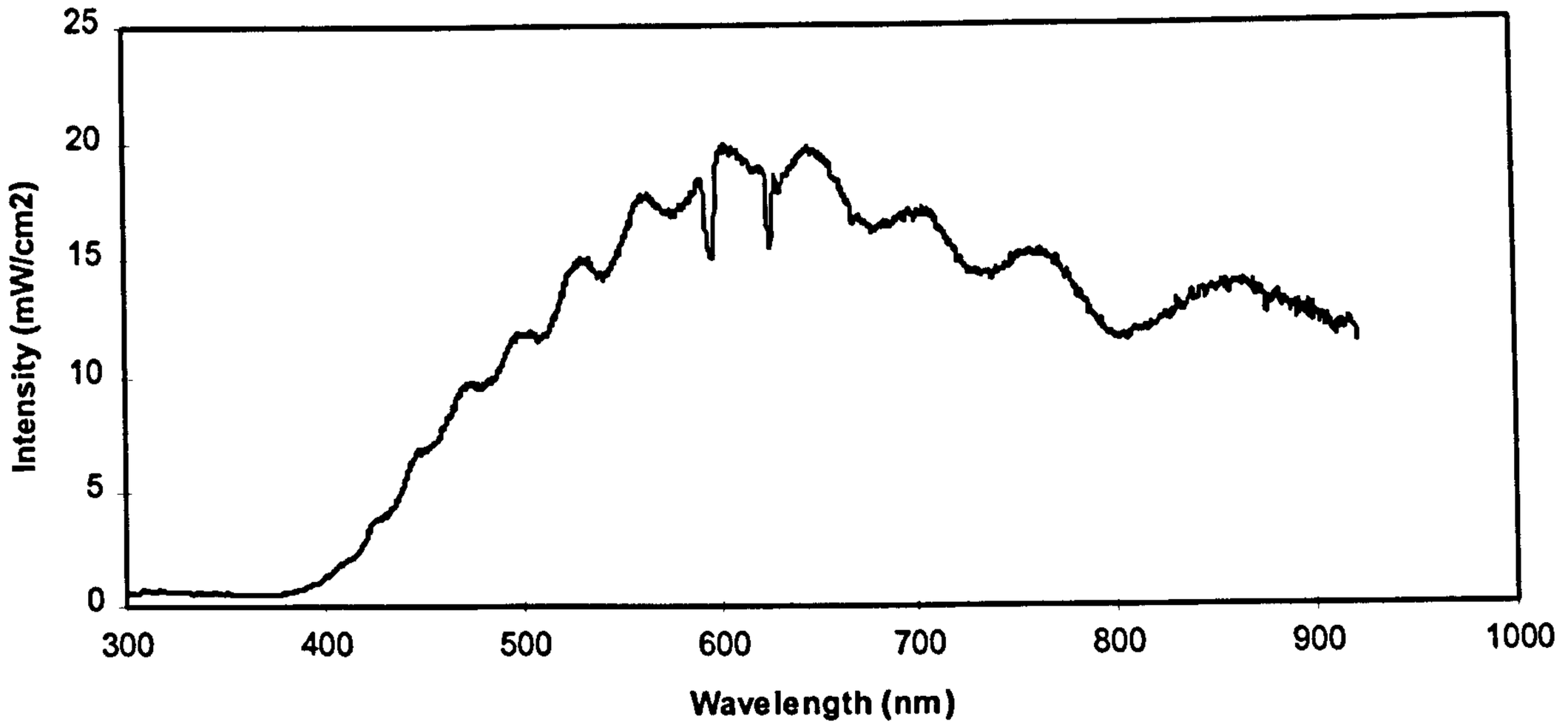

Figure 7.3 Spectral distribution of light from a 1.0mm thick mild steel sheet welded with a CW Nd:YAG laser at 2kW and 4m/min with helium gas shielding. Off-axis detector.

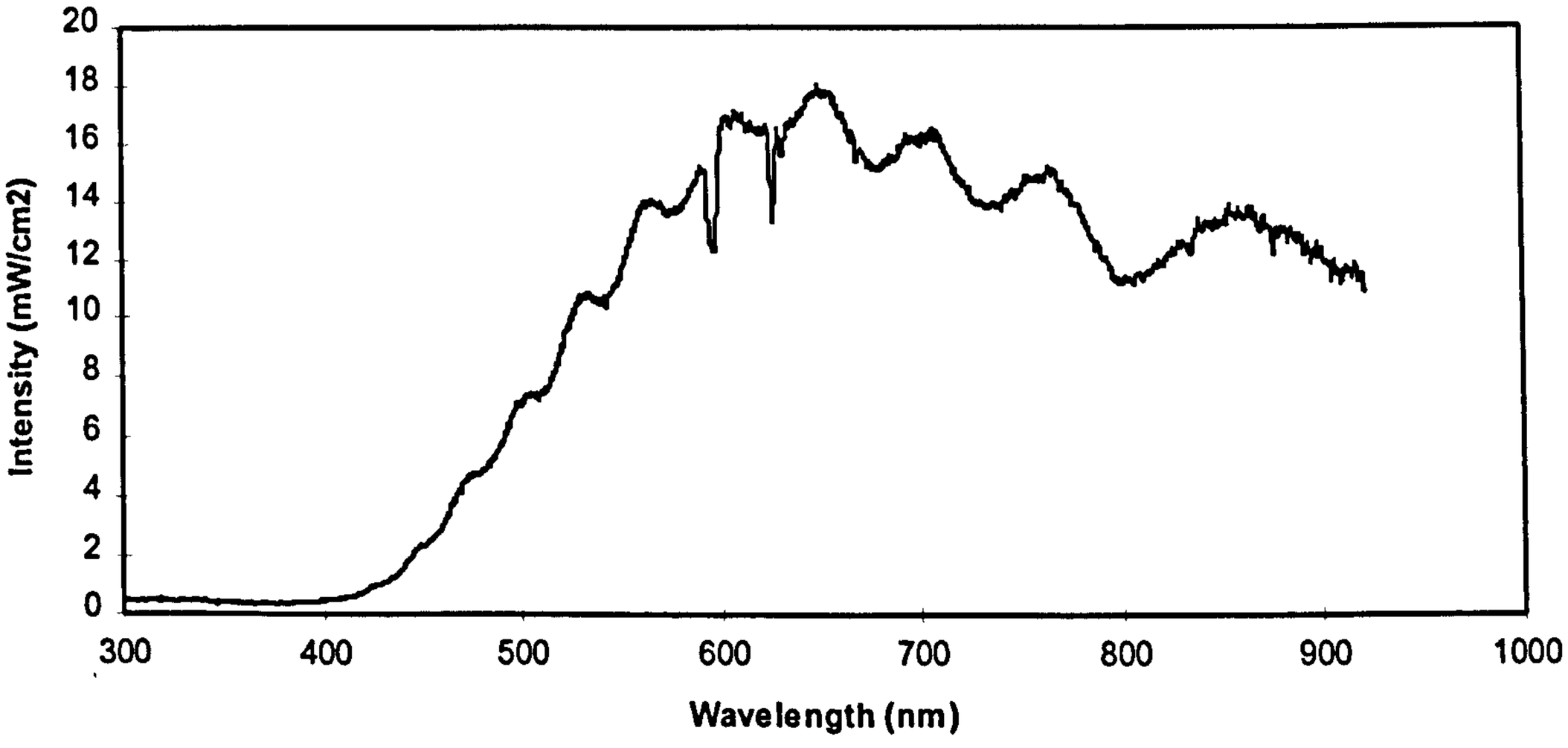

Figure 7.4. Spectral distribution of light from a 1.0mm thick mild steel weld made with a CW Nd:YAG laser at 2kW and 4m/min with nitrogen gas shield. Off-axis detector.

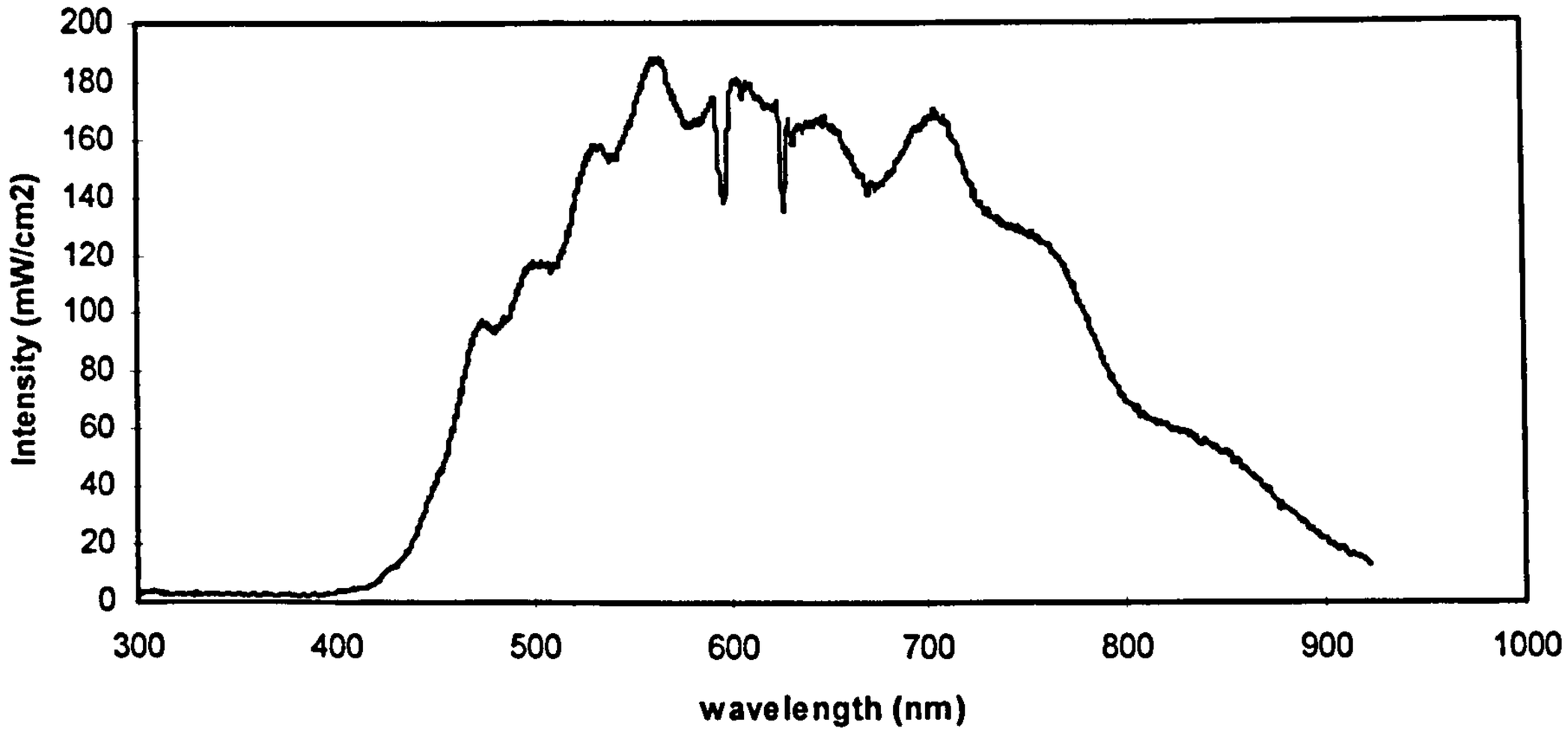

Figure 7.5. Spectral distribution of light from a 1.0mm thick mild steel sheet weld made with a CW Nd:YAG laser at 4kW and 12m/min with helium gas shield. Off-axis detector.

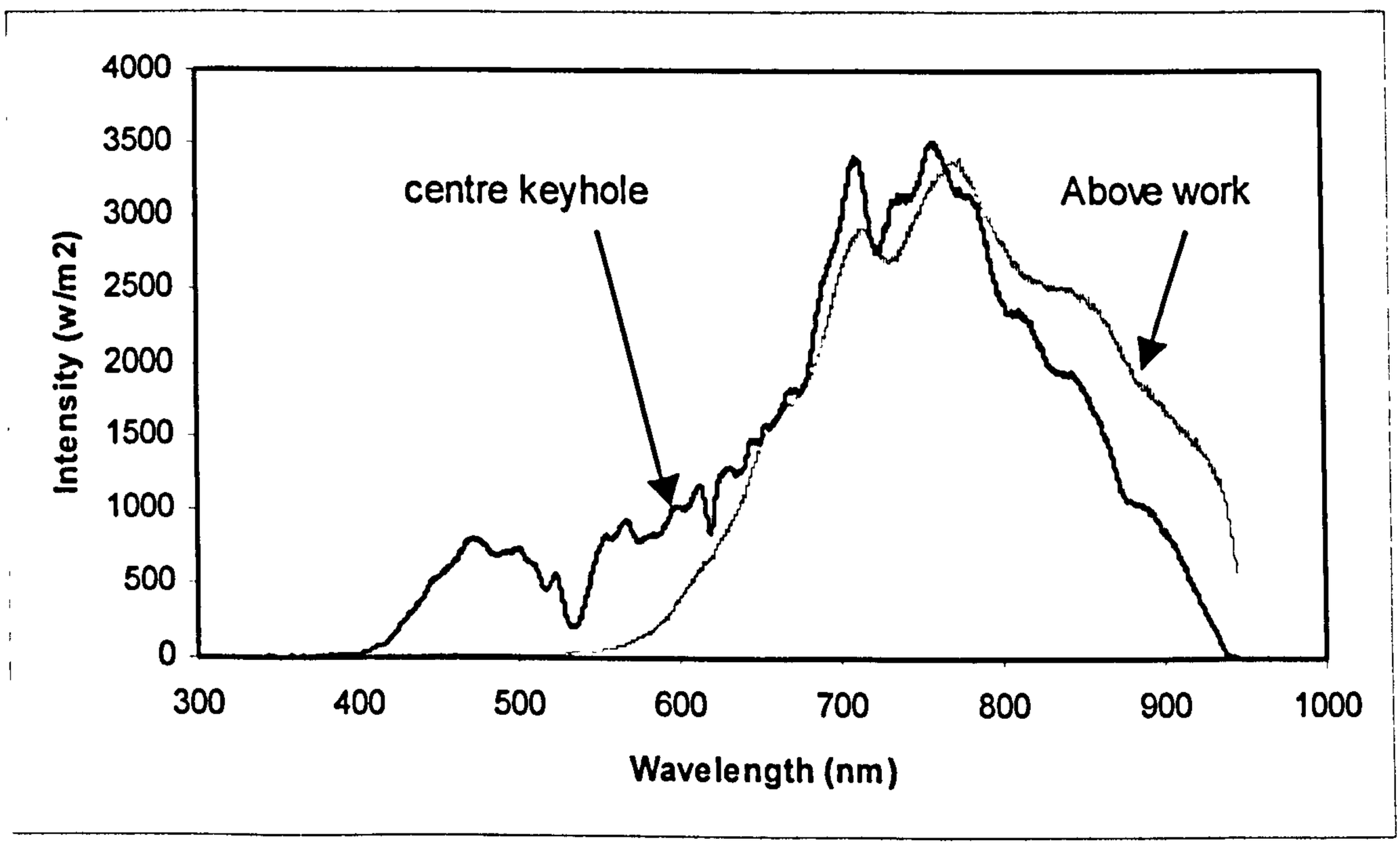

Figure 7.6. Spectral distribution from1.0mm thick mild steel sheet using a CW Nd:YAG laser at 2kW and 4m/min with argon gas shield. Viewed from side, 4.3mm above work-piece surface and through the core monitor

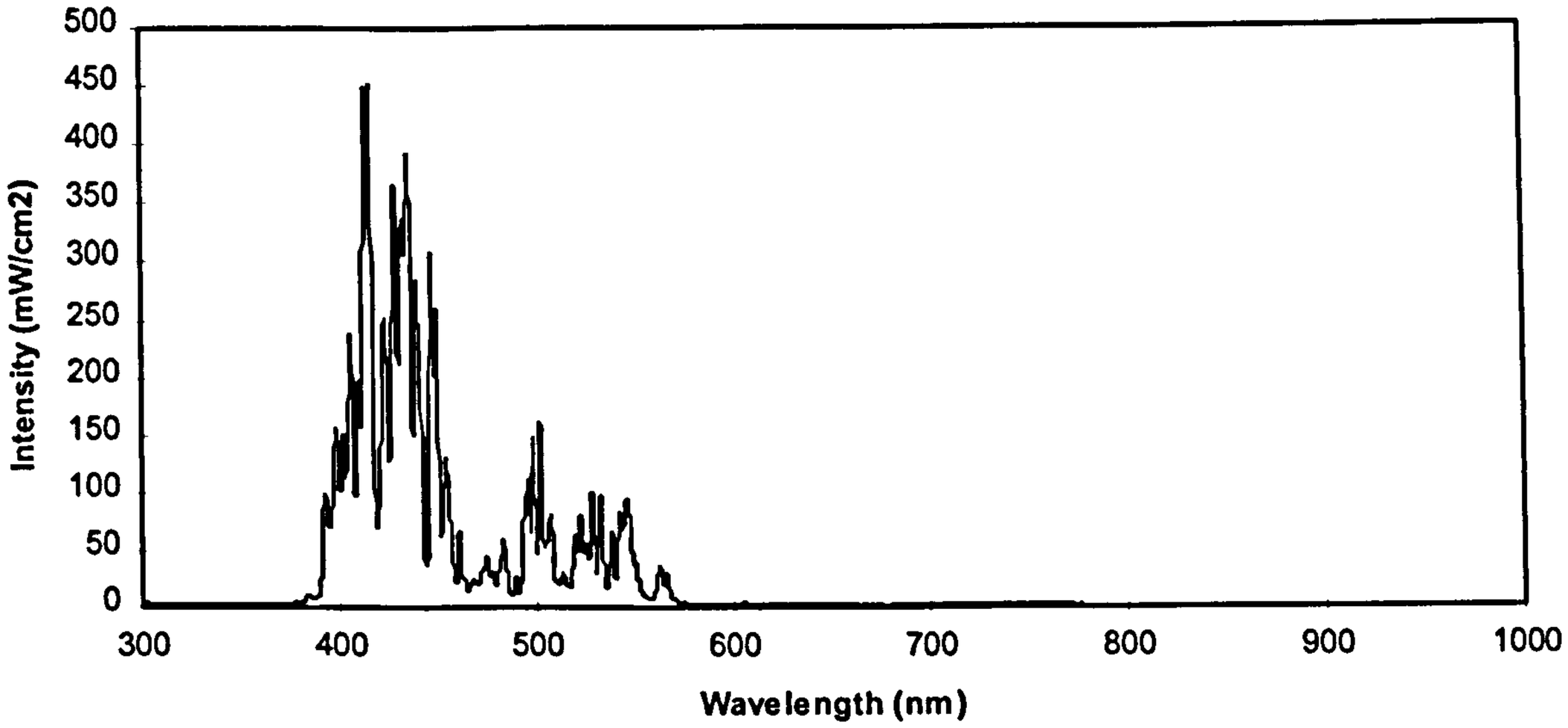

Figure 7.7. Spectral distribution of light from a 1.0mm thick mild steel sheet welded with a CW Carbon Dioxide laser at 2kW and 4m/min with helium shield gas. Off-axis detector.

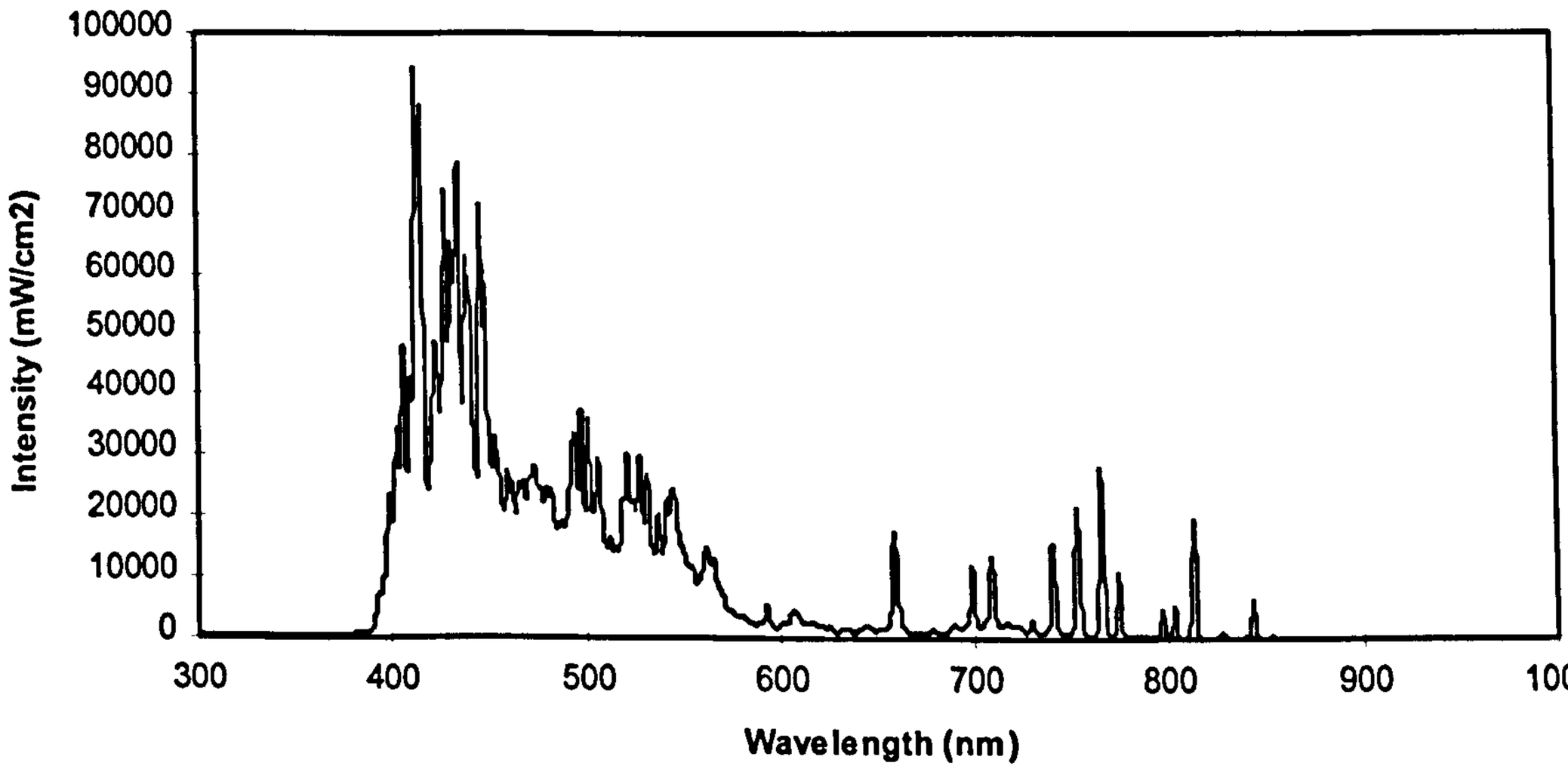

Figure 7.8 Spectral intensity distribution from mild steel welded with a carbon dioxide laser at 2kW and 5m/min. Argon shield. Off-axis detector.

7.3 Validation of Process Monitoring by Sensing Through the Fibre Optic Beam Delivery

7.3.1 Objectives

The objective of this set of experiments was to capture the temporal characteristics of the signal measured in the return leg of the cladding power monitor to determine whether the signals observed were representative of processes occurring at the work-piece. Actual events occurring at the work piece related to signals picked by the sensor were not easily determined during welding so a statistical approach was adopted in an attempt to positively determine that signals were indicating events occurring at the work-piece and not just a characteristic of the beam delivery.

7.3.2 Experimental Procedure

A cladding power monitor of core diameter 1.0mm and monitor fibre diameter 200μm was fitted to a Lumonics JK 702H, 350W pulsed Nd:YAG laser, using a 17mm beam collimation and 60mm focus lens to focus the beam into the core of the fibre.

A single silicon diode arrangement with fixed amplification was positioned at the output end of the return leg of the monitor fibre with the output end butted to the glass window of the detector aligned with the diode junction. A digital storage oscilloscope was used to capture the returned signals. Initially a pulse was taken without any target to determine the signal amplitude associated with the beam delivery.

A 50mm x 50mm x 0.7mm thick copper (C100) coupon, bright and free from surface scale, with surface roughness R_a in the x and y direction of 5.5μm and 6.5μm respectively was marked off

into 10 rows and 10 columns of equally sized squares across one of its surfaces. The copper coupon was placed under the focusing optics at the output end of the beam delivery fibre, at the waist position of the laser beam. The waist was located by taking burns in kapton film.

Each row of squares was exposed to an increasing number of shots from the laser i.e. row one was exposed to one shot, row two, 2 shots, row three shots etc. using the pulse parameters 5.5ms, 25J, 10.0Hz. These parameters were optimised so as not to produce melting on the first shot. After exposure each sector was examined under an optical microscope for signs of melting. Where melting had occurred, the diameter of the molten zone was measured using a calibrated graticule on a microscope eyepiece, at a magnification of 100x. In addition multiple shot welds were produced on the surface of a mild-steel plate.

7.3.3 Results

The signal level without a target was found to be between 0.02 and 0.035 volts per kW laser peak power. Typical returned signal values at the same peak power were between 1.7 and 3.5 volts per kW with the same electrical amplification. This gives a signal to noise ratio of between 70 and 85. This gives a good indication that the detector is capable of discriminating between background signal levels associated with reflections from optical faces, such as the cover slide, focusing lenses and output end of the fibre.

Table 7.1 shows the results of measurements taken at the surface of the copper coupon after exposure to the laser.

Position	Column1	2	3	4	5	6	7	8	9	10
Row 1	No Melt	No Melt	No Melt	No Melt	No Melt	No Melt	No Melt	No Melt	No Melt	No Melt
2	No Melt	No Melt	No Melt	No Melt	No Melt	No Melt	No Melt	No Melt	No Melt	No Melt
3	No melt	ϕ0.04 mm	ϕ0.068 mm	No melt	ϕ0.108 mm	No melt	ϕ0.04 mm	No melt	No melt	No melt
4	ϕ0.075 mm	ϕ0.025 mm	ϕ0.22 mm	ϕ0.2 mm	ϕ0.46 mm	ϕ0.090 mm	ϕ0.025 mm	ϕ0.08 mm	ϕ0.14 mm	No melt
5	No melt	ϕ0.04 mm	ϕ0.07 mm	No melt	ϕ0.118 mm	No melt	ϕ0.05 mm	No melt	No melt	No melt
6	ϕ 0.13 mm	ϕ0.25 mm	ϕ0.33 mm	ϕ0.27 mm	ϕ0.43 mm	ϕ0.45 mm	ϕ0.35 mm	ϕ0.35 mm	ϕ0.23 mm	ϕ0.38 mm
7	ϕ0.39 mm	ϕ0.16 mm	ϕ0.41 mm	ϕ0.44 mm	ϕ0.51 mm	ϕ0.45 mm	ϕ0.04 mm	ϕ0.45 mm	ϕ0.35 mm	ϕ0.3 mm
8	ϕ0.24 mm	ϕ0.33 mm	ϕ0.5 mm	ϕ0.42 mm	ϕ0.45 mm	ϕ0.52 mm	ϕ0.13 mm	ϕ0.21 mm	ϕ0.45 mm	ϕ0.45 mm
9	ϕ0.35 mm	ϕ0.38 mm	ϕ0.54 mm	ϕ0.5 mm	ϕ0.42 mm	ϕ0.52 mm	ϕ0.41 mm	ϕ0.36 mm	ϕ0.35 mm	ϕ0.10 mm
10	ϕ0.39 mm	ϕ0.23 mm	No melt	ϕ0.54 mm	ϕ0.31 mm	ϕ0.48 mm	ϕ0.46 mm	ϕ0.04 mm	ϕ0.38 mm	ϕ0.43 mm

Table 7.1 Measurements taken of melt zones on the surface of a copper coupon exposed to an increasing number of laser pulses

From table 7.1 it can be seen that the probably of melting of the copper plate surface with just two shots was nil and the probably of melting occurring after more than five shots was virtually

100%. Between 3 and 5 shots the chances of melting occurring every time was between 40 and 90%.

Figure 7.9 shows a typical sequence of sensor output for a series of 10 shots onto the copper target.

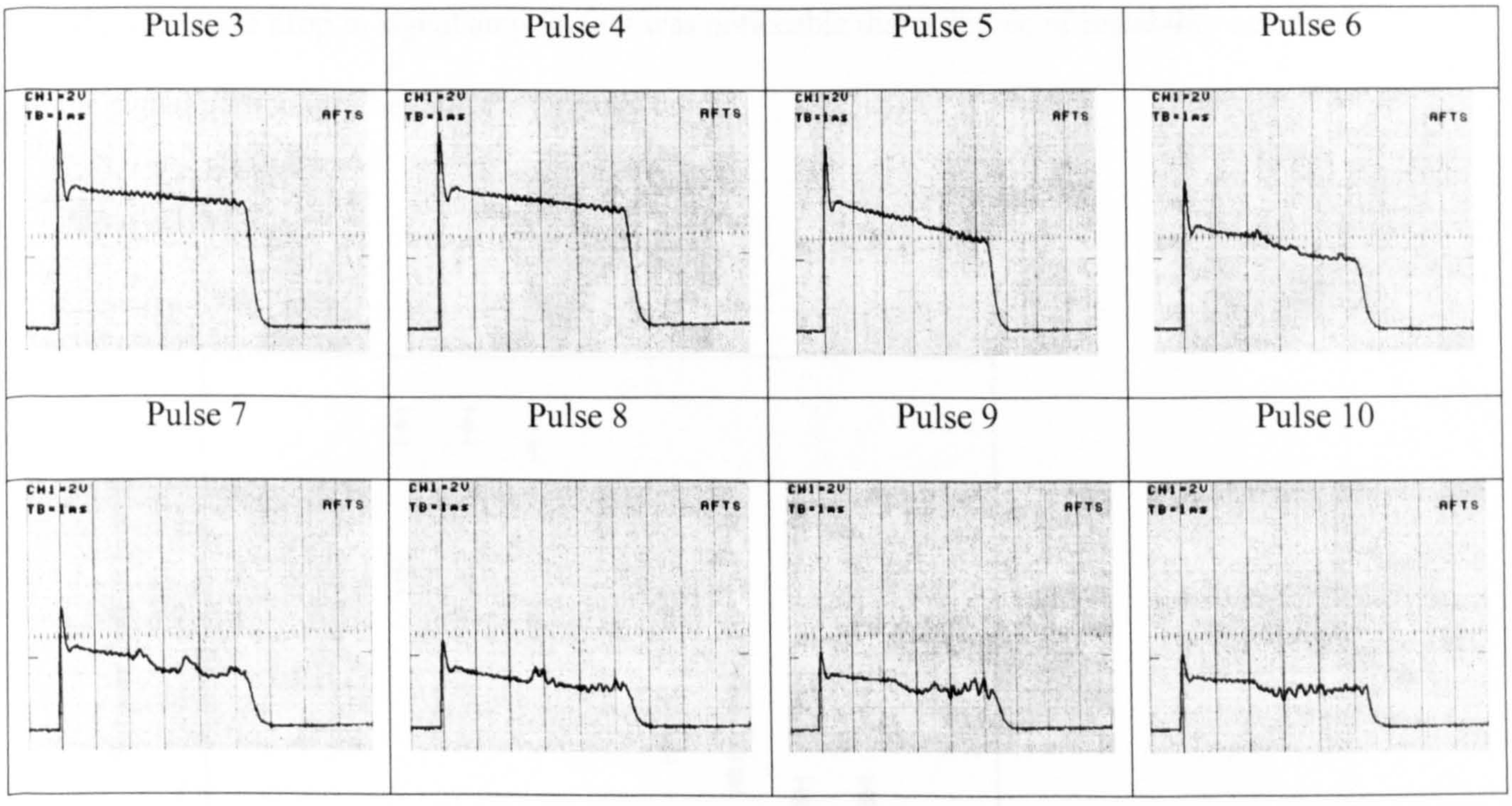

Figure 7.9 Typical sensor output for a sequence of laser pulses during spot welding of copper target

To assist in the understanding of the changes in the signal that have taken place in the peak and average signal the amplitude of sensor output has been plotted in figure 7.10. It can be seen that the amplitudes of the peak value at the initial part and the final part of the returned signal decreases from a steady state were there is a very low probability of melting occurring to a lower steady state were there is virtually 100% probability of melting.

In addition to the drop in signal amplitude it was noticeable that a degree of instability occurred in the signal particularly beyond the halfway point.

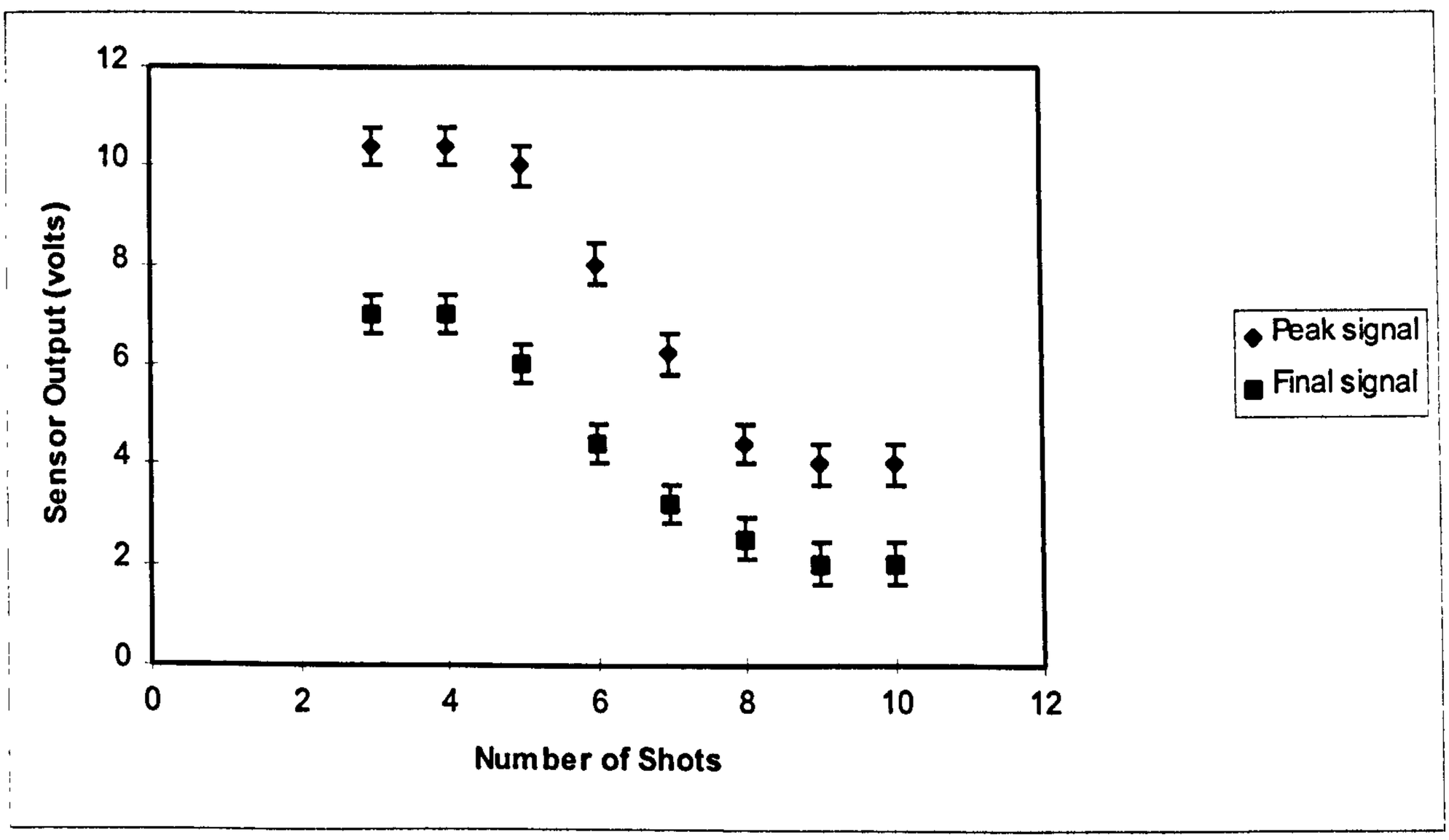

Figure 7.10 showing the amplitude of sensor output for spot welds made with a number of shots

Of particular interest is that this instability appears to have periodicity of 0.286ms associated corresponding to a frequency of 3500Hz.

Mild steel was more easily melted even at quite low peak power and power density at the work-piece.

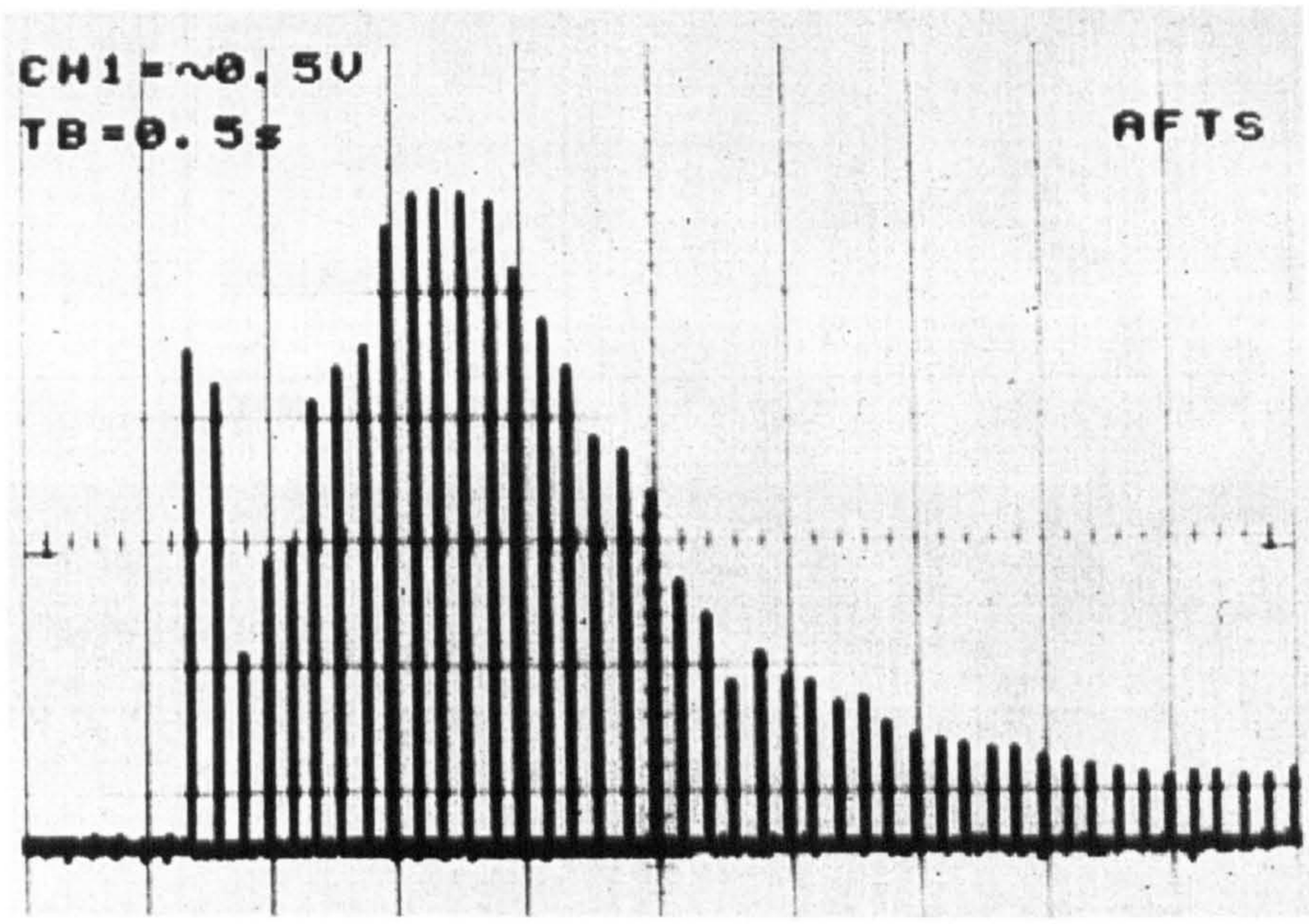

Figure 7.11 relative amplitude of signals observed during spot welding of a mild steel.

.

It can be seen from figure 7.11 that initially as the laser shutter is opened the sensor signal is high; it then reduces, rises again to then reduce to become steady state. This was found to be typical of behaviour when multiple shots were used to produce spot welds.

By selectively delaying the trigger point of the oscilloscope it was possible to capture in detail the characteristics of each pulse, each having experienced the thermal effects of the preceding pulses. These are shown in Figure 7.12.

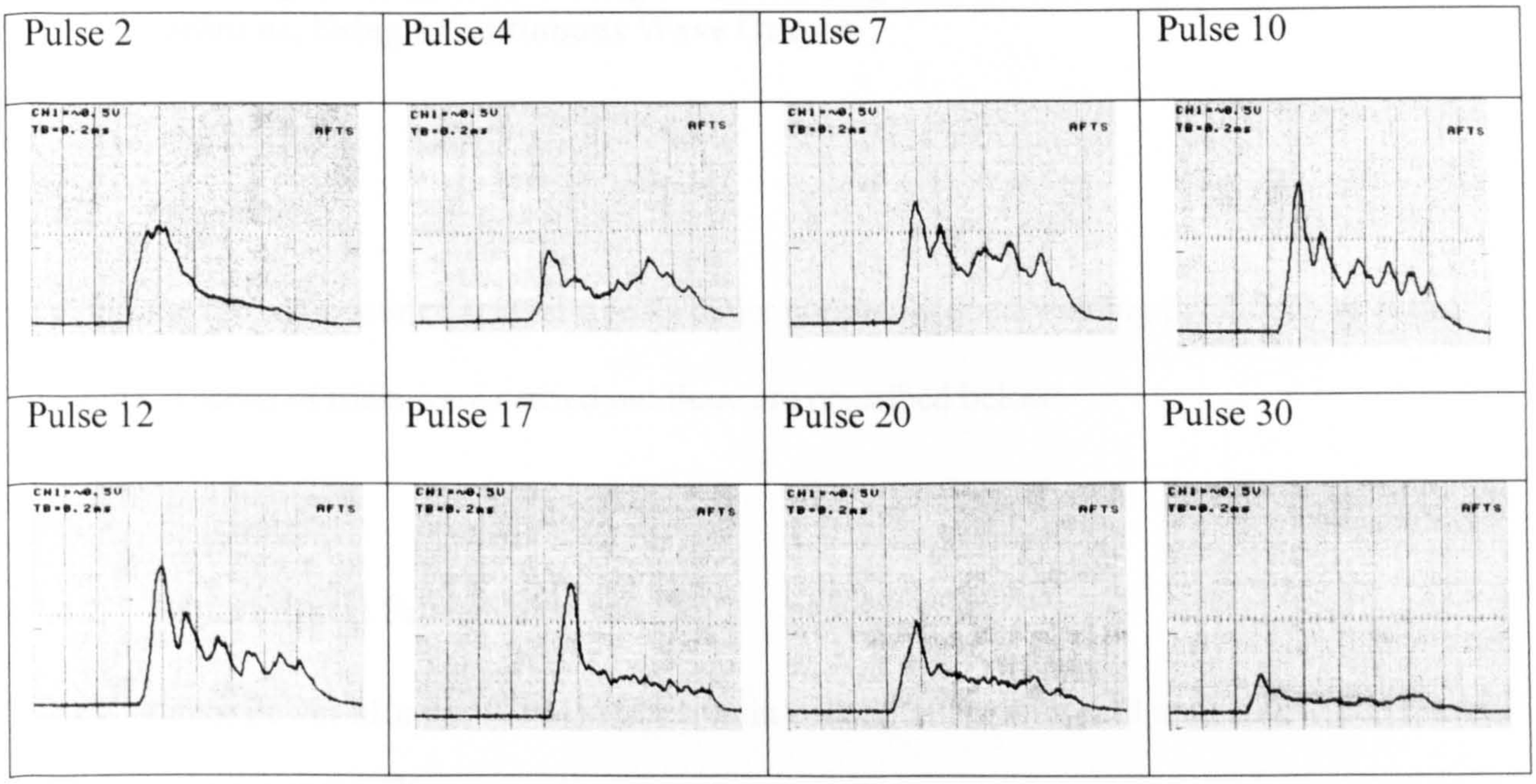

Figure 7.12 Sensor signals from successive pulses producing a spot-weld on a mild steel plate

It can be seen that the early pulse has little or no structure except a high initial peak. This then decays to form a structured pulse with reduced peak and average amplitude. As the pulse amplitude begins to rise again there appears to be an increase in the amount of periodic activity occurring during the pulse. Pulses 10 and 12 show periodic structure of 0.15 to 0.2ms, corresponding to frequencies in the range 5000 – 6700Hz.

7.4 Optical Signal Behaviour During Seam Welding Under Nominally Good Welding Conditions, Using a Continuous Wave Output.

7.4.1 Objectives

To observe the behaviour of several signals under nominally good welding conditions of seam welding, a series of trials were carried out these are described below:

7.4.2 Experimental Procedure

The Cladding Power Monitor (CPM) with 1.0mm core diameter was used with a 2kW continuous wave laser (MultiWave^{TM} 2000). The return fibre from the CPM was connected to the wavelength splitter equipment. The sensors within the splitter were aligned using a bright white light source directed back along the forward-going side of the CPM monitor fibre. The target material was 1.0mm thick mild steel with the beam focused with a 160 and 80mm lens combination giving a 0.5mm focused spot. Argon gas shielding was used to prevent oxidation. This was introduced through an 8mm diameter side pipe, positioned in front of the weld with respect to beam translation relative to the work-piece.

Bead-on-plate welds were also made in the surface of a 4mm thick mild-steel plate at different speeds and laser power to determine the response of the backscattered laser wavelength.

A tapered work-piece with angle 3^0 was used to assess the effect of changing work-piece thickness.

7.4.3 Results

Figure 7.13 shows typical traces of the IR signal and the UV/Visible signal for welds made in 1.0mm thick mild steel sheet material whilst fully penetrating the coupon.

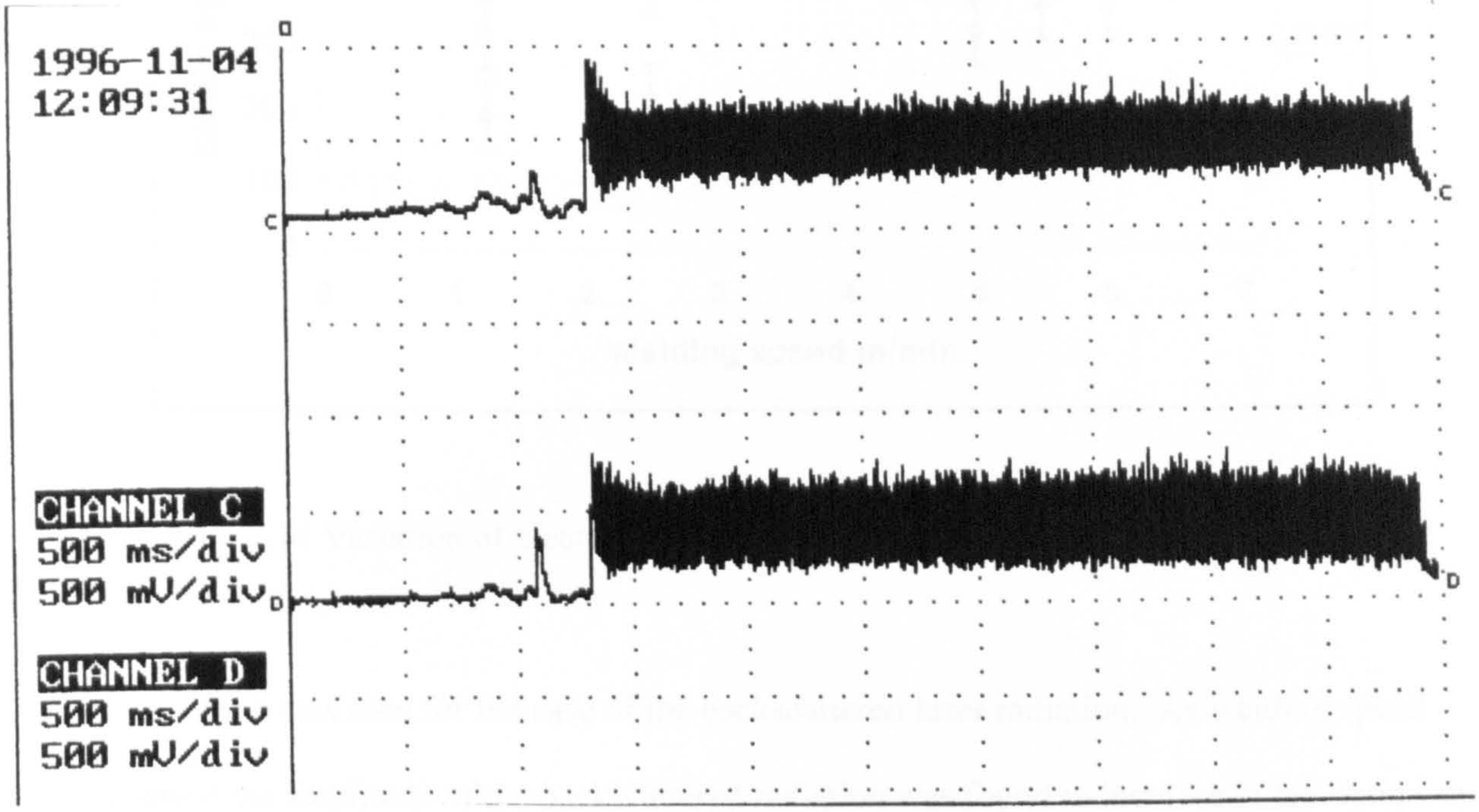

Figure 7.13 Typical IR (channel D) and UV/Visible (Channel C) signal during welding

This signals where found to be highly repeatable under a given set of conditions. A reduction in laser power did produce a reduction in both signal amplitudes. Figure 7.14 shows the behaviour of the UV/visible signal and IR signal for variation in speed.

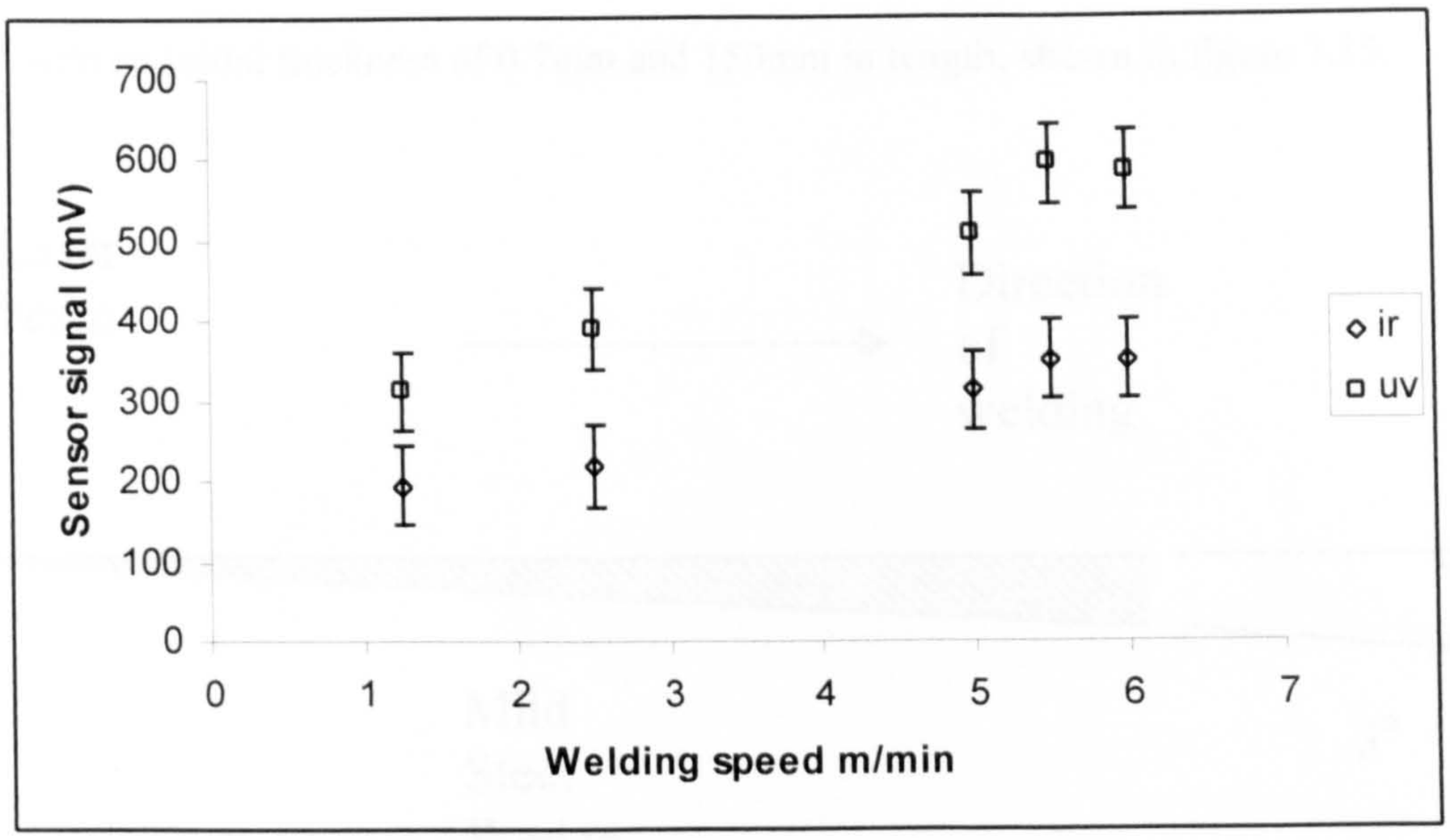

Figure 7.14 Variation of mean UV and IR signal amplitude with welding speed.

A different effect was seen for the case of the backscattered laser radiation. As welding speed was increased the amplitude of the backscattered radiation was found to increase in the same way as the UV and IR radiation signals. However, as power was decreased the backscattered signal was found to increase, opposite behaviour to that of the UV and IR signals.

It was noticeable that the amplitude of oscillation about a mean point increased with decreasing speed for both the UV and IR signals. Of particular note is the high degree of oscillation within the signals even with a nominally stable continuous wave output.

A fast Fourier analysis of these signals under various conditions was carried out and showed, during full penetration at the slower speeds, distinctive peaks of oscillation corresponding to frequencies in the range 2500 – 3500Hz and occasionally, particularly in the UV signal, higher frequencies in the region of 7000Hz

To try to understand the nature of these frequencies welds were made over a tapered steel wedge angled at 3^0 with an initial thickness of 0.7mm and 150mm in length, shown in figure 7.15.

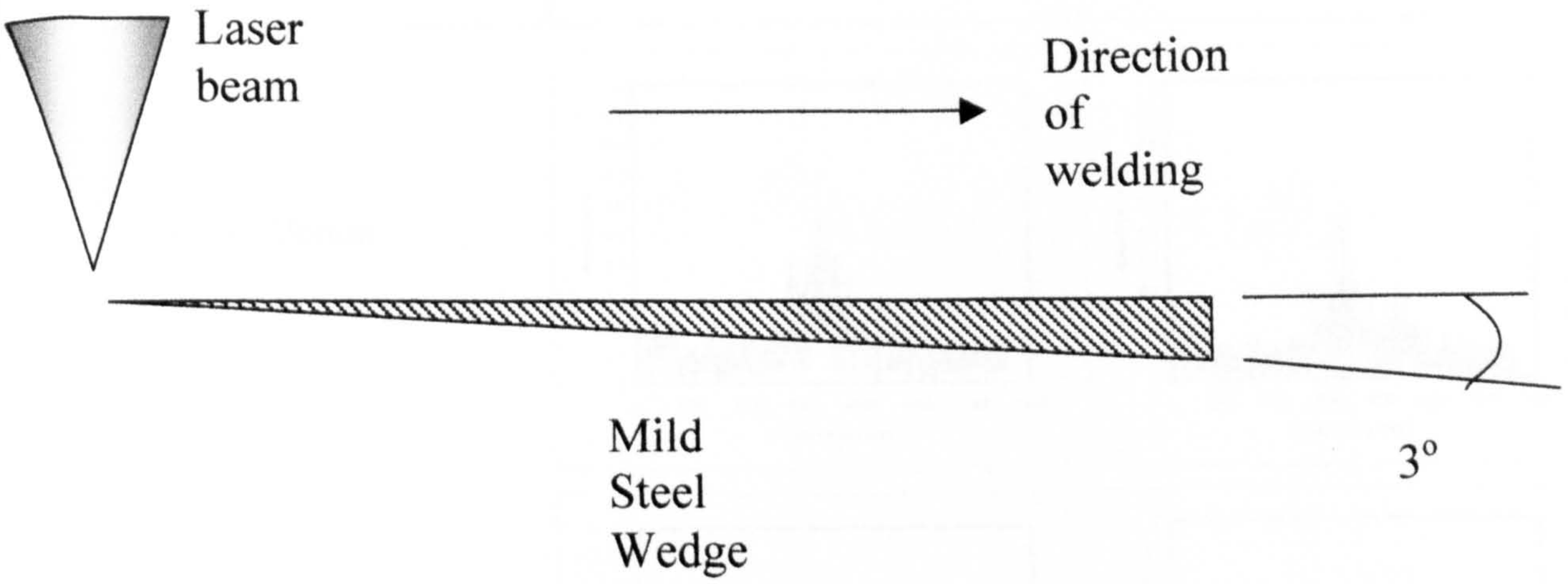

Figure 7.15 Schematic of experimental set-up involving a tapered work-piece

The flat side of the wedge was positioned upper-most so that the beam focus position relative to the work-piece was maintained during translation. This arrangement allowed a weld to be produced over a constantly varying material thickness. The UV and IR signal was recorded through the core monitor during welding. Welds were performed at constant power and varying speed. A Fast Fourier Transform (FFT) was performed on each signal against time, and time-correlated to the thickness of the material under the beam at any one time. The results are shown in figure 7.16 below for two speeds, 3 and 4m/min. The figure shows the characteristic oscillation frequencies observed in the infrared signal. Both UV and IR signals exhibited similar characteristics. It is evident that considerable oscillation is present indicating that there is considerable activity within the keyhole. It is noticeable that within the spectrum of oscillation some frequencies were more prevalent than others, indicated by the peaks. It can be seen from the results that as time elapsed, and thickness increased the maximum oscillation frequency also decreased, moving from approximately 3500Hz to 2000Hz. It is also of note that the oscillation

frequency is approximately the same for both speeds at similar positions along the tapered work-piece.

Time from start of weld (secs)/Thickness (mm)	**Speed 3 m/min**	**Speed 4 m/min**
0.102 secs/0.736mm	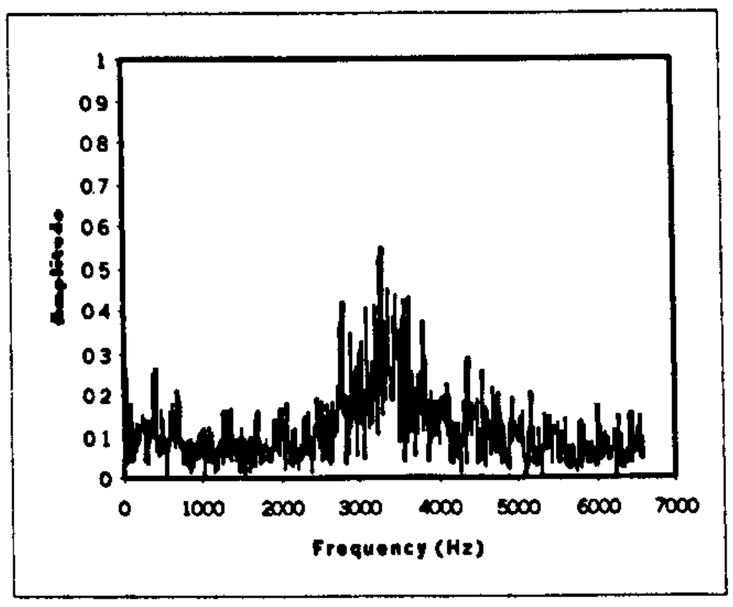	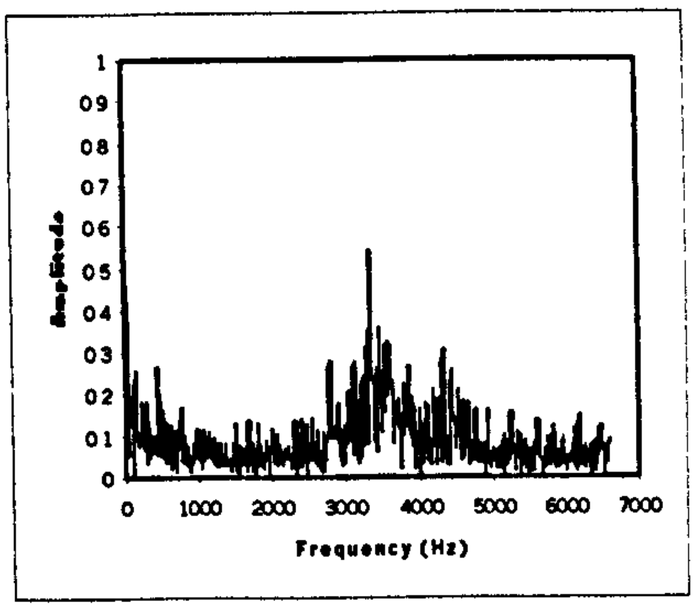
0.307 secs/0.808mm	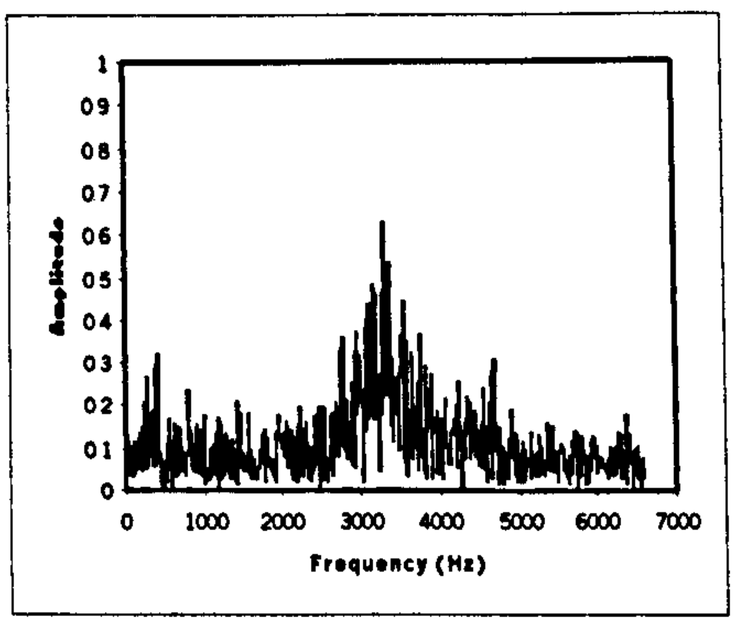	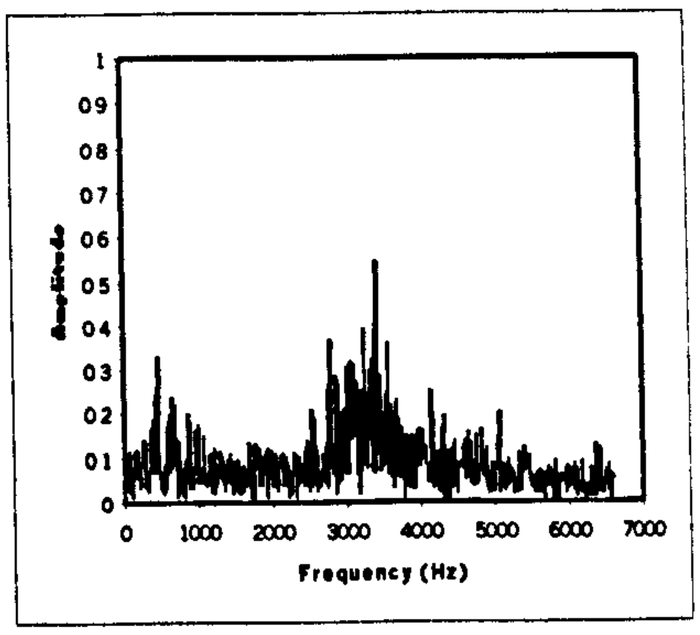
0.614 secs/0.916mm	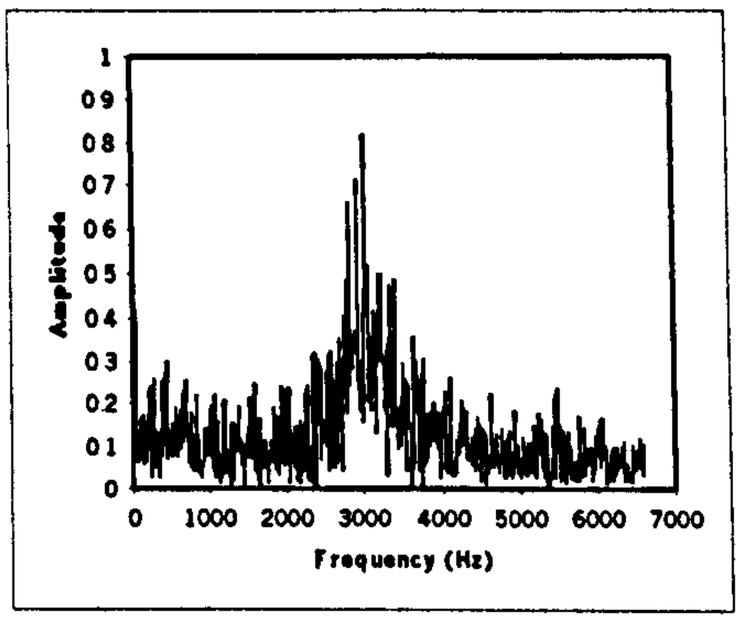	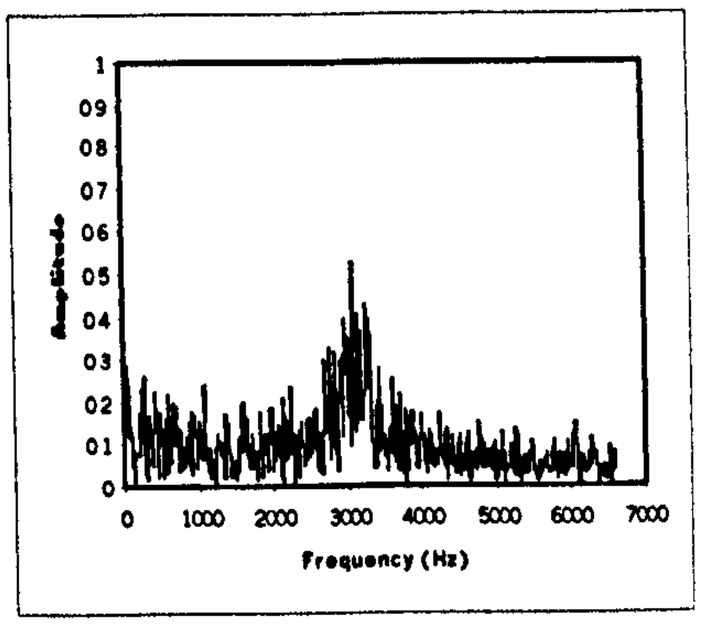
0.922 secs/1.02mm	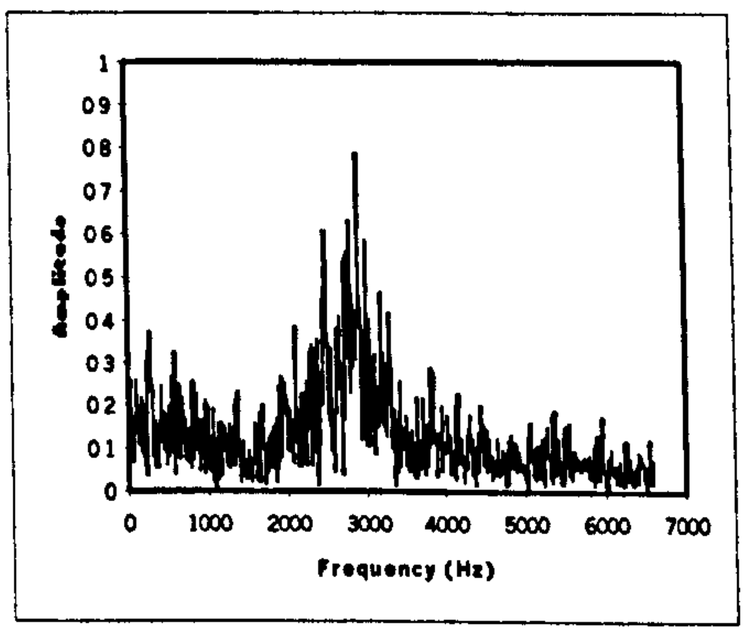	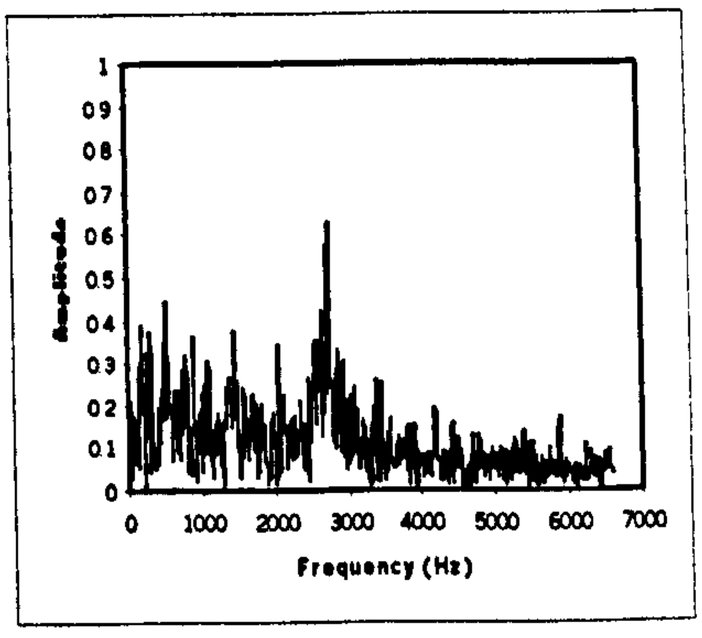

Figure 7.16 Oscillation frequencies observed during welding of a mild steel wedge

Time from start of weld (secs)/Thickness (mm)	Speed 3 m/min	Speed 4 m/min
1.22 secs/1.13mm	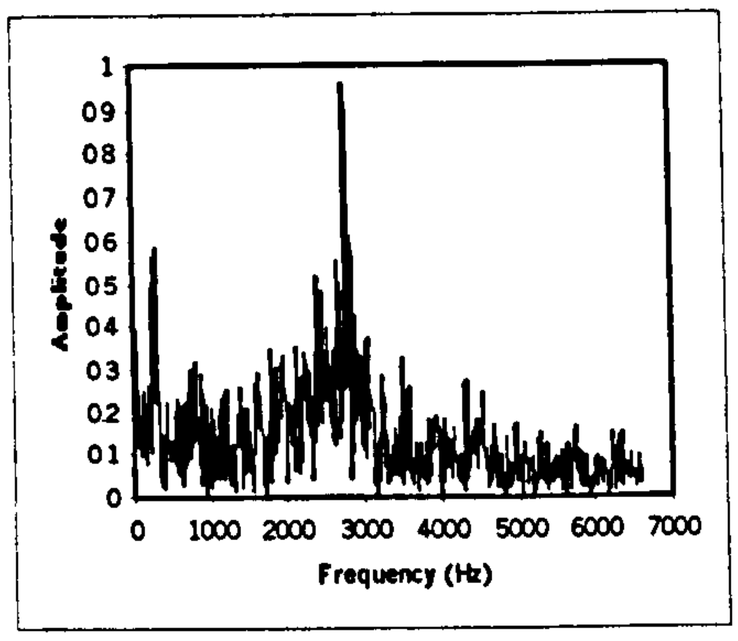	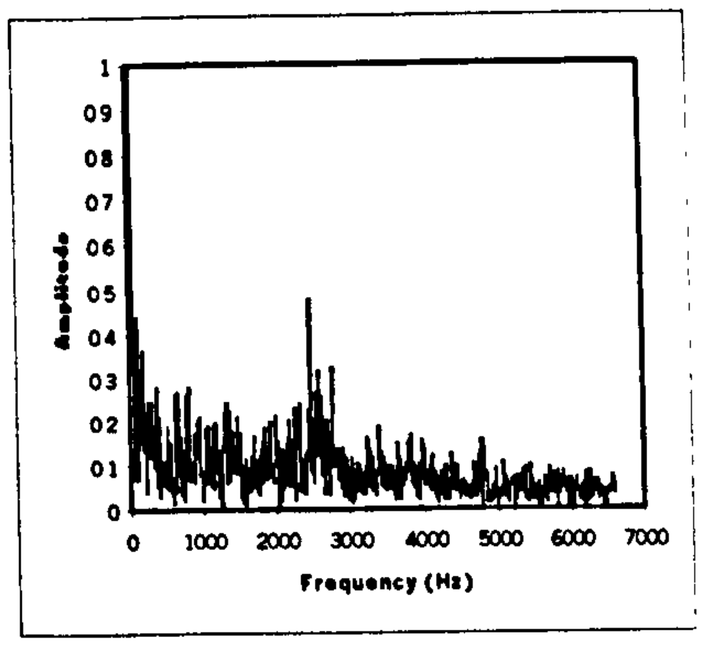
1.43 secs/1.20mm	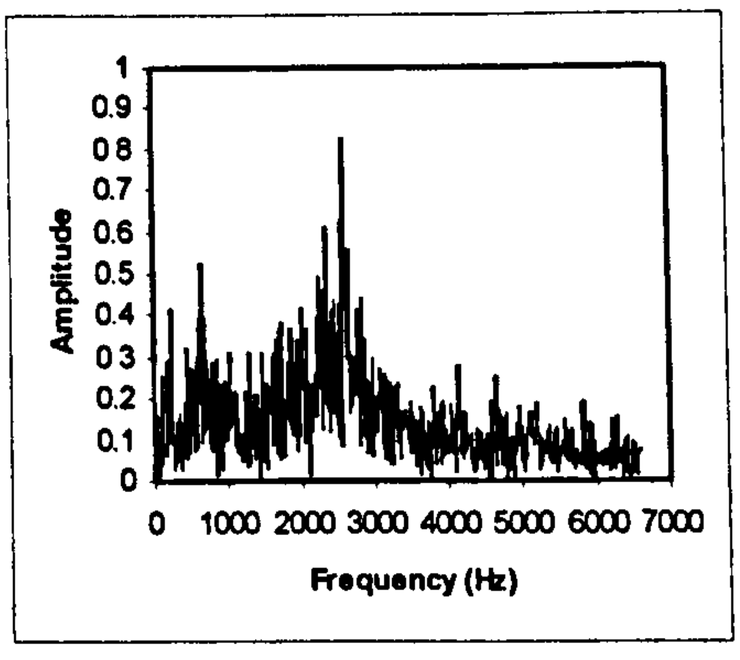	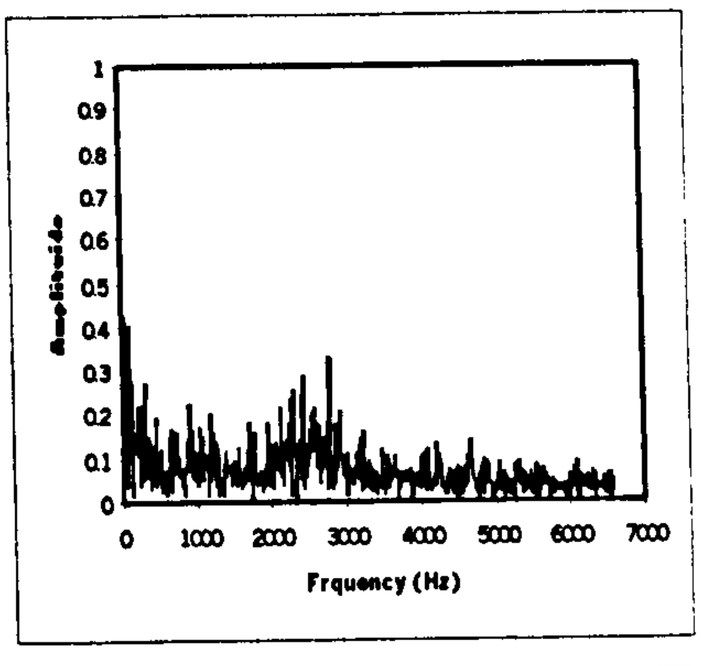
1.74 secs/1.31mm	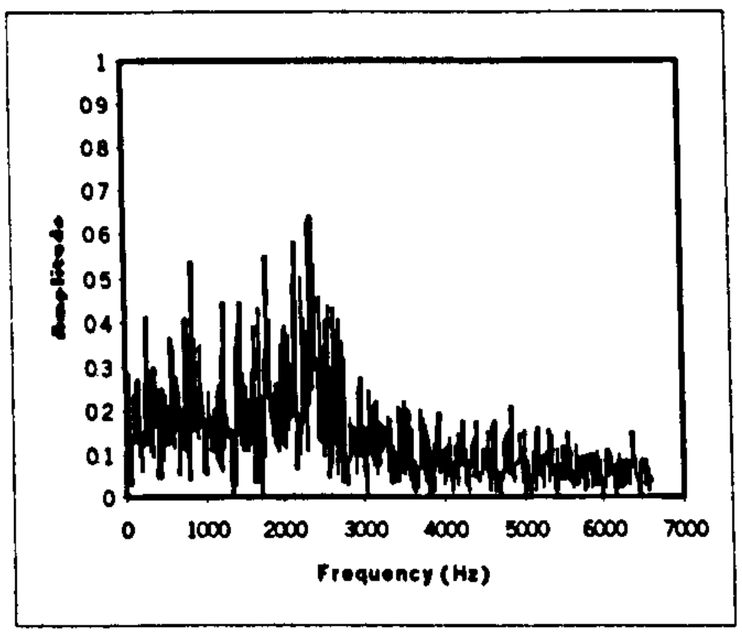	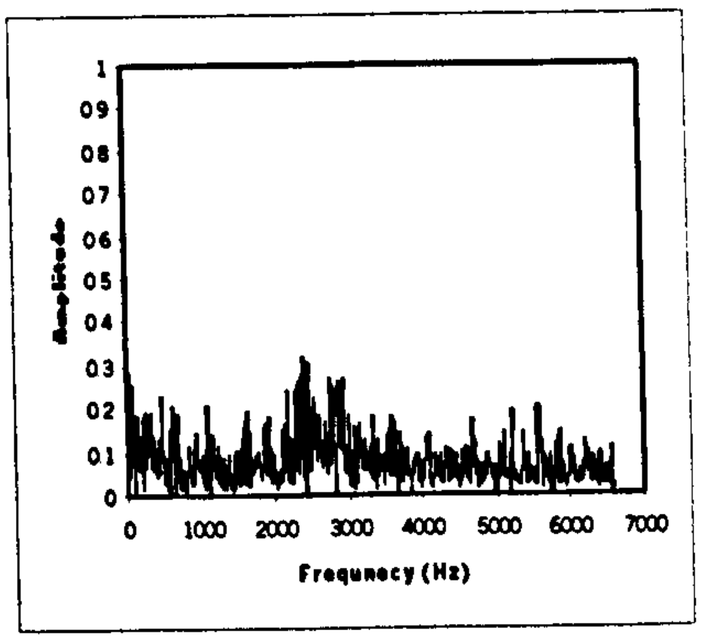
2.05 secs/ 1.42mm	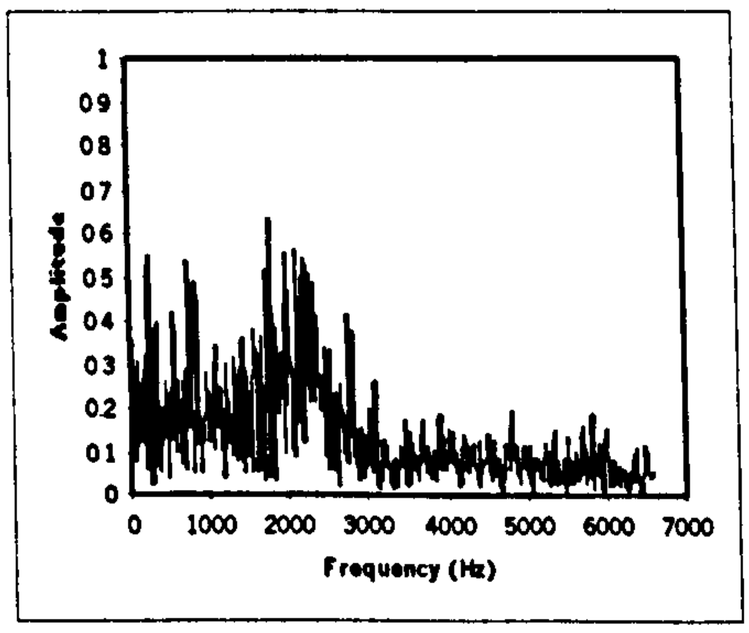	

Figure 7.16 (cont) Oscillation frequencies observed during welding of a mild steel wedge

7.4.4 High Speed Video Filming of the Laser Keyhole

A high-speed video recording at up to 40,500 frames per second was taken using a Kodak Ektrapro camera. The camera was positioned behind the turning mirror within the laser focusing head optics, such that it could view the beam impingement area coaxially with the laser beam. Illumination was provided by a copper vapour laser, delivered via optical fibre, through a frosted glass slide positioned, approximately 2cm above the beam impingement point. This arrangement was found to give more diffuse illumination leading to better image quality. Welds were made at constant speed and power.

Figure 7.17 shows a set of images produced during a continuous seam weld, showing the welding keyhole from directly above the beam impingement point on the work piece. The keyhole can be identified as the bright circular object in the centre of the image. The edge of the front of the weld pool can also just be made out at the top of each picture. The correct sequence of images is viewed from left right with the frame number printed next to the image. The images appear to show the view through the keyhole to the backside of the sheet where the keyhole exit can be seen. During the image sequence it becomes apparent that whilst the keyhole entry stays largely constant in size and shape the exit appears to be opening and closing every 12 frames corresponding to a frequency of approximately 3375Hz.

Figure 7.17 Images showing opening and closing of the keyhole during welding

		42765	42766	42767
Frame 42764	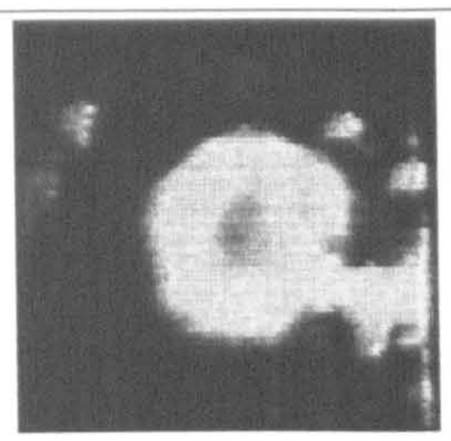	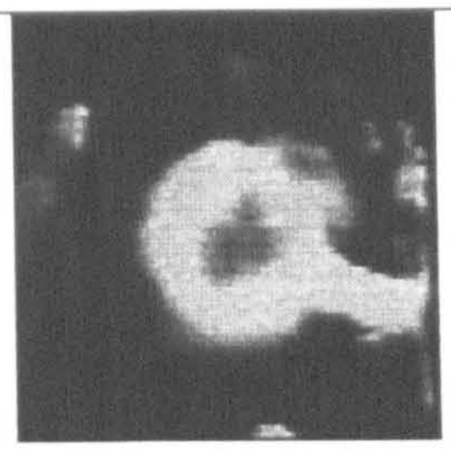	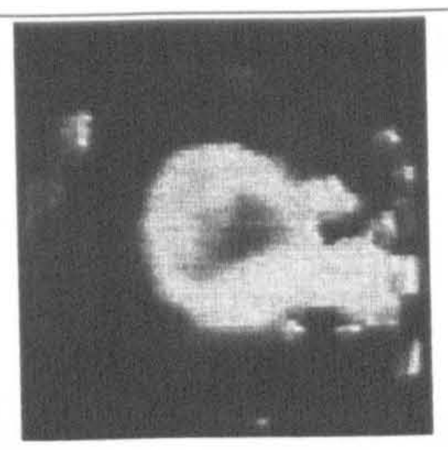	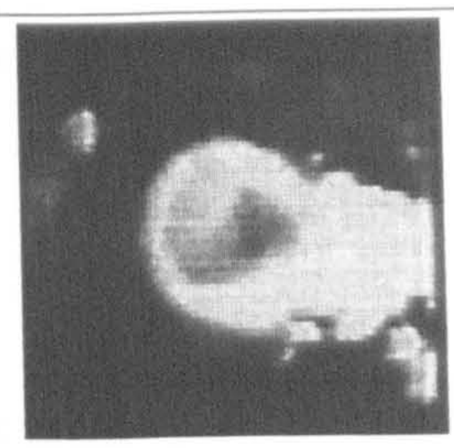
Frame 42768	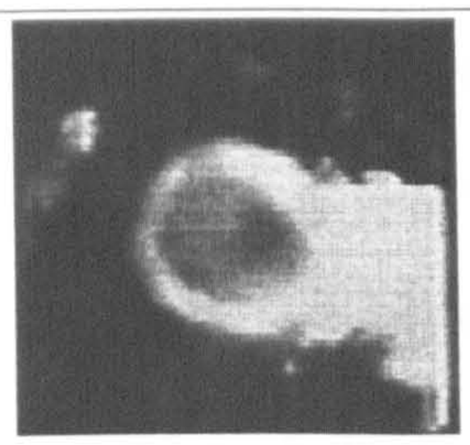	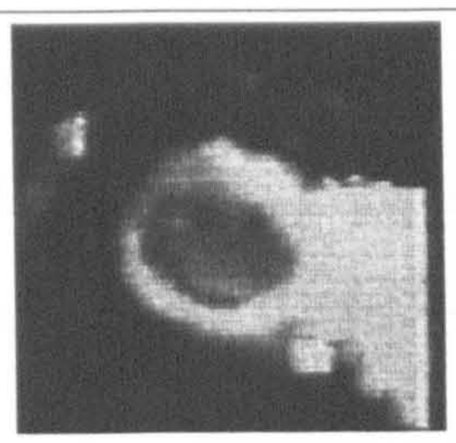	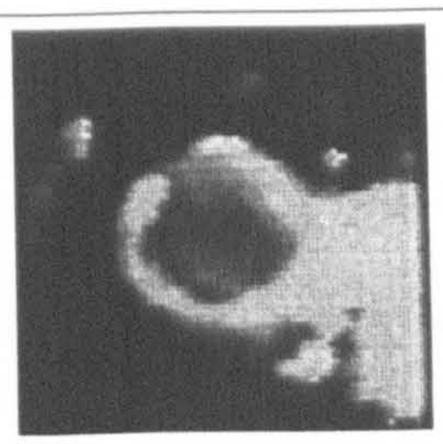	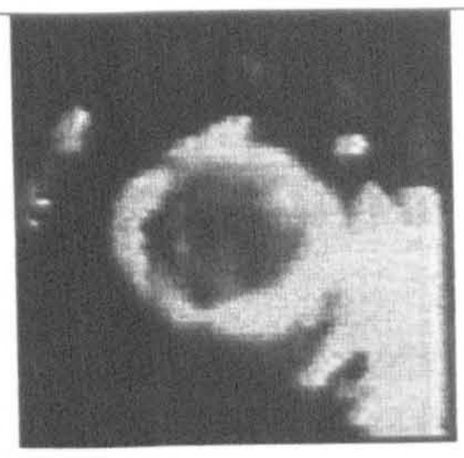
Frame 42772	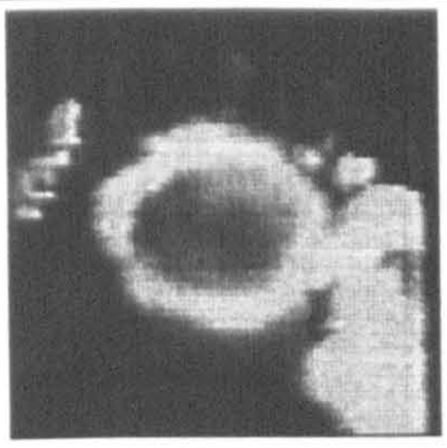	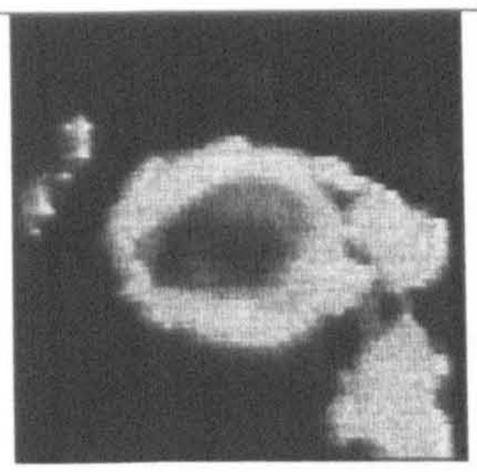	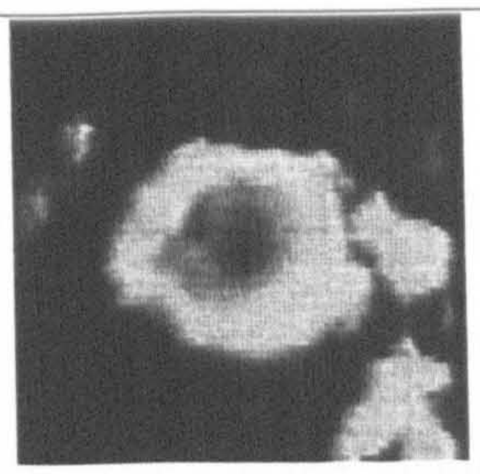	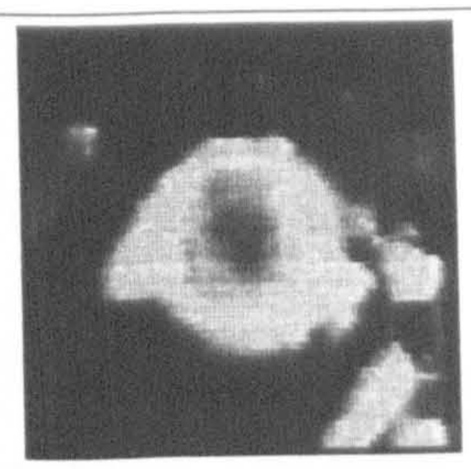
Frame 42776	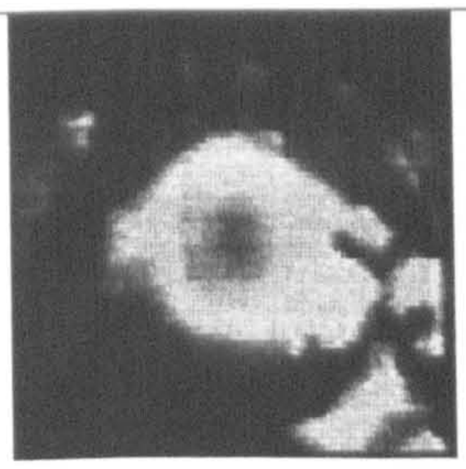	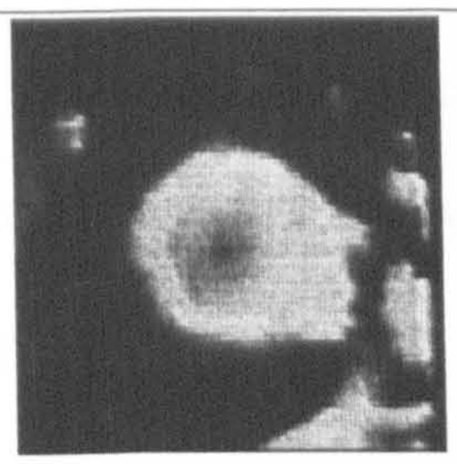	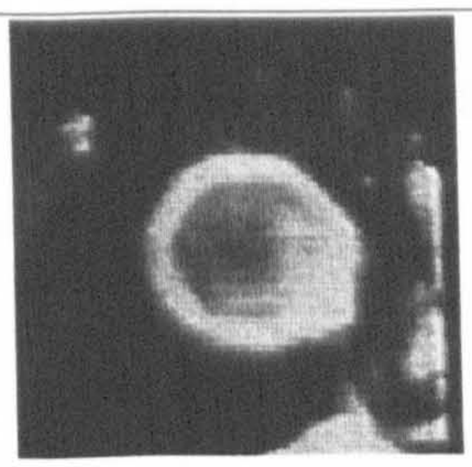	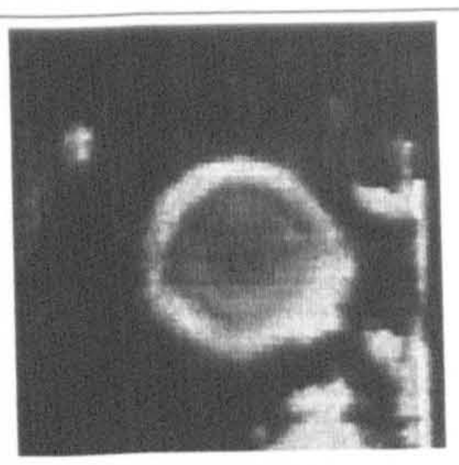
Frame 42780	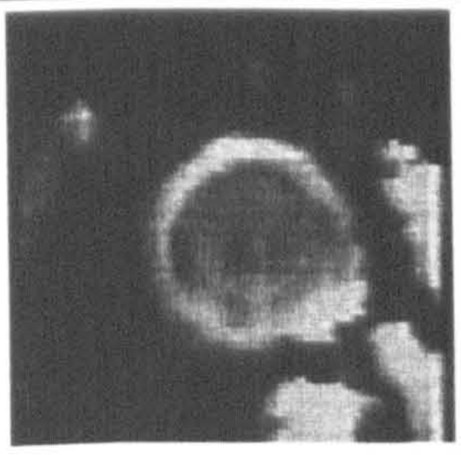	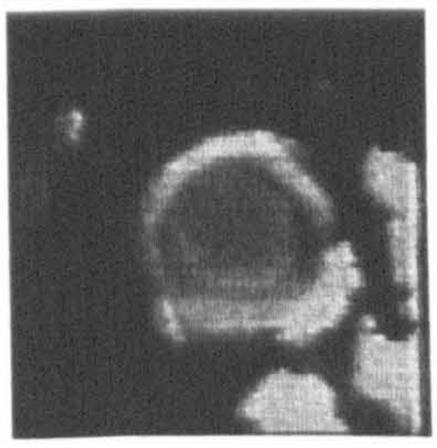	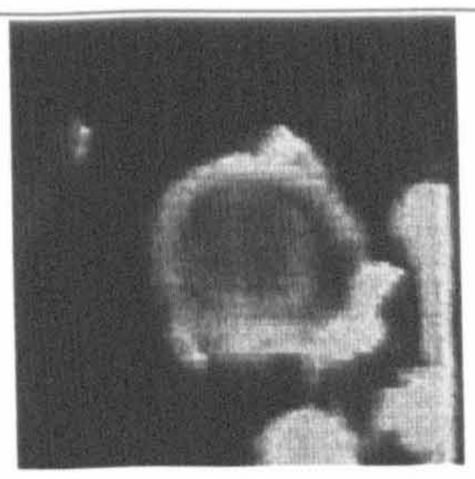	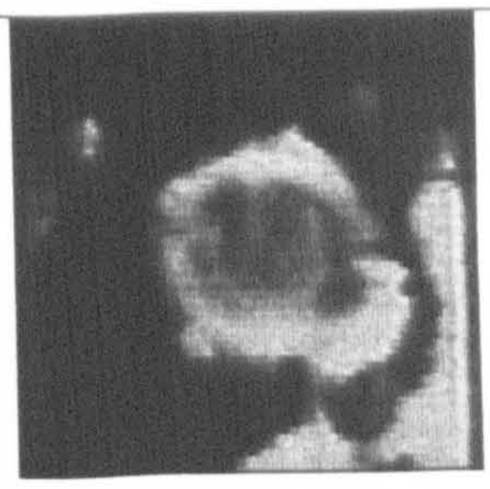
Frame 42784	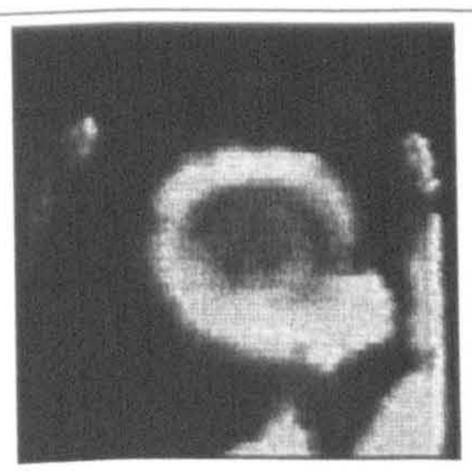	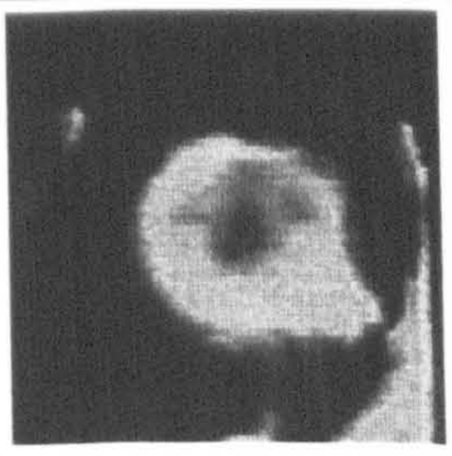	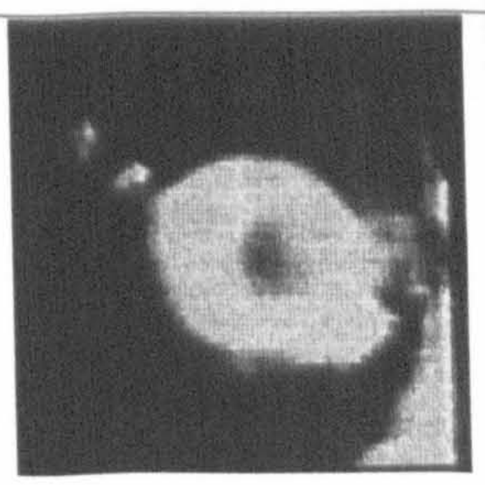	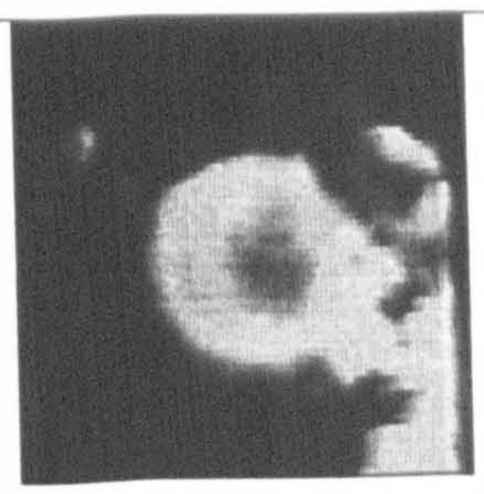

Also of note, from the high-speed images was the presence of small waves moving from the front edge on both sides of the keyhole. Low density particles (possibly silicates) could also be seen on the surface of the weld-pool that appeared to move forwards and backwards just behind the keyhole, very much like surfers on a wave.

High speed images of welding in aluminium zinc alloy (7475) using the same technique showed the keyhole to be far less stable. In this case the keyhole entry was seen to be unstable with molten material periodically flowing back into the keyhole from behind momentarily closing it completely. Note that it was not possible to carry out extensive trials as the laser would barely couple into the work-piece.

Under extreme conditions of low speed (0.9 – 1.0m/min) and high power (2kW) whilst welding 1mm thick mild steel, a condition was observed where the weld widened considerably and the keyhole elongated such that a large hole appeared in the plate surface during welding. This effect had previously been thought to be associated with molten material dropping out of the weld-pool under its on weight and is known in some circles as weld 'drop through' or 'drop out'. Images of this condition are shown in figure 7.18.

1. Keyhole at start of welding	
2Keyhole begins to elongate	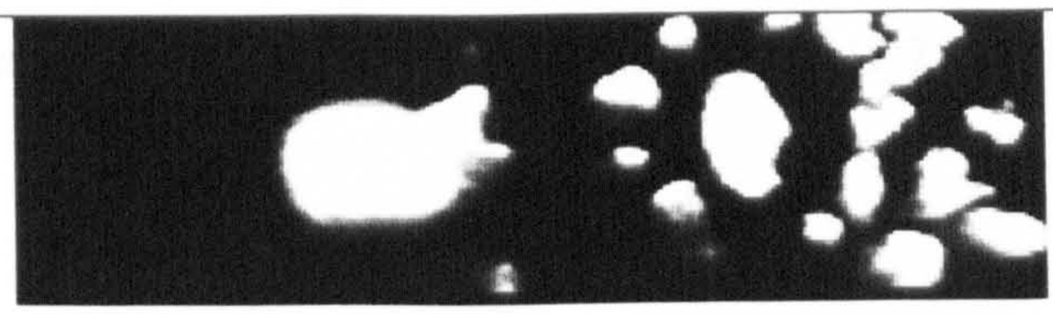
3 Becoming a large circular hole	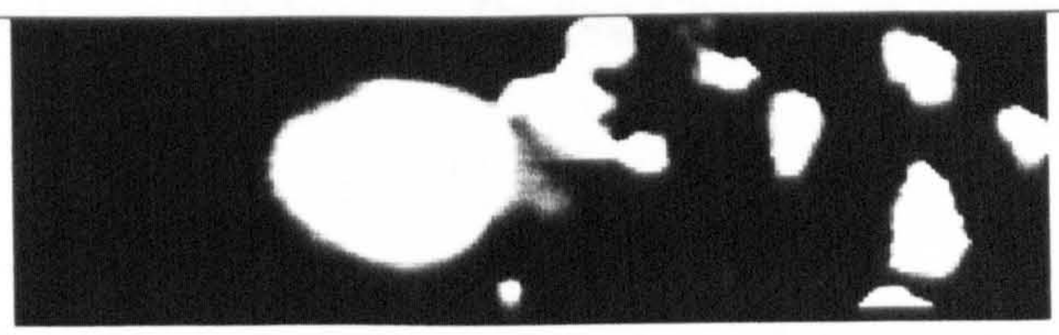
4 The front of the hole becomes pointed. Capillary waves can be seen travelling around the circumference from the front of the hole.	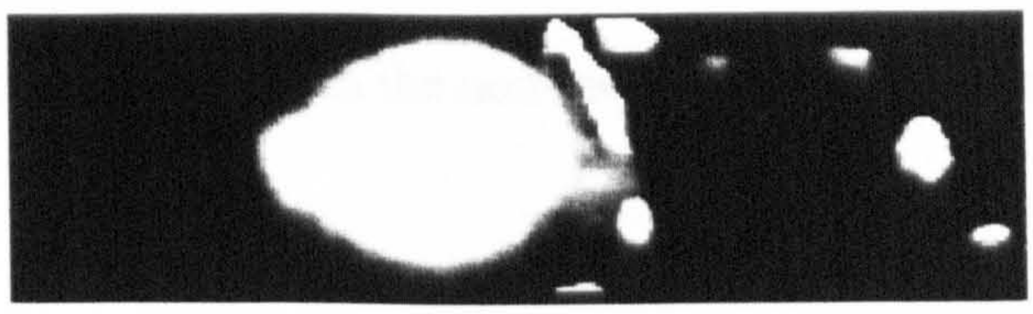
5 The point becomes more pronounced. A molten sphere appears behind the hole. Skating bottom right	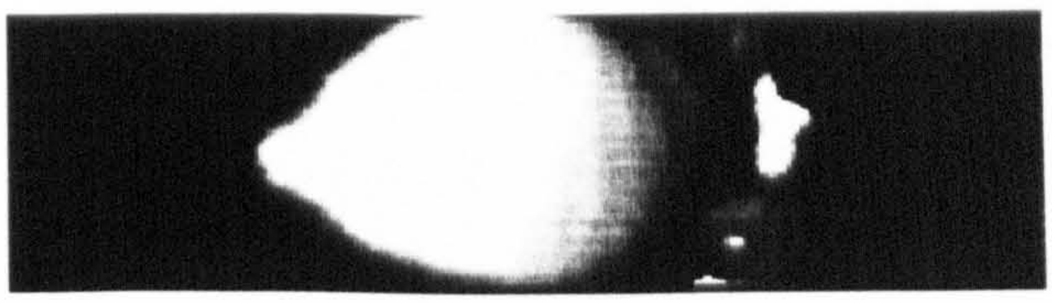
6 The hole becomes so large that plate is sectioned as though cut.	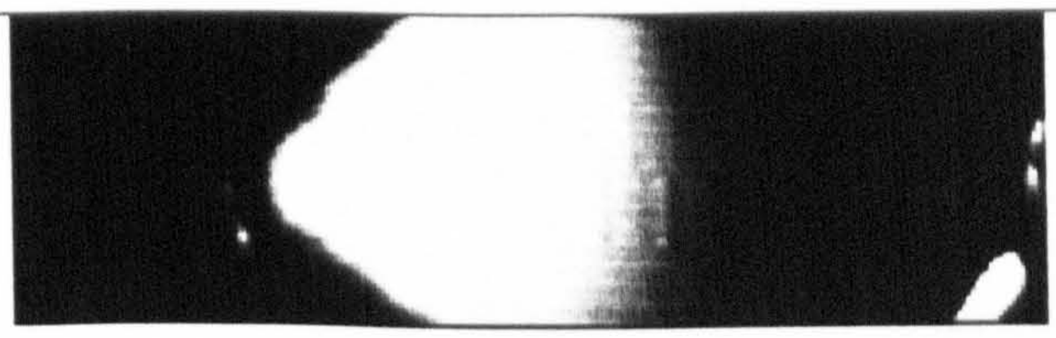

Figure 7.18 Keyhole enlargement at low speed (1 m/min)

In simulating these conditions, the high-speed video revealed a possible alternative mechanism whereby this condition can occur. From 7.18 the keyhole can be seen to enlarge to many times its original size as the laser beam traverses across the plate. It is the enlarged keyhole that produces the hole in the plate after solidification, not loss of material. Also worth noting was the disappearance of principle oscillation frequencies seen in slightly faster (1.25m/min) welds.

7.5 Observation of the Optical Signal Behaviour During Changes of Focus Position

7.5.1 Objectives

The objectives were to observe the behaviour of the monitored signal during changes in work-piece to optics distance, simulating changes in focus position that might be encountered in an industrial application. This was observed for both the non-melting and melting case.

7.5.2 Experimental Procedure

A Cladding Power Monitor (CPM) of core diameter 1.0mm and monitor fibre diameter 200μm was fitted to a 350W pulsed Nd:YAG laser Lumonics JK 702H. The beam was focused into the fibre by collimating to 17mm and focusing onto the fibre core using a 60mm cemented achromat focus lens.

The return fibre from the CPM was connected to the wavelength splitter equipment with the filters selected to only detect wavelengths in the range 1064nm +/- 10nm, i.e. corresponding to the returned laser radiation. The sensors within the splitter were aligned using a bright white light source passed back along the forward-going side of the CPM monitor fibre.

It was found to be relatively difficult to prevent melting on the surface of a mild steel plate so a 1.0mm thick copper coupon was used as the target material. The beam was focused using a 160 and 80mm lens combination giving a 0.5mm focused spot. The focus position or waist of the beam was found by making single shots into 0.1mm thick Kapton film at different elevations relative to the focus lens. The smallest hole produced in the Kapton film was selected as corresponding to the waist position. Initially the copper target was placed in the same plane as the waist position in the beam path. Individual shots were taken and the signals at various wavelengths observed for various focus positions either side of the waist position.

7.5.3 Results – Non-melting Case

Figure 7.19 shows a typical trace of the radiation signal received by the process monitor with a copper target positioned at the laser beam waist position i.e. at focus.

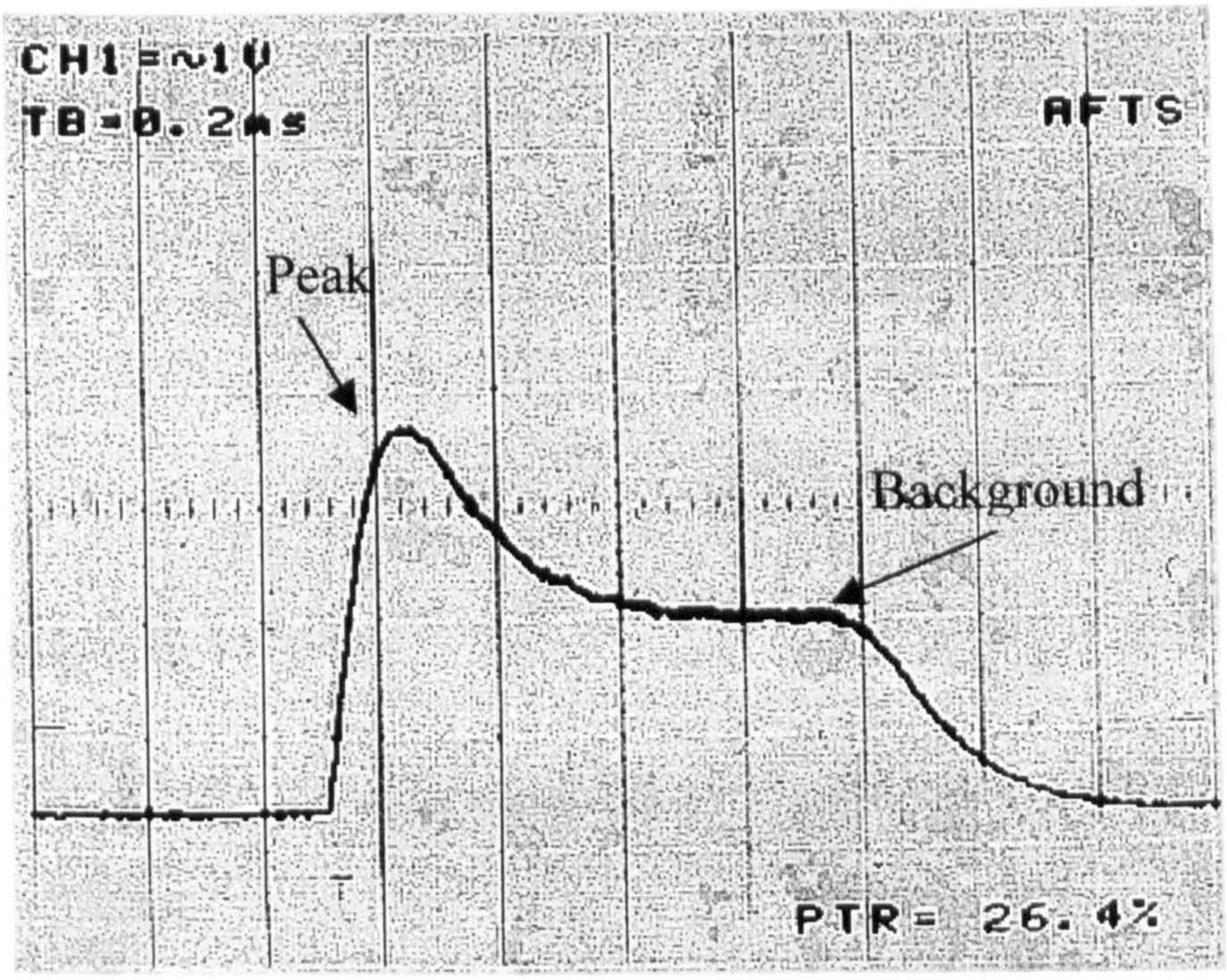

Figure 7.19 returned signal from copper target positioned 'at focus'

It was found that the levels of IR and UV/Visible that could be detected from the copper target were insignificant, but the signal detected from the laser wavelength was very large in comparison. Figure 7.20 shows a plot of the sensor signal for the backscattered laser light returning from the surface of a copper target positioned at various focal positions relative to the waist position.

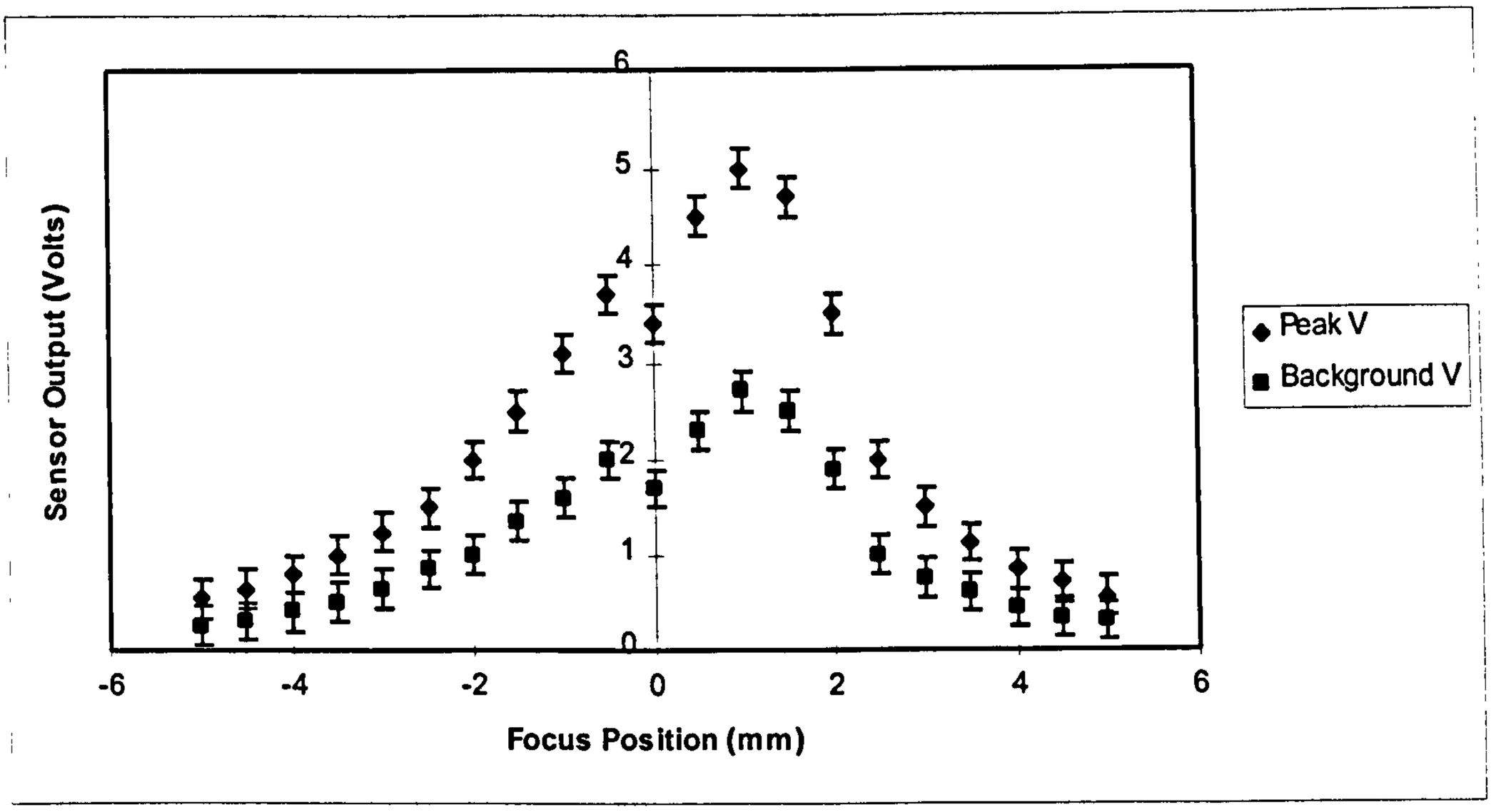

Figure 7.20 Sensor output at various focal positions relative to copper target. Note: negative focus position corresponds to waist above target surface

Starting from a beam waist position below the surface of the plate (positive value) it can be seen that as the waist is raised so that it approaches the plane of the plate surface, the amplitude of the sensor signal (peak and background) increases. The ratio of the peak to background remains constant. The sensor signal reaches a maximum with the waist 1 mm below the surface of the plate whereupon the signal drops as the waist continues to be raised above the plate surface. It can be seen that the shape of the curve is not symmetrical about the maximum point with the rate of increase below the plate surface greater than that above.

7.5.4 Results - Melting Case

The peak amplitude of the collected signal for each wavelength was recorded and is shown in figure 7.21 below.

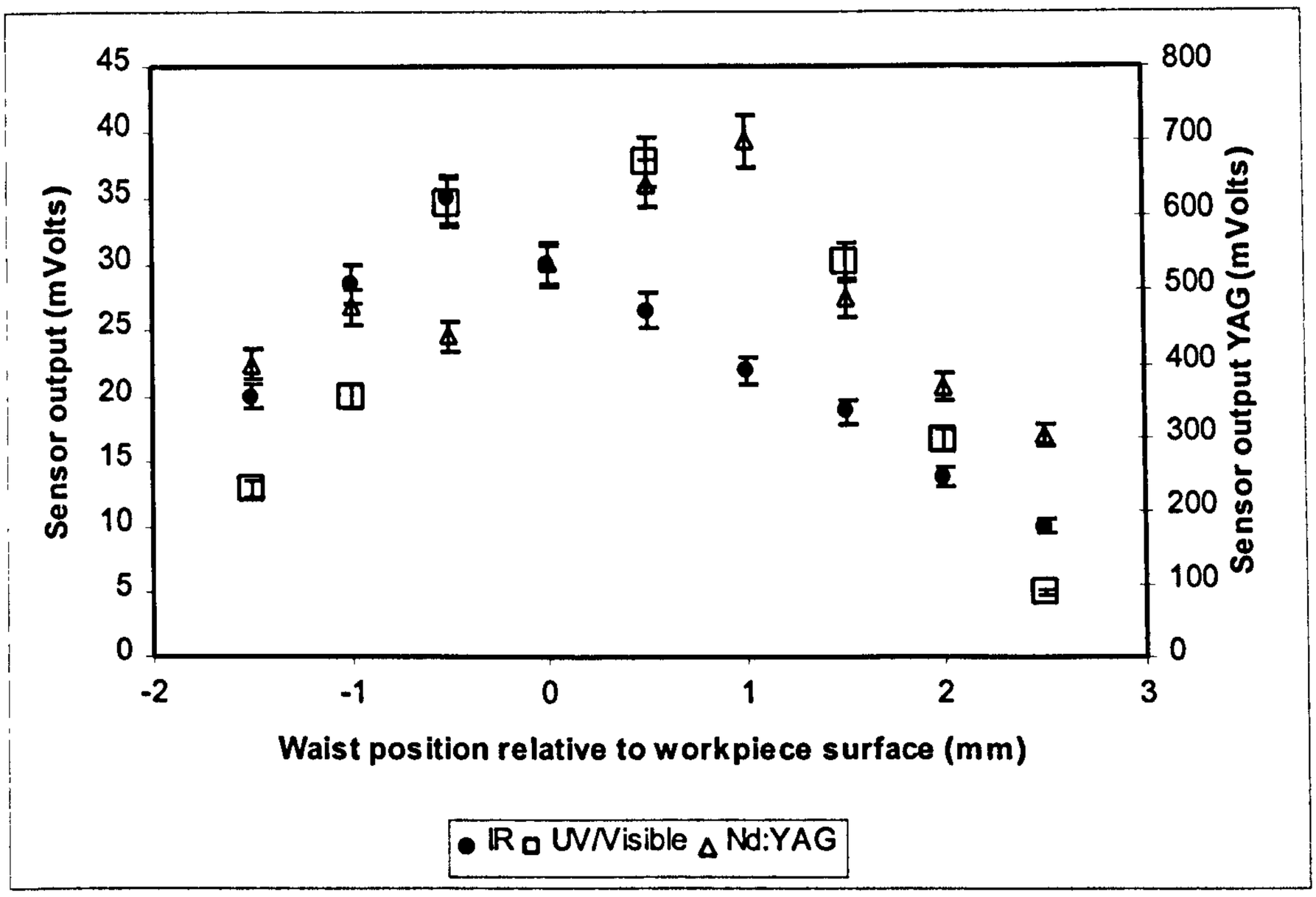

Figure 7.21 peak amplitude of detected YAG, IR and UV/Visible wavelengths at different focal positions

With the mild steel target it was possible to detect significant levels of UV and IR signal. It can be seen from figure 7.21 that the behaviour is similar to the non-melting case that is the signals rise and fall as the focus is adjusted from above to below the plate surface. However in the case of the plate melting the UV and IR signals are available, their peaks appearing to straddle the waist position.

7.6 Experiment to Observe the Optical Signals During Melting – Continuous Wave Laser

Note: It was not possible to carry out continuous wave trials for the non-melting case as excessive backscatter and reflection of the laser wavelength would cause damage to the output end of the fibre.

7.6.1 Procedure

Because of the nature of a continuous wave laser it was not thought possible to be able to get a reliable single shot mode to carry out focus trials so a different method was used to introduce focal errors. A mild steel sheet, 1.0mm thick, was tilted at an angle of 2.5 degrees to the horizontal plane. The laser beam waist position was set initially above the surface of the sheet. The sheet was traversed under the stationary laser beam so that the beam waist position moved through the plane of the sheet until at the end of welding the beam waist was positioned below the sheet surface.

Focusing optics were selected (160mm recollimating lens, 80mm focus lens) to give a nominal focussed laser beam waist of 0.5mm. Welding was carried out using a continuous wave output and with power measured at the work-piece of 1300 watts. Argon gas was introduced using a side pipe of 8mm internal diameter and 10 litres /min flow directed at the beam impingement area so that good cover was maintained over the entire length of the plate. A variety of welding speeds were used, typically in the range 2.0 – 3.0m/min. Melt runs were also made through overlapping sheets by clamping two 1.0mm thick sheets on top of one another and welding at a slower welding speed of 1.0m/min.

Bead on plate runs were made using core monitor and cladding power monitor arrangements connected to the wavelength splitter apparatus. The behaviour of the different wavelengths ranges was monitored simultaneously.

7.6.2 Results

Figures 7.22 show the characteristic UV/visible signal from a weld made across the length of an inclined single mild steel sheet.

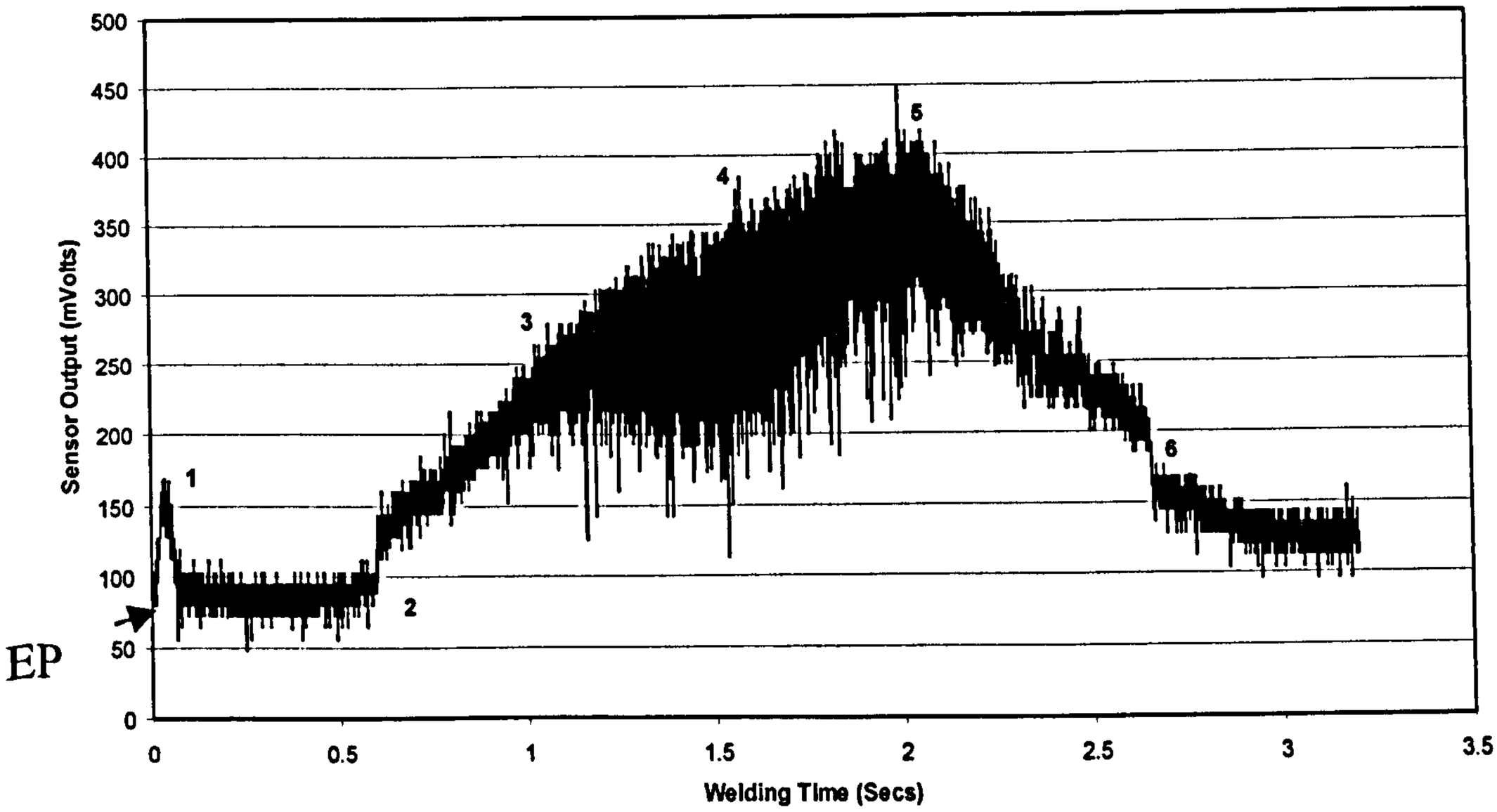

Figure 7.22 Typical signal from UV/Visible sensor during welding of inclined steel plate

The results have been plotted so that the edge of the plate is coincident with time equal to zero (marked by EP). As the beam moves onto the plate there is an increase in signal indicated at position 1 which reduces as the beam is fully onto the plate. This is believed to be associated with an edge effect. Beyond position 1 the signal remains at a constant level for approximately 0.5 seconds even though the beam is constantly changing focus, until position 2. At 2, there is a step increase in signal of approximately 40mV over a time period of 11.8ms, or a linear translation of the beam across the surface of the sheet of 0.5mm. Between positions 2 and 3 the signal increases constantly, with a signal modulation depth of approximately 32mV, similar to the base noise level from the detectors when not welding. At position 3 the signal still increases at a

largely constant level but the depth of modulation starts to increase until position 4 where the modulation depth reaches a maximum of 200mV. At position 5 the sensor signal reaches peak amplitude then begins to decay along with the modulation depth. At position 6 there is a step decrease in signal level of approximately 60mV. Both the step changes observed at positions 2 and 6 corresponded to a discontinuity observed on the surface of the sheet. Figure 7.23 shows a plot weld top bead and under bead width against welding time.

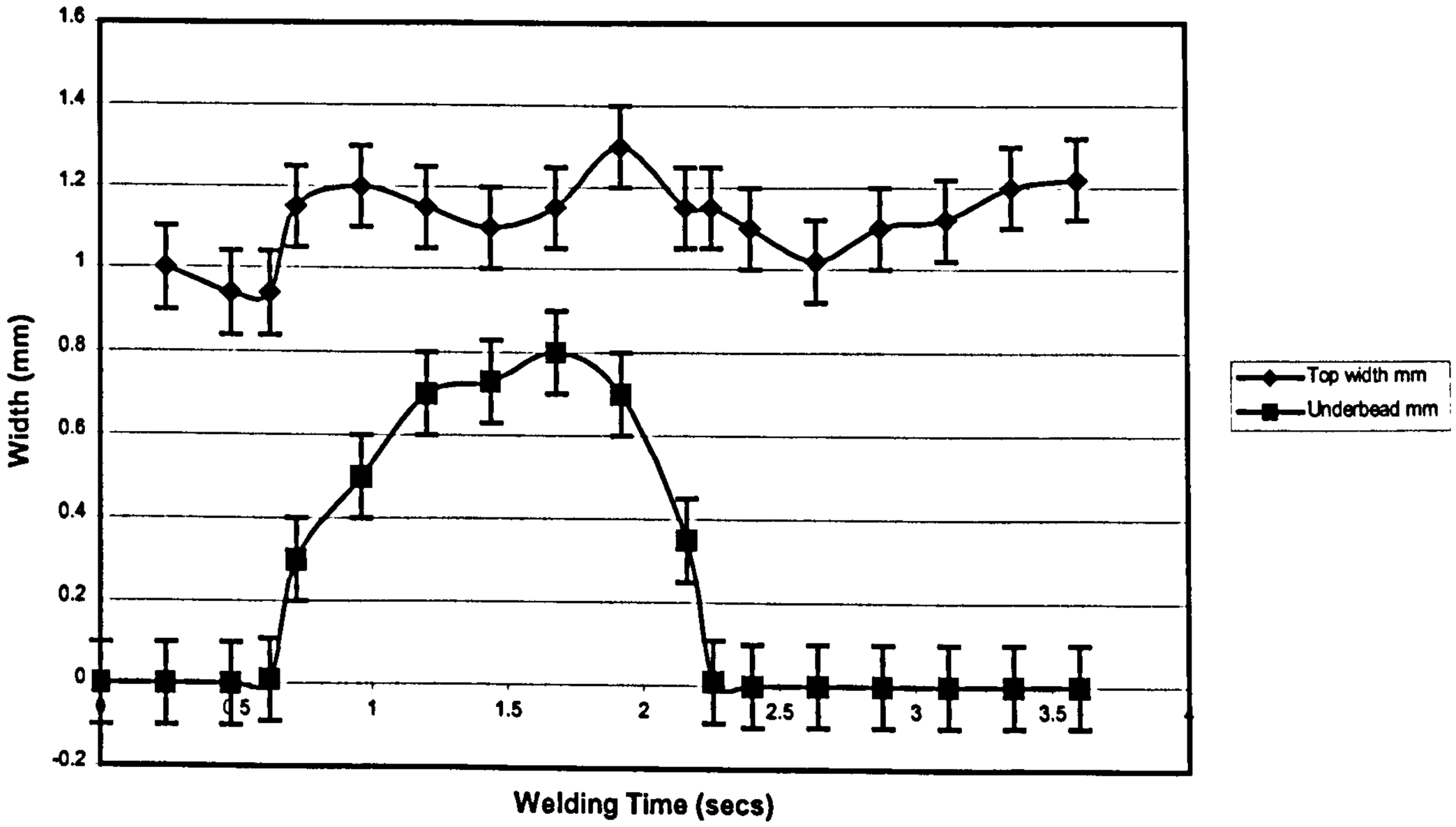

Figure 7.23 Typical plot of weld top bead and under-bead width for a weld made in 1.0 mm inclined mild steel sheet

Cross referencing figures 7.22 and 7.23 it can be seen that the time corresponding to the first step change in signal position 2, (0.6secs) appears to be coincident with an increase in top bead width and the onset of full penetration. Top bead width reduces to a minimum at the point of the second step change at 6 but full penetration is lost before this time.

Figure 7.24 below shows a photograph of the weld top bead at the position corresponding to the position 2. It can be seen that there appears to be a transition point where the weld bead increases width. Also significant is the increase in oxidation on the top bead surface that since the weld-pool was protected by inert gas immediately at the welding point, must be occurring after

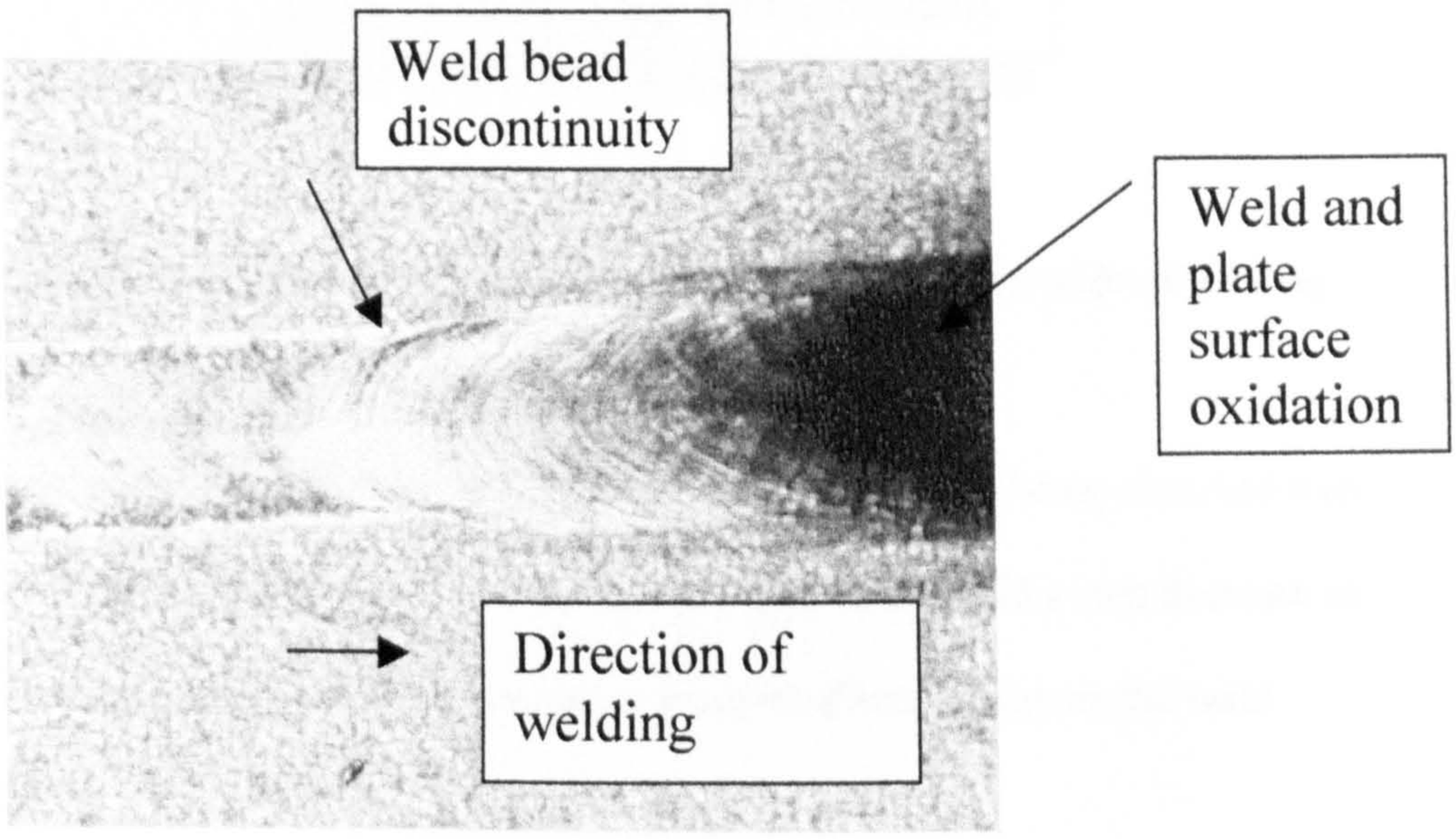

Figure 7.24 Transition point on bead on plate weld made on an include 1.0mm mild steel sheet.

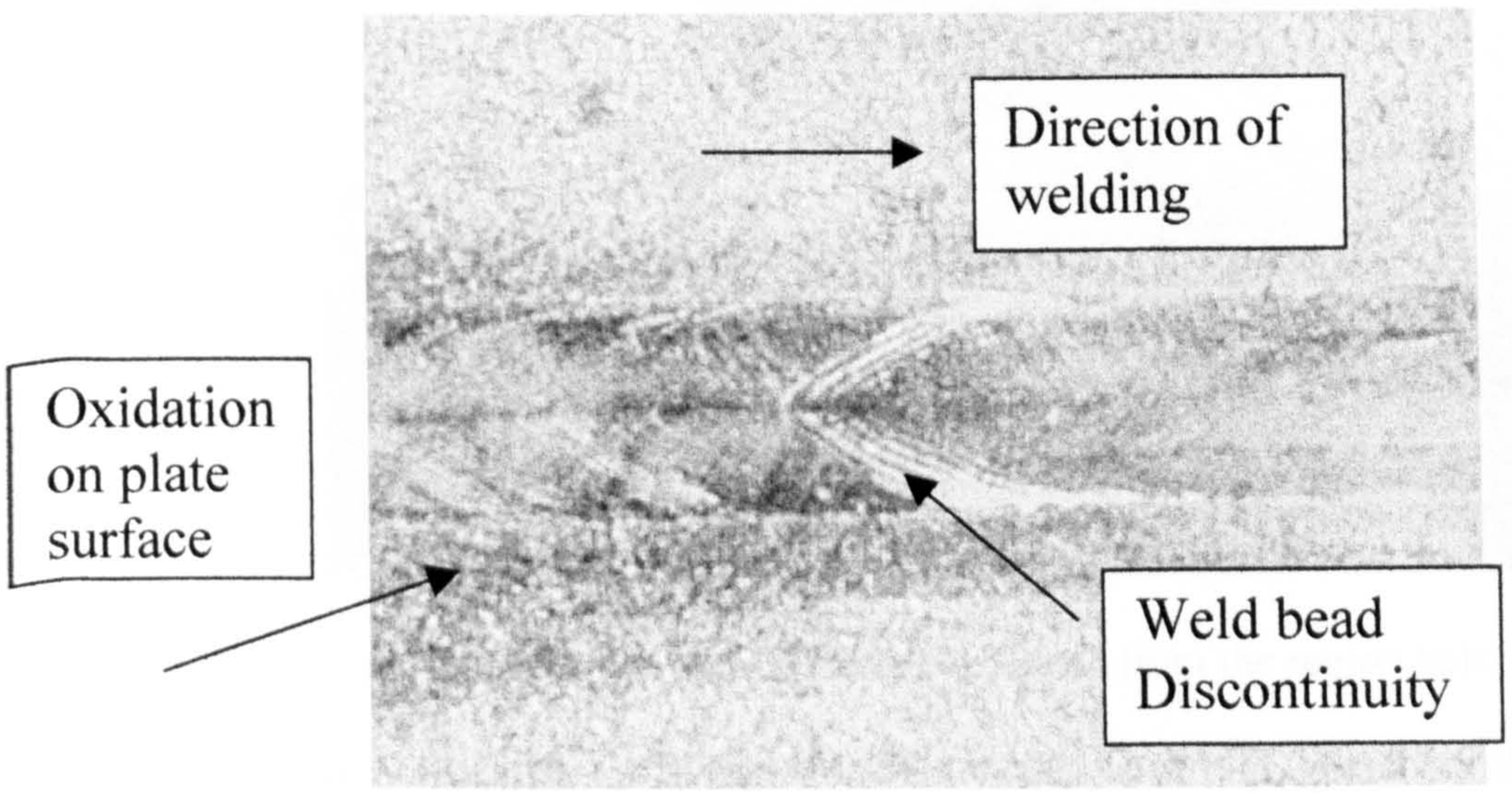

Figure 7.25. Discontinuity or transition in the surface of the weld after 2.5 seconds of welding.

solidification of the weld and is thought to be an indication of increased heat being absorbed into the weld per unit length. Approximately 2.5 seconds after the start of the weld a step decrease in both optical signals could be seen which corresponded to a visible discontinuity on the weld surface; see figure 7.25.

Metallographic cross sections of the welds made on an inclined plate were taken at points either side of the two transition points and at the centre of the plate. These are shown below.

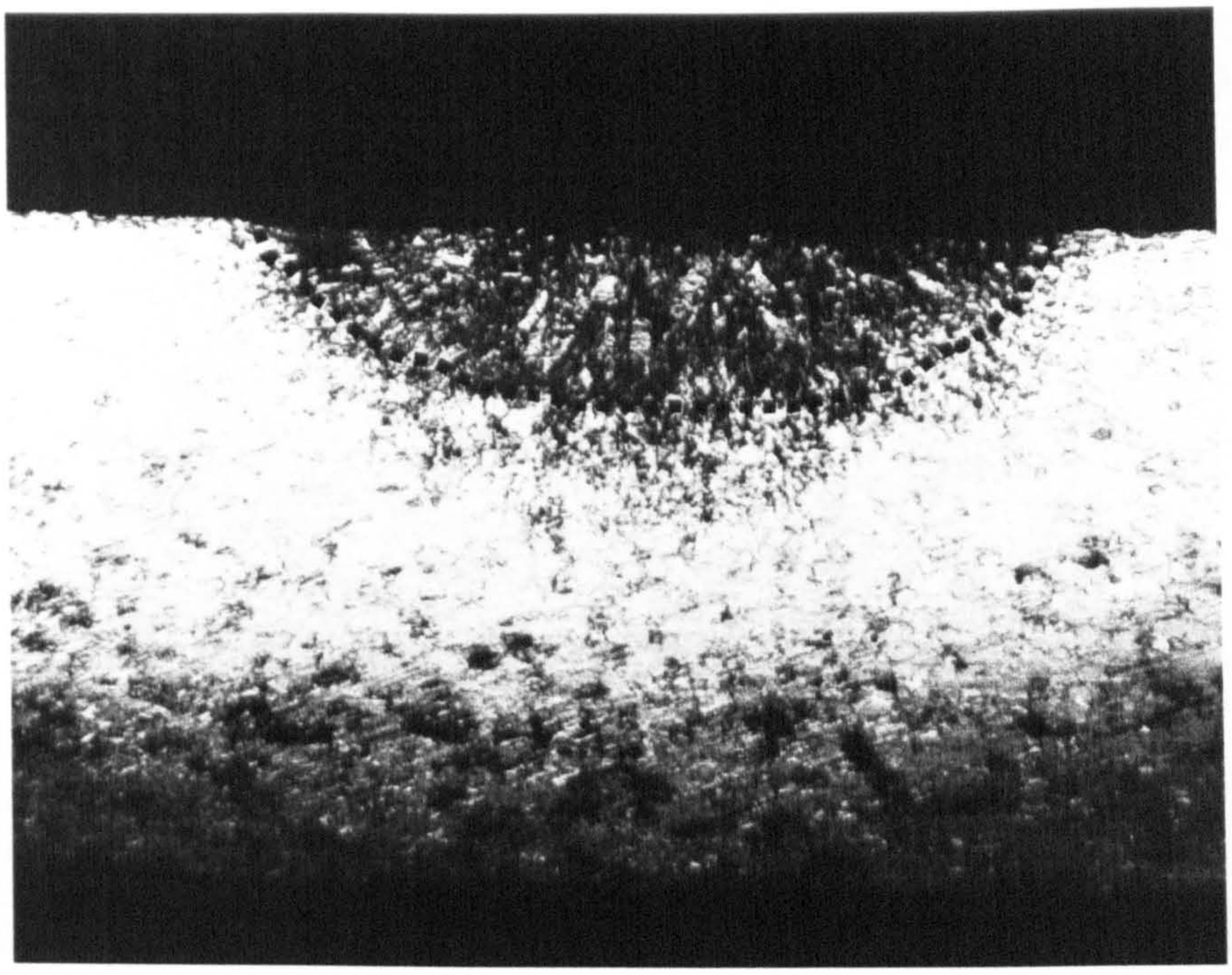

Figure 7.26. Typical weld cross-section (mag 60x) taken from the region before initial transition point. Etched in 2% Nital. Fusion zone has been highlighted for clarity.

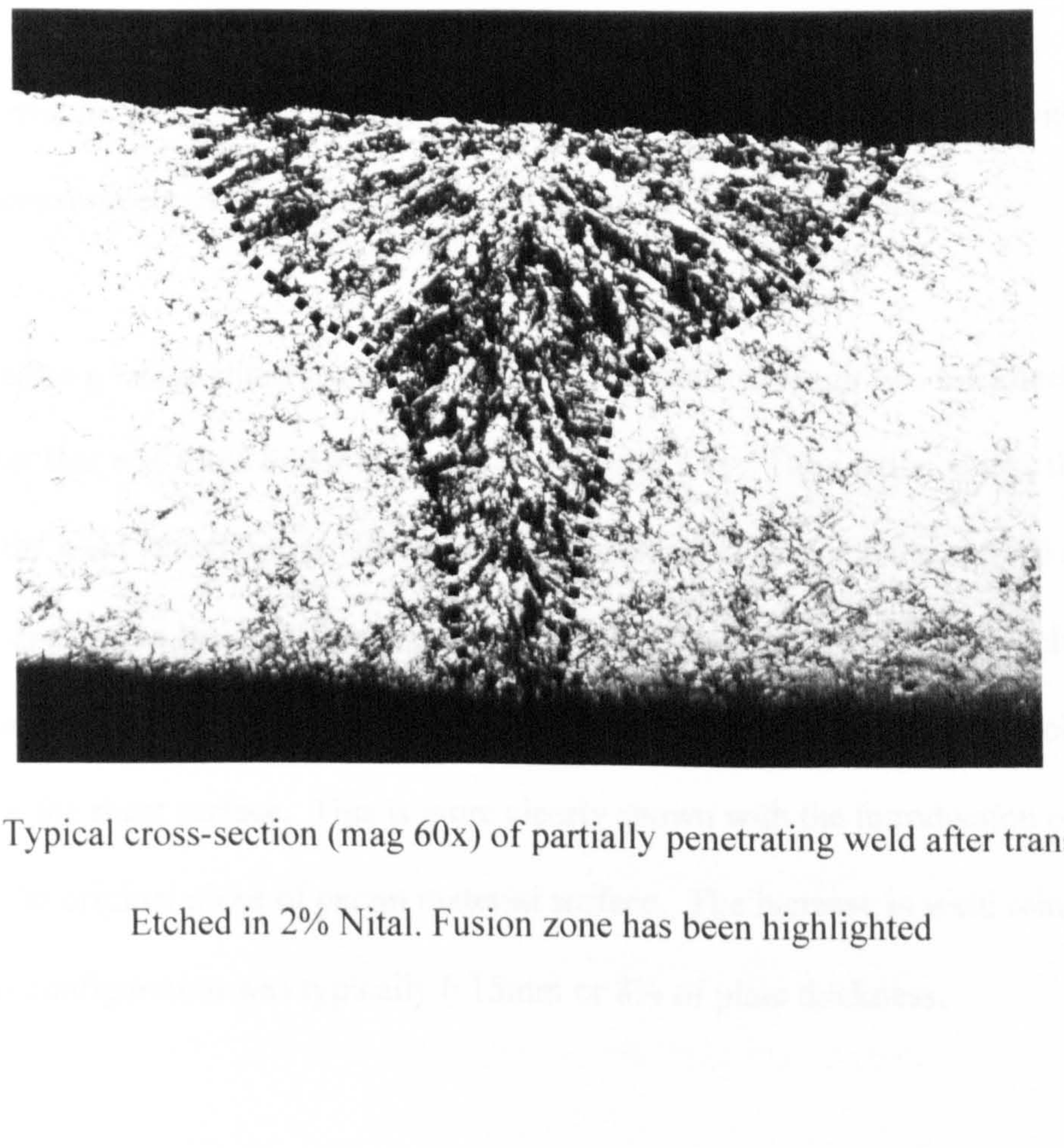

Figure 7.27 Typical cross-section (mag 60x) of partially penetrating weld after transition point. Etched in 2% Nital. Fusion zone has been highlighted

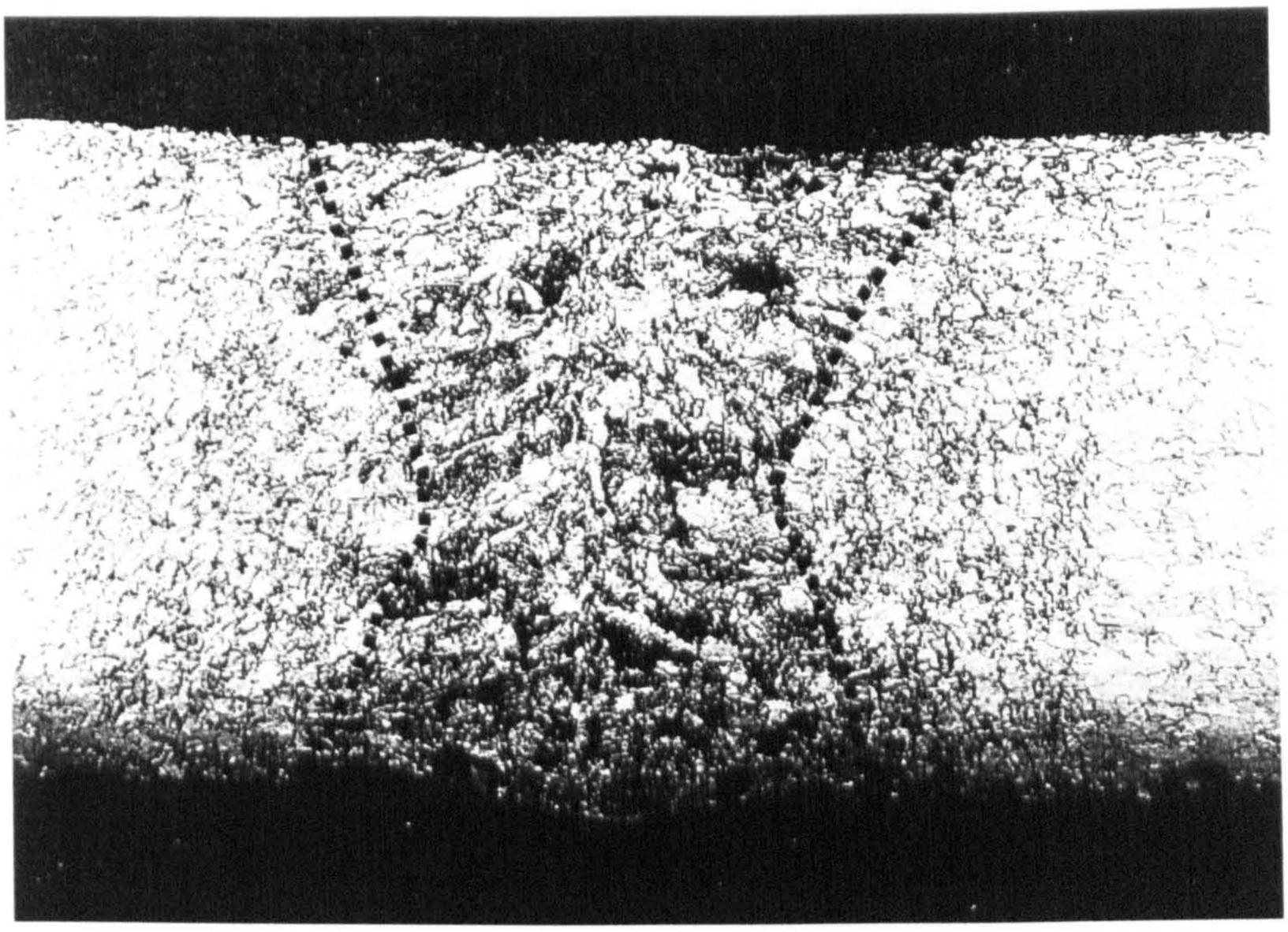

Figure 7.28. Typical cross-section through a weld (mag 60x) taken from mid point showing full penetration of the plate. Etched in 2% Nital. Fusion zone has been highlighted.

The fully penetrating weld can be seen to exhibit a characteristic hourglass shape with a waist positioned approximately centrally relative to the thickness of the metal sheet

Figure 7.29 shows a longitudinal section of overlap weld made through two thickness of 1.0mm mild steel sheet that was tilted under the beam in a similar way. The section shows the area at the beginning of the weld where the initial step increase in signal is seen and the surface discontinuity is present. A dotted line has been introduced to show the lower boundary of the melted zone within the material. Above the plate it can be seen that there is an increase in the volume of material above the sheet surface. This is more clearly shown with the introduction of a marker line showing the original plane of parent material surface. The increase in weld reinforcement height for this configuration was typically 0.15mm or 8% of plate thickness.

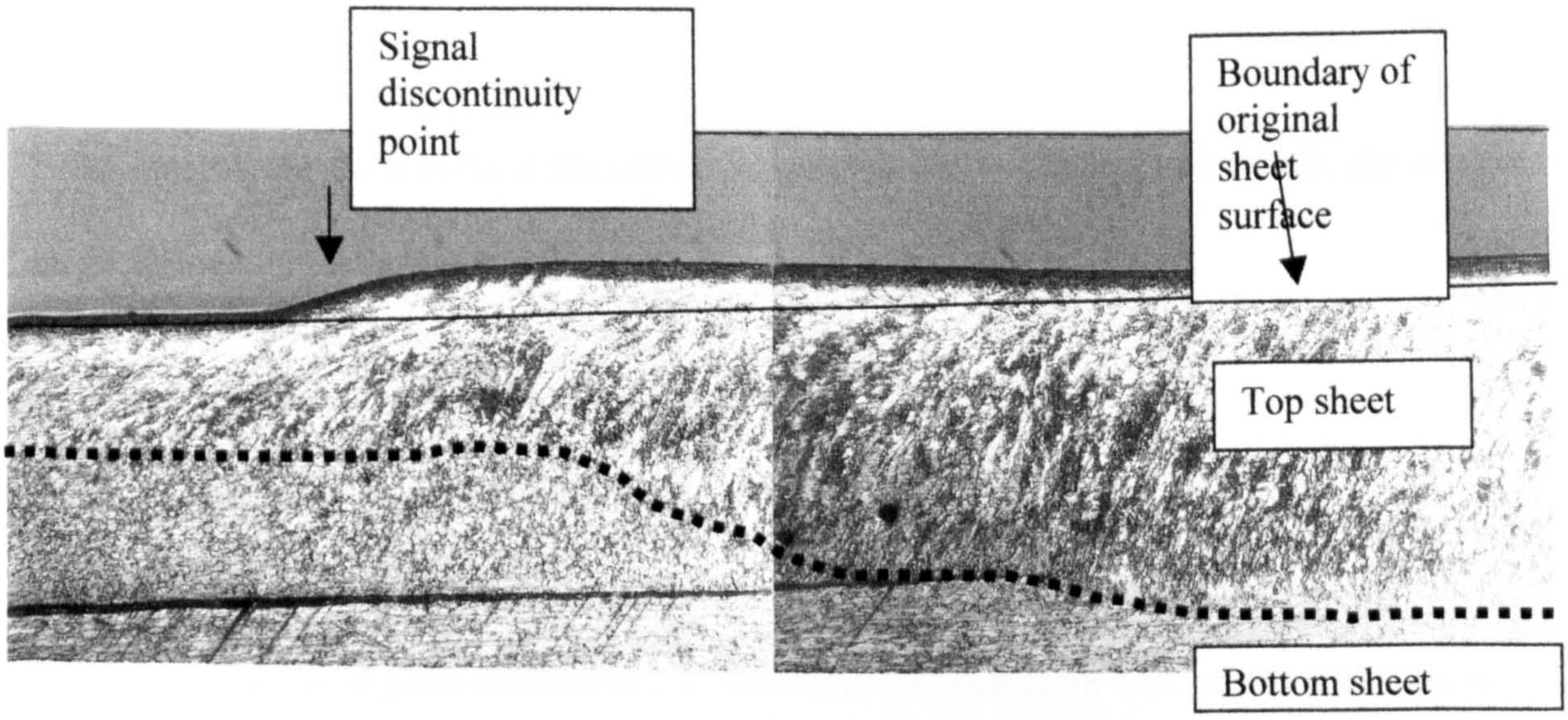

Figure 7.29 Typical longitudinal weld section (mag 50x) taken through the centre-line of a weld made in two overlapping sheets of 1.0mm steel showing the weld discontinuity point at the beginning of welding. Etched in 2% Nital. Fusion boundary profile has been highlighted for clarity.

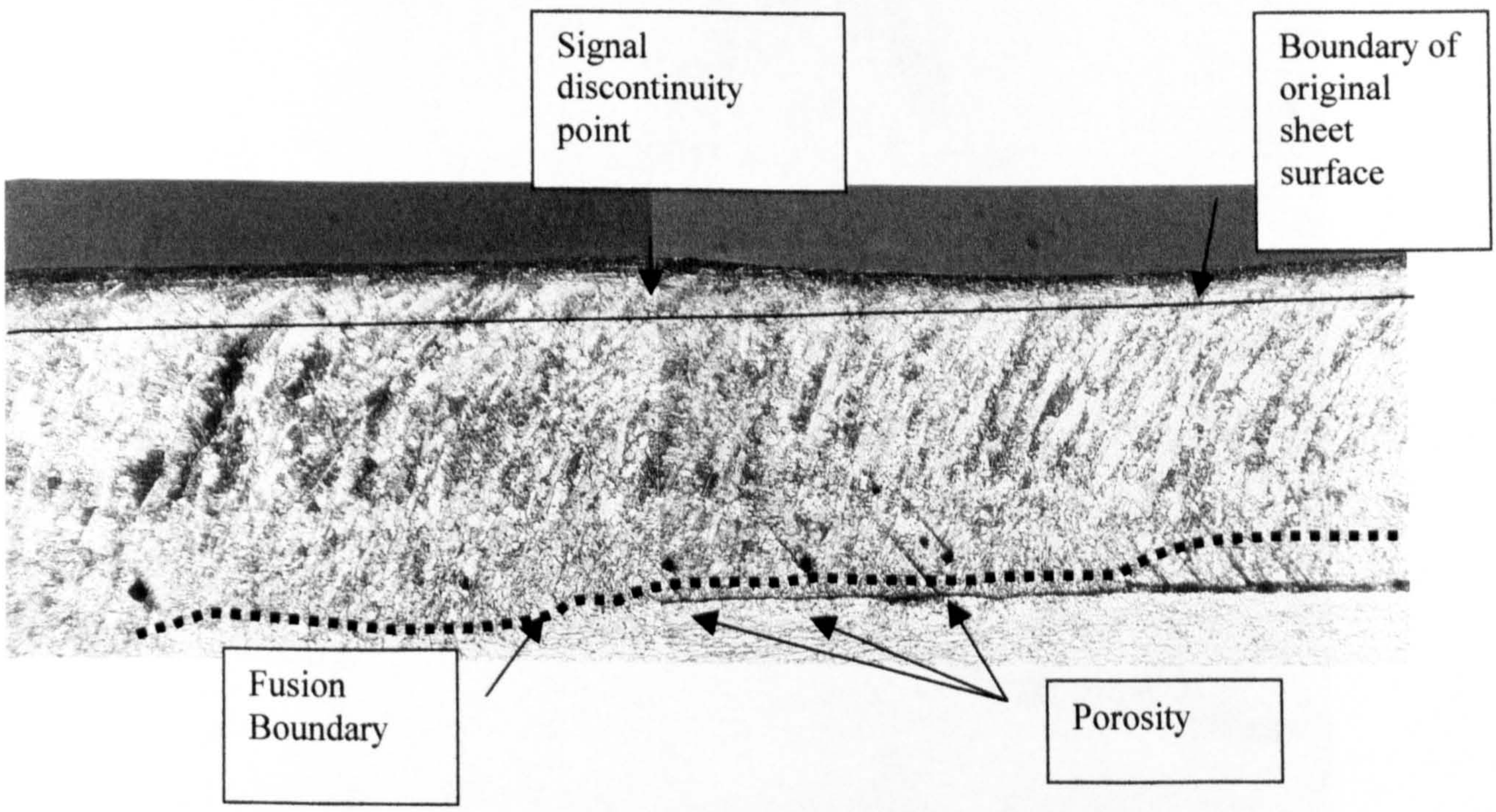

Figure 7.30 Longitudinal weld section (mag 50x) taken through the centre-line of a weld made in two overlapping sheets of 1.0 mm steel showing the weld discontinuity point towards the end of the weld. Etched in 2% Nital. Fusion boundary profile has been highlighted for clarity

Following the transition point at the end of the weld there is a slight but noticeable dip in weld height below the plane of the sheet surface.

7.6.3 Dual Wavelength Sensing

Observation of both the UV/visible and IR wavelengths together during the production of melt runs over a mild steel plate inclined at 2.5^{O} demonstrated that there was a distinct change in signal amplitude at different focus positions as seen above. More interestingly the changes in amplitude relative to focus position appeared to be different for each wavelength range.

A trace of UV/visible and IR amplitude is shown in figure 7.31.

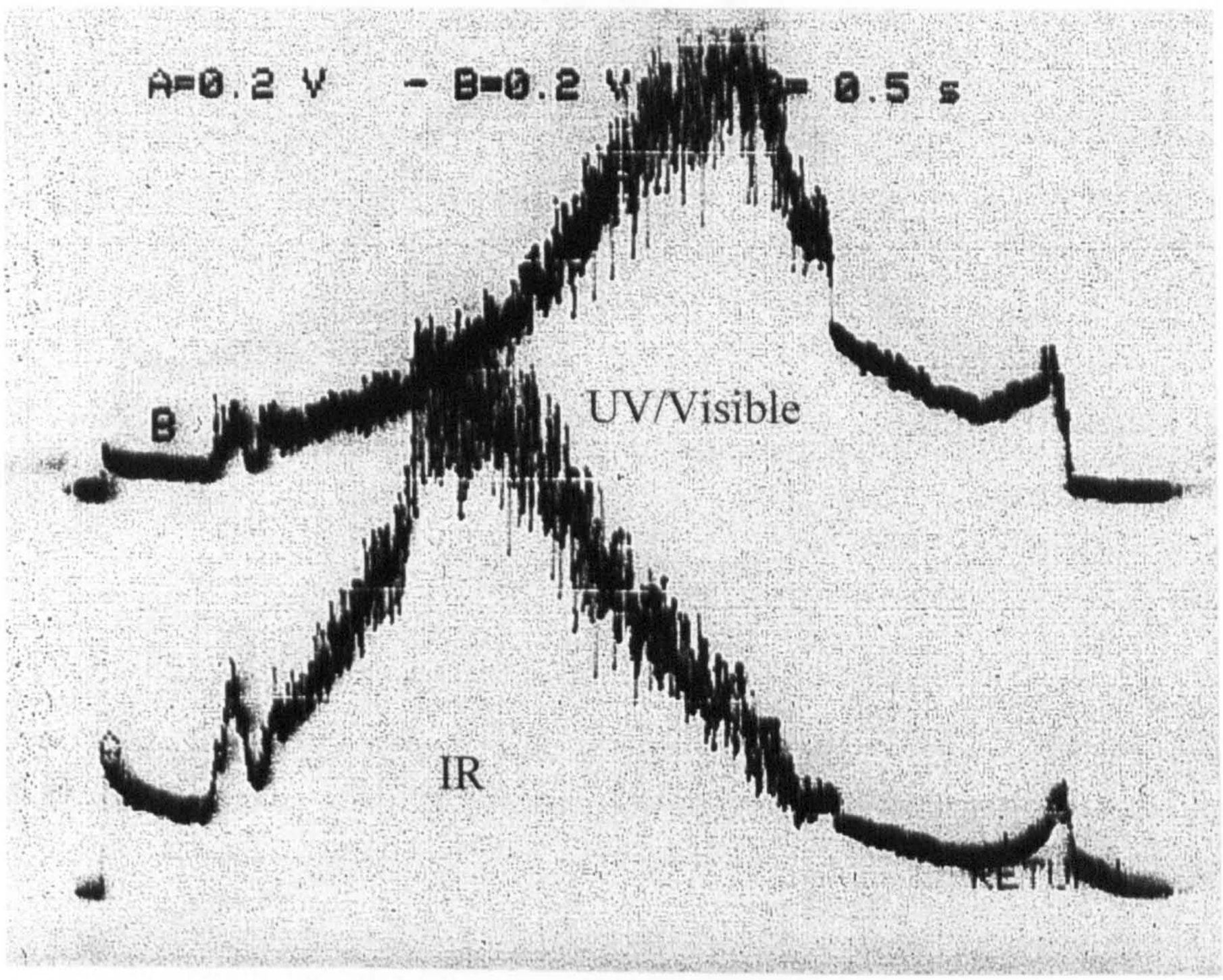

Figure 7.31. Infrared and 'UV/Visible' signals taken simultaneously while welding over an inclined mild steel plate

Figure 7.31 shows that the IR (trace A) and UV/visible (trace B) signals both increase and decrease as the laser beam is translated along the length of the tilted plate, each reaching a maximum amplitude at different positions along the plate.

Figure 7.32 shows the mean values (calculated over 1000 points, note the sample size 100,000 data points) for the trace plotted against focus position. Optimum or laser focus was determined from the point on the plate where maximum penetration was achieved. It can be seen that the UV

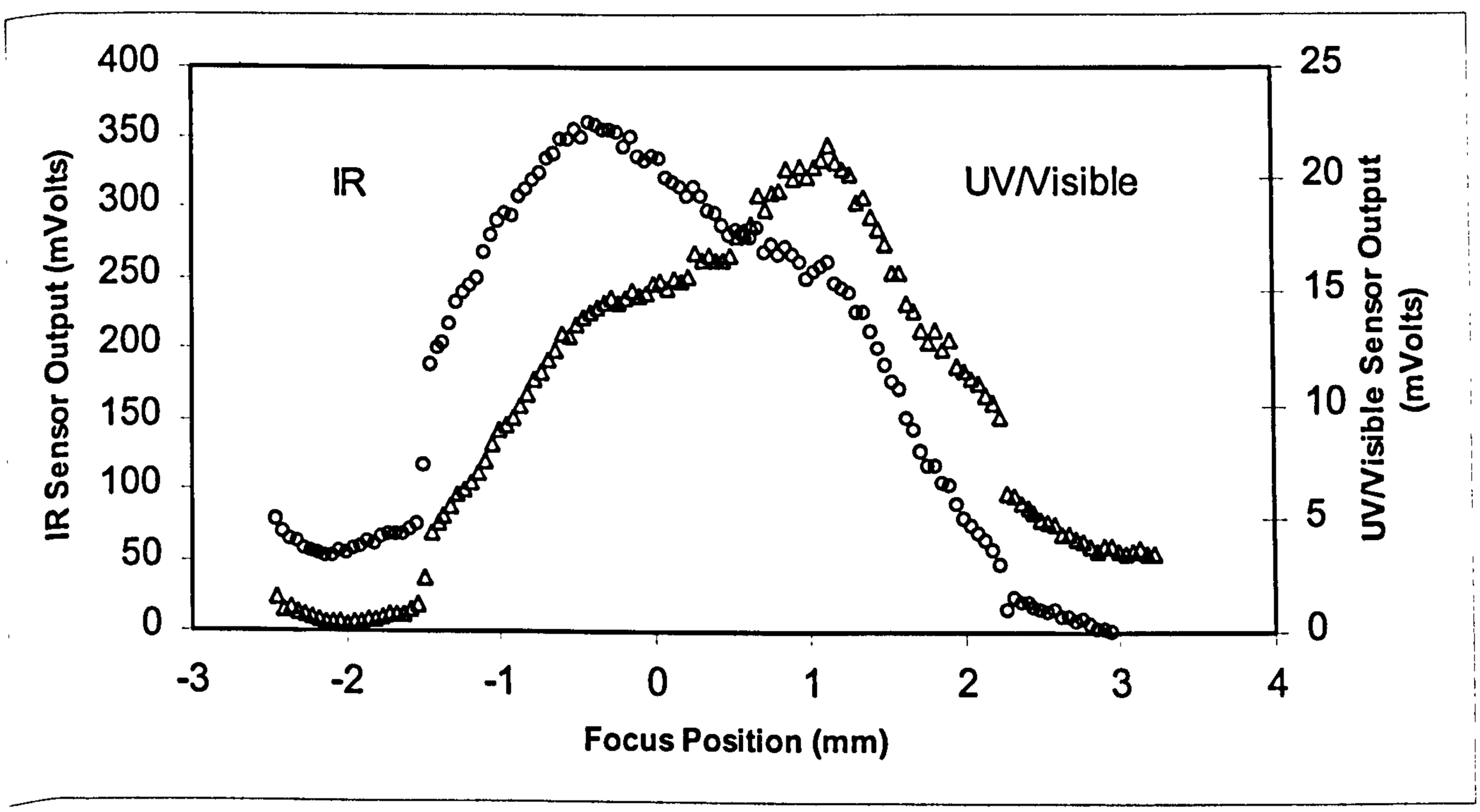

Figure 7.32 Average values of signal amplitude plotted relative to optimum laser focus position.

and IR signatures straddle the laser focus almost symmetrically.

7.7 Discussion of Results

7.7.1 Spectrometer Measurements

From figures 7.1 and 7.2 it can be seen that the spectra from the welding process for the Nd:YAG laser looks very much like black body radiation, following a similar contour to that described by Planck's law. There is little structure in either of the traces except in the region 590-600nm and 620-630nm where there are clear dips in the intensity.

Wien's law, see equation 3.13, shows the wavelength at the maximum intensity corresponding to a given temperature. This allows the temperature of the radiation detected by the spectrometer to be calculated. It can be seen for both figures 7.1 and 7.2 that the wavelength giving the maximum intensity are 630 and 650nm respectively, corresponding to temperatures of 4603K and 4461K. The difference in the two temperatures may be associated with experimental repeatability but may also be associated with the greater heat input per unit length of weld with the slower weld causing additional heating.

The spectra from the welds made with helium and nitrogen gas show similar characteristics to that of argon. The main difference appears to be a much greater relative intensity in the tail of these two signals in the wavelength range 700 to 950nm. There is also a decrease in minimum wavelength in the helium case. The reason for this is not fully understood but is believed to be a real phenomenon as all of the above results were achieved using the same equipment set up and subsequent checks welding in argon, yielded consistent results.

Figure 7.5 shows the spectra from a weld made at a higher mean power of 4kW at the work-piece. This gave increased heat input 15 J/mm and a higher intensity of 2.4MW/cm^2 when compared with the previous results. It can be seen that this has not significantly changed the profile of the spectra but has moved the peak intensity to a shorter wavelength of approximately 560nm corresponding to a blackbody temperature of 5178 K (5451°C)

A number of workers have carried out spectroscopic analysis of the beam work piece interaction for different laser sources including carbon dioxide [94, 95, 96, 97], carbon monoxide [98] and Nd:YAG [99].

The results of welds made using the carbon dioxide laser for comparison are quite different to those with the Nd:YAG. Figures 7.7 and 7.8 show the spectral results from welds made in mild steel with the carbon dioxide laser using argon and helium gas shielding. It can be seen that there is a significant difference between the two spectra. If a direct comparison is made it is immediately clear that in the case of the weld made in argon the spectrum is greatly extended and includes a number distinctive peaks at wavelengths above 650nm. These have been identified from tables of spectra as being lines associated with the first level of ionisation of argon, the lines being 696.54, 706.72, 727.29, 738.39, 750.38, 751.46, 763.51, 772.37, 772.42, 794.81, 800.61, 811.53 and 842.46nm. The spectra to the left of the 650nm peak appears to have a profile with much more structure associated with it and is quite unlike the smoother profile from the Nd:YAG laser.

During welding it was noticeable that the brightness of the light generated from the argon was much greater than for helium. This impression was confirmed, as light incident on the detector for the argon shielding, was found to be some 190 times greater in intensity than for the helium.

7.7.2 Signal Behaviour During Melting

The signals taken from the spot welding on the copper target were dominated by the back reflection and scattering of the laser radiation wavelength. It was apparent that by increasing the number of pulses a threshold was reached which firstly reduced the backscattered signal by approximately one half, which ties in closely with the findings where a high intensity pulsed laser was used [28] to melt a copper target. The initial drop in intensity is thought to be associated with the break down of reflectivity (increase in absorptivity) and is probably associated with the introduction of oxidation on the surface of the plate. This is supported by the fact that melting of the plate at this intensity could not be achieved when using gas shielding.

The onset of modulation seen in the signal was confirmed as being associated with melting of the metal surface and displacement of the melt by the vapour pressure.

When the CPM was used to monitor the backscattered laser radiation it was found that the signal at the Nd:YAG wavelength appeared to change in the opposite sense to the UV and IR wavelengths. That is, as the power was decreased the YAG signal was found to increase, indicating that the signal may be associated with changes in coupling. In an attempt to try to normalise the data the depth of penetration at each condition was measured, using metallographic techniques and compared to the signal amplitude. Figure 7.33 shows a plot of penetration depth against sensor signal.

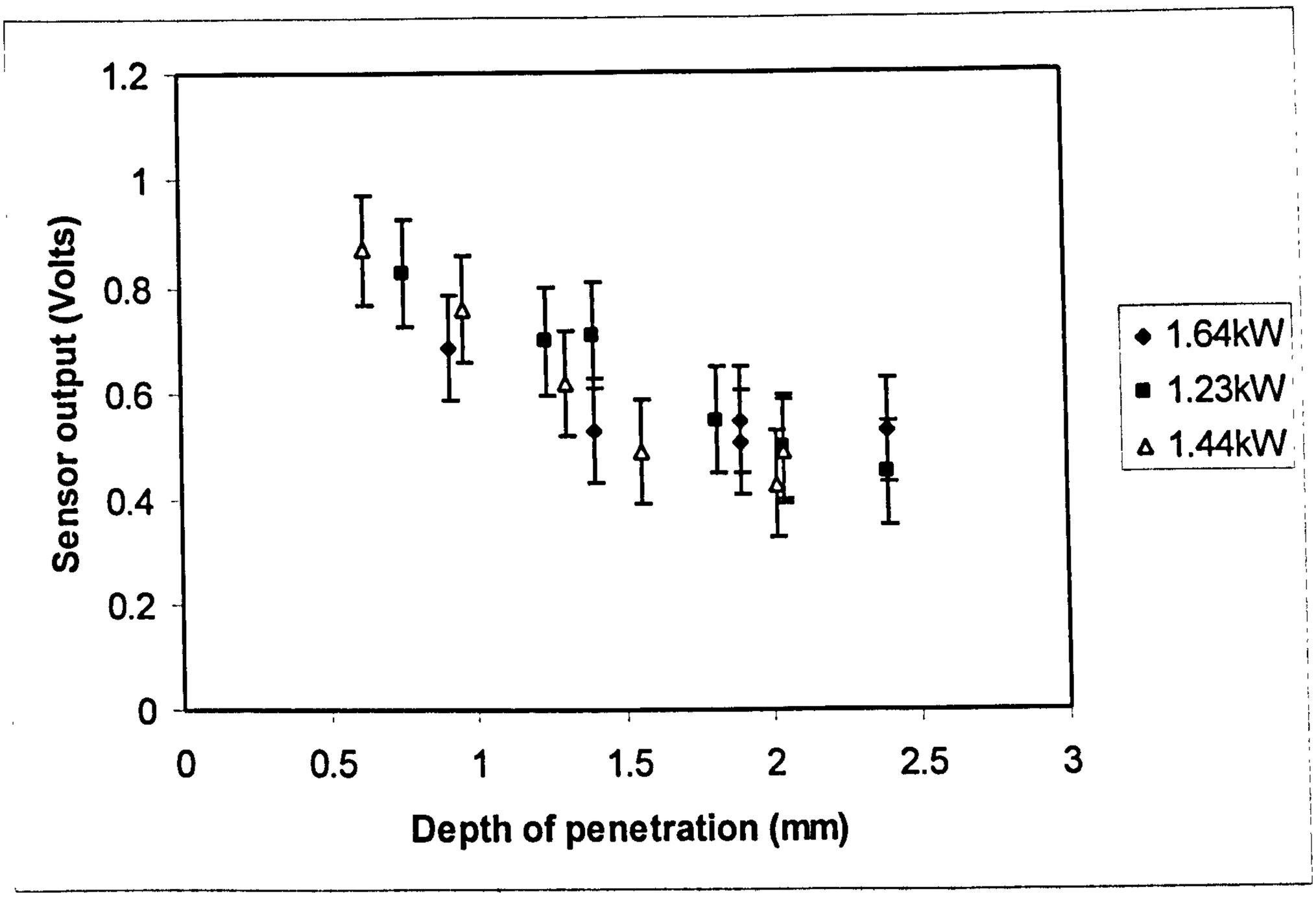

Figure 7.33 Plot of penetration depth for three different speeds and power levels

It can be seen that to a close approximation the sensor signal corresponds closely to the penetration depth even for changes in speed and laser power. This is an interesting result as it seems to indicate that for a given penetration depth a backscatter signal exists which is independent of speed and power.

7.7.3 Oscillation Behaviour

Figure 7.34 shows a plot of natural frequency for the weld pool calculated using the Postacioglu model [68,69], for two axial mode numbers 4 and 5. To aid calculation the surface tension and density of the melt have been assumed to remain constant, the figures used being 0.85N/m for surface tension and an average density of 7200kg/m^3.

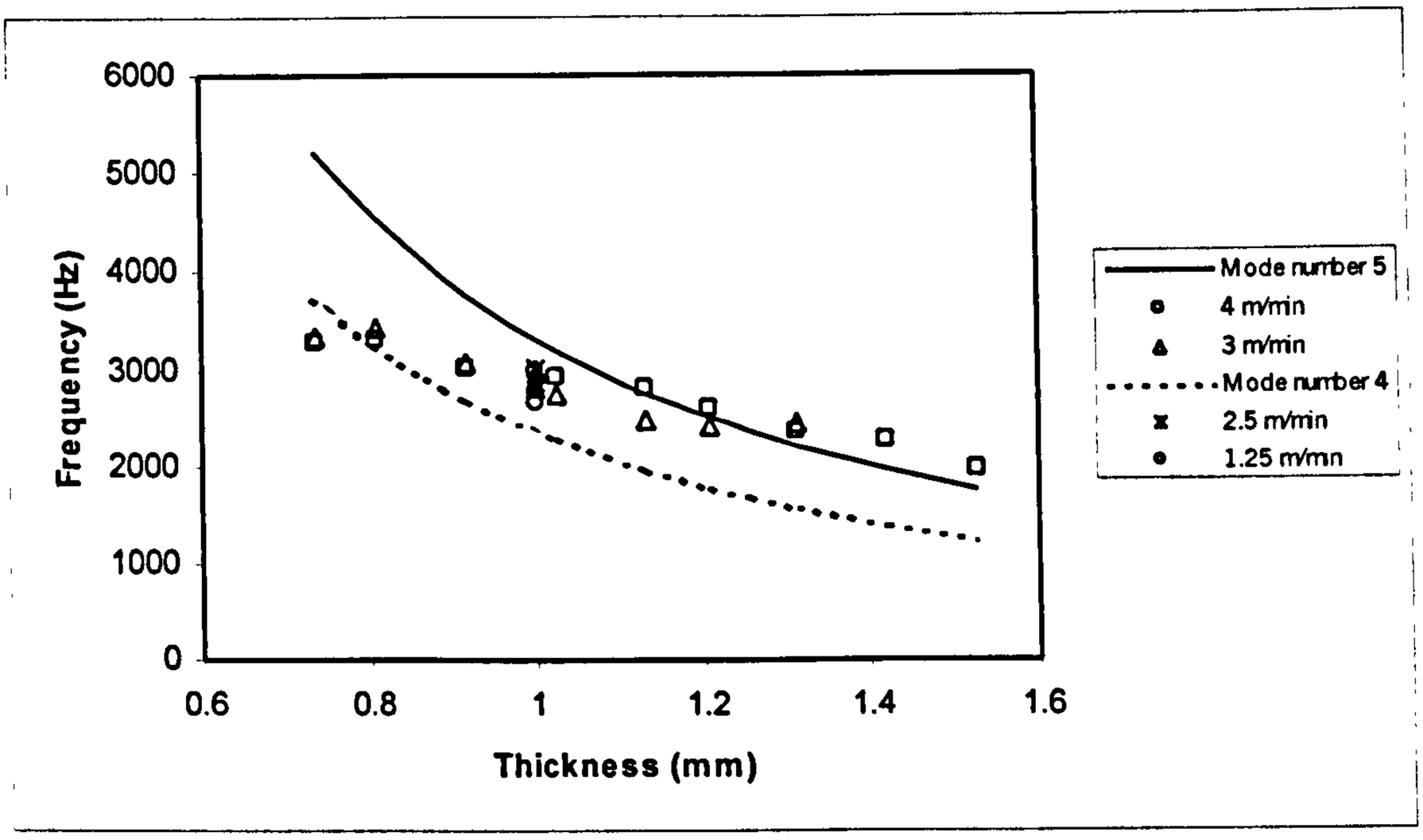

Figure 7.34 Natural frequency of weld-pool oscillation compared with measured values at different material thickness

These have been plotted together with the actual frequencies observed during the welding operation carried out across the tapered work-piece as a function of material thickness. Additional points have been added from individual welds made in single thickness of 1.0mm at various travel speed.

It can be seen that the actual measured frequencies follow closely the calculated predicted natural frequencies, lying approximately half way between the natural frequencies of the two modes. They show a clear correlation between thickness, and length of keyhole and oscillation frequency as predicted.

The high-speed video showed clearly that for a 1.0mm thick plate that the keyhole entry remains static whilst the exit appears to open and close periodically. The frequency of oscillation

calculated from the frame speed corresponded to that observed on the optical signals and to that predicted, demonstrating that this was the origin of the oscillation.

The reason for the opening and closure of the keyhole is thought to be associated with the way the beam interacts with the molten liquid within the pool. It is thought that the interaction is not continuous but periodic. The beam is thought to initially couple with the front portion of the keyhole, vaporising the material in the process. This creates sufficient recoil pressure to produce a pulse which forces molten metal downwards and away from the interaction point. The pulse of molten material is forced to the bottom of the keyhole whereupon it produces full or partial closure. Restoring forces (surface tension), in the absence of significant vapour or recoil pressure within the weld-pool then re-present the melt interface to the beam again and the process is repeated. The action of the beam is stimulating the natural frequency of the pool and visa versa. This analysis is partly supported by the limiting case of speed observed in figure 7.18, where the keyhole became extended. These conditions were marked by the disappearance of characteristic natural frequencies that would have been expected from a fully penetrating keyhole. The reason for this is that the keyhole exit has become so enlarged that the keyhole can no longer close. This perhaps explains the departure of the measured frequency data from that predicted towards the thinner end of the tapered work-piece. Here the relative speed to work-piece thickness is such that the keyhole is enlarged, reducing the ability for the keyhole to close.

7.7.4 Changes in Focus Position

The highly dynamic nature of the backscattered laser light signal is believed to be associated with melting of the plate surface and subsequent displacement of the surface such that normal specular reflection is no longer possible, thereby greatly reducing the level of radiation returning back up the laser beam delivery optics and being captured by the sensor.

In the case of the copper target, no melting of the surface was occurring and the temporal characteristics of the returned signal remained constant at the various focal positions. The origin of the increase in signal amplitude as the target surface approached the waist position is believed to be associated with a number of effects including the aperturing effects of the fibre, the diverging or converging beam on the surface of the target either side of the waist and the size of the image relayed from target to fibre.

7.7.4.1 Divergence Effect.

The rays from the lens converge as they approach the waist position. As these converging rays strike the surface of the target, if the laws of reflection apply as they should from a reasonably smooth flat surface then, the reflected rays will fall within the aperture of the beam delivery optics and will therefore be collected. This is shown diagrammatically in figure 7.35.

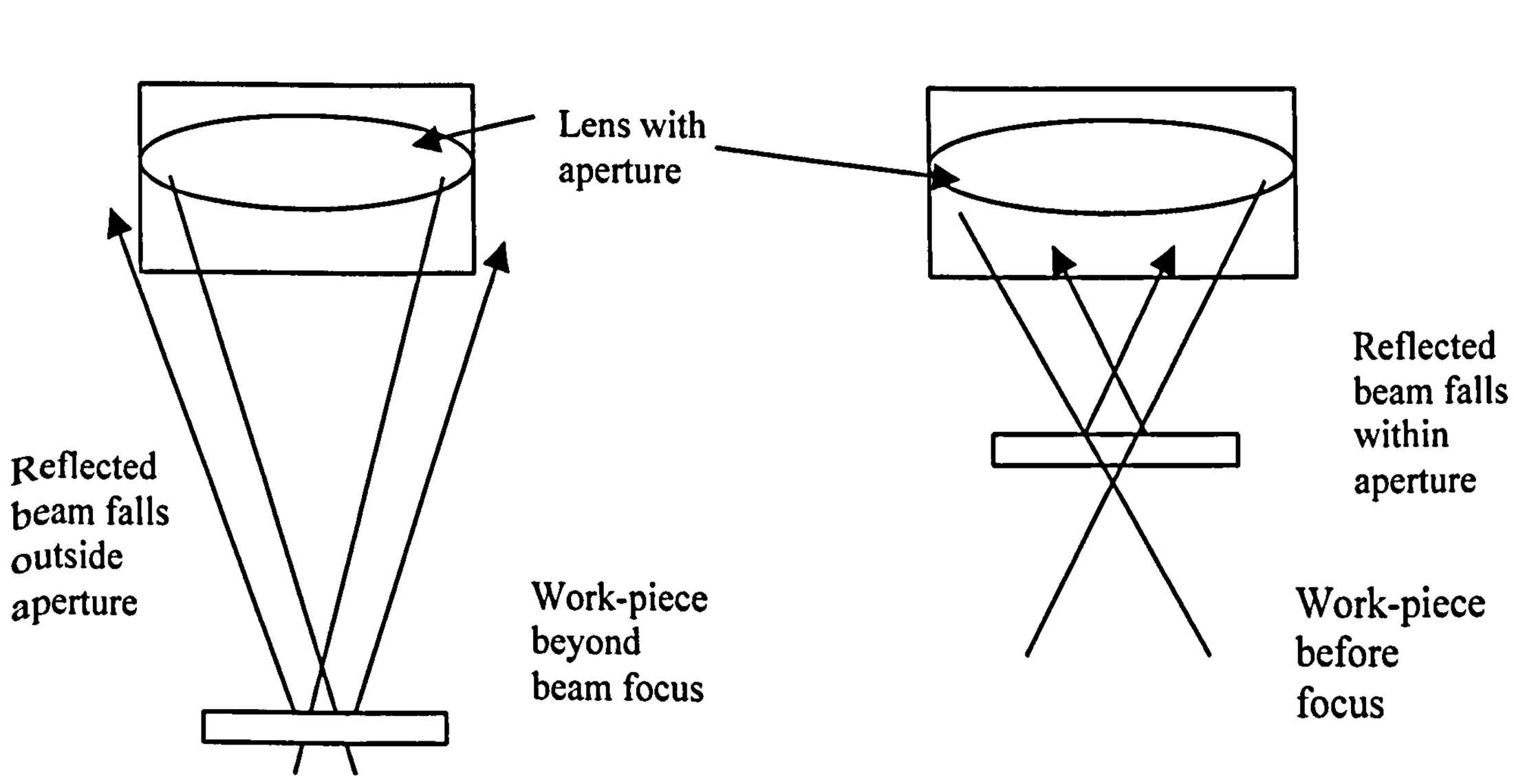

Figure 7.35 showing effect of beam divergence on the amount of light available for through the fibre detection

7.7.4.2 Image Effect

Calculations with the combination of lenses used revealed that the position of the waist and image planes could differ by up to 1.0mm. Thus the image of the fibre end does not correspond to the position of highest intensity. If the target is positioned at the image position, the backscattered light will be imaged back into the fibre in its entirety. If however, the target is positioned at the waist position (the position of highest intensity) not all of the light would be imaged back into the fibre and the amplitude of the signal would be correspondingly less.

The inclination of the sheet material below the laser beam to produce a continuously variable focus has yielded some interesting results. The discontinuity observed consistently on the UV/visible signal shown in figure 7.22 (and also on the IR signal not shown), after 0.6secs correspond to changes on the surface of the weld profile perhaps indicating a transition in the way the beam is coupling into the work-piece. A distinct change in the weld profile can be seen from sections taken either side of the transition point but not immediately at this point. This suggests that the change in signal is associated with a change in the characteristics of a welding regime, most probably moving from conduction limited melting to key holing, shown by the characteristic 'wine glass' shape in the weld cross-section.

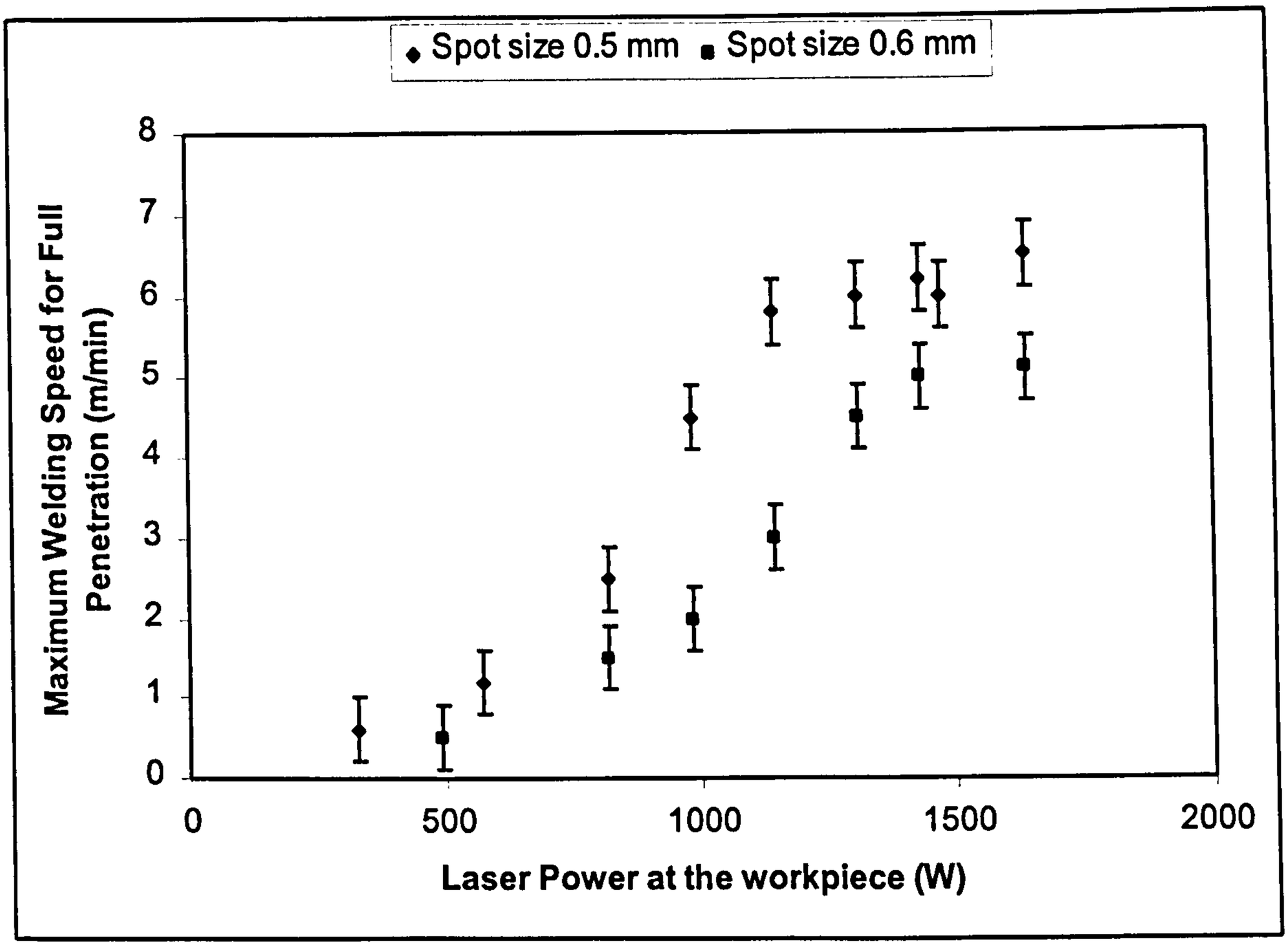

Figure 7.36. Effect of laser power at two spot sizes, on maximum speed for full penetration in 1.0mm thick mild steel.

Several workers [33, 39] have determined that at low intensity, such as that encountered with a defocused beam, heating of a metal target below its surface will be by conduction of heat. At higher intensity there is a change in the regime that creates vaporisation and an increase in coupling efficiency.

An investigation was carried out to determine the conditions of power and spot-size needed to produce this transition. This was achieved by welding across a horizontal 1.0mm thick steel sheet at different power levels and optimising the welding speed until full penetration could just be produced. Two lens combinations were used;

i. Recollimating lens of 160mm and a focus lens of 80mm giving a spot size of 0.5mm diameter.

ii. Recollimating lens of 160mm and a focus lens of 120mm giving a spot size of 0.6mm diameter.

The results of these trials are shown in figure 7.36.

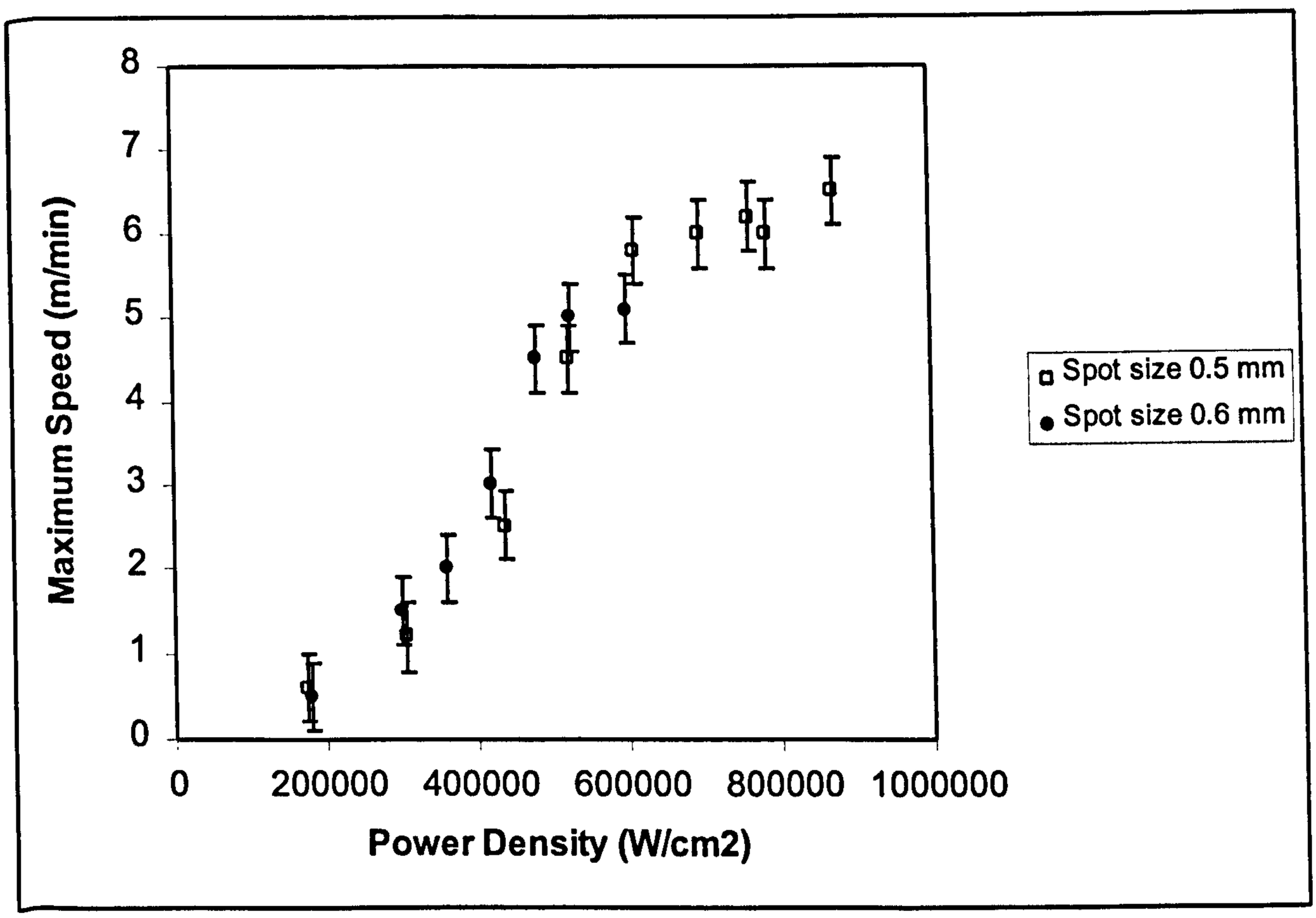

Figure 7.37 plot of calculated power density against optimum welding speed

The intensity (power at the work-piece divided by the area of the focused spot) was calculated using results from figure 7.36 and plotted in figure 7.37. To improve the accuracy the spot size calculation included the contribution from spherical aberrations. This revealed that the transition

from a conduction-limited regime to that of a vaporisation regime occurred at power density in the range between 2 and 6MW/cm^2.

An estimate of the average power density occurring at the transition point seen on the inclined plate can be made by using geometric principles. If it is assumed that the centre of the full penetration region corresponds to the point where the beam waist is coincident with the plane of the sheet surface, simple geometry can be used to calculate the approximate spot size of the beam above the work plan at the transition point. It can be shown that the power density at the transition point is approximately 163kW/cm^2. It is therefore believed that the discontinuity observed on the tilted work-piece surface is associated with the transition point between a conduction limited and vaporisation regime.

7.7.5 Chromatic Effects

The origin of the separated signals with the IR and UV/visible ranges is believed to be associated with the chromatic aberration of light passing through the laser focusing lenses. Chromatic

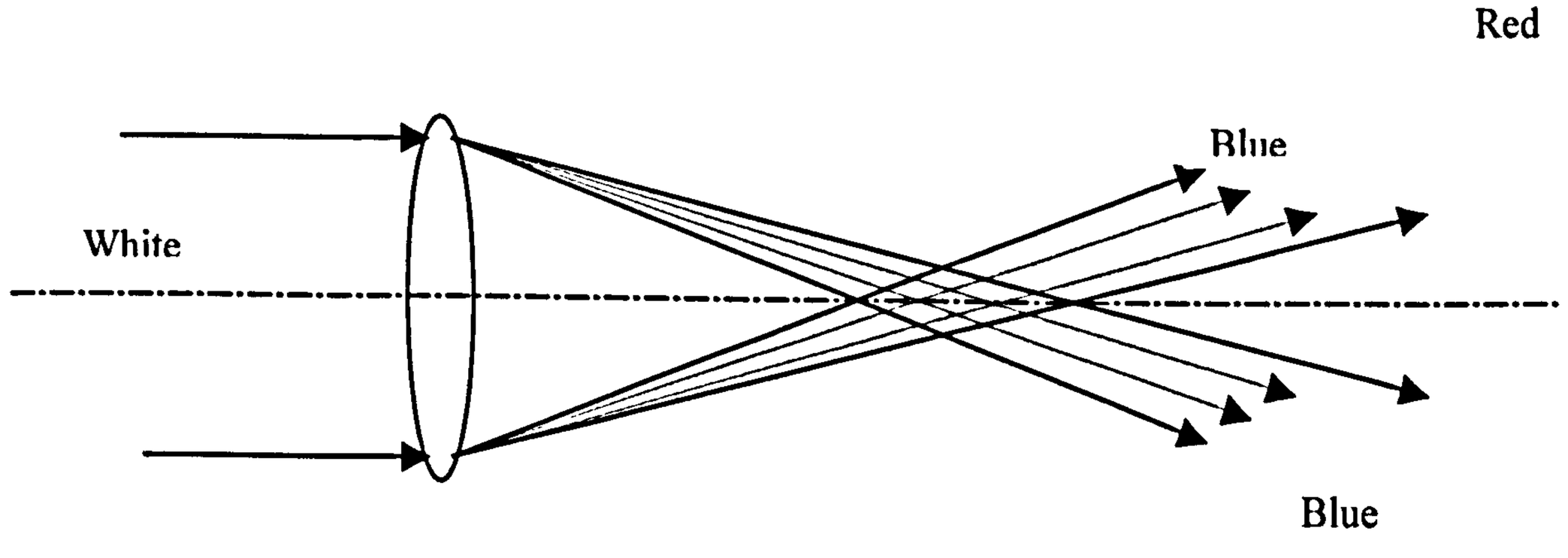

Figure 7.38 schematic showing principle of chromatic aberration (after Hecht)

aberration is a well known phenomenon which describes the effect when light of different wavelength passing through the same lens is focused in different planes. If we consider the thin lens equation 7.1 (lens maker's formula) below:

$$\frac{1}{f} = (n_{lens} - 1)\left(\frac{1}{R_1} - \frac{1}{R_2}\right) \tag{7.1}$$

It can be seen that the focal length (f) of the lens (in air) is a function of the lens surface radii (R_1 and R_2) of the lens surface and the refractive index (n_{lens}) of the lens material. We know however, from dispersion theory that the refractive index of a material is not only dependent on the material but also on the frequency of the radiation propagating through it,

that is; n_{lens} is a function of λ,

and therefore from equation 7.1 it can be seen that the focal length of a simple lens is also dependent on wavelength.

Figure 7.38 shows a schematic diagram of a lens focusing a source of white light. It can be seen that the positive lens has a separate focal point for each frequency (or colour) of light. For convenience the range of colour has been shown from red to blue. With a positive lens made of common lens material, such as fused silica, the focal position of the red is pushed out to the right of the blue. This type of chromatic aberration where an axial displacement of the image is experienced is known as axial (or longitudinal) chromatic aberration.

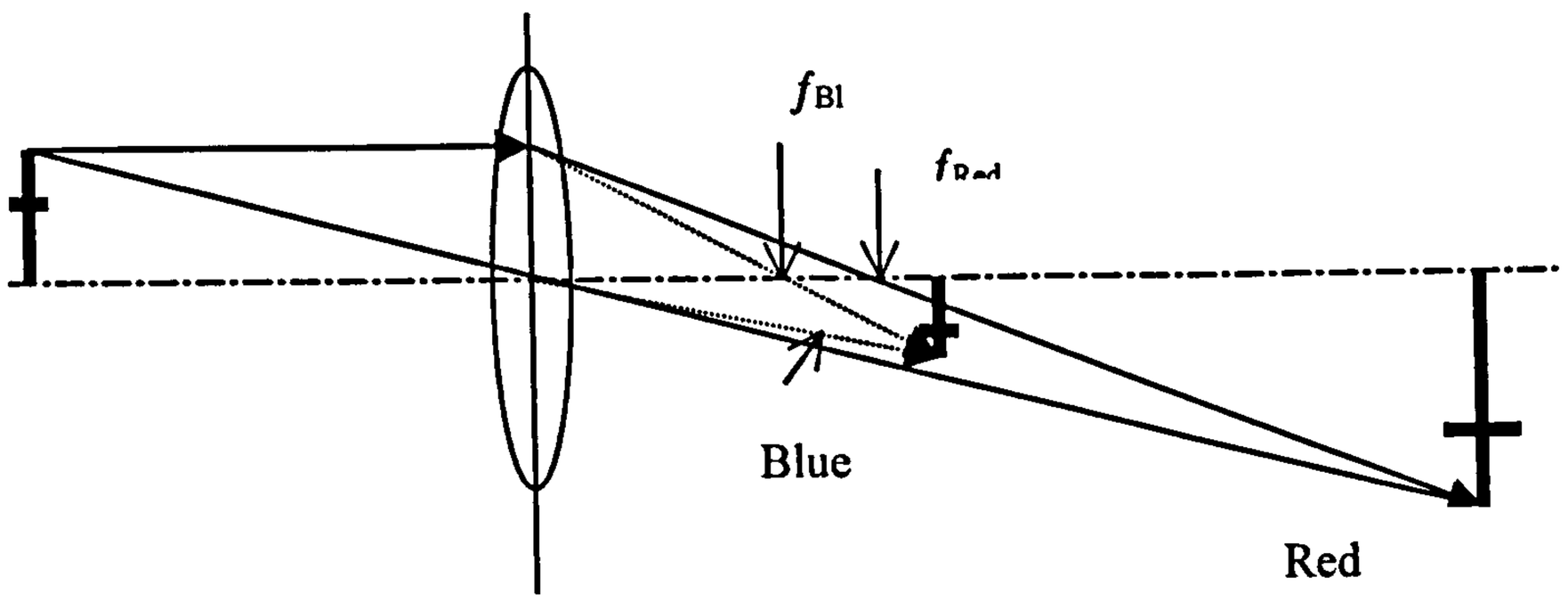

Figure 7.39 schematic showing effect on image position and size of chromatic aberration (after Hecht)

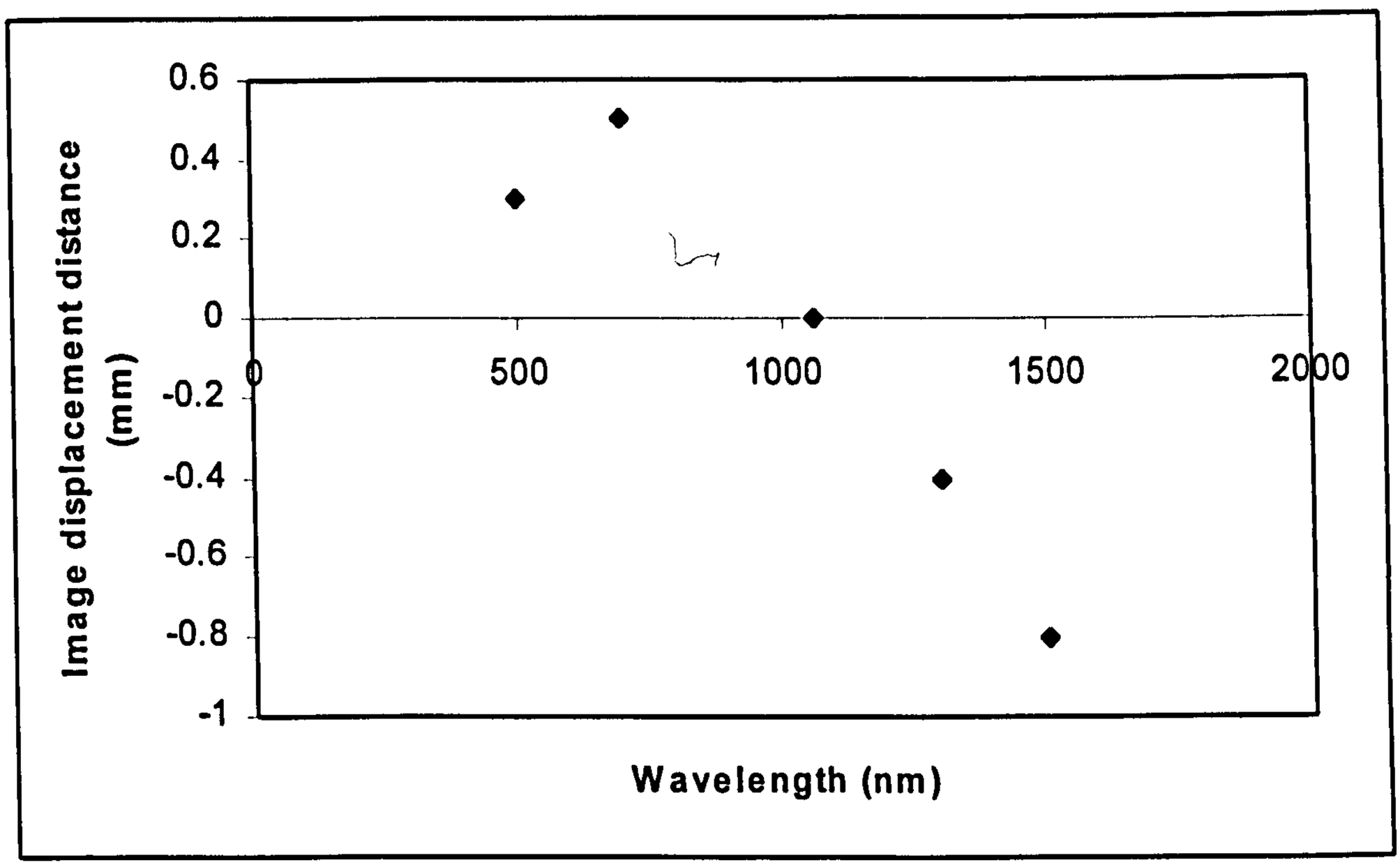

Figure 7.40 Variation of image distance with focal length for lens system used in process trials

Another effect is where the image of an off-axis point causes transverse magnification. This is known as lateral chromatic aberration, an effect illustrated in figure 7.39.

The lenses used in the trials were of positive cemented achromat type, each consisting of two elements one positive the other negative. The achromat design allows for some correction of chromatic aberration but not all. The relative image displacement distance for the lenses used is shown in figure 7.40. It can seen that although the lenses used were achromatic, chromatic aberrations still occur at other wavelengths these are known as the secondary spectrum.

Figure 7.41 shows a schematic of the principles involved in the chromatic aberration observed during defocus. For simplification (and to ease drawing) the two positive achromat lenses used in practice have been idealised as a single lens. An explanation of the principles is given below with reference to the figure.

1. The work-piece is situated at the focal point of the lens, with the laser radiation forming an image of the fibre onto the work-piece. Process light consisting of broadband wavelengths, and illustrated by the two wavelength ranges infra-red (IR 1100 –1600nm) and Ultra-Violet/Visible (UV/visible 300 – 700nm) is generated by the interaction of the beam with the work-piece. The effective focal points of the IR and UV/Visible wavelengths respectively are less than and greater than the laser wavelength (1064nm), so their images are formed before and after the fibre face.

Figure 7.41 Principle of signal behaviour with changes in focus due to chromatic aberration

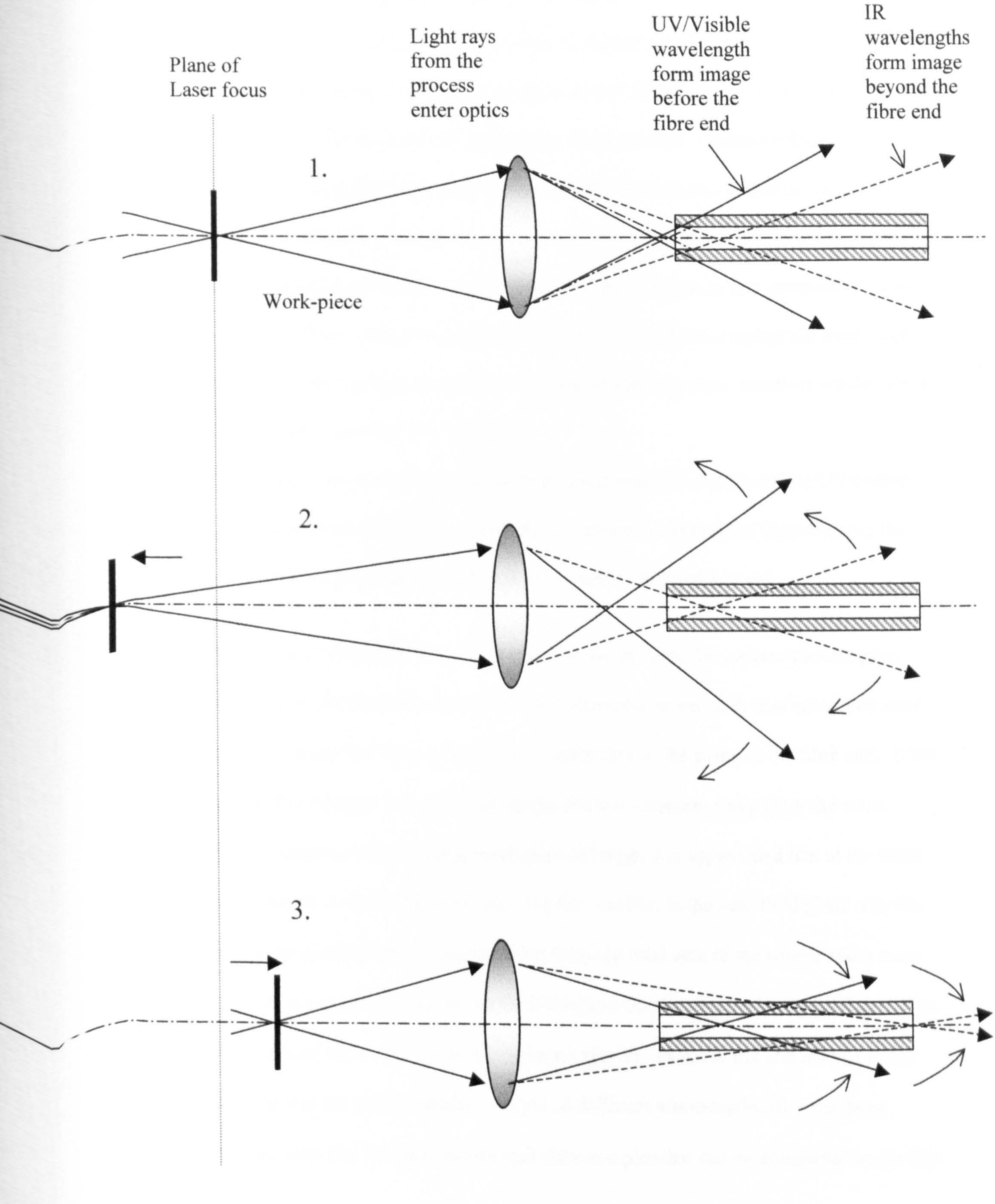

At the plane of the fibre end the circle of confusion of the two wavelength bands is of similar size and the signal is therefore similar (assuming equal intensity). Therefore the core of the fibre can be seen to act as an aperture discriminating between intensities.

2. The work-piece has been moved further away from the lens. Correspondingly the IR image has moved closer to the lens and more of the IR radiation is able to enter the fibre. The UV/visible has also moved closer to the lens but because it is focusing before the IR image it diverges more before the fibre face and less radiation at this wavelength band can centre the fibre. As a consequence a detector at the opposite end of the fibre (core monitor), or detecting light in the fibre cladding (Cladding power monitor) would detect more IR radiation and less UV radiation.
3. The work-piece has moved back towards the focus lens that shifts both the UV/visible and IR images beyond the fibre end. In this condition the amount of light entering the fibre in the IR band is reduced and increased for the UV/Visible band.

Figure 7.42 shows a plot of calculated relative spot size on the fibre for various wavelengths. Manufacturer's data on the chromatic aberration characteristics of the each lens have been used. For each wavelength a plot has been made of the relative area in the plane of the fibre end. It has been assumed that the intensity across the across the beam is constant, away from the waist position. This is thought to be a valid approximation although it is appreciated that at the waist position the distribution is of constant intensity 'top hat' profile; in the near field plane only the central portion of the distribution will receive light from the total area of the source and a more conical distribution is expected [100]. In the far field plane the distribution is expected to receive flux almost evenly from the source. It is also assumed that the source is flat and normal to the axis of the lens and that the source consists of light of different wavelengths all at the same intensity. It can be seen that for each wavelength there is a plot that can be interpreted as the flux

entering the fibre end. Thus at a value of unity all of the light from that wavelength enters the fibre.

It can be seen that the prediction matches very closely the behaviour observed during the trials suggesting that it is predominantly chromatic aberration producing the effects seen.

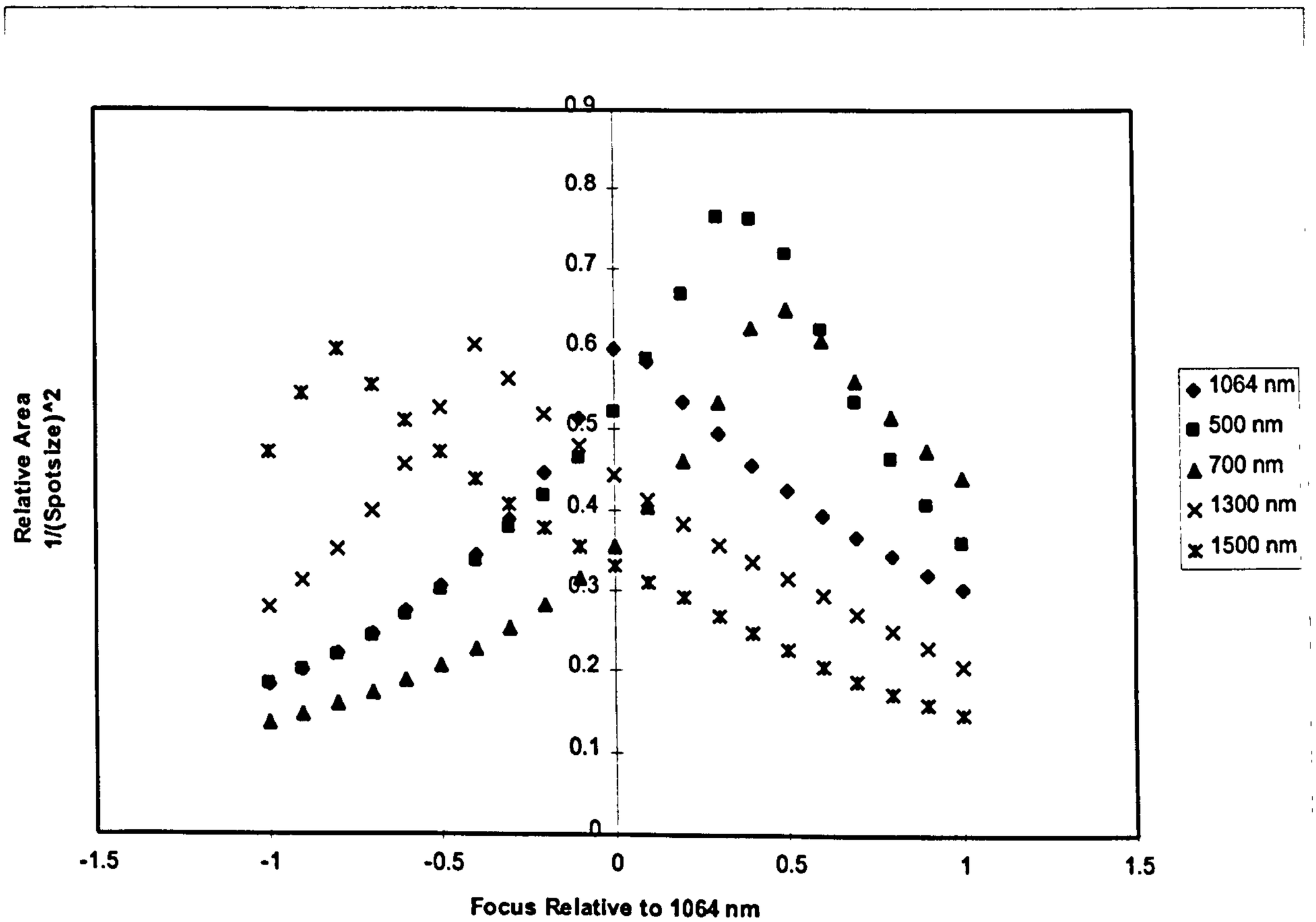

Figure 7.42 Calculated relative spot area in the plane of the fibre for several wavelengths

8 Experimental Trials to Observe the Spatial Behaviour of the Optical Signals During Welding

8.1 Objectives

Use of equipment to observe the spatial characteristics of the optical radiation emanating from the laser interaction zone is perceived as being a more complex issue than simply observing the temporal profile. The main reasons are that instead of a single sensor point it is necessary to use multiple sensors such as an array to track the movement of intensity over the area of the interaction zone. The complexity of such a system may also be diametrically opposed to the need for an industrially rugged device. In addition signal interpretation becomes more difficult since there is more information to interpret.

On the other hand, with both temporal and spatial information available the probability of achieving a device that has greater ability is perceived as higher. The work in this chapter examines the changes both temporal and spatially changes in optical signals during variation in process parameters.

8.2 Sensor Equipment

A CCD camera-based sensor was used to observe spatial information from the laser beam interaction at the work-piece. The CCD camera was placed behind a fused silica 45° turning mirror, coated to reflect 1064nm laser radiation, so as to view the interaction point through the mirror. A schematic diagram of this arrangement is shown in figure 8.1. The arrangement allowed selective optical filters to be placed between the work-piece and the camera to allow the radiation of interest to be viewed and the unwanted radiation to be removed.

An image processing software (Big Sky) was used to digitally collect the signal from the camera and show an image graded according to the signal intensity. The software also allowed the digitised data to be saved and accessed as data arrays.

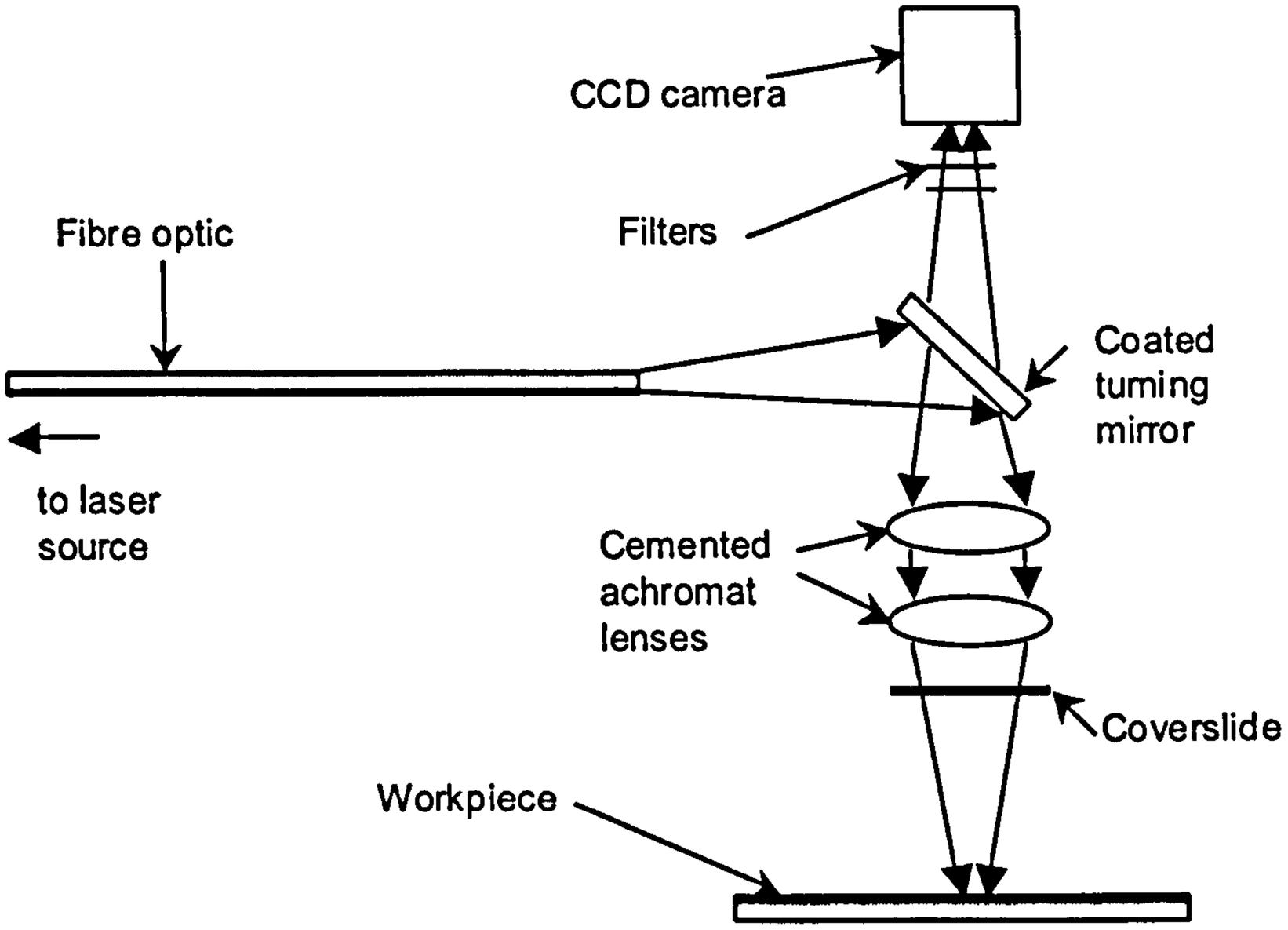

Figure 8.1 schematic of CCD camera-based sensor arrangement

A second arrangement was used whereby a single miniature X-Y stage was placed at the con-focal point of the laser beam focus optics, behind a fused silica mirror with coating centred on 1064nm. The X-Y stage was designed so that a fused silica fibre with 100μm core could be attached to it and moved manually in a raster parallel to the con-focal plane so as to allow light to enter the end of the fibre. Using this arrangement signals could be captured from a circular image

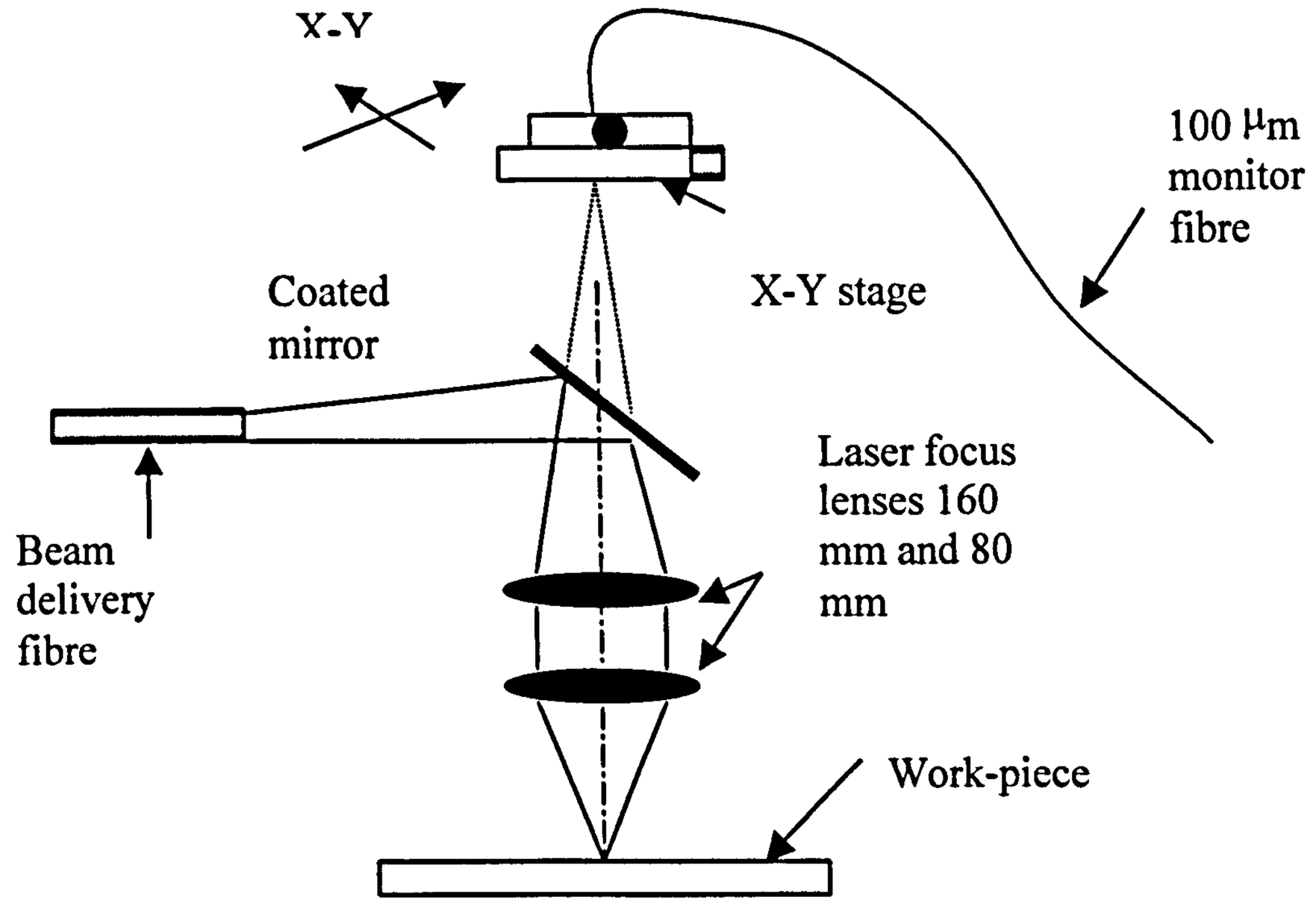

Figure 8.2. Miniature stage arrangement for gathering radiation signals from different areas in and around the beam interaction point in the plane of the work-piece.

corresponding to 50μm diameter (taking into account the imaging ratio of the laser focus optics) in the plane of the work-piece.

8.3 CCD Camera Sensor Experimental Procedure

The sensor arrangement used is shown schematically in figure 8.1. A silicon based CCD camera was placed behind a 45°-turning mirror within the beam delivery optics. This mirror was coated to reflect the 1064nm laser wavelength but still had a transmittance at this wavelength of approximately 0.2%. Other wavelengths in the visible and near infrared were transmitted with very little attenuation. The camera was positioned such that the two lenses formed an image of the work-piece on both the CCD array and the fibre end-face (at a wavelength of 1064nm). The lenses used were both positive cemented achromats with the closest to the fibre having a focal

length of 160mm and the other 80mm. The fibre core diameter was 1.0mm, and the focused spot size at the work-piece 0.5mm diameter. A band pass filter centred to pass 1064nm with a bandwidth of 10nm was placed between the camera and mirror; additional attenuation was controlled using appropriate glass neutral density filters. Bead-on-plate welds were produced on 4.0 and 5.0mm thick mild steel plate using a 2kW Nd:YAG laser, a Lumonics Multiwave^{TM} 2000. The laser gave 2kW at the source and after losses (measured as 18%) through the beam delivery, which included an optical fibre, lenses and an uncoated cover-slide, gave 1840W at the work-piece.

The beam was focused at the surface of the steel plate that was clamped securely into a fixture and moved beneath stationary focusing optics using an appropriate motorised linear table and CNC controller. Initially, optimum focus was found by sectioning welds made at a constant speed at various focal point elevations and, selecting the focal point corresponding to the greatest depth of penetration.

To simulate conditions where laser power and speed were varying a series of welds were made at laser power (measured at the source) in the range 1kW to 2kW and at different speeds in the range 0.5m/min to 3.0m/min. To simulate a focal error welds were made with different lens-to-work-piece distances over a range +/- 1.5mm either side of the optimum focal position.

To investigate the influence of work-piece temperature the work-piece was preheated. This was achieved by clamping the steel plate onto the surface of an electrical heater itself fixed to the linear table. The temperature of the plate to be welded was measured using surface thermocouples. Welding trials were carried out at three work-piece temperatures 26, 230 and 400°C. Each weld was produced with a constant parameter setting and the camera image captured using software that stored the image as a graduated intensity scale.

To ensure that no oxidation could occur, all welds were made with argon gas shielding introduced via gas-shoe arrangement.

After welding each weld was subsequently sectioned, polished and etched (Nital 2%) and the depth of penetration measured using a stage microscope and graticule.

Optical images were collected mid-way through each weld to ensure that a steady state had been reached and stored using image analysis software (Blue Sky) for later analysis. The software allowed the image to be viewed as a graduated scale of intensity and allowed stored of this image as a 2 dimensional data array.

The images obtained from the CCD camera were firstly analysed visually to determine whether there were any obvious trends. A computer programme was then used to analyse the data files by locating the centroid of the 2-dimensional data file array and plotted out the relative intensity from side to side and front to the rear of the weld-pool.

8.4 Results

Figure 8.4 shows the intensity profile of the laser beam taken at the beam waist position after the laser focusing lenses at mutually perpendicular directions, X and Y.

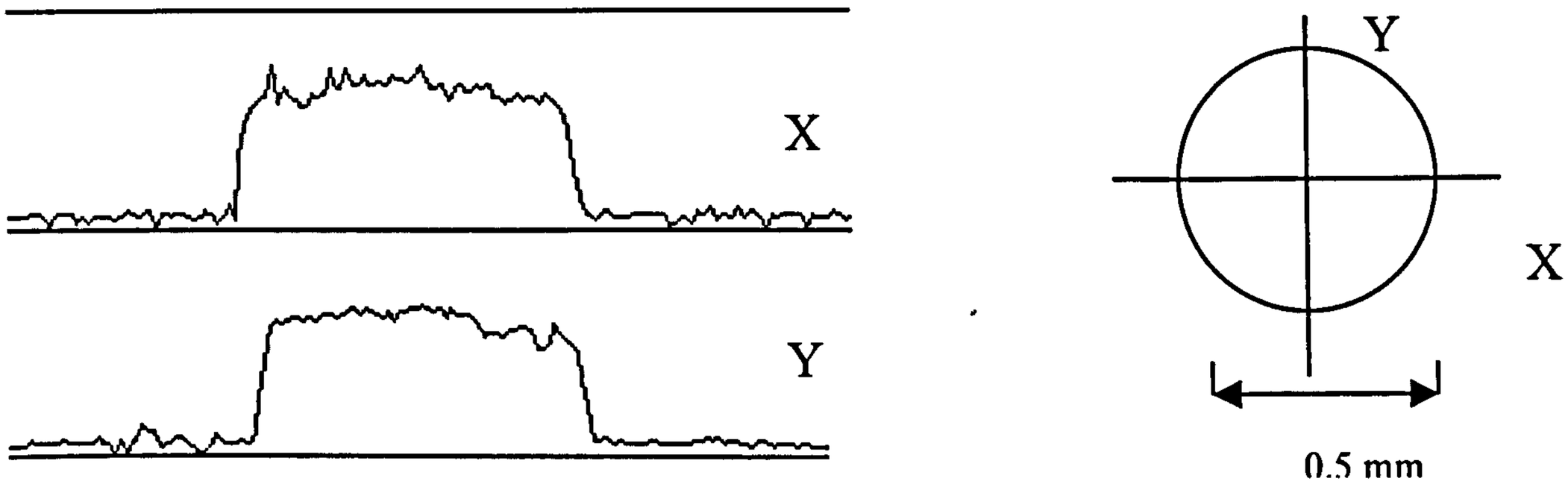

Figure 8.4 Beam profile at focus position

It can be seen that the beam profile is 'top hat' in shape, which is typical of beams delivered through fibre optic beam delivery. The results of welding trials using the through focus head CCD camera system are presented below:

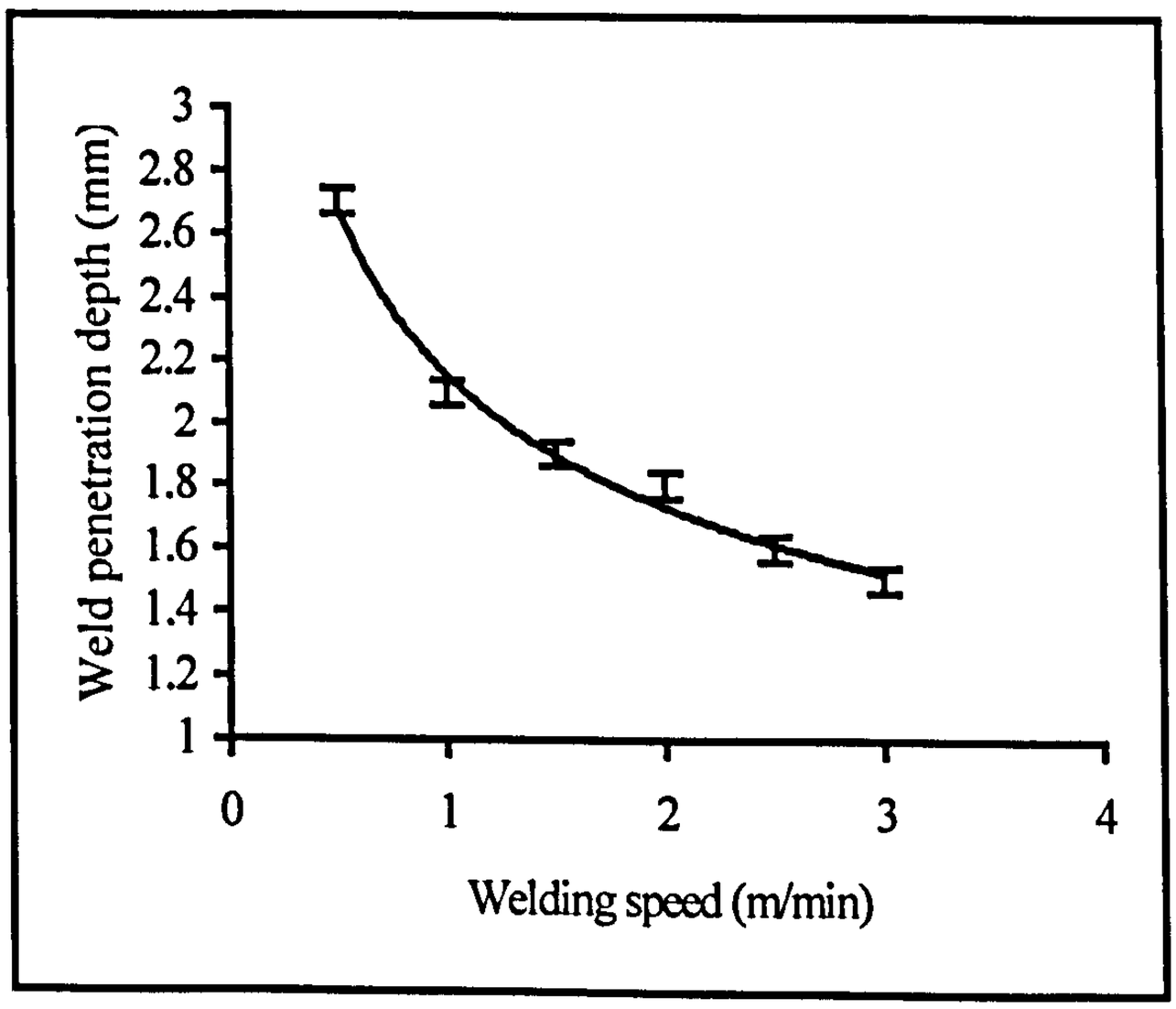

Figure 8.5 weld penetration depth at various welding speeds and a constant mean power of 2kW

Figure 8.5 shows a plot of weld penetration depth variation for the trials at a constant mean power of 2kW. It can be seen that the weld depth decreases as speed increases.

Figure 8.6 shows a plot of the intensity profile from front to back of the weld for welds made at various welding speeds and constant mean power. The centre of the laser beam impingement point corresponded to the 100 position on the x-axis. The scale corresponds to 88.79 divisions per mm. Therefore the focused spot size of 0.5mm would span from graduations 78 to 122 inclusive.

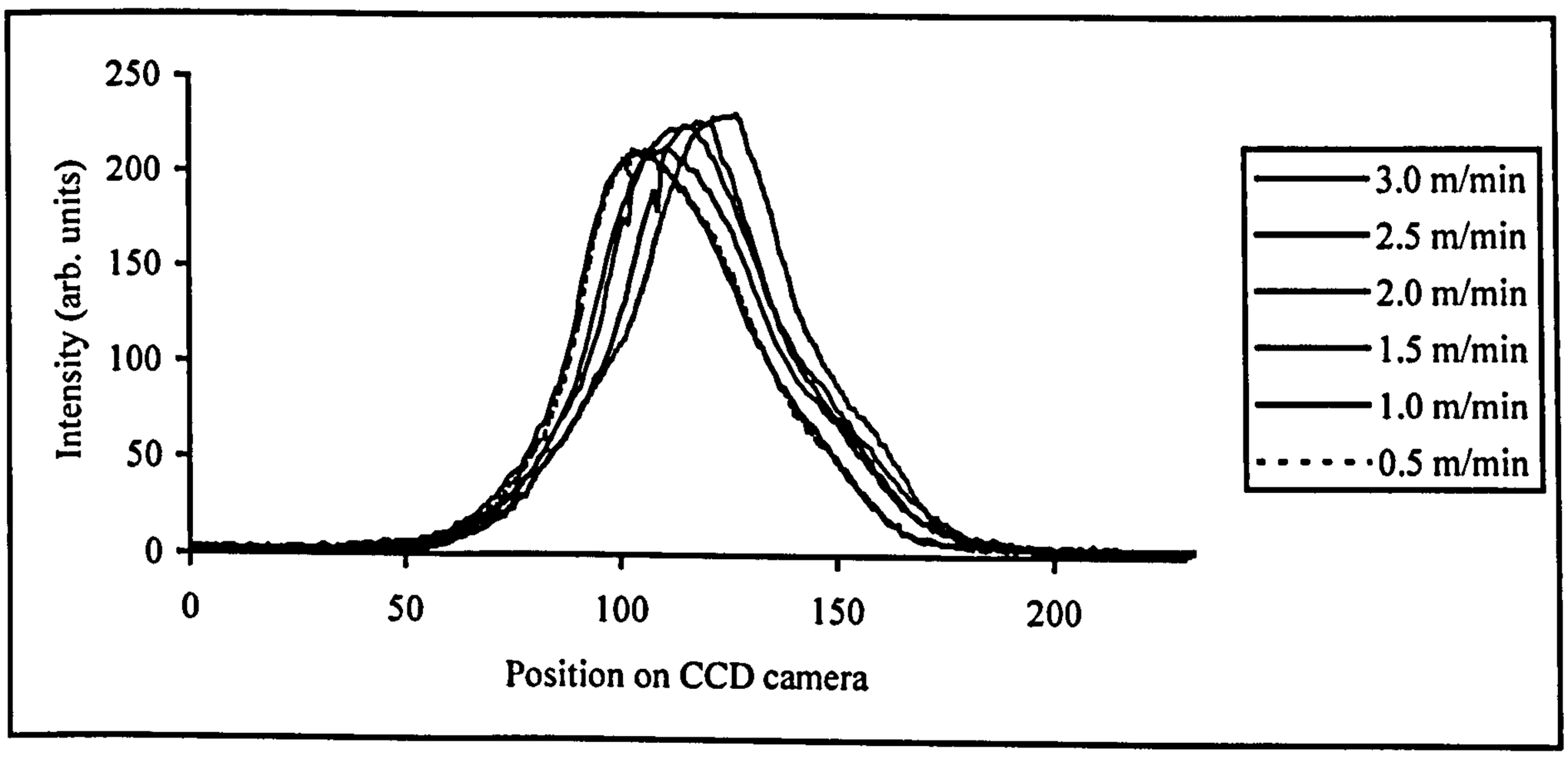

Figure 8.6 Intensity distribution for welds made at various speeds

The CCD camera scale can be calibrated as 61 divisions equal to 0.5mm at the work-piece. Therefore the peak has moved a distance equivalent to 0.2mm at the work-piece surface.

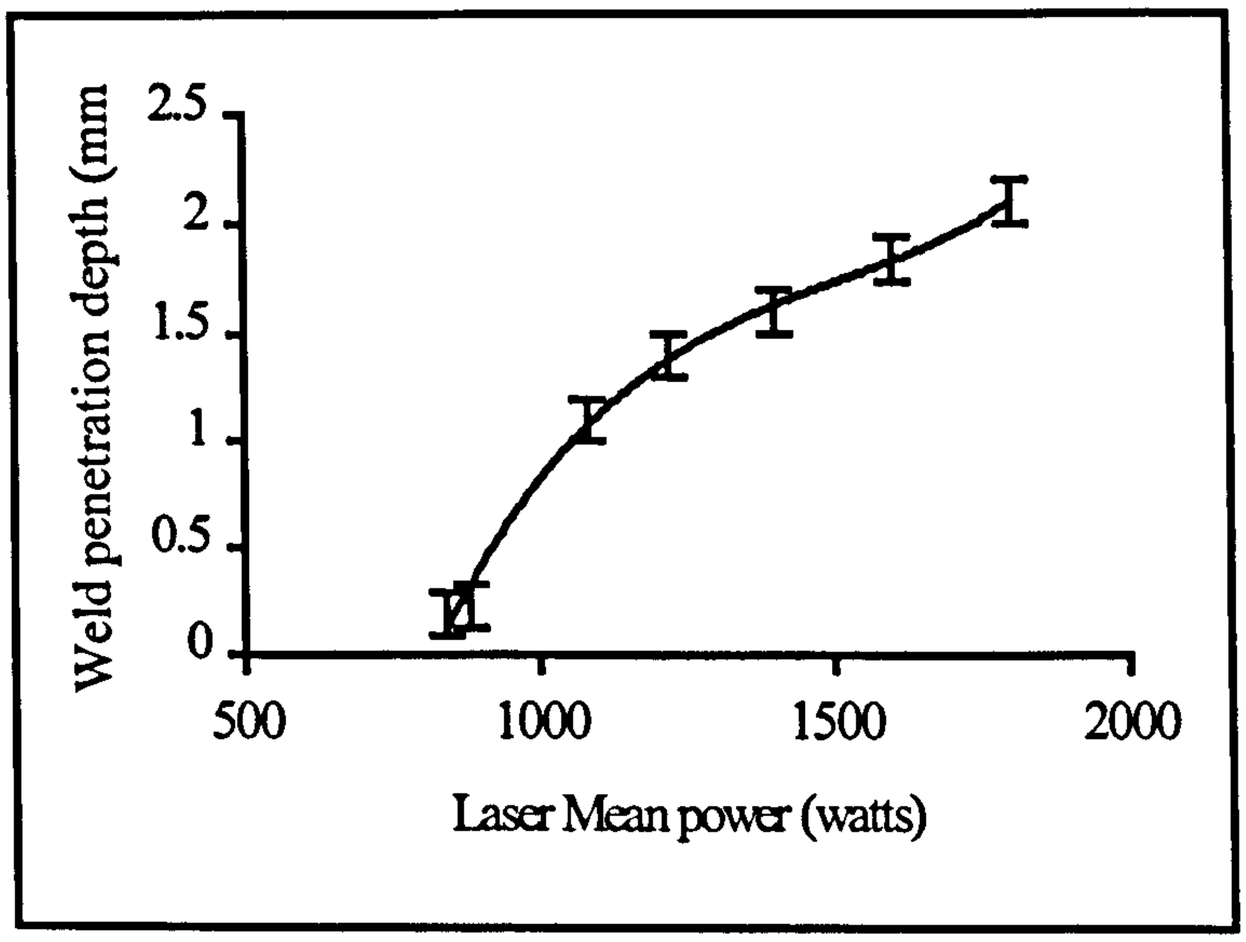

Figure 8.7 Penetration depth of welds made at various laser mean powers at constant welding speed

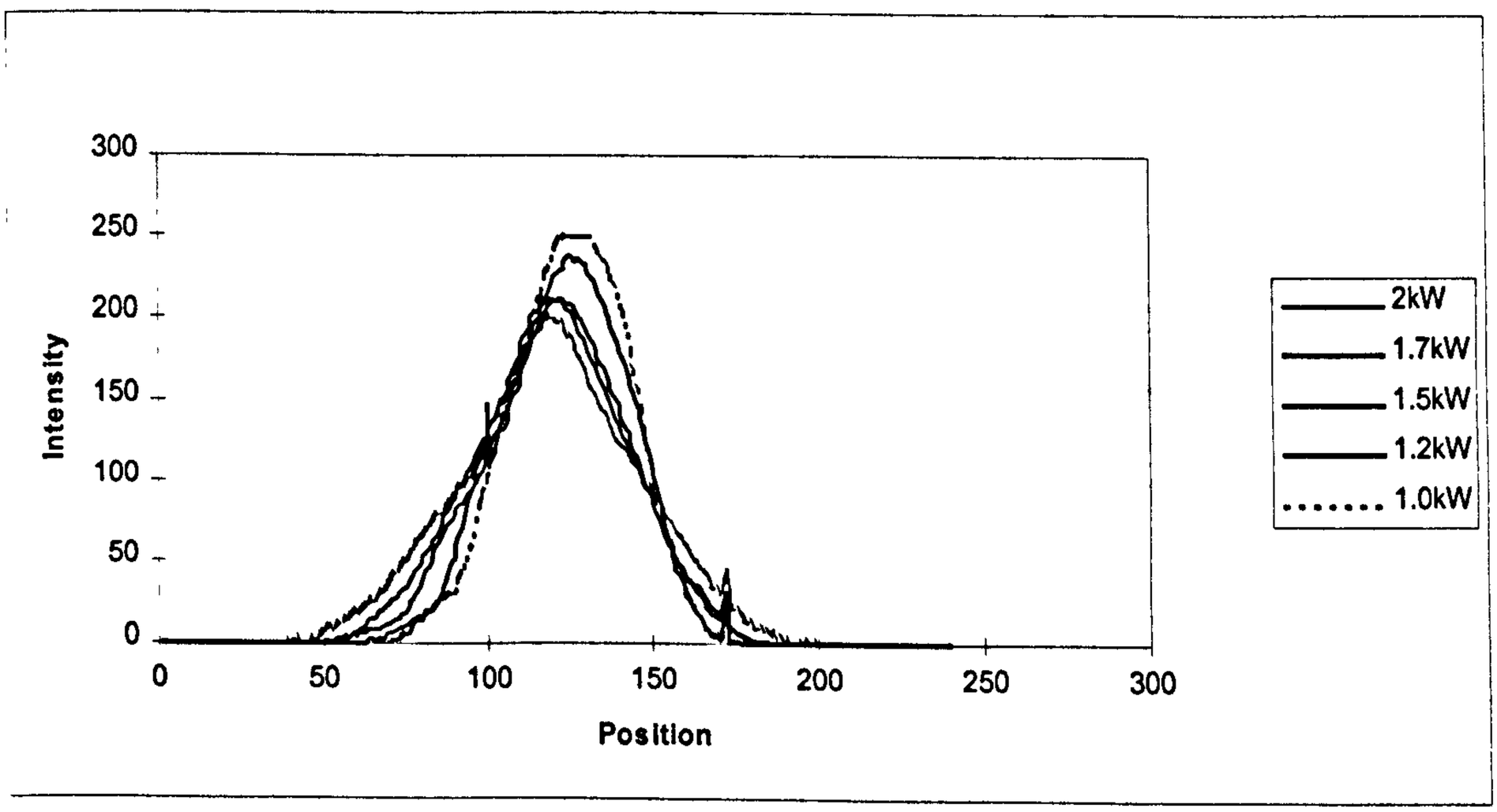

Figure 8.8 Intensity profile for welds made with various mean powers at a constant speed.

For the condition of variable speed it can be seen that as welding speed is increased and penetration decreased, the peak intensity of back-scattered light both increases and moves backwards relative to the motion of the beam to work-piece. However the general profile shape remains constant.

For the condition of variable laser power see figures 8.7 and 8.8, the peak intensity of the back-scattered light decreases with increasing laser power, whilst the position of the peak does not move significantly.

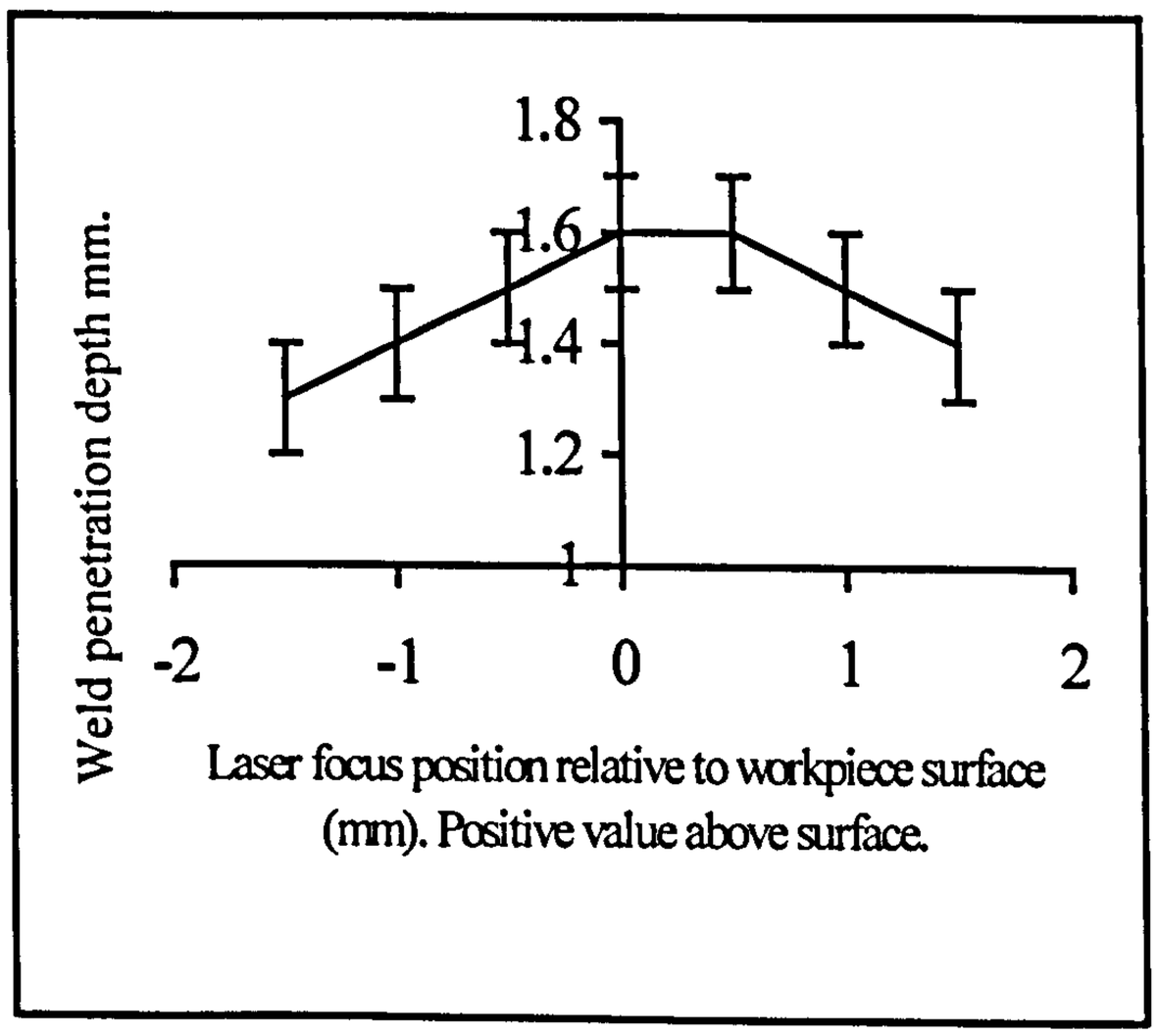

Figure 8.9 variation of penetration depth with focal position

However the base of the profile does broaden as power is increased.

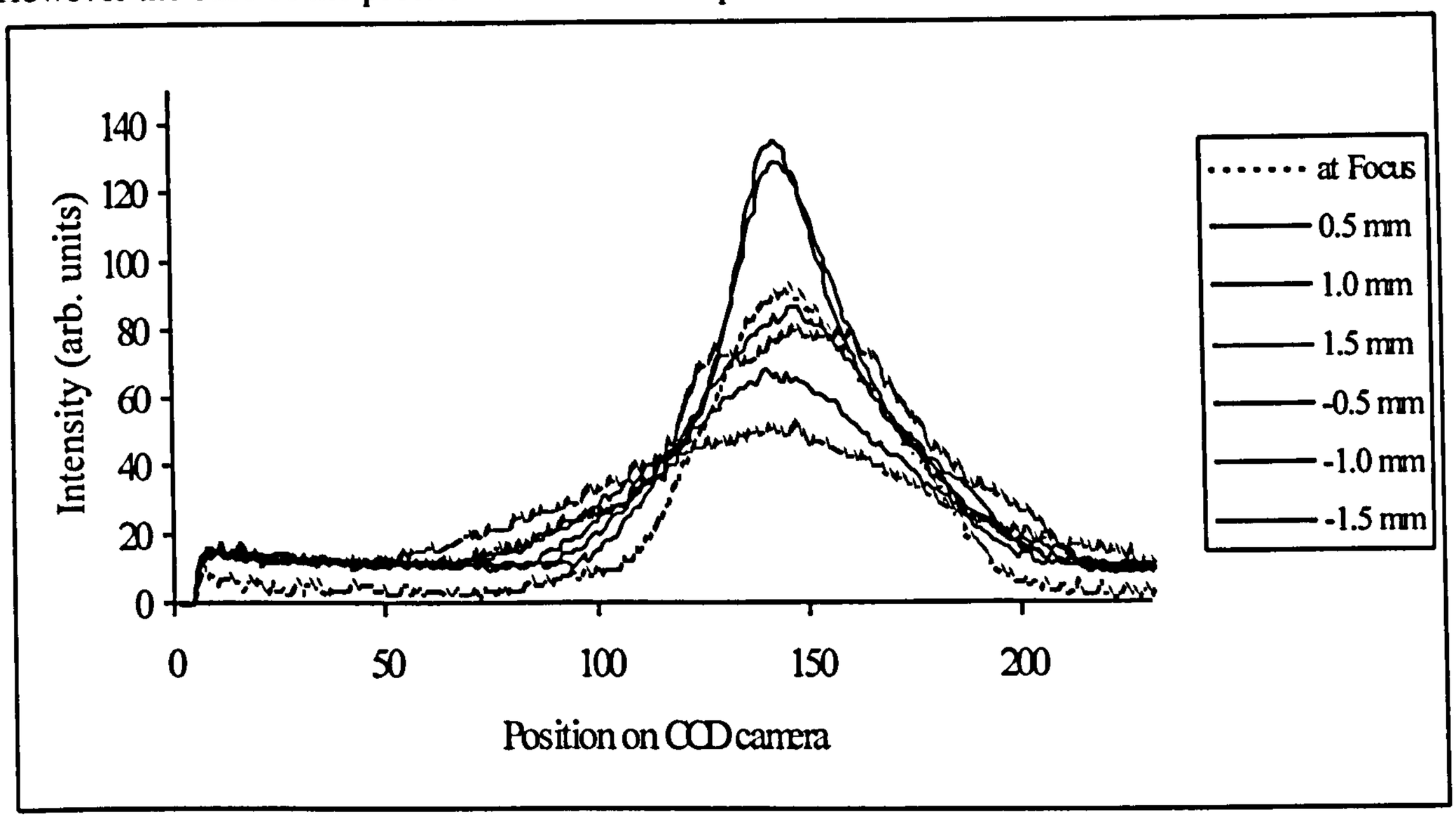

Figure 8.10 Intensity profile as a function laser focus

In varying focus position relative to the work-piece surface, see figures 8.9 and 8.10, the trend as the focus is raised above the work-piece (in a positive sense), is for the intensity of the back-scattered light to increase until a focus position of -1.5mm, whereupon it decreases. As the relative intensity decreases a broadening of the peak is also evident. This is commensurate with laser and camera defocusing at the work-piece.

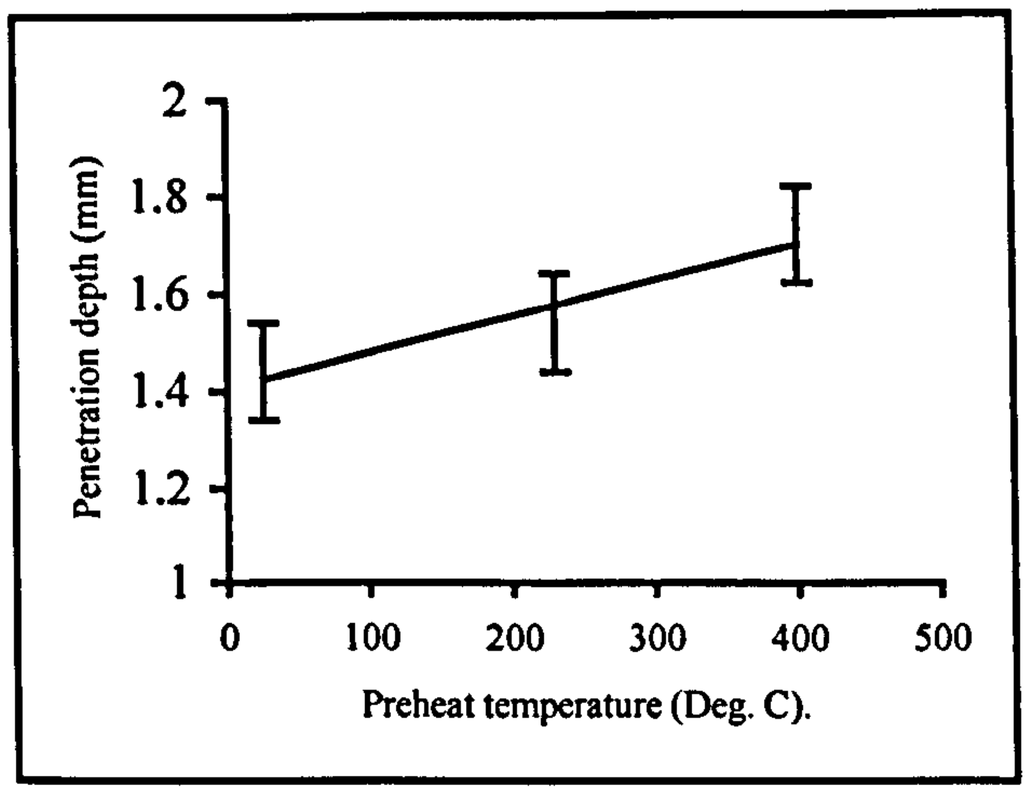

Figure 8.11 Variation of penetration due to preheat

In the case of the preheat condition see figures 8.11 and 8.12, as preheat is increased, corresponding to an increase in penetration, the relative intensity of the backscattered radiation decreases but the position of the peak remains constant.

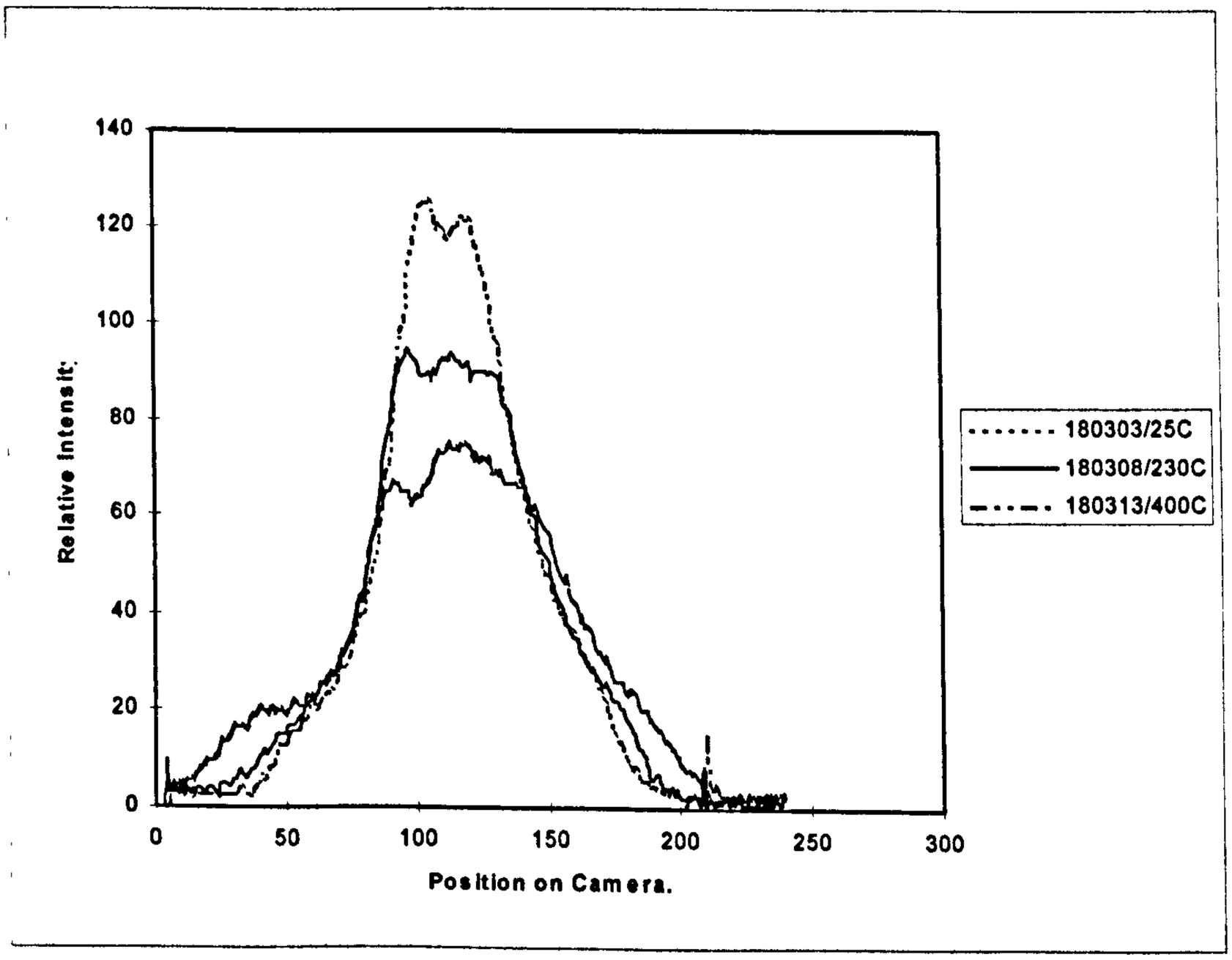

Figure 8.12 Intensity profile associated with varying degrees of pre-heat

Table 8.1 shows a summary of the effects described above, for convenience the convention has been adopted where process errors are varied to produce a decrease in penetration depth.

	Welding Speed Increase	**Mean Power Decrease**	**Focus Above Work-piece**	**Focus Below work-piece**	**Work-piece Temperature Reduction**
Peak Position	Moves Backwards	No Change	No Change	No Change	No Change
Peak Amplitude	Increases	Increases	Decreases	Increases	Increases
Width	No Change	Broadens	Broadens	Narrows	No Change

Table 8.1 showing a summary of spatial changes to signals with variation in welding conditions

8.5 X-Y Stage Experimental Procedure

The fibre was aligned to the interaction point by firstly producing a small burn mark on the plate by gating the laser and opening the shutter for 0.3 sec. Then a white light was shone through the monitor fibre to image on the surface of the plate. The image being approximately one tenth the size of the laser spot it was relatively easy to place the monitor fibre centrally to the mark. The output end of the fibre was connected to the wavelength splitter apparatus where upon the wavelengths in the ranges, <900nm, 1064nm +/-10nm and >1100nm were monitored separately.

A series of welds were made in 4.0mm thick mild steel plate at various conditions of speed and mean power. For each combination of parameters the monitor fibre was positioned at different locations front to back in relation to the laser beam movement relative to the work-piece, bearing in mind the movement of the miniature stage was in the opposite sense to the location on the work-piece, so as to collect light coming from different locations relative to the laser beam interaction point. Two welding conditions were explored, variation in power and variation of speed.

8.6 Results

To simplify interpretation of the highly modulated signals picked up from the process the mean was found for each of the signal traces and plotted as a function of speed and power at each position. It was found that the changes where not significant when positioned at the centre of the weld. Changes in signal amplitude were observed 0.4 and 0.6mm from the centre towards to the front of the keyhole. Figures 8.13 and 8.14 show the results plotted for each of the positions.

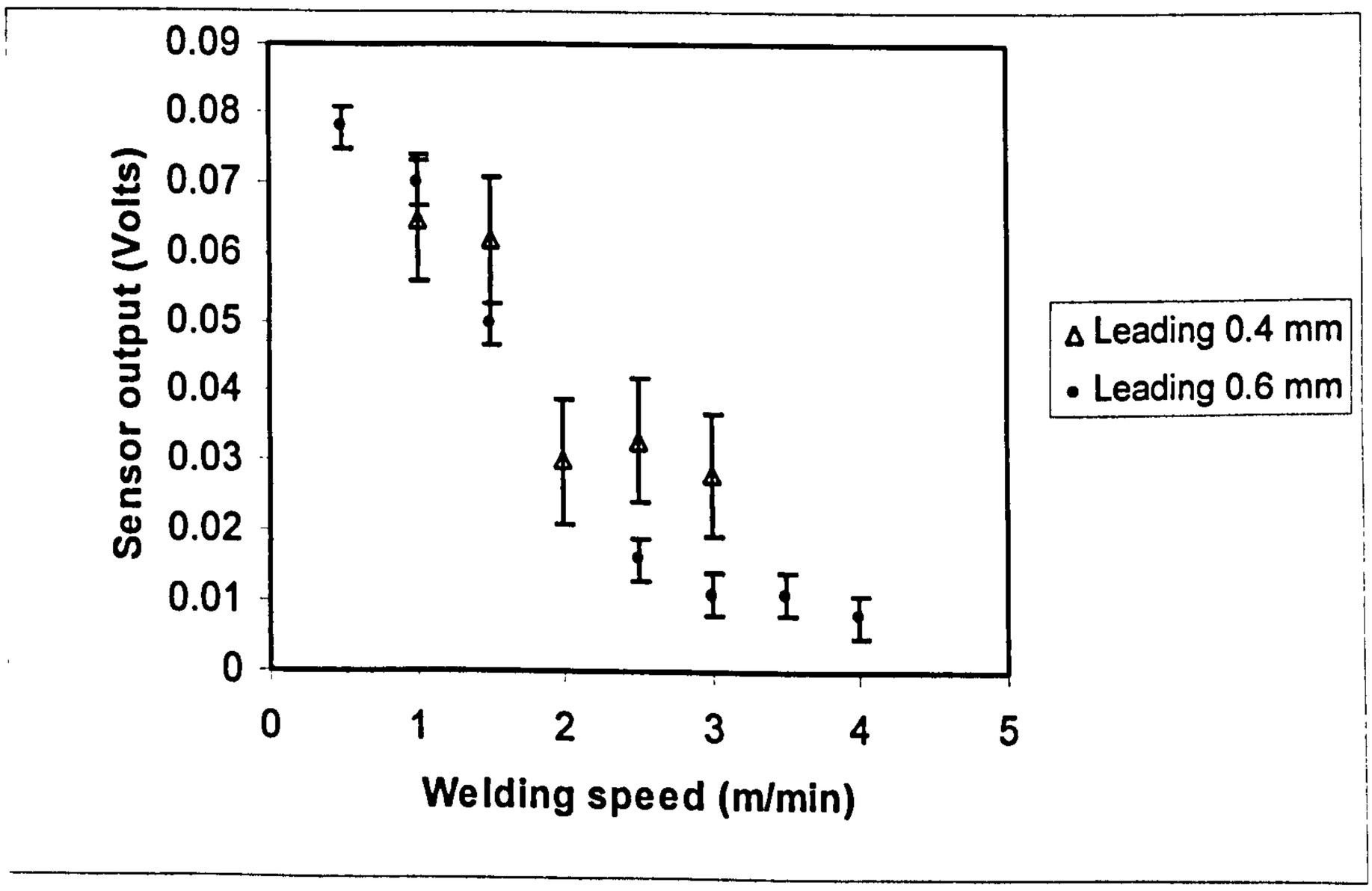

Figure 8.13 Behaviour of 1064nm radiation taken at positions ahead of the beam interaction point.

It can be seen that the response of the signal to an increase in speed is when the sensor is positioned ahead of the interaction point is to reduce with increasing speed. When the sensor is positioned behind the interaction point, trailing with respect to movement of the beam relative to the work-piece, the response is in the opposite sense, increasing with increased speed. A similar response was seen when monitoring wavelengths >1100nm and in <900nm although the level of the signal was much smaller by a factor of 100 to 200 reduced compared to the 1064nm wavelength.

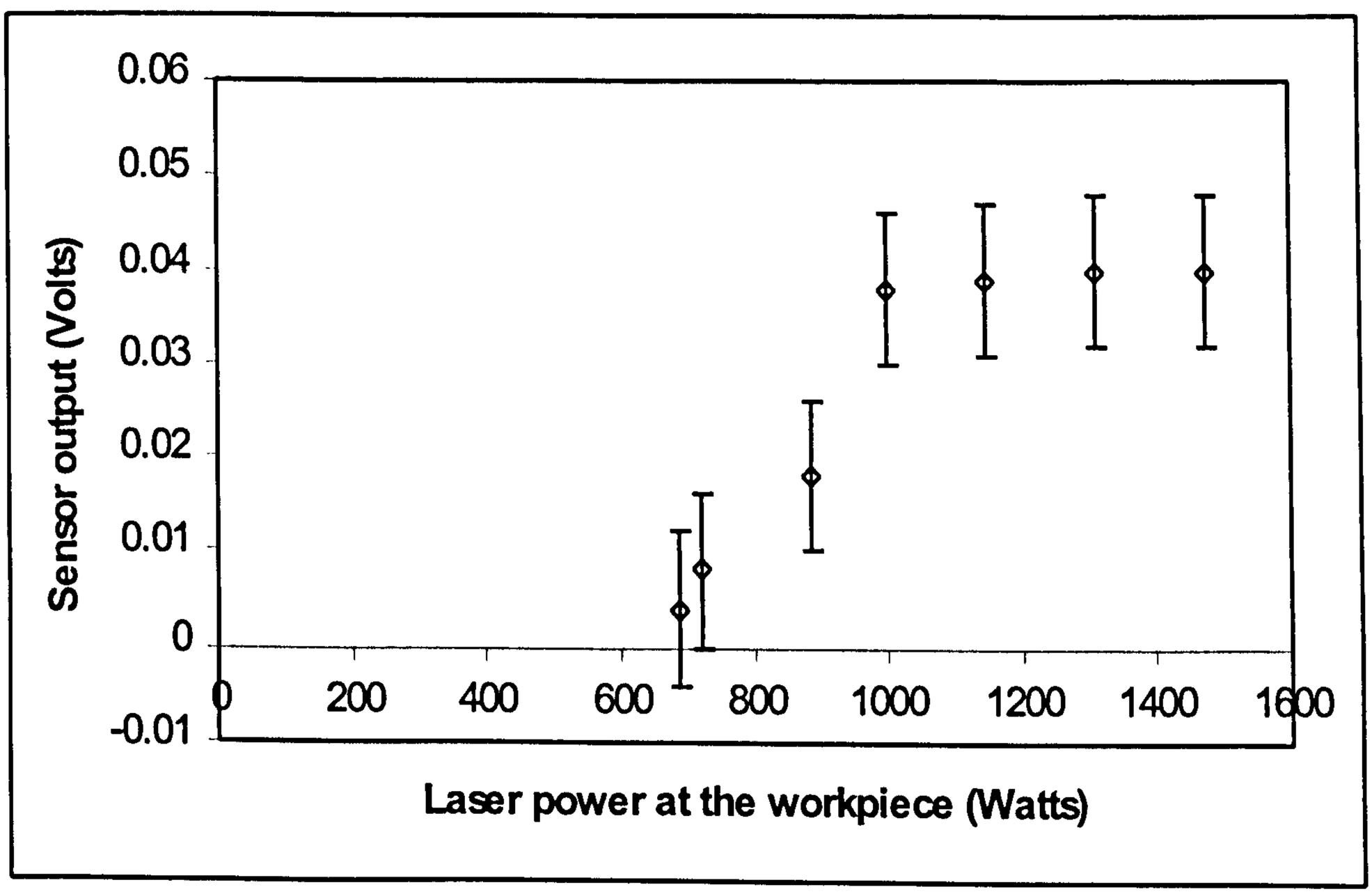

Figure 8.14 shows a plot of the sensor response for changes in laser power at the work-piece, at a constant speed of 1.5m/min, for the sensor positioned 0.6mm leading the interaction point.

It can be seen from figure 8.14 that as power is initially increased there is a rapid rise in signal that then begins to plateau, continuing to rise at a reduced rate. The point where the signal levels corresponds to a power density at the work piece of approximately 420MW/cm^2.

8.7 Discussion of results

The beam profile measured at the focus position is typical of that expected from fibre optic beam delivery. The multimode beam from the laser on entering the fibre is subject to repeated reflection at the sidewalls of the fibre core and subsequently fills the fibre aperture losing any spatial effects as it propagates. As a consequence of this 'scrambling' of the beam this profile is not expected to change significantly with changes of entry conditions such as laser beam profile or with power.

The origin of the 1064nm radiation detected by the CCD camera is believed to be dominated by backscatter and back reflection of the incident laser beam. Some radiation at this wavelength is expected from by the hot metal and plume within the keyhole but this is believed to be of much lesser intensity compared with that originating from the laser. The origin of the changes in the images collected by the CCD camera is believed to be associated with shape changes in the weld pool and keyhole. Changes in the keyhole shape have been observed by a number of workers [101, 102, 103].

We will consider the influence of each parameter change on the keyhole in turn. Changes in speed have produced both an increase in peak intensity and movement backwards of the peak intensity relative to the centre of the impingement point with increasing speed. Semak [104] described results of observations made with high speed and Schlerien photography of the keyhole during welding CO_2 laser sources. The results showed that during welding with 2 to 3.3kW the

position of the impingement point tended to be at the front of the keyhole. With reference to figure 8.15, at low speeds the keyhole dimension (b') tended to enlarge so that it was 2-3 beam diameters larger than the focused spot size (d). At higher speed the keyhole dimension (a) reduced in size but became elongated in dimension (b'), creating a space or void behind the impingement point. Also as speed increased the thickness of molten material ahead of the impingement point (T_{ip}) reduced and the weld width significantly decreased.

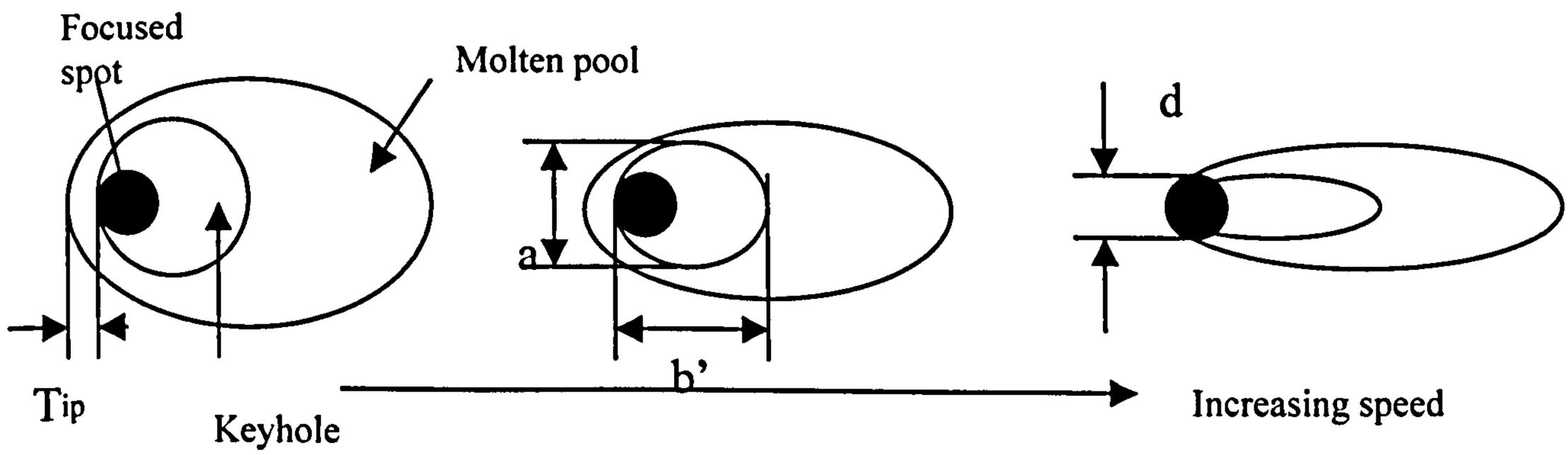

Figure 8.15 Changes in keyhole shape with increasing welding speed. Semak [104]

Measurements of keyhole and weld-pool characteristics were taken from images generated by high-speed video, using a similar technique to that described in chapter 7. The results are summarised in figure 8.16.

It can be seen that over a relatively large change of speed of 1 and 3m/min there is little change in the keyhole dimensions. However the melt thickness ahead of the keyhole did change significantly over the same range by approximately 0.15-0.2mm.

High-speed film was also taken of thinner 1mm thick section material (as described in chapter 7) where the exit to the keyhole could clearly be seen. With speed changes over the same range the

keyhole was found to exhibit similar behaviour to the thicker material. However little or no change in keyhole inlet shape was observed, the keyhole remaining approximately circular with a diameter between 0.55 – 0.6mm, 10 and 20% larger than the focussed spot size of 0.5mm. In these trials the keyhole exit could be clearly seen on fully penetrating welds and it was noticeable that the centre line of keyhole exit moved backwards relative to the centre of the keyhole entry as speed was increased. The shape of the exit remained circular but the diameter reduced. Figure 8.17 shows a summary of the dimensions taken from the work on thinner plate.

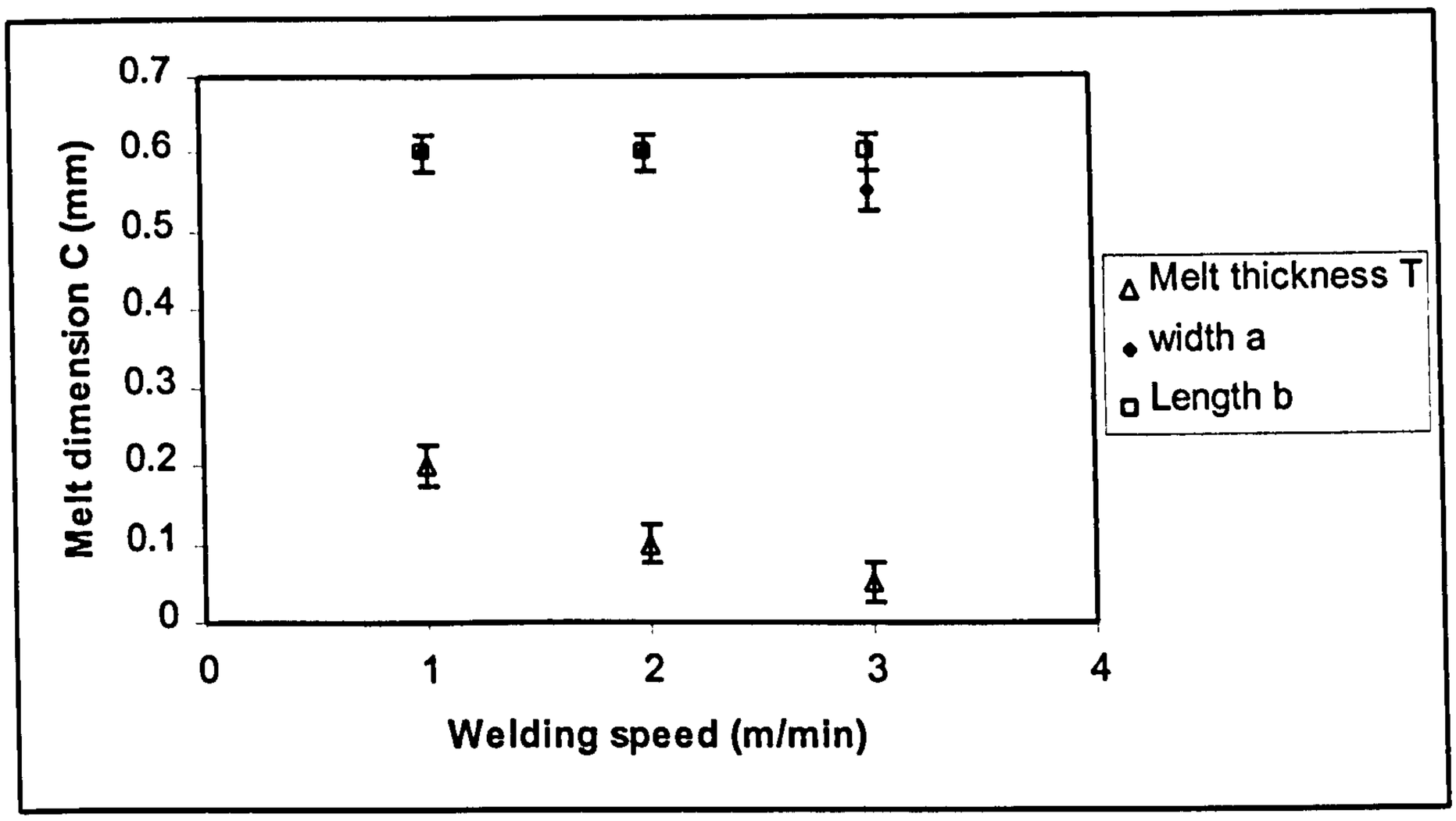

Figure 8.16 Keyhole dimensions taken from melt runs made on 4mm thick mild steel plate

From Figure 8.17 it can be seen that over a welding speed change of 1 to 3m/min the exit of the keyhole shifts backwards by approximately 0.15mm. The effect of increasing speed is to bend the keyhole backwards relative to the forward motion of the beam, which is consistent with observations made by other workers [105, 106, 107]. It is believed therefore that the changes in peak position are associated with a shift backwards of the laser beam interaction point within the keyhole.

The variation in power is known below a certain threshold value to have a marked effect on the way the beam couples into the work-piece. At low intensity the coupling mechanism is one of conduction limited, above a threshold intensity vaporisation begins to occur and a keyhole forms which increases the efficiency of the coupling process.

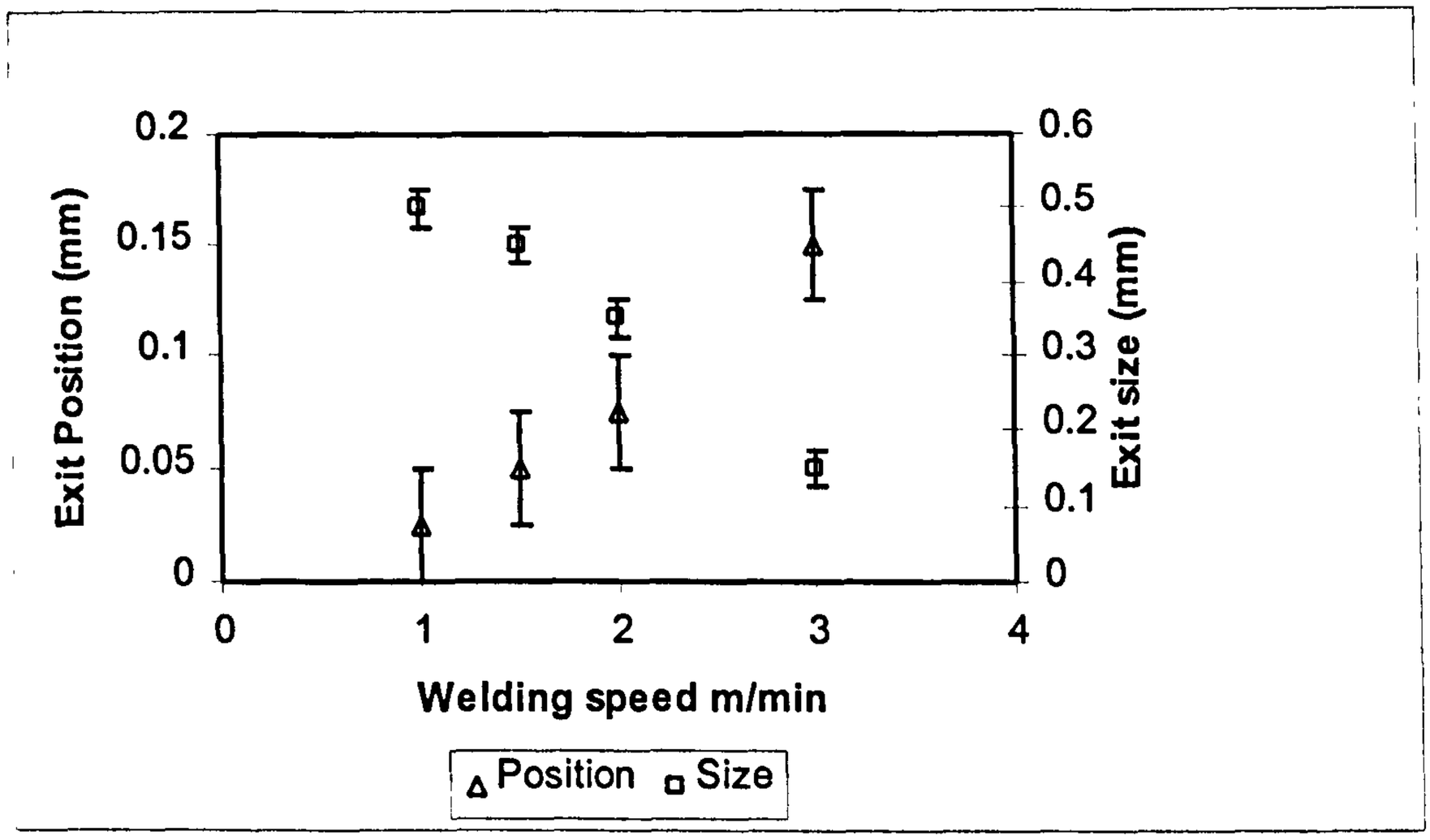

Figure 8.17 Keyhole exit relative to the leading edge of the keyhole entry

Video film of the weld area demonstrated that over the power range explored a keyhole was present in the melt pool. The reduction in power did however have an influence on the keyhole dimension, which reduced in diameter from 0.6mm diameter to 0.45mm going from 2kW at the source to 1.5kW respectively. Interestingly as the power was increased at the work-piece the level of signal measured decreased, directly opposite to the increase in signal in the UV/Visible range that increased. Suggesting that the level of activity within the keyhole had increased whilst the level of laser radiation being backscattered was reduced. This might suggest that the absorption had increased or the geometry within the keyhole was such that the backscattered laser radiation was directed away from the sensor.

The movement of peak amplitude associated with changes in focus is consistent with the geometric effect associated with the aperturing by the fibre and the offset of the beam waist relative to the focus described within chapter 7.

The preheat result is particularly interesting as it has produced changes in monitored signal and weld penetration with constant beam and work-piece movement parameters . The fact that the penetration has increased means that the amount of energy absorbed by the material must have increased. This is consistent with the reduction of measured peak amplitude in the returned signal for increases in penetration observed with changes in power and speed. The question remains however whether the signal amplitude changes are associated with absorption changes or whether they are a function of geometric changes within the keyhole. It is possible that the two go hand in hand. If the signal intensity changes were independent of geometry and only a function of absorption then similar signal intensity would be expected for similar weld geometry.

8.7.1 Trials with Miniature X-Y Stage.

These trials demonstrated that by selectively positioning the detection point around the keyhole the spatial effects observed through the CCD camera could be seen using a simple detector.

9 Discussion and Implications

9.1 Optical Signals

The combined plots of spectra taken from the centre of the weld-pool, using the core monitor and the plume 4.3mm above the work-piece have very similar peak value and correspond to a temperature (assuming perfect black body radiation) of approximately 3870K (4140 °C).

The result through the core monitor was initially surprising since the spectrum was effectively being taken from the centre of the keyhole where it was expected to be very hot. However considering that these conditions produced full penetration it is perhaps more understandable and may be more indicative of a keyhole temperature for a stable, open keyhole and where there is insignificant contribution coming from the walls of the keyhole, as in the off-axis case. This makes the temperature above the keyhole surprising since it might be expected to be significantly cooler than in the keyhole. The high velocity that the metal vapour is being ejected means that there is not sufficient time for it to cool, may be one explanation. The other more likely one is that the laser is heating the plume above the work-piece to the same temperature as the plume/plasma in the keyhole.

From the spectra it is clear that process monitoring during the Nd:YAG process would not benefit from using selective sensors looking for specific changes in signal behaviour at different wavelengths, as might be the case for the CO_2 process because this information is simply not present. This confirms, unlike the findings of Li [89], that there are no differences in the temporal behaviour of the two wavelength ranges (IR and UV/visible) associated with defects in the process.

9.2 Monitoring of Backscattered Laser Radiation

The origin of backscattered laser radiation is thought to be from the walls of the keyhole. The spatial profile of the backscatter indicates that the origin of the signal comes from near the centre of the keyhole and can move as speed is increased or decreased. At relatively high speeds, as in the partially penetrating case, the keyhole is know to bend backwards, away from the direction of travel. It is thought that this change in shape is the origin of the profile movements. The fact that the signal at the laser wavelength appears to follow the relative coupling of the beam is perhaps not surprising since the amount of material melted has to be related to the amount of energy absorbed. We know that increased absorption will tend to increase depth of penetration. The question is which comes first. Increased absorption, a drop in signal and a change in depth or a change in depth followed by an increase in absorption followed by a drop in signal. This phenomenon provides a possible method correlating penetration depth with changes in speed and power. Thus if a change of power is observed an automatic compensating change in speed might be possible to return the signal level and therefore penetration to their correct level.

9.3 Oscillation Frequencies

The presence of characteristic oscillation frequencies relating the length of a fully penetrating keyhole to the depth of penetration has very interesting implications for penetration monitoring. For example if a particular component of particular thickness is to be welded then there should be a condition during full penetration so that a characteristic oscillation frequency can be seen. If this frequency is present then the keyhole is known to be fully penetrating and full penetration of the weld can be confirmed. This approach may be quite acceptable since it was postulated in chapter 4 that we should assume that the process is inherently stable and that process monitoring should be used to detect the situation where the process departs from this stable point. A possible

draw-back is that the characteristic frequencies become less apparent at the maximum speed where full penetration occurs, and can only really be resolved at slower than optimum welding speed. Thus there may be a compromise between the need for process assurance and the production rate. On the basis that it is no use producing 100% scrap at high speed this may be acceptable.

9.4 Changes in Focus Position

The significance of the separate behaviour observed in the two wavelength ranges for focus control may not be fully appreciated without considering the problem of ensuring good maintenance of the focus position, relative to the work-piece. Because the chromatic aberration effects the position of peaks in the two wavelength bands of signal, either side of the optimum focus position they can be used to monitor and potentially control focus position. Focal errors occur when the work-piece moves relative to the focus lens, perhaps through distortion, variability of fixturing or robotic manipulation or perhaps just natural variability of sheet metal after pressing. If we consider a focus error where the work-piece moves away from the focusing lens, then the laser wavelength behaviour would reduce in amplitude. Similarly if we consider a change in focus the other way, so that the work-piece approaches the focusing lens the amplitude of the signal will again reduce. Thus, there is information that the focus has changed but no information regarding the direction of change. Information relating to the direction of the focal error would be a prerequisite to correcting the error if a closed loop control system is to be considered.

By sensing a single wavelength, offset from the laser wavelength it can be seen that directional information would be available. For example, if a wavelength in the UV/Visible range was chosen then if a negative focal error or positive focal error was experienced the amplitude of the

signal would go up or down respectively. The problem in single wavelength is that a control system would have to be calibrated to recognise that a particular value of sensor signal represented a particular focal position. This might be difficult to set up initially particularly when considering different materials and applications. By using dual wavelength bands it should be possible to produce a much more discriminating measure of focus position. If, for example a negative focal error (one that moves the plate away from the optics) was experienced, the amplitude of the IR signal would increase and UV/Visible signal would decrease. If a positive focal error was experienced (bringing the work-piece closer to the focus lens) the IR signal would decrease and UV/Visible increase. By subjecting each signal to individual gains such that their amplitudes were made equal, one signal could be subtracted from the other to generate an error signal. The sign of the signal would indicate the direction of defocus i.e. if the IR signal was subtracted from UV/visible a negative signal would be produced, indicating direction of error with a magnitude indicative of the size of the error.

Figure 8.1 shows the result of subtracting one signal from the other during a welding over an included mild steel plate at three power work-piece power levels, 820W, 1230W and 1640W. It can be seen that at each power level a clear linear portion of the signal can be seen which is approximately symmetrical about the zero volts position. The feasibility of using these signals for focus control has been proven by Haran et al [67] for a number of materials including mild steel, stainless steel and titanium alloys.

Power	Figure 8.1 Error signal
820W	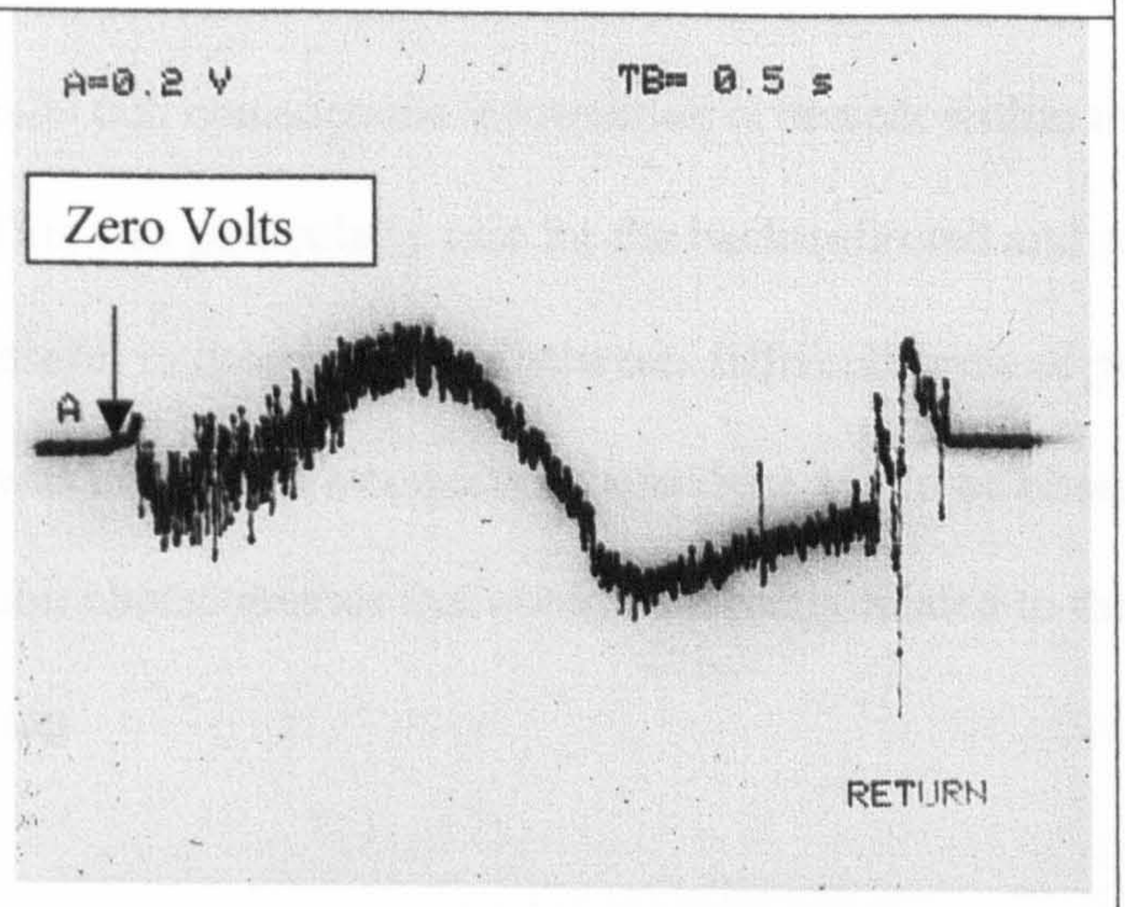
1230W	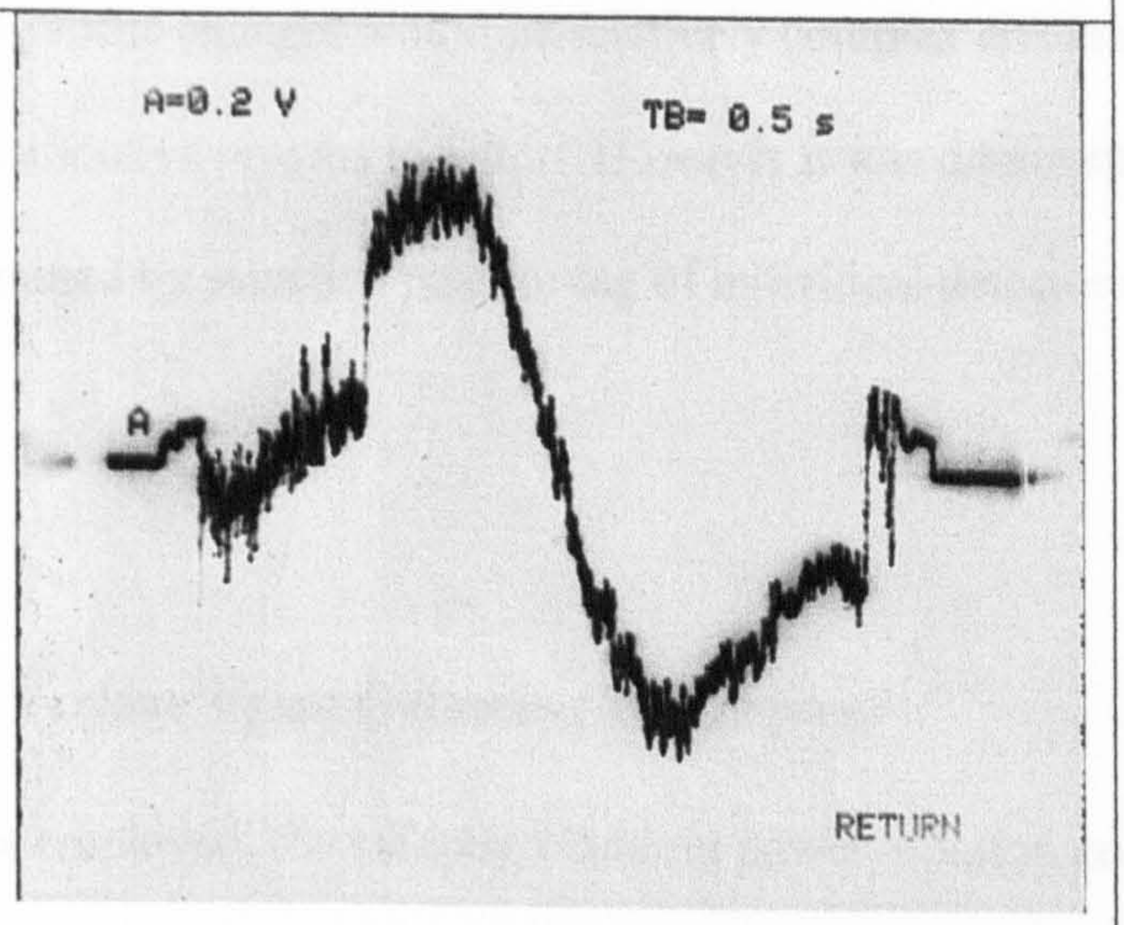
1640W	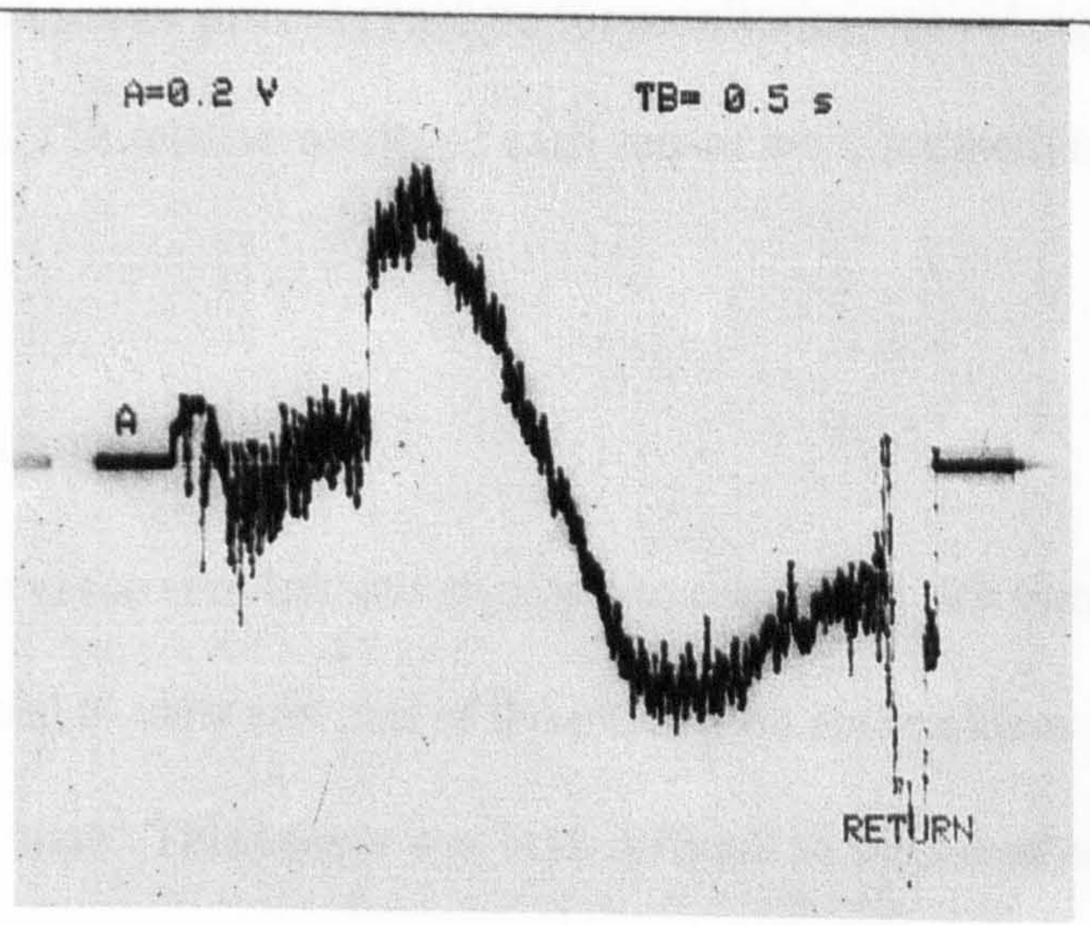

9.5 Spatial Monitoring

It is clear from the results that considerable information is present within the spatial profile around the keyhole. This was particularly true for the back-reflected and scattered laser radiation that was shown to be useful in discriminating between different forms of process fault affecting penetration depth. It was hoped that a consistent behaviour would be observed in the spatial profile that might exhibit characteristics that could be directly related to the penetration depth but this was not forthcoming.

Analysis of the spatial profile changes would be relatively complex and maybe prohibitive in the development of a cost effective process monitor. However it was demonstrated that the spatial effects could be determined by selective positioning of individual detector around the keyhole/weld-pool.

9.6 Assessment of Various Signal Gathering Techniques

Each of the techniques employed, the off-axis, cladding power monitor, core monitor and the on-axis CCD-camera based sensor proved practical for monitoring optical signals, which represented changes in the process. The relative merits of each sensor are discussed in more detail below:

9.6.1 Off-axis Monitor

The off-axis monitor was the simplest and cheapest to construct. By virtue of its location the system could be adjusted to view any part of the interaction area or areas outside of the immediate interaction zone. This sensor was both difficult to align and prone to being easily misaligned if it was knocked. To compound this, the location and position of this type of detector made it more vulnerable to being knocked. The nature of the location of this detector meant that

it would add to the overall size and weight at the work-piece this may be restrictive particularly if robotic manipulation is to be used.

9.6.2 Cladding Power Monitor

The cladding power monitor (CPM) arrangement proved to be very easy to align using a white light source prior to processing. If constructed properly this sensor gave good performance however, it did prove difficult to construct particularly in joining the monitor fibre to the main fibre and as a consequence was not always repeatable from one CPM to another. In addition it was felt that the discontinuity introduced by attaching a small fibre to the main beam delivery fibre would cause an area of potential weakness that might lead to premature failure of the main fibre when operated under dynamic conditions.

9.6.3 Core Monitor

The core monitor arrangement proved to be simple to use, easy to align using a simple white light source technique and repeatable. Of all the monitors it was the most robust being located well away from the processing area and benefiting from the protection of the laser cabinet. However it did prove impractical for use when monitoring back reflected laser radiation as the signal from the process was often swamped by the high signal from Fresnel reflection coming from the fibre end face.

9.6.4 CCD Camera -based Monitor

A system employing a CCD monitor proved to be the most flexible: both temporal and spatial information could be gathered. By virtue of the fact that the fibre does not restrict its field of view it could be positioned to view both the area within the keyhole and the area around it giving

much greater potential for information gathering. However, there were perceived drawbacks in locating a relatively delicate piece of equipment so close to the work-piece where it could easily be damaged by knocks, fumes and spatter.

Initial alignment proved difficult, since the optical filtering necessary to attenuate some of the process light was so dense that an image of the work-piece surface and beam impingement point could not be resolved under normal lighting conditions.

Monitor Type	Ease of alignment	Good signal to noise	Minimal intrusion and weight	Robust	Temporal information	Spatial information
Off- Axis Monitor	X	√	X	X	√	X
Cladding Power Monitor	√	√	√	√	√	X
Core Monitor	√	√	√	√	√	X
CCD Monitor	X	√	X	X	√	√

Table 9.1 Summary of the benefits of various optical detectors

10 Summary and Conclusions

10.1 Summary

There is a clear drive towards the use of more process monitoring to provide quality assurance in automated environments. This is particularly true for welding, which is expected to experience rapid growth over the next 5-10 years. Growth is thought to be primarily within the automotive industry where the application of lasers to welding of car body parts is rapidly increasing. This work has concentrated on developing techniques that are applicable to materials used in the automotive industry.

The problem of locating universal signals from the process, which are indicative of the process quality, was not found to be a trivial one. The dynamics of the beam interaction with metal is inherently unstable and the permutations of process parameters numerous. The problem is simplified, at least in the mind, if it is accepted that a particular welding process is inherently stable, the process has been developed and qualified such that it does not sit on a knife-edge, so the process monitor only needs to be aware of changes from the nominal. A degree of practicality was also exercised by ignoring situations that are unlikely to arise.

To be really useful, process monitoring needs to be discriminating: that is, not only able to determine that there has been a change, but also able to pinpoint the probable cause of that change. It is often the case that a number of parameter changes will cause similar effects in monitored signals. In order to achieve this, both the temporal and spatial behaviour of signals were examined over a range of different wavelengths. A technique of monitoring the spatial

profile of the back-scattered laser light during welding has been developed which makes it is possible to discriminate between different root causes of changes in weld penetration.

Where possible the practicalities of closed loop control and therefore correction of process errors has been considered. It is a prerequisite to closed loop control that an element of discrimination is required so that appropriate correction can be made. The best example of the potential for closed loop control was the technique developed for detection of focus error which uses chromatic aberration of the process light within the beam delivery. Subsequent to the initial discovery of this phenomenon this technique has been used successfully to control focal errors by Haran [67].

During this work the techniques for process monitoring have been identified which can determine

- Loss of focus (and provide the necessary components for correction).
- Changes in coupling.
- Changes in speed.
- Changes in power.
- Method of measuring penetration as a function of speed and power.
- Detection of loss or achievement of full penetration.
- Changes in penetration depth associated with changes in preheat, speed, power and focus.

10.2 Conclusions

1. Through-the-fibre monitoring is a practical method for in-process monitoring for Nd:YAG laser welding. Both the CPM and core monitor demonstrated the capability of detecting subtle changes in the processing regime.

2. The technique of incorporating sensing within the beam delivery also serves to restrict the impact on space around the processing zone and reduces the payload that a robot may have to carry.
3. Initial coupling of the laser light into the surface of the work-piece can be observed as an increase in UV and IR signal intensity. Conversely, a reduction in coupling can also be detected.
4. Oscillation in the keyhole can be shown to be dependent on the thickness of the plate material and may form the basis for a go/no-go penetration monitor.
5. Chromatic aberration within the optics of the beam delivery can be used to determine the relative focus position of the laser beam to work-piece.
6. Chromatic focus effects also provide the means for closed loop control of focus, since they indicate position and direction of focus error.
7. Monitoring of the laser wavelength appears to provide information on coupling efficiency and may be useful for monitoring penetration depth.
8. Monitoring of the spatial profile of back-scattered laser light can provide a discriminating method of penetration monitoring which can be used to identify the root cause of penetration errors

References

1. Einstein. A. Phys. Z, 18,121, 1917.
2. Gordon, J.P., Zeiger, H.Z., and Townes, C.H., Phys. Rev. 95, 282,1954
3. Maiman, T.H. Nature, 187,493, 1960
4. Steen. W. M. Laser Material Processing. Pub: Springer-Verlag.
5. Anderson S. Review and Forecast of Laser Markets 1999. Laser Focus World. January 1999
6. Belforte D.A. Notes From Laser Focus World Market Place 2000.Jan 26, 2000.
7. Bransch H.N. Cutting and Welding Performance of High Power CW and Pulsed Nd:YAG Lasers. ICALEO (Florida, Oct 1992), Vol 75, pp 70 – 76
8. Naeem M. Riches S. Russell D. Material Processing With a High Average Power and High Beam Quality Continuous Wave Nd:YAG Laser. ICALEO Florida, Nov 1998, section G pp 8-17
9. Lewinski R. Operating Cost Analysis of Laser Blank Welding Systems. 7th Annual Automotive Laser Applications Workshop (ALAW) Detroit, March 9-10 1999.
10. GSI Lumonics Product literature.
11. Trumpf Gmbh Product literature.
12. GSI Lumonics' Applications and Custom Systems Groups.
13. Withnall K. Calculating the Cost of Ownership. The industrial laser user. Aug 1996
14. Peters. C.N.D. The Manufacture of Heat Exchangers Using High Power Nd:YAG Lasers. TWI 'Make it with lasers' Case study. Presented at British Steel Co.Port Talbot, S.Wales. Nov. 1996.
15. Hecht J. Understanding Lasers. Pub. Howard W Sams and Co. ISBN 0672272741
16. Koechner. W. Solid-State Laser Engineering. Pub: Springer-Verlag 1976
17. GSI Lumonics proprietory data.

18. Rosseler M. David. An Introduction to the Laser Processing of Materials. The industrial laser review handbook. 1986 Edition. Ed: Belforte and Levitt

19. Luxon. T. James. Optics for Material Processing. The industrial laser review handbook. 1986 Edition. Ed: Belforte and Levitt

20. Verboven E.P. Beam delivery for Nd:YAG Lasers. Optical Engineering, September 1995, Vol 34. No 9, 2683 – 2686

21. Tyndall. J. Royal Institution of Great Britain, proceedings, 6, (1870-1872), 189.

22. Boechat, A.A.P. Optical Fibre Beam Delivery of High Average Power Nd:YAG Laser Radiation. PhD Thesis. Heriot-Watt University. 1992

23. Beck T. Reng N. Richter K. Fibre Type and Quality Dictate Beam Delivery Characteristics. Laser Focus World. Oct 1993 pp 111 – 115

24. Leong K. and Hunter B.V. High Power Fibre Optic Laser Beam Delivery Moves Forward. Industrial laser review. May 1996, pp 7 – 12

25. Ireland C.L.M. Fibre Optic Beam Delivery for use with High Power Lasers Producing ms Pulses. Internal Lumonics document. March 98.

26. Matsuura Y. Miyagi M. German A. Nagli L. and Katzir A. Silver Halide Fiber Tip as a Beam Homogeniser for Infrared Hollow Wave guides. Optics letters. Vol 22, no 17, Sept 1997 pp 1308 – 1310

27. Matsuura Y. Hiragea H. Wang Y. Kato Y. Miyagi M. Abe S-I. Onodera S. Lensed-taper Launching Coupler for Small-bore Infrared Hollow Fibers. Applied optics. Vol 36 No 30 20 Oct 1997 pp 7818 – 7821

28. Hecht. Optics. 2nd Ed. Pub. Addison-Wesley Pub.Co.

29. Prokhorov, A.M. Konov, V.I. Ursu, I. Mihailescu, I.N. Laser Heating of Metals. Pub. Adam Hilger. 1990 ISBN 0-7503-0040-X

30. Carslaw H.S. and Jaeger J.C. Conduction of Heat into Solids, 2nd Ed, University Press, 1959)

31. Olsen F.O. Theoretical Investigations in the Fundamental Mechanisms of High Intensity Light Reflectivity. SPIE Vol. 1020, 1988.

32. Roessler D.M. and Gregson V.G. Journal 1978 Appl. Opt. 17, 992

33. Herziger G. The Influence of Laser-induced Plasma on Laser Materials Processing. Industial Laser Handbook 1988, Ed. Belforte and Levitt

34. Chen F.F. Introduction to Plasma Physics. Plenum Press 3rd Ed.

35. Hughes T.P. Plasmas and Laser Light. Pub: Adam Hilger.

36. Bloembergen. Material Interactions; Fundamentals and Applications. LAMP '92

37. Drude P. The Theory of Optics, Dover Publications, INC. New York, 1959

38. Banas C. High Power Laser Welding. The Industrial Laser Handbook 1988. edited by Belforte and Levitt

39. Kristian B. and Flemming O. Investigation into the Absorptivity Change in Metals with Increased Laser Power. SPIE vol. 3092.

40. Miyamoto I., Maruo H. and Arata Y. Beam Absorption Mechanism in Laser Welding. SPIE Vol 668 1986.

41. Ursu I, Apostol I, Cracium D, et al. J. Phys. D Appl. Phys. 17, 709. 1984.

42. Ursu I, Mihailescu I N, Apostol I, et al. J.Phys. D: Appl. Phys.17 1315. 1984

43. Bekefi G. Principles of Laser Plasmas. John Wiley and Sons

44. Cairns R.A. and Sanderson J.J Ed Laser-Plasma Interactions. Proceedings of the Twentieth Scottish Universities Summer School in Physics 1979.

45. Malvezzi A.M. Fundamentals of High Excitation Phenomena in Laser Processing. Proceedings of the Society of Photo-Optical Instrumentation Engineers (SPIE) Volume 801 High Power lasers. 31 march – 3 April 1987. pp 68 – 74.

46. Matsunawa A. and Ohnawa T. Beam-Plume Interaction in Laser Material Processing. Trans. Japanese Welding Research Institute. Vol 20, No 1 1991. pp 9 –15

47. Essien. M., Keicher D.M., and Jellison J.L. Sandia National Labs. Observation of Refractive Index Gradients in Laser-generated Plume using Schlieren Imaging.

48. Beck M. Berger P. Dausinger F. Hugel H. Aspects of keyhole/melt Interaction in High Speed Laser Welding. Proc 8th Int. Symp. On gas Flow and Chemical Lasers. Madrid 1990, SPIE vol 1397 p 768.

49. Norris I.M. High Power Laser Welding of Structural Steels – Current status. Proceedings of the International Conference; Advances in joining and cutting processes 89. Harrogate 31 Oct – 2 Nov 1989.

50. Douay D. Daniere F. Fabbro R. and Sabatier L. Plasma Blowing in Deep Penetration CO_2 Laser Welding. ICALEO Detroit Oct 1996. Vol 81 section D, pp54 – 63.

51. Semak V.V. Hopkins J.A. McCay M.H. and McCay T.D. A Concept for a Hydrodynamic Model of Keyhole Formation and Support During Laser Welding. ICALEO 1994 pp 641-650.

52. Metzbower E.A. On Temperature and Size of Keyhole. ICALEO 1992, Florida. Oct 25 – 29. Vol 75, pp 140 – 155

53. Duley W.W., Olfert M. Bridger P. Mao Y-L. What CO_2 Laser Welding of Liquids Tells Us about Penetration Welding of Metals. ICALEO 1992, Florida. Oct 25 – 29. Vol 75, pp 156 – 162

54. Fujinaga S. Takenaka H. Narikiyo T. Katayam S. Ohmori A. Observation of Keyhole Behaviour During High Power YAG Laser Welding with Microfocused X-ray Transmission Imaging System. ICALEO Florida 1998, Vol 85, pt 1, Section C, pp158 – 167.

55. Semak V.V. Hopkins J.A. McCay M.H. McCay T.D. Dynamics of Penetration Depth during Laser Welding. Proc. ICALEO 1994,

56. Matsunawa A. Seto N. Mizutani M. Katayama S. Liquid Motion in the Keyhole Laser Welding. Proc. ICALEO Florida Nov 1998, Vol 85. Section G pp 151 – 160.

57. Williams K. O'Neill W. Steen W.M. Melt-pool and Keyhole Dynamics During Thin Plate Laser Welding of Steel. SPIE Vol 1810 Gas Flow and Chemical Lasers (1992) pp 594-597

58. Semak V.V. Hopkins J.A. McCay M.H. and McCay T.D. Melt Pool Dynamics during Laser Welding. J. Phys. D: Appl. Phys. 28 (1995) 2442 – 2450)

59. Shannon G.J. and Steen W.M. Investigation of Keyhole and Melt Pool Dynamics during Laser Butt Welding of Steel Sheet Using High Speed Camera. ICALEO (Oct 1992) Vol 75, pp130-138

60. Duley W. Olfert M. Bridger P. Mao Y-L. What CO_2 Laser Welding of liquids tells us about penetration welding in metals. ICALEO Florida, Oct 1992, Vol 75, pp156 – 162.

61. Hugel H. Dausinger F. Berger P. Beck M. and Griebsch J. Investigations into the fundamental phenomena as basis for high quality laser welding. 5th European Conference on Laser Treatment of Materials. (ECLAT). Sept 1994. Bremen-Vegesack. Pp 63 –74

62. Girardeau–Montaut J-P. Dynamical Coupling Parameters for laser material interactions. Proceedings of the Society of Photo-Optical Instrumentation Engineers (SPIE) Volume 801 High Power lasers. 31 march – 3 April 1987. pp 75 - 80

63. Gasser A, Herziger G. Holtgen B. Kreutz E.W. Treusch H.G. Capillary waves and energy coupling in laser materials processing. Proceedings of the Society of Photo-Optical Instrumentation Engineers (SPIE) Volume 801 High Power lasers. 31 march – 3 April 1987. pp 170 - 177

64. Beyer E. Herziger G, Gasser A. and Sokolowski W. Plasma fluctuations during laser machining with CW – CO_2 lasers. Proceedings of the Society of Photo-Optical Instrumentation Engineers (SPIE) Volume 801 High Power lasers. 31 march – 3 April 1987. pp 75 - 80

65. Rayleigh lord. On the instability of cylindrical fluid surfaces. The London, Edinburgh and Dublin Philosophical Magazine 34,177, 1892.

66. Klein T. Vicanek M. Kroos J. Decker I. Simon G. Oscillations of the keyhole in penetration laser beam welding. J Phys.D: Appl. Phys. 27 (1994) 2023 – 2030.

67. Haran F.M. Hand D.P. Ebrahim S.M. Peters C. and Jones J.D.C. Optical signal oscillations in laser keyhole welding and potential application to lap welding. Meas. Sci. Technol. 8 (1997) 627 –633.

68. Postacioglu N. Kapadia P. Dowden J. Capillary waves on the weld pool in penetration welding with a laser. J.Phys. D. Appl. Phys. 22 (1989) 1050 –1061

69. Postacioglu N. Kapadia P. Dowden J. Theory of oscillations of an ellipsoidal weld-pool in laser welding. J.Phys. D. Appl. Phys. 24 (1991) 1288 –1292

70. BS5750, Quality Assurance Systems. British Standard Institute

71. The International Institute of Welding (I.I.W.), Commission XI.

72. Rogerson, J.H. Sept 1981. Cranfield University (formally Cranfield Instiute of Technology) lecture notes.

73. Lancaster. J.F. Ed The Physics of Welding 2nd Ed. Pub: Pergamon Press

74. Kim J.S., Watanabe T., Yoshida. Y. The effect of the beam-defocusing characteristics on porosity formation in laser welding. Journal of Materials Science Letters, 14,(1995) 1624-1626.

75. Katayama, S. Seto, N. Kim, J-D. Matsunawa. A. Formation mechanism and suppression procedure of porosity in high power laser welding of aluminium alloys. ICALEO Nov. 16 –19, 1998. Section C, pp 24

76. Shannon G.J. and Steen W.M. Investigation of Keyhole and Melt Pool Dynamic during Laser Butt Welding of Sheet Steel using a High Speed Camera. Proceedings of ICALEO (1992). pp 130-138.

77. Steen W. M Dowden J., Davis M and Kapadia. P. A point and line source model of laser keyhole welding. Phys.D:Appl.Phys.21 (1988) 1255-1260.

78. Tönshoff, H.K. Ostendorf, A. Kral, V. Hillers, O. Process and condition monitoring features incorporated in laser heads. ICALEO 1999, Nov. 15 –18. San Diego, Cal. Section E, pp 109 – 118

79. Decker, I. And Wohlfahrt, H. Laser beam welding - quality assurance by using process simulation. 5th European Conference on Laser Treatment of Materials. Bremen, 26 – 27 September 1994. pp 75 - 82

80. Bruce R. Madigan and Harvey R. Castner Survey of weld penetration techniques.EWI Research report MR9002. Jan 1990.

81. A review of sensor systems for top face weld penetration.TWI Researh board document 7254.02/93/780.02. Nov 1993.

82. Peters. C. N. D. Backface Penetration Control in Synergic MIG Welding. Msc Thesis. Cranfield Institute of Technology. (1985)

83. Monsoor A. Saifi and Sotiros J. Vahaviolos. Laser spot welding and real time evaluation. IEEE Journal of quantum electronics, Vol. QE-12, N° 2 Feb 1976.

84. Hamann C. , Rosen H-G, LaBiger. B. Acoustic emission and its application to laser spot welding. SPIE.1989. High power lasers and laser machining technology. pp275-281 Vol.1132.

85. Li.L and Steen W.M. Non-contact acoustic emission monitoring during laser processing. ICALEO 1992 pp719-728

86. Farson D., Hillsley K, Sames J. and Young R. Frequency-time characteristics of airborne signals from laser welds. ICALEO pp 86-94.

87. Li L, Qi N., Brookfield D.J. and Steen W.M.. Laser weld quality monitoring and fault diagnosis

88. Li L, Qi N., Brookfield D. J and Steen W.M. On-line laser weld sensing for quality control. ICALEO (1990) pp 411-421

89. Chen H.B., , Li L, Brookfield D.J., Williams K. and Steen W.M. Laser process monitoring with dual wavelength optical sensors.ICALEO 1991, San Jose, USA, Nov 3-8.

90. Semak V., McCay T.D., Hopkins J.A, Kahlen F.J, McCay M.H. and Eraslan AH. Development of a weld keyhole monitoring technique for laser welding. HTD-Vol.259 Transport phenomena in nonconventional manufacturing and materials processing. ASME 1993

91. Miyamoto I., Kamimuki K., Maruo H, Mori K., Sakamoto M.In-process monitoring in laser welding of automotive parts.ICALEO (1993) pp 413-424 H.R.Griem, Plasma Spectroscopy, Pub: McGraw-Hill.

92. Griebsch J, Hugel H., Dausinger F., Jurca M. Quality assurance in pulsed laser welding.ICALEO (1995)

93. Boechat A.P.Alvaro. Optical Fibre Beam Delivery of High Average Power Nd:YAG Laser radiation. PhD Thesis March 1992, Dept of Physics, Heriot-Watt University.

94. Bermejo D, Fabbro R, Sabatier L., Leprince L., Orza J.M. Spectroscopic studies of iron plasmas induced by continuous high power CO_2 laser. SPIE Vol. 1279 Laser assisted processing II (1990). pp 118-126

95. Sokolowski W., Herziger G., Beyer E. Spectral Plasma Diagnostics in welding with CO_2 lasers. SPIE Vol 1020 High power CO_2 laser systems and applications (1988). pp 96-102

96. Autric M., Vigliano P., Astic D., Bournot P., Dufresne D. Visible spectroscopy of laser produced plasma. SPIE Vol 1020 High power CO_2 laser systems and applications (1988) pp 103 - 112.

97. Matsunawa A., Kim J-D., Takemoto T., and Katayama S. Spectroscopic studies on laser induced plume of aluminium alloys

98. Schellhorn M. and Eichhorn A. Spectroscopic investigations of CO and CO_2 induced aluminium welding plasmas. SPIE Vol. 3092. pp 522- 525

99. Lacroix D., Jeandel G. and Boudot C. Spectroscopic characterisation of laser -induced plasma created during welding with a pulsed Nd:YAG laser. J. Appl. Phys. 81 (10), 15 May 1997. pp 6599-6606.

100. Fujii, H. Asakura, T. Matsumoto, T and Ohura, T. Output power distribution of a large core optical fiber. Journal of Lightwave Technology, Vol. LT-2, No 6, Dec 1984

101. Fujinaga, S. Takenaka, H. Narikiyo, T. Katayama, S. and Ohmori, A. Observation of keyhole behaviour during high power YAG laser welding with microfocused X-ray transmission imaging system. ICALEO November 16 –19, 1998. Section C, pp 158 - 167

102. Trappe, T. Kroos, J. Tix, C. and Simon, G. On the shape and location of the keyhole in penetration laser welding. J. Phys. D: Appl. Phys, 27 (1994) 2152 – 2154

103. Semak V.V. West, J.C. Hopkins, J.A. McCay M. H. McCay, T. D. Shape and position of keyhole during laser welding.

104. Matsunawa A. Semak V. The simulation of front keyhole wall dynamics during laser welding. J.Phys. D: Appl. Phys. 30 (1997) 798 -809

105. Chen, M. M. and Bos, J. A. Melt flow in deep penetration welding. ICALEO November 16 –19, 1998. Section F, pp 187 – 196

106. Kar, A. and Mazumder, J. Mathematical modelling of keyhole laser welding. J.Appl.Phys. 78 (11), 1 December 1995

107. Solana, P and Negro, G. A study of the effect of multiple reflections on the shape of the keyhole in the laser processing of materials. J. Phys. D: Appl. Phys. 30 (1997) 3216 – 3222

108. Ellis H. Ed. Nuffield Advanced Science Book of Data. Pub. Longman, 2nd Edition.

Publications

1. **Peters C, Fox M.D.T, Haran F.M, Hand D.P. Jones J.D.C, and Steen W.M.** Nd:YAG welding penetration monitoring using back-scattered laser light from in and around the keyhole. ICALEO 98 Florida Nov 98.
2. **Peters C.** On-line quality monitoring for Nd:YAG laser welding: a look at opportunities. The Industrial Laser User. Issue 16, Aug 1999. pp 29-31.
3. **Hand.D.P, Peters C, Fox M.D.T, and Jones J.D.C.** Automatic detection of errors in laser overlap welding of zinc coated steel. ICALEO 98. Florida Nov 98.
4. **Hand.D.P, Peters C, Fox M.D.T, and Jones J.D.C.** Optical sensor for detection of errors in Nd:YAG laser overlap welding of zinc-coated steel. Proc Instn Mech Engrs Vol 214 Part B, pp 793-798.
5. **Haran F.M., Hand, D.P., Ebrahim, S.M. Peters, C. Jones J.D.C.** Optical signal oscillations in laser keyhole welding and potential application to lap welding. Meas. Sci. Technol.Vol 8: 1997 pp627 –633.
6. **Haran F.M, Hand D.P, Peters C, and Jones J.D.C.** Process control in laser welding utilising optical signal oscillations. ICALEO 96 Florida October 96
7. **Haran F M, Hand D.P, Peters C, Jones J.D.C.** Real-time focus control in laser welding. Meas.Sci. Technol. 7 (1996) 1095-1098
8. **Haran F.M., Hand D.P., Peters C., Jones.** Focus control system for laser welding. J.D.C. Applied Optics Vol 36 (1997) pp. 5246 –5251)
9. **Hand D.P., HaranF.M., PetersC, Jones J.D.C.** Full penetration detection in Nd:YAG laser welding by analysis of oscillatory signals: application to overlap seam tracking.
10. **Morgan S.A,. Hand D.P, Haran F.M., Peters C.,.Steen W.M, Jones J.D.C..** Origin of oscillations in in optical signals for Nd:YAG laser welding.. ICALEO October 14-17, Section D, Vol 81 pp28-35.

11. **Hand D.P., Peters C., Jones J.D.C..** Nd:YAG laser welding process monitoring by non-intrusive optical detection in the fibre optic delivery system. 1995 Meas. Sci. Technology, 6: 1389 – 1394.
12. **Fox M.D.T., Peters C., Blewett I.J., Hand D.P., Jones J.D.C..** Real-time optical monitoring of gas shield condition during Nd:YAG laser welding. ICALEO 1998. Orlando Florida November 16-19, Section C, pp 62 – 68
13. **Fox M.D.T. French, P. Hand, D.P. Peters, C. Jones J.D.C.** Optical focus control for laser percussion drilling. ICALEO 1999 November 15 –18, San Diego, Cal. Section C. pp 1- 10
14. **Fox M.D.T. Peters, C. Hand, D.P. Jones, J.D.C.** Applications of optical sensing for laser cutting. ICALEO 1999. November 15 –18, San Diego, Cal. Section C. pp 106- 114

Patents

1. United States Patent 5,850,068. Focus Control of Lasers in Material Processing Operations